ARO 2249.2-EG

(1)

ARMY RESEARCH OFFICE FINAL SCIENTIFIC REPORT
ARO CONTRACT DAAG29-K-0216

MODELING HOW EDGES AND CORNERS AFFECT THE IGNITION OF HOMOGENEOUS REACTIVE SOLIDS

BY

L. G. VORSTEVELD,
C. E. HERMANCE, PI

PREPARED FOR
UNITED STATES ARMY LABORATORY COMMAND
ARMY RESEARCH OFFICE
RESEARCH TRIANGLE PARK, NC 27709 - 2211

FINAL REPORT FOR PERIOD AUGUST, 1985 TO AUGUST, 1988

THE UNIVERSITY OF VERMONT
COLLEGE OF ENGINEERING AND MATHEMATICS
DEPARTMENT OF CIVIL ENGINEERING
AND MECHANICAL ENGINEERING
BURLINGTON, VERMONT 05405 - 0156

UNCLASSIFIED
SECURITY CLASSIFICATION OF THIS PAGE (When Data Entered)

REPORT DOCUMENTATION PAGE

READ INSTRUCTIONS BEFORE COMPLETING FORM

1. REPORT NUMBER	2. GOVT ACCESSION NO. N/A
3. RECIPIENT'S CATALOG NUMBER N/A	
4. TITLE (and Subtitle) Modeling How Edges and Corners Affect the Ignition of Homogeneous Reactive Solids	5. TYPE OF REPORT & PERIOD COVERED Final, Aug. 18, 1985- Aug. 18, 1988
	6. PERFORMING ORG. REPORT NUMBER
7. AUTHOR(s) Vorsteveld, L. G. and Hermance, C. E.	8. CONTRACT OR GRANT NUMBER(s) -k- DAAG29-85-0216
9. PERFORMING ORGANIZATION NAME AND ADDRESS CEME Dept./ 213 Votey Bldg. University of Vermont Burlington, VT 05405-0156	10. PROGRAM ELEMENT, PROJECT, TASK AREA & WORK UNIT NUMBERS
11. CONTROLLING OFFICE NAME AND ADDRESS U. S. Army Research Office Post Office Box 12211 Research Triangle Park, NC 27709	12. REPORT DATE 14 October 1988
	13. NUMBER OF PAGES 170
14. MONITORING AGENCY NAME & ADDRESS(if different from Controlling Office)	15. SECURITY CLASS. (of this report) Unclassified
	15a. DECLASSIFICATION/DOWNGRADING SCHEDULE

16. DISTRIBUTION STATEMENT (of this Report)

Approved for public release; distribution unlimited.

17. DISTRIBUTION STATEMENT (of the abstract entered in Block 20, if different from Report)

NA

18. SUPPLEMENTARY NOTES

The view, opinions, and/or findings contained in this report are those of the author(s) and should not be construed as an official Department of the Army position, policy, or decision, unless so designated by other documentation.

19. KEY WORDS (Continue on reverse side if necessary and identify by block number)

Solid Propellants
Ignition
Ignition Modeling
Reactive Solids
Homogeneous Reactive Solids

20. ABSTRACT (Continue on reverse side if necessary and identify by block number)

The effect of geometry on the ignition behavior of solid propellants has been investigated both theoretically and experimentally. Physical and mathematical formulations of the theoretical problem are presented, where extensive use is made of the reactive solid concept, with ignition being controlled by a solid phase exothermic chemical reaction. Mathematical equations are described in different two dimensional domains, and solved numerically over a wide range of physico-chemical parameters utilizing the explicit finite difference method. Geometries considered are: acute wedges having included angles of $\pi/2$, $\pi/4$ and

DD FORM 1 JAN 73 1473 EDITION OF 1 NOV 65 IS OBSOLETE

UNCLASSIFIED
SECURITY CLASSIFICATION OF THIS PAGE (When Data Entered)

$\pi/8$, and in addition, the effect of rounding $\pi/2$ and $\pi/4$ angles is investigated by inclusion of a radius of curvature γ.

Theoretical results are presented for these various geometric cases; they show dramatically faster ignition times for strictly acute wedges, with ignition proceeding approximately three times faster with each halving of the included angle. Introduction of edge rounding reduces significantly the geometrically induced speed up in ignition; the extent of rounding depends predominantly on the relative magnitudes of the thermal penetration wave at ignition and rounding parameter γ.

Temperatures at ignition are influenced by the convexity of the investigated geometry; a more convex shape yields higher ignition temperatures. Reactant depletion plays an increasingly important role for the more acute cases as the ignition process becomes more localized and more rapid reactant consumption limits the overall range in ignition. Conversely, the introduction of rounding removes the extreme acuteness from the solution domain, delocalizes the ignition site and suppresses the rate of reactant consumption.

Experimental investigations, performed with a CO_2 laser to ignite an AP-based propellant in an atmospheric N_2 environment, demonstrate appreciably faster ignition for 90° and 60° samples, compared to the baseline planar samples. However, the effect of geometry on ignition times diminishes with increasing flux levels, which indicates additional contributing mechanisms besides solid phase heat conduction. Experimental observations suggest gas phase chemical diffusion and surface regression becoming more important. These remarks and the reasonable agreement between theory and experiment lead to the recommendation that inclusion of gas phase and/or surface processes is imperative in future modeling attempts of geometric aspects of solid propellant ignition as possible avenues for improved correlation between theory and experiment.

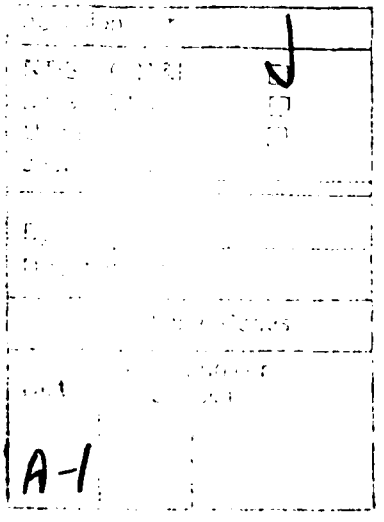

ARO FINAL SCIENTIFIC REPORT

ARO DAAG29-85-K-0216

MODELING HOW EDGES AND CORNERS AFFECT THE IGNITION OF HOMOGENEOUS REACTIVE SOLIDS

by

L.G. Vorsteveld and C.E. Hermance

GRANT ARO-DAAG29-85-K-0216

October, 1988

Transmitted by:

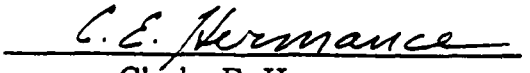

Clarke E. Hermance
Principal Investigator

Department of Civil Engineering and Mechanical Engineering
University of Vermont, Burlington, Vermont

TABLE OF CONTENTS

ACKNOWLEDGMENTS

It is with pleasure that we gratefully acknowledge the help of external organizations during the conduct of this research program. Firstly we wish to thank Sandia National Laboratories, Livermore, CA for the use of the Combustion Research Facilities laboratories during the experimental phase of the work reported herein. Special thanks are due Dr. Robert Carlson for his encouragement and help in arranging the cooperative effort, and to and Dr. Steven Vosen for his help and letting us use his laser and laboratory area. Financial assistance for Dr. Vorsteveld from Associated Western Universities Inc. during the time at Sandia is gratefully acknowledged. We also wish to acknowledge the essential help rendered by the Naval Weapons Station, China Lake, CA through Mr. Thomas Boggs and his associates for providing the propellant material used in the experiments.

ABSTRACT

The effect of geometry on the ignition behavior of solid propellants has been investigated both theoretically and experimentally. Physical and mathematical formulations of the theoretical problem are presented, where extensive use is made of the reactive solid concept, with ignition being controlled by a solid phase exothermic chemical reaction. Mathematical equations are described in different two dimensional domains, and solved numerically over a wide range of physico-chemical parameters utilizing the explicit finite difference method. Geometries considered are: acute wedges having included angles of $\pi/2$, $\pi/4$ and $\pi/8$, and in addition, the effect of rounding $\pi/2$ and $\pi/4$ angles is investigated by inclusion of a radius of curvature γ.

Theoretical results are presented for these various geometric cases; they show dramatically faster ignition times for strictly acute wedges, with ignition proceeding approximately three times faster with each halving of the included angle. Introduction of edge rounding reduces significantly the geometrically induced speed up in ignition; the extent of rounding depends predominantly on the relative magnitudes of the thermal penetration wave at ignition and rounding parameter γ.

Temperatures at ignition are influenced by the convexity of the investigated geometry; a more convex shape yields higher ignition temperatures. Reactant depletion plays an increasingly important role for the more acute cases as the ignition process becomes more localized and more rapid reactant consumption limits the overall range in ignition. Conversely, the introduction of rounding removes the extreme acuteness from the solution domain, delocalizes the ignition site and suppresses the rate of reactant consumption.

Experimental investigations, performed with a CO_2 laser to ignite an AP-based propellant in an atmospheric N_2 environment, demonstrate appreciably faster ignition for 90° and 60° samples, compared to the baseline planar samples. However, the effect of geometry on ignition times diminishes with increasing flux levels, which indicates additional contributing mechanisms besides solid phase heat conduction. Experimental observations suggest gas phase chemical diffusion and surface regression becoming more important. These remarks and the reasonable agreement between theory and experiment lead to the recommendation that inclusion of gas phase and/or surface processes is imperative in future modeling attempts of geometric aspects of solid propellant ignition as possible avenues for improved correlation between theory and experiment.

LIST OF TABLES

TABLE #

LIST OF FIGURES

FIGURE #

CHAPTER I

MOTIVATION

1.1 Introduction

The study of ignition of solid propellants has been a research topic both in the development of operational solid rocket motors and gun systems for quite some time. Both double-base and composite propellants have been the subject of numerous investigations whose main concern has been to determine and characterize the mechanisms responsible for ignition of these materials. In practical situations the response of a solid propellant containment has to be reliable and repeatable after functioning of an igniter system. Predictive capabilities of the propellant ignition process are especially important in solid rocket motors as the subsequent processes of transient flame spreading, pressurization of the chamber and steady propellant burning are influenced by the ignition characteristics.

A great deal of work has been done in understanding the ignition process, which can now be predicted contingent upon selection of an appropriate and sufficient set of qualifiers. Important factors include propellant ingredients, igniter characteristics such as mode and intensity of stimulation, and environmental conditions such as its composition, temperature and pressure.

Theoretical work has advanced three major ignition mechanisms which are categorized into: (i) solid phase thermal ignition theory where thermal runaway is based on exothermic chemical reactions in the solid, (ii) heterogeneous or surface ignition as a result of chemical reaction between gaseous oxidizer attacking the solid fuel surface, and (iii) gas phase ignition where the solid propellant decomposes into fuel and oxidizer vapors which diffuse and react exothermically in the adjacent gas phase. Extensive numerical and analytical analyses have established limits of applicability for these theoretical formulations based on experimentally observed phenomena.

Experimental studies have frequently reported on multi-dimensional observations despite exercising extreme care in maintaining one dimensionality in the execution of the experiments. A partial list includes effects such as localized ignition at a propellant surface presumably due to its surface inhomogeneity and irregular surface morphology after extinguishment of an ignited propellant surface.

In all these cases the tested propellant samples have a flat planar surface. In practice however, the geometry of the solid propellant undergoing ignition is usually not one

dimensional as is exemplified by the perforated stick propellants used in many small arms and the tips of sharp fins, consisting of solid propellant material, which exist in the interior of a solid rocket motor. Secondly, the presence of roughness on a propellant surface might augment the predictions based on one dimensional laboratory tests because of the generally small time scale involved during ignition. It is important therefore to consider the effect that a muiti-dimensional geometry could have on the ignition delay and ignition characteristics of a solid propellant. It is precisely the study of this geometric effect which forms the basis of this thesis.

1.2 Problem Statement

This research deals with the determination of the ignition behavior of solid propellants in multi-dimensional geometries. To meet this objective, the study consisted of two parts: 1) an extensive numerical investigation of proposed ignition models having different geometric configurations; and 2) a small experimental program to gain insight in the effect of geometry during the radiant ignition of a practical propellant.

In the numerical investigations major emphasis is placed on the study of the ignition behavior of the simplest model of a solid propellant, the homogeneous reactive solid, which has a geometric shape that presents a specified degree of convexity towards the ignition stimulus. Various geometries will be considered to obtain quantitative information concerning these geometric aspects on the ignition delay. Results for the different geometries are then compared to those reported for a planar surface of the same material and ignited by the same ignition stimulus. Predictive methods will be developed for the determination of the ignition delay in different geometries. Guidelines are formulated stating the degree of convexity and other conditions required for significant reduction of the ignition delay.

Primary objective of the experimental study is to assess the extent of geometry augmenting the one dimensional ignition behavior. This is to be accomplished by exposing small propellant samples of different configurations to radiation from a CO_2 laser and determining the ignition delay dependence on the applied heat flux. The comparison between acute and planar sample results provides then a means of interpreting the effects of geometry.

It is anticipated that through current modeling efforts and experimental work an estimate can be made of the effect of geometry on the ignition behavior of real solid propellants. In addition, present work may provide a partial explanation to unexpected experimental ignition behavior.

CHAPTER II

LITERATURE SURVEY

2.1 Introduction

For centuries mankind has searched for highly energetic materials capable of producing a large thrust force or a large destructive force in a small time period. One only needs to look at the invention of black powder and its effect on warfare. These investigations arise not only from the desire to develop weapons for defensive and offensive purposes, but also out of curiosity and scientific interest to expand human knowledge beyond the boundaries of planet Earth.

A category of materials capable of fullfilling these needs are liquid and solid propellants. A partial list of their applications include providing propulsion for a variety of applications in rockets, guns, artillery and air-breathing propulsion systems, rapid generation of gaseous products for automotive safety air bag systems, ejection of pilots from aircraft and gas and pressure generators (Kuo, 1987).

Solid propellants are defined as solid materials which generate a large quantity of gas and are capable of self-sustained combustion without the presence of ambient oxidizer. Fuel and oxidizer components are chemically linked in homogeneous or double-base propellants. Heterogeneous or composite propellants consist of small oxidizer crystals embedded and held together in a plastic fuel binder matrix, the conglomorate thus forming a physically linked heterogeneous system. The effects of these physical characteristics are clearly demonstated in the different nature of the flame structures associated with this broad classification of solid propellants.

A typical example of a homogeneous propellant is nitrocellulose. Upon thermal decomposition its large molecules break up into two main fragments; one set containing C/H and C/H/O structures acts as the fuel component whereas the other fragment having NO_2 acts as the oxidizer. The flame structure for homogeneous propellants appears uniform and one-dimensional as ingredients are mixed microscopically and react chemically in a premixed flame.

Commonly used ingredients in composite propellants are NH_4ClO_4 (ammonium perchlorate or AP) and high energy nitramines as energetic oxidizers. Organic binders such as polyurethane and polybutadiene act as fuel and provide structural support to the mixture. Its combustion zone displays definite heterogeneous characteristics. Kubota (1984) shows typical flame structures for both propellant types under various atmospheric conditions. Observed cellular flames for both AP and RDX composites are a direct result of interdiffusion of

decomposed gases from AP or RDX crystals into fuel pyrolysis products producing the typical diffusion flame structure.

Major emphasis in solid propellant research is directed towards their use in solid rocket motors. Research areas as ignition, flame spread behavior and erosive burning, steady state burning of double-base and composite propellants, and combustion instability all have direct connections to their usage in solid rocket motors. In addition, chemical, thermal and kinetic aspects of different types of solid propellants and the role of various ingredients and additives have been investigated in depth with a comprehensive compilation done by Summerfield and Kuo (1984). As each of these topics forms a major area of research in itself, they are simply enumerated here to give the reader a flavor of the wide variety of problems and processes associated with solid propellant research. In the current work attention is restricted to further understanding the processes during the initial phase of operation of a solid rocket motor: the ignition process.

2.2 Physical Description of the Ignition Process

Before reviewing the historical development of ignition theories and experiments of solid propellants, it is appropriate to describe in some detail the physical and chemical aspects involved during the transient ignition process. Although this process depends heavily on the constituents making up the solid material, it is generally agreed that the following processes are present.

Figure 2.1, taken from Price *et al.* (1966), shows a diagrammatic representation of some classes of chemical reactions thought possible for composite propellants. Starting wih the solid phase, Price *et al.* (1966) identified oxidizer and fuel decomposition reactions to either a solid or a liquid state, direct solid-phase reactions between oxidizer and fuel as well as direct oxidizer and fuel decomposition to gaseous intermediates. At the surface, heterogeneous reactions between oxidizer gases and solid fuel intermediates as well as gaseous binder products attacking condensed phase oxidizer were assumed to occur. In the gas phase a diffusion flame was identified between oxidizer and binder products, as well as several reactions between environmental gases and binder and oxidizer gas products. Depending upon one or a few dominant chemical reactions, three different theories of ignition have evolved which have as their primary distinction the physical location of the primary exothermic reaction assumed to control the ignition process.

Another detailed description of the ignition process put forward by Kulkarni, Kumar and Kuo (1980) is portrayed in Figure 2.2. Starting initially with a solid at a low, nonreactive

temperature, energy is transferred to the surface by some external means. Following an inert heating period, the solid phase starts to decompose at or near the surface caused by heat conduction, in-depth radiation and photochemical decomposition. Depending upon specific propellant formulations and environmental conditions, a foam or liquid melt layer is frequently observed at the surface (Boggs, Derr and Beckstead, 1970). At this point chemical reactions may occur in the solid-phase, in the melt layer and at or near the surface along with gasification of species into the gas phase and direct sublimation of the solid. Species evolved from the surface can react in the gas phase in a diffusion or cellular flame between binder pyrolysis products and oxidizer originating from either the solid or the ambient surroundings. Due to the large number of species present, the exact delineation of chemical processes remains rather obscure. Heat generated in the gas phase is both radiated and transported back to the surface and into the solid which further enhances species generation and chemical reactions. Some of the reactions are endothermic, others are exothermic. To attain a state of sustained ignition, the net heat evolved from chemical reactions must overcome conductive and radiative heat losses. Depending upon operating conditions, a steady combustion wave may result. The overall ignition process therefore involves processes of heat transfer, fluid flow, phase changes, chemical kinetics and mass diffusion of several species. Further complications arise because of high rates of chemical heat release and extremely small length and time scales.

2.3 Areas of Ignition Research

Major areas of research in solid propellant ignition have primarily revolved around: (1) the mechanistic understanding of the ignition process with respect to formulation effects, modes of heating and environmental conditions, (2) determination of a single or global chemical reaction rate capable of numerically predicting observed ignition behavior for a particular propellant and igniter system, and (3) determination of ignition delay and its dependence on formulation, environmental and ignition stimuli effects (Hermance, 1984).

2.4 Ignition Delay Criteria

The time period from start of the ignition stimulus to the instant of sustained ignition is called the ignition delay. Its determination for a particular propellant system forms one of the main areas of interest in solid propellant studies. However, no universally accepted definition of ignition delay has emerged yet after over 30 years of openly published work.

In numerical studies it is frequently defined in terms of reaching some kind of thermal

runaway condition, particular elevated temperature level, or in terms of continued and sustained chemical reactivity after removal of the external stimulus. Experimental results are commonly reported based on either first detection of a visible flame or 50% of the samples ignited at a particular interrupted flux level. However, there exists no direct straightforward connection between numerically defined ignition, first light detection and the actual state of combustion. In response, Kumar and Hermance (1971) developed a new theoretical ignition criterion based on thermal emission of product species in the gas phase, and noted theoretical traces quite similar to actual experimental photo detector output, depending on the sensitivity of the theoretical criterion. Both theoretical and experimental approaches require careful interpretation before statements concerning the mechanistic steps leading to ignition can be made. Various ignition criteria are frequently tested in modeling efforts to assess their sensitivity on the reported results. In addition, theoretically employed criteria frequently are difficult to implement in experiments and vice versa. It is therefore imperative in reporting results that the employed ignition criterion is carefully defined.

2.5 Ignition Theories

2.5.1 Evolution of Ignition Theories

Openly published work in solid propellant ignition started in the early fifties with works from Frazier and Hicks (1950), Altman and Grant (1953) and Hicks (1954). The first theory advanced considered thermal runaway conditions as a result of solid phase heat generation. This development led to the concept of a homogeneous reactive solid having a typical bulk or surface solid-to-solid exothermic decomposition reaction. Hicks's work (1954) was the first sophisticated attempt at a "surface-ignition" model as he considered the transient heating of a solid undergoing an Arrhenius exothermic decomposition reaction. An unique feature of his model was the consideration of the ignition behavior after removal of the ignition stimulus. This approach tested the "state of ignitedness" of the solid and set minimum required heating times leading to thermal runaway. Other solid phase models were developed differing mainly in the manner of external heating and nature of chemical self-heating (Price, Bradley and Fleming, 1963; Baer and Ryan, 1965).

Double-base propellants were considered at that time to ignite due to a solid-phase exothermic reaction. Because of the heterogeneous nature of composite propellants, it seemed unlikely that their ignition characteristics were controlled in a similar fashion. This prompted development of a "gas phase" ignition model where fuel and oxidizer mixed in the gas phase

initiated chemical reactions which then led to a self-sustaining system.

Early work at Princeton University by Hermance, Shinnar and Summerfield (1965) considered fuel diffusing from the solid surface into the gas phase and oxidizer diffusing inward to the surface. The solid, which represented fuel binder, gasified upon contact with the hot stagnant oxidizing environment. The vapors mixed by counter-diffusion reacted in a second-order fashion releasing chemical energy. Ignition was defined in terms of the maximum gas phase temperature reaching a specified level. Shortcomings included constant assumed solid/gas interface temperature and treatment of a pure fuel, not a propellant.

A third body of solid propellant ignition theory was developed in the early sixties at the United Technology Center as a result of experimental ignition studies in which the propellant surface was attacked chemically by powerful oxidizing agents such as fluorine. No external heating was included in these models. The resulting hypergolic theory consisted of a one dimensional model involving transient gas phase diffusion of reactants and products with simultaneous heat conduction in solid and gas phases. Ignition was defined in terms of an arbitrarily selected fast rise in surface temperature. The sole site for chemical reaction was restricted to the propellant surface where gaseous oxidizer reacted exothermically with the solid fuel surface. It was argued that the hypergolic theory correctly predicted the experimentally observed dependence of ignition delay on ambient oxidizer concentration.

A modification of the hypergolic theory led to the "heterogeneous" theory, which originated initially to incorporate ignition of composite propellants by external heating in inert atmospheres. Its major phenomelogical component considered AP oxidizer decomposing upon heating into anhydrous perchlorate acid ($HClO_4$) which then chemically attacked the fuel surface in a hypergolic manner. However, no early analytical work was performed to model this sequence consisting of external heating, oxidizer decomposition, diffusion of its products and surface fuel oxidation.

Price *et al.* (1966) noted several shortcomings of these theories and difficulty in comparing the theories as far as composite propellant ignition by external heating in inert environments was concerned. Solid phase theory shortcomings included nonagreement with respect to observed AP solid phase decomposition and inability to account for experimentally observed pressure effects. Heating boundary conditions were differently formulated for the solid and gas phase models, making direct comparison to each other and to experimental results of dubious significance.

Following these early efforts, modeling of solid propellant ignition processes was directed more or less along three distinct paths, leading to advancements in the solid phase, heterogeneous and gas phase theories. To maintain clarity in the subsequent description, each

of these theories is discussed seperately.

2.5.2 Solid Phase Thermal Ignition Theory

In this branch of ignition theory the characteristic rapid temperature rise is assumed to be caused by an exothermicity located at or within the solid surface. Gas phase composition and pressure effects can not be incorporated in the theoretical description except possibly in the formulation of the boundary condition. A general mathematical description has been formulated by Price *et al.* (1966), including field equations and initial/boundary conditions for a semi- infinite, one dimensional physical model as:

$$\rho_c c_c \frac{\partial T}{\partial t} = k_c \frac{\partial^2 T}{\partial x^2} + \rho_c c_c r \frac{\partial T}{\partial x} + \beta q e^{-\beta x} + Z_c Q_c C_i^a f^a e^{-E_c/RT} \tag{2-1}$$

$$\frac{\partial f}{\partial t} = -Z_c C_i^{a-1} f^a e^{-E_c/RT} \tag{2-2}$$

$$q_n + \rho_c r Q_s = -k_c \frac{\partial T}{\partial x} \quad \text{at } x=0 \tag{2-3}$$

$$T(x,0) = 0,\ f=1 \quad \text{at } t=0 \tag{2-4}$$

$$T(x,t) = T_i \quad \text{or} \quad \frac{\partial T}{\partial x} = 0 \quad \text{at } x=\infty \tag{2-5}$$

The physical interpretation of the terms in Eq. (2-1) in sequential order is: 1) rate of accumulation of energy; 2) rate of energy gain due to solid phase conduction; 3) rate of energy convection due to surface regression; 4) rate of in-depth radiation absorption due to nonopacity of the solid; and 5) rate of chemical heat generation by an a^{th} order bulk chemical reaction.

Eq. (2-2) represents the rate equation for the a^{th} order chemical reaction, where C_i is the initial concentration and f the fraction of reactant present at any time. Eq. (2-3) expresses the exposed boundary condition; its details vary depending upon the particular model formulation. Eqs. (2-4) and (2-5) constitute initial conditions and the boundary condition far away from the exposed surface. A substantial number of studies are reported dealing with various parts of the above general formulation.

The simplifying assumptions made in the above general formulation and possible physical implications have been discussed by Price *et al.* (1966). Major conditions scrutinizing these

assumptions are: 1) constant physical properties, debatable because of the heterogeneous nature of composite propellants, likely temperature effects and changes in chemical composition caused by chemical reactions; 2) assumed one dimensional heat conduction which is open to discussion for composite propellants; and 3) description of chemistry by an overall Arrhenius reaction rate which drastically simplifies the actual chemical kinetics.

Ignition delay times are frequently defined for solid phase ignition theories by (i) attainment of a thermal runaway condition at or near the surface or (ii) a "go no-go" criterion where the successful ignition is based on the thermal behavior of the solid material after external flux removal.

The majority of recent theoretical models have considered the transient conduction equation augmented with the exothermic heat production term solved either by numerical integration or asymptotic analysis. Specific formulation of the boundary condition has introduced gas phase effects in the analysis. Bradley (1970) and Liñán and Williams (1971) have reported a decrease in ignition time with increasing flux levels. However, the noted increasing ignition times under constant pressure conditions reported by Baer and Ryan (1968) for increasing heating rates was never verified experimentally (Kulkarni, Kumar and Kuo, 1980).

Gas phase pressure, surface regression, surface absorption and exothermic reaction at the surface were included in a model formulated by Baer and Ryan (1968). The applied surface flux was complemented with a kinetically limited chemical heat release due to chemical reaction at low surface temperatures and a convection limited heat addition corresponding to steady surface regression. Successful ignition was based on a "go no-go" criterion by monitoring the behavior of the regression rate at a time twice as long as the igniter exposure period. Major results indicated that ignition times approached simple thermal ignition theory at low flux levels, pressure effects were nonexisting at high pressure and low fluxes but strong at low pressures and high fluxes. Further, different ignition time asymptotes were approached at low pressures depending on the igniter flux level. It was noted that the low pressure limit depended strongly on the steady state surface temperature. Finally, the manner of igniter flux termination drastically affected the transition to steady deflagration.

Detailed numerical computations of a model described by Eqs. (2-1) through (2-5) without inclusion of surface regression and in-depth radiative absorption by Bradley (1970) indicated minimal dependence of results on reaction order, the ignition temperature limited by the adiabatic reaction temperature and a minimum activation energy of 20 kcal/mole below which external heating did not produce typical ignition behavior. In general a long inert heating period was observed, followed by rapid onset of chemical reactivity resulting in ignition. He also developed an empirical correlation between dimensionless heat release parameter A,

activation energy E and ignition time τ_c which related all numerical data within 4%.

$$A = \frac{E^{1/2} e^{E/[1+2(\tau_c/\pi)^{1/2}]}}{(\pi\tau_c)^{1/4}[1+2(\tau_c/\pi)^{1/2}]}, \quad \text{where } A = \frac{Q\nu k T_i}{q^2}, \text{ and } \tau = \frac{kt}{kpcT_i^2} \tag{2-6}$$

Liñán and Williams (1971) later derived this expression analytically using asymptotic methods based on expansions in terms of a high activation energy. This work formed the basis of several subsequent studies employing similar techniques, which resulted in approximate relations between τ_c and system parameters. As the different researchers have attempted to express results in a format similar to Eq. (2-6), major phenomenological results will be enumerated below. In these studies the effects of in-depth radiative absorption and inclusion of heat losses to the adjacent gas phase were investigated for a range of chemical parameters.

In-depth radiation effects were studied by Thompson and Suh (1970), Liñán and Williams (1972) and Bush and Williams (1975, 1976). Ignition was specified by the occurence of a thermal runaway condition in the solid due to an exothermic condensed phase reaction.

Thompson and Suh (1970) achieved excellent agreement between low flux radiative heating ignition experiments and a proposed model which included a bulk exothermic reaction and in-depth radiative absorption. Values of heat of reaction, frequency factor and activation energy were determined based on experimental results. They reported using an absorption coefficient μ of 250 cm^{-1} based on transmittance tests.

Liñán and Williams (1972) reported that as the absorption coefficient α increased from very small values, the ignition behavior changed from a thermal explosion without any appreciable heat conduction in the solid to a transition zone with spatially distributed chemical heat release, and, for very large α, to surface heated ignition results as expressed by Eq (2-6). For small absorption coefficients corresponding to distributed chemical heat generation, they obtained the following relation between ignition time τ_c and parameters A and E:

$$\tau_c = [\frac{E}{\ln(A/\alpha)} - 1]/\alpha \quad \text{where } \alpha = \frac{\mu k T_i}{q}, \quad 10^{-4} \leq \alpha \leq 10^{-2} \tag{2-7}$$

Figure 2.3 shows typical results for the entire absorptivity range.

The effects of in-depth radiative absorption and conductive heat losses to an inert gas phase adjacent to the reactive solid were investigated by Bush and Williams (1975, 1976). They introduced the ratio of gas to solid thermal responsivity Γ expressed as $[\rho_g \lambda_g c_g / \rho_s \lambda_s c_s]^{1/2}$

to account for this surface heat loss.

In their first work, the analysis was done for small values of Γ where 3 regions were identified depending upon the magnitude of the absorption coefficient α. They noted that for decreasing α the position of the thermal runaway moved from the surface inward into the interior and that the ignition time became less dependent on Γ. Parameter Γ had the largest effect on ignition time for large α in which case the ignition took place at the surface. Three approximate relations were obtained depending on the nature of the thermal field as affected by the absorptivity α.

For very small α which corresponded to explosion type ignition behavior, Γ had no effect and results were related by Eq. (2-7). Larger α values produced the following expression:

$$\alpha(\theta_o - 1) = \alpha\left(\frac{E}{\ln(A)} - 1\right) + \frac{\alpha E}{(\ln A)^2}[t_c + \ln(\alpha g_c)], \quad \text{where} \quad \theta_o = 1 + 2\frac{(\tau_c/\pi)^{1/2}}{1+\Gamma} \tag{2-8}$$

The contribution of the second term is generally small; t_c is concerned with the interior position of the thermal runaway site. For large α corresponding to radiative absorption in a thin layer near the surface, Bush and Williams (1975) reported strongest dependence of ignition times on Γ and obtained, where C was a complex function of Γ, α and τ_c, the following:

$$\tau_c = \frac{\pi}{4}\left[\left(\frac{E}{\ln(A/\alpha^{1/2})} - 1\right) - \frac{E}{\ln^2(A/\alpha^{1/2})}\ln[(\pi\tau_c)^{1/4}C/0.65] + \cdots\right]^2 \tag{2-9}$$

The effect of strong conductive cooling to an inert gas phase, expressed via the same parameter Γ, was discussed in a follow-up paper by Bush and Williams (1976). Again, the reactive solid was taken to be transparent. For a strictly opaque reactive solid they developed a modification to Eq. (2-6) to account for the surface heat loss as:

$$A = \frac{.65E^{1/2}e^{E/[1+2(\tau_c/\pi)^{1/2}/(1+\Gamma)]}}{(\pi\tau_c)^{1/4}(1-\Gamma)^{1/2}[1+2(\tau_c/\pi)^{1/2}/(1+\Gamma)]} \tag{2-10}$$

Figures 2.4, 2.5 and 2.6 display results for Γ ranging from 0 to ∞ and for values of α equal to ∞, 10, 1 and .1. It is clear that Γ has a large effect on the ignition time τ_c only if the incident flux is absorbed at or near the surface.

Since many practical situations involve convective rather than radiative heat transfer to

the exposed propellant surface, convective heating of a reactive solid by sudden immersion in a hot gas flow was considered by Niioka and Williams (1977). Thermal runaway was attained at the surface via an Arrhenius reaction rate without considering reactant consumption. The gas phase was treated in a quasi-steady fashion where its temperature was assumed constant resulting in Newtonian heating. Results were formulated using previous definitions for parameters A, E and τ_c, complemented with θ_e, the nondimensional free stream temperature, as:

$$A = \frac{.65E^{1/2}\, g_c}{1-(\theta_e-1)(1-g_c)} \left[\frac{1}{\sqrt{\pi\tau_c}} - \frac{g_c}{\theta_e-1}\right]^{1/2} \exp\left[\frac{E}{1+(\theta_e-1)(1-g_c)}\right] \qquad (2\text{-}11a)$$

where:

$$g_c = \exp[\tau_c(\theta_e-1)^{-2}]\ \mathrm{erfc}[\tau_c^{1/2}(\theta_e-1)^{-1}] \qquad (2\text{-}11b)$$

Figure 2.7 shows typical results for different θ_e's; for θ_e approaching infinity, Eq. (2-11a) reduces to Eq. (2-6) as is displayed in Figure 2.7.

The general solid phase ignition model, expressed by the system equations (2-1) through (2-5), has been thoroughly investigated with several different effects incorporated. Direct comparisons are easily facilitated since identical parameter definitions are employed. Manipulation of the implicit ignition time equations (2-6) through (2-11) and plotting the quantity $(A\tau_c)$ versus $(1/A^{1/2})$, being equivalent to graphs of ignition time t_c versus applied heat flux q, produces curves whose slopes range from -1.52 for E= 20 kcal/mol to -2.0 for E= 60 kcal/mol. Experimental results exhibiting similar slopes can be fully explained by the solid phase ignition mechanism. However, a pressure effect built in via the surface cooling parameter Γ yields longer ignition times for increasing Γ's; a prediction contrary to experimental evidence. Hermance (1984) stated that convective transport in both solid and gas phases must be incorporated for complete description of the reactive solid ignition model as these effects tend to limit the thermal runaway and possibly alter the predicted pressure effect. Baer and Ryan's work (1968) in this regard included only solid surface regression and correctly predicted the low pressure ignition limit.

Recently, in a different fashion with major emphasis placed on gas phase heating and pressure conditions, Kumar and Kuo (1980) formulated a model describing the ignition of a propellant located at the tip of a crack under rapid pressurization conditions. In a detailed discussion they argued that ignition was attributed to 1) turbulent diffusion of hot igniter product gases into the crack and stagnation heating of propellant surface and 2) compression heating of

this gas and stagnation heating of the propellant surface by the hot gases at the crack tip. No chemical heat generation was included in the theoretical formulation. Numerically, ignition occured once the surface temperature exceeded 850 °K; experimentally, ignition was defined as the onset of luminous light emitted from the propellant surface. Figure 2.8 shows both experimental and theoretical ignition times versus pressurization rate. Its excellent agreement is somewhat skewed, as acknowledged by the authors, as the gas phase turbulent thermal conductivity was selected based on its close agreement with one measured ignition delay. The "ignition" surface temperature was based on the best available data.

At this point in time the idealized concept of a reactive solid has been frequently employed to determine several mechanistic effects on the ignition characteristics. Important qualitative and quantitative observations have been made. In those cases where the solid heating time is much longer than gas phase diffusion or chemical reaction times, solid phase ignition theory predictions may agree closely with experimental observations (Kulkarni, Kumar and Kuo, 1980). However, the major shortcoming of the solid phase ignition model is its inability to correctly predict the effect of atmospheric conditions if so present in experiments. Secondly, its concepts do not hold in cases where pressure plays a role in the ignition process. These major deficiencies have led to further developments in both the heterogeneous and gas phase ignition theories.

2.5.3 Heterogeneous Ignition Theory

The major premise of this theory is based on the heterogeneous reaction between gas phase supplied oxidizer and solid fuel, which forms the propellant surface. Physical models presented in the literature all possess some of the following characteristics: 1) semi-infinite one dimensional inert solid, 2) semi-infinite gas phase region, 3) uniform but not necessarily equal temperatures in each half domain at time zero and 4) an exothermic heterogeneous surface reaction between gas phase supplied oxidizer and solid fuel.

Three branches of this theory have developed depending on initial gas phase temperature and solid surface heating conditions. A low gas phase temperature with no applied surface heating constitutes a hypergolic model, a heterogeneous model includes external surface heating and finally, shock tube conditions are simulated by a high temperature gas phase. These three physically different circumstances are frequently discussed in a single work as a shift in parameter dominance usually alters the physical model description.

Price *et al.* (1966) listed the hypergolic ignition model of Anderson and Brown, which contains the basic structure of the heterogeneous ignition theory, and is detailed next:

solid phase energy:

$$\frac{\partial T_c}{\partial t} = \alpha_c \frac{\partial^2 T_c}{\partial x^2} \tag{2-12}$$

gas phase energy:

$$\frac{\partial T_g}{\partial t} = \alpha_g \frac{\partial^2 T_g}{\partial x^2} \tag{2-13}$$

oxidizer species diffusion:

$$\frac{\partial C_o}{\partial t} = D_o \frac{\partial^2 C_o}{\partial x^2} \tag{2-14}$$

product species diffusion:

$$\frac{\partial C_p}{\partial t} = D_p \frac{\partial^2 C_p}{\partial x^2} \tag{2-15}$$

Initial conditions are:

$$T_c(x,0)=T_i,\ T_g(x,0)=T_i,\ C_o(x,0)=C_{oi},\ C_p(x,0)=0 \tag{2-16}$$

Boundary conditions for this model are:

$$T_c(\infty,t)=T_i,\ T_g(-\infty,t)=T_i,\ C_o(-\infty,t)=C_{oi},\ C_p(-\infty,t)=0 \tag{2-17}$$

Interface conditions at x=0 are described as:

$$T_g = T_c = T_s \tag{2-18a}$$

$$D_p\left(\frac{\partial C_p}{\partial x}\right) = -\phi D_0\left(\frac{\partial C_o}{\partial x}\right) \tag{2-18b}$$

$$-D_0 Q_s \frac{\partial C_0}{\partial x} = -k_c \frac{\partial T_c}{\partial x} + k_g \frac{\partial T_g}{\partial x} + c_p(T-T_s)D_p \frac{\partial C_p}{\partial x} + c_o(T-T_s)D_o \frac{\partial C_o}{\partial x} \tag{2-18c}$$

$$-D_o \frac{\partial C_o}{\partial x} = C_o^a Z e^{-E/RT} \tag{2-18d}$$

Major assumptions consist of the representation of heat and mass diffusion by the concept of semi-infinite, one dimensional slabs, constant and temperature independent thermodynamic and physical properties, representation of the chemical reaction by an Arrhenius rate expression and equal binary diffusion coefficients.

Frequently employed ignition delay criteria in the theoretical efforts are based on a

rapid rise in surface temperature, attainment of a certain surface temperature or a "go no-go" type criterion. Initial investigations employed Laplace transform techniques to solve the above equations.

Williams (1966) considered radiative heating of an opaque propellant with equal initial temperatures for solid and gas phases. A single, exothermic surface reaction of order n was assumed for thermal runaway; ignition times reported for zero incident flux (hypergolic case) depended strongly on the activation energy, but rather weakly on reaction order and a parameter α based on solid and gas phase thermal properties. An empirical ignition time formula in dimensional quantities was reported for purely hypergolic ignition as:

$$t_{ign} = \left[(kc\rho)_2^{1/2} + (kc\rho)_1^{1/2}\right]^2 T_o^2 Y_o^{-2n} (QZ)^{-2} e^{2\beta - 11.5 + 100/\beta} \quad \text{where } \beta = E/RT_o \tag{2-19}$$

The effect of a hot, stagnant reactive gas adjacent to the solid surface was investigated by Waldman and Summerfield (1969). In a nearly identical formulation as Williams (1966), shock tube ignition was modeled and computed ignition times were compared to a gas phase based theory (Hermance, Shinnar and Summerfield, 1966). Figure 2.9 demonstrates numerical results for both theories applied to the shock tube situation. It was concluded that based on these results, both theories predicted a similar relation between ignition time and partial oxidizer pressure in the hot gas.

Further work into shock tube ignition conditions by Waldman (1970) produced similar results by employing a local similarity method. The resulting ignition time formula is expressed as:

$$\tau_{ign} = \frac{\pi^2}{4}\left[\frac{\theta^* \exp(-\beta\theta^*)/(1+\theta^*)}{(1-\alpha\theta^*)}\right]^2 \tag{2-20a}$$

where:

$$\theta^* = \frac{\beta - 2 + [(\beta-2)^2 - 4(1+\alpha\beta)]^{1/2}}{2(1+\alpha\beta)}, \quad \text{and} \quad \alpha = \left[(kc\rho)_1^{1/2} + (kc\rho)_2^{1/2}\right]\frac{T_o}{\rho_1 Y_o Q D_1^{1/2}} \tag{2-20b}$$

and:

$$\tau = \left[(kc\rho)_2^{1/2} + (kc\rho)_1^{1/2}\right]^{-2} \pi \left(\frac{QBY_o^n e^{-\beta}}{T_o}\right)^2 t \tag{2-20c}$$

with α being the ratio of thermal diffusion to chemical diffusion. Dimensionless ignition delay times (τ_c) depended very minimally on reaction order n, increased with larger α, and decreased about two orders of magnitude with β activation energy parameter.

An extensive numerical model was formulated for heterogeneous ignition of solid propellants by Bradley and Williams (1970) which included an exothermic surface reaction between solid fuel and gaseous oxidizer of order n and in-depth radiative absorption. The radiant and hypergolic branches of the heterogeneous ignition theory were incorporated by proper adjustment of system parameters. Effects of different ignition criteria on ignition time were investigated. Criteria under consideration were (i) constant ignition temperature (τ_θ), equality in chemical and external heating rates (τ_γ), time of occurence of important reactant consumption effect (τ_2) and a "go no-go" criterion (τ_1), based on attainment of a positive $d\theta/d\tau$ after flux removal. Important parameters, defined in the same fashion as before, included α, the ratio of thermal diffusion and oxidizer diffusion, β, the dimensionless activation energy and γ, the ratio of the external heating rate q to the initial chemical surface heating. In all results an infinite absorption coefficient was used.

For the radiant heating case ($\gamma > 0$), reasonable agreement was seen for all criteria except the constant ignition temperature criterion. Increasing α tended to increase ignition times by about 10% as temperatures in the reaction zone were depressed by enhanced heat conduction. However, for more hypergolic ignition (decreasing γ), growing disparities appeared between τ_γ and τ_1 ignition results when compared to the τ_2 and τ_θ cases. Clearly, for hypergolic ignition τ_θ and τ_2 remained the only criteria physically possible and showed reasonable agreement for realistic ignition for activation energies above 12 kcal/mole.

For radiant ignition, Bradley and Williams (1970) reported higher required surface temperatures at higher heating rates and dimensional ignition delays related to the applied flux as:

$$t_{ign} \propto q^{-b}, \quad \text{where } b = 2-(8.4/\beta) \tag{2-21}$$

Slopes of ignition time versus applied heating rate range from -1.16 to -1.83 for increasing activation energy. Secondly, ignition times were related to heat of reaction Q, rate factor Z and oxidizer mass fraction Y_o as $t_{ign} \propto (QZY_o^n)^{-8.4/\beta}$.

Pressure effects were embedded in parameters Z ($\propto p^n$), gas phase thermal responsivity Γ ($\propto p^{1/2}$) and α ($\propto \Gamma/T_o p^{1/2}$). At low pressures ignition times were decreasing with increasing pressures as a result of higher oxidizer concentrations near the surface. But at high pressure ignition times could possibly increase with pressure because of enhanced heat loss to the gas

phase through higher gas phase thermal responsivities.

A somewhat different, analytically based analysis using the reactive solid concept, was developed by Andersen in the early seventies (1970, 1972a, 1972b). Radiant heating was decoupled from the chemical reactivity in his approximate analysis of a surface ignition model. The total ignition time was composed of the sum of an inert heat-up time t_c, and the adiabatic reaction time t_r associated with the surface temperature T_c attained at time t_c. The general ignition time was then obtained by noting that the total ignition time possessed a minimum with respect to time. For an inert, opaque solid the surface temperature was expressed below along with the adiabatic exothermic reaction time t_r as:

$$T = T_o + \frac{2I_r(1-r)t^{1/2}}{(\pi\rho ck)^{1/2}}, \quad t_r = \frac{cRT^2}{ZQE}e^{E/RT} \tag{2-22}$$

Based on the noted minimum in ignition time with respect to time, from $[dt_c/dt + dt_r/dt]_{T_c}=0$, an implicit expression for the effective ignition temperature T_c was developed as:

$$T_c = \frac{(E/R)}{\ln\left[\dfrac{\pi\rho kZQE(T_c-T_o)}{2[(1-r)I_r]^2(E-2RT_c)}\right]} \tag{2-23}$$

Using this simple theory good comparison was obtained with experimental results at low incident flux levels. In addition, this analytical theory could be fitted to experimental results to extract the values for activation energy E and prefactor ZQ. The agreement obtained between kinetic parameters computed from surface ignition of an M-2 double-base propellant with the current simple model and those used in numerical solutions for more rigorous ignition equations proved to be quite good. Modifications to include in-depth radiative absorption effects were indicated.

The above formulated model was extended by Andersen (1972b) to account for the time needed to attain a state of self-sustained burning. The nonsteady burning time t_s was estimated from the ratio of the total heat stored in the solid during steady regression to the surface heating rate. It was reported that total time to steady burning depended both on t_{ig} and t_s, the first one being dominant at moderate to high pressures or low heating rates; the other controlling ignition times primarily at low pressures and high heating rates. This

observation indicates the importance of convective transport in ignition model formulations.

Asymptotic methods were also applied to the heterogeneous ignition theory. Liñán and Crespo (1972) considered simultaneously hypergolic, shock tube and radiant heating conditions of the ignition proposed by Bradley and Williams (1970). Identical parameters were employed. For large γ's, corresponding to radiant heating conditions, they developed the following relation which states the dependence of ignition time on other parameters:

$$e^{.431}\beta^{1/2}(\tau_c/\pi)^{1/4}\frac{1}{1+2\sqrt{(\tau_c/\pi)}}e^{2\beta\sqrt{(\tau_c/\pi)}/[1+2\sqrt{(\tau_c/\pi)}]} = 1 + \frac{qe^{\beta}}{QBY^n} \qquad (2\text{-}24)$$

For shock tube or hypergolic conditions (γ=0), ignition times were related to the thermal-chemical diffusion parameter α and activation energy parameter β as:

$$\tau_c = .864\beta^{-2}(1+2\alpha n/\beta) \quad \text{where } \alpha = (\Gamma_1+\Gamma_2)T_o/\rho_1 D^{1/2}QY_o \qquad (2\text{-}25)$$

This approximation provided an accurate correlation to numerical results presented by Bradley and Williams (1970) and Waldman (1970) for the hypergolic case.

Heterogeneous ignition in a hot stagnation point flow was considered by Niioka (1978). The formulation followed the previous development by Niioka and Williams (1977) except for the surface reaction between solid fuel and high temperature gas phase oxidizer and inclusion of subsurface radiative absorption. Ignition was defined in terms of a rapid surface temperature rise. Under quasi-steady gas phase conditions which involved a constant oxidant mass fraction and a constant heat transfer coefficient, the following correlation equation was obtained:

$$A = .65\frac{[(\theta_e-1)(1-g_c)+1]}{E^{1/2}}\left[\frac{1}{\sqrt{(\pi\tau_c)}}-\frac{g_c}{\theta_e-1}\right]^{1/2}\exp\left[\frac{E}{1-(\theta_e-1)(1-g_c)}\right] \qquad (2\text{-}26a)$$

where:

$$g_c = \exp[\tau_c/(\theta_e-1)^2]\mathrm{erfc}[\tau_c^{1/2}(\theta_e-1)^{-1}] \qquad (2\text{-}26b)$$

Figure 2.10 displays dimensionless ignition times versus the surface reaction rate parameter for different activation energies and flow temperature. In addition, they developed correlation formula for special limiting cases which compared well to those reported in previous studies.

Comparison with numerical integrations indicated a high degree of agreement.

Significant accomplishments of the heterogeneous ignition theory when compared to experimental observations consist of its ability to explain slope values of ignition time versus flux plots, as is clear from the works of Williams (1966), Waldman and Summerfield (1969), Bradley and Williams (1970) and Liñán and Crespo (1972), its ability to demonstrate the qualitative oxidizer mass fraction effect on ignition time (Bradley and Williams, 1970) and mechanistic explanation for the increased pressure sensitivity of ignition time at low pressures (Bradley and Williams, 1970). Shortcomings are enumerated by Hermance (1984) as the treatment of pure fuels instead of propellants, consideration of only the onset of exothermicity in the analyses instead of attainment of a steady combustion wave. Inclusion of convective transport appears necessary to reach this quasi-steady region. Finally, the heterogeneous theory does not contain a mechanism to predict ignition in inert gaseous environments.

2.5.4 Gas Phase Ignition Theory

Two major deficiencies reported for the solid phase ignition theory led to the development of the theory of gas phase ignition. Price *et al.* (1966) quoted these shortcomings as being the theoretical inability to predict observed dependence of ignition on gaseous composition ingredients and pressure as well as the observed lack of condensed phase exothermic reactions in many solid propellants.

The essence of the gas phase theory is that upon external heating the solid propellant surface decomposes, producing both fuel and oxidizer components which are transported away from the surface by diffusion and convection. In the gas phase these species participate in an exothermic reaction which is possibly influenced by gas phase pressure and the presence of other species. These chemical reactions are frequently limited by the degree of fuel and oxidizer mixing and the local temperature via an Arrhenius type reaction rate. Upon build-up of gas phase reactants and increased chemical reactivity, energy is fed back to the surface leading to a quite strong, quasi steady gasification of the solid surface. Eventually sufficient reactants are present in the gas phase at sufficiently high temperatures to cause a rapid rise in chemical reactivity, the occurence of locally flame like temperatures and a sharp rise in solid surface temperature. Sustained ignition results next.

The physical evolution of the above mentioned processes is relatively insensitive to the manner of thermal stimulus application, it being either by radiant heating (arc-image or laser) or a conductive type heat input (shock tube). Experimentally determined ignition times usually differ by at least an order of magnitude for these two heating modes. Since these experimental

cases present a significant difference in boundary condition at the solid/gas interface and initial gas phase temperature in the theoretical formulations, gas phase theory developments have proceeded seperately for shock tube and radiant heating cases.

2.5.4.1 Gas Phase Ignition: Shock Tube Case

A typical set of partial differential equations, frequently quoted in the literature, were formulated to describe mass and energy transfer in the reacting gaseous mixture with simultaneous exothermic reactions, and presented by Hermance and Kumar (1970). The species and energy diffusion equations were expressed in a density weighted coordinate system using the Howarth transformation defined as:

$$\psi = \int_0^z (\rho/\rho_g)dx \tag{2-27}$$

The species and energy diffusion equations were then formulated as follows:
Fuel:

$$\frac{\partial y_f}{\partial t} + (m/\rho_g)\frac{\partial y_f}{\partial \psi} - D\frac{\partial^2 y_f}{\partial \psi^2} = -\rho Z y_f y_{oz} e^{-E/RT} \tag{2-28}$$

Oxidizer:

$$\frac{\partial y_{oz}}{\partial t} + (m/\rho_g)\frac{\partial y_{oz}}{\partial \psi} - D\frac{\partial^2 y_{oz}}{\partial \psi^2} = -n\rho Z y_f y_{oz} e^{-E/RT} \tag{2-29}$$

Gas phase energy equation:

$$\frac{\partial T}{\partial t} - (m/\rho_g)\frac{\partial T}{\partial \psi} - D\frac{\partial^2 T}{\partial \psi^2} = (\rho Q Z/c_p) y_f y_{oz} e^{-E/RT} \tag{2-30}$$

Solid phase energy equation:

$$\frac{\partial T_s}{\partial t} + (m/\rho_s)\frac{\partial T_s}{\partial x} = \alpha_s \frac{\partial^2 T_s}{\partial x^2} \qquad x<0 \tag{2-31}$$

These equations were solved numerically with the following initial conditions:

$$y_f(\psi,0)=0,\ y_{oz}(\psi,0)=y_{oz}^{\infty},\ T(\psi,0)=T_o,\ T_s(x,0)=T_{so} \tag{2-32}$$

and the following boundary conditions:

$$my_f(0,t)-\rho_g D\frac{\partial y_f(0,t)}{\partial \psi}=\alpha m,\ my_{ox}(0,t)-\rho_g D\frac{\partial y_{ox}(0,t)}{\partial \psi}=(1-\alpha) \tag{2-33a}$$

$$T_s(0,t)=T(0,t),\quad \lambda_s\frac{\partial T_s}{\partial x}-mh_v=\rho_g D c_p\frac{\partial T}{\partial \psi} \tag{2-33b}$$

$$y_f(\infty,t)=0,\ y_{ox}(\infty,t)=y_{ox}^{\infty},\ T_s(-\infty,t)=T_{so},\ m=\rho_s B e^{-E_s/RT_s(t)} \tag{2-33c}$$

Primary assumptions were: 1) one-dimensional diffusion of heat and mass, 2) mass decomposition rate of the solid surface was expressed by an Arrhenius rate expression, 3) uniform gas-phase temperature and pressure initially, and 4) identical physical and chemical properties for external gas phase oxidizer and oxidizer produced from solid surface decomposition.

Prior to solving the above system of equations, simpler formulatione were proposed and solved numerically. Early modeling efforts decoupled gas and solid phase processes by prescribing a constant surface temperature and either a constant fuel concentration or constant fuel mass flux at the solid surface (Hermance, Shinnar and Summerfield, 1965). Ignition was defined in terms of the attainment of a selected temperature level exceeding the initial level. Selection of the ignition criterion affected results significantly. Curves of $\log(t_{ign})$ vs $\log(Y_{ox}^{\infty})$ exhibited a variable slope which became more apparent at high initial gas temperatures.

A follow-up study by Hermance, Shinnar and Summerfield (1966) investigated the effects of heat feedback to the solid surface with the fuel gasification rate strongly dependent on the surface temperature. The main result indicated that non volatile fuels were ignitable through rapid feedback of energy to the surface compared to their previous work (1965). Ignition delays showed strong dependence on pressure and oxidizer mole fraction.

A subsequent study achieved coupling between gas and solid phases through an energy balance at the interface with the fuel concentration at the surface being related via a Clausius-Clapeyron equation to its temperature (Chang and Schultz-Grunow, 1970). Approximate analytical solutions were derived for gas temperature, fuel and oxidizer concentration, and temperature and fuel concentration at the surface. The solution methodology was based on the method of successive substitutions where one iterates on a set of constants until a predetermined accuracy is achieved (Hildebrand, 1956). Ignition was achieved if somewhere in the gas phase a balance existed between heat loss due to diffusion and heat generation due to chemical reaction.

It was found that ignition times at specific gas phase temperature decreased with

pressure, and decreased as well for higher gas phase temperatures. In addition, the physical location of the ignition site in the gas phase was determined, ranging from 0.1 mm to 1.25 mm. Experimental verification was done using an organic fuel ($n-C_{16}H_{34}$) in a gas-driven shock tube. Theoretically predicted ignition times agreed reasonably well with experimental results as displayed in Figure 2.11 with ignition times plotted against initial gas temperature. Experimental results included samples having nonplanar geometries which exhibited more rapid ignition according to the degree of convexity of the sample surface to the incident hot gas.

Returning to the gas phase ignition theory expressed by Eqs. (2-27) through (2-33c), Hermance and Kumar (1970) noted that the endothermic value of the heat of pyrolysis of the solid phase has very little effect on the subsequent ignition behavior. This current formulation incorporated transient convective transport in solid and gas-phases, variable gas phase density, endothermic solid surface gasification, and coupling of gas and solid phase energy equations across the solid/gas interface. As a result, this model was able to describe the ignition process from the initial solid phase heating all the way to the attainment of quasi steady-state conditions in the solid and gas phases.

The authors somewhat arbitrarily defined two distinct ignition criteria. The first was termed a "short time" criterion as it was based on the first occurence of a 50 % rise in maximum local gas phase temperature. The second criterion was called the "near steady-state" criterion as it pertained to a state of ignitedness approaching steady state conditions in terms of gas phase species and temperature distributions. It was observed that for a wide range in compositions of the mass flux originating from the surface decomposition, for both neutral and oxidizer containing environments, and for a wide range in gas phase reaction stoichiometry, the first criterion was reached an order of magnitude earlier in time than the steady burning conditions, which corresponded closely to the second criterion.

Under conditions of high fuel mass flux, high oxidizer reaction stoichiometry and an oxidizing gas phase, a secondary reaction zone was reported to exist which was caused by the reaction of fuel vapor unconsumed in the primary reaction zone and oxidizer present in the external gas phase. The existence of this secondary reaction zone drastically changed the dependence of ignition delay on ambient oxidizer concentration and a reference pyrolysis mass flux m_o when compared to results using the "short time" criterion. It was shown that ignition delay dependence changed from $m_o^{-2/3}$ to no dependence, and its dependence on initial gas phase oxidizer mole fraction y_{ox}^{∞} from $(y_{ox}^{\infty})^{-2/3}$ to $(y_{ox}^{\infty})^{-2}$ upon changing the definition of ignition from the first to the second criterion. In addition, ignition times for pure fuels were larger than for propellants when using the same "near steady-state" ignition criterion. This observation was in

excellent agreement with fuel and propellant shock tube ignition data (McAlevy, Cowan and Summerfield, (1960). It was therefore concluded that the present gas phase ignition theory predicted results obtained in shock tube experiments well.

In a subsequent paper Kumar and Hermance (1971) developed a new theoretical ignition criterion for gas phase ignition of homogeneous solid propellants under shock tube conditions. The major impetus was to investigate whether theoretical predictions using a particular ignition definition have any correspondence to experimentally obtained results and to develop an criterion which related observed light emission from experimental work to the transient gas-phase distributions of species and temperature. This new definition was based on the thermal emission of CN molecules as its strong spectral line at 3590 A is frequently employed for experimental ignition detection. Equations (2-27) through (2-33) were expanded to include diffusion of reaction products. Ignition was defined in terms of the time required for the theoretical photo detector signal to reach a specific level.

Results indicated a significant level of agreement between theoretical and experimental results in terms of temporal light emission behavior and ignition delay dependence on initial oxidizer mole fraction y_{ox}^{∞}. It was noted that experimental results should include a statement about the sensitivity of the detection device and careful definition of the ignition criterion. Usage of two sensitivities for the recording device was advocated where the highly sensitive output corresponded to the previously defined "short time" definition, and the low sensitivity output would correspond to the "near steady state" criterion, indicative of intense light emission. Finally, it was reported that the secondary reaction zone was the major contributor to the detected light intensity.

Shock tube ignition of composite or heterogeneous propellants was modeled by Kumar and Hermance (1972) where a cylindrical oxidizer particle was surrounded by a fuel ring. Axial and radial diffusion and conduction were included as well as possible different decomposition rates for fuel and oxidizer. Ignition criteria were either a 50 % rise in maximum gas phase temperature or the previous developed theoretical light emission criterion (Kumar and Hermance, 1971). Results displayed excellent agreement with respect to oxidizer mole fraction and total gas phase pressure compared to experimental work. (See Figure 2.12). They concluded that ignition of composite propellants under shock tube conditions is controlled by gas phase chemical reactions.

Based on the degree of agreement between experiment and theoretical work when considering ignition of solid propellants by conduction from a hot gas, as occuring in shock tube experiments, Hermance (1984) stated that both double-base and composite propellants ignite via a gas phase controlled mechanism. Experimental results discussed later will provide

evidence of this statement. Theoretical results predicted similar trends with respect to environmental factors such as pressure and gaseous oxidizer mole fraction as observed in shock tube ignition experiments. It should be noted however, that the degree of match between theory and experiment depends heavily on the similarity in employed ignition delay criterion. Emphasis must be placed on the use of a "strong" ignition criterion for experimental and theoretical work to achieve the best match in results.

2.5.4.2 Gas Phase Ignition: Radiant Case

A second branch of gas phase ignition theory evolved to gain understanding involving processes presumed active during arc-image experiments. Contrary to shock tube modeling, where a hot gas is adjacent to the solid surface, in radiant heating a cold gaseous environment is in contact with the solid surface. The fundamental difference entails the manner of solid phase heating and possible heat loss from the surface to the gaseous zone. All this leads to the introduction of a thermal induction time for heating of the solid phase prior to vigorous gas phase chemical reactions.

The implications are mathematically conceptionalized by a basic change in initial and boundary conditions of the general formulation expressed by Eqs. (2-27) through (2-33). Primary changes involve: 1) identical initial uniform temperatures for both gas and solid phases, and 2) inclusion of an applied energy flux term in the heat balance equation at the solid/gas interface.

Two physical models were proposed by Ohlemiller and Summerfield (1968) in which major emphasis was placed on the effects of incident radiation. Model formulations involved either a purely gas phase or a purely heterogeneous ignition mechanism based on the possible site for the exothermic reaction. The proposed gas phase model is described first.

The theoretical description of radiative interaction with solid propellant material involved processes as in-depth absorption due to non-opacity of the propellant, in-depth pyrolysis of the polymer and photochemical reaction having wavelength dependency. Fuel vaporization was caused by both thermal degradation or gasification and photochemical degradation. Gas phase equations included fuel, oxidizer and energy diffusion augmented with a convective term, as well as the second order exothermic reaction responsible for ignition.

The proposed heterogeneous model envisioned ignition caused by the reaction between gas phase oxidizer and surface polymer molecules. Mathematically, the polymer vaporization and convective transport were ignored and the exothermic reaction was incorporated in the solid/gas interface energy equation. Although the postulated models were not solved in their

entirety, approximate theoretical solutions were reported based on certain physical conditions. Ignition was approximated as the sum of a chemical diffusion, a radiative absorption and a conduction characteristic time scale.

$$t_{ign} = t_{chem-diff} + \frac{1}{\alpha}\left[\frac{\rho c \Delta T^*}{I_o(1-r)}\right] + \frac{\pi}{4}k\left[\frac{\rho c \Delta T^*}{I_o(1-r)}\right]^2 \qquad (2\text{-}34)$$

By judicious selection of propellant property values and applicable operating conditions, a reasonable degree of agreement was reported between their theory and experiments conducted by Beyer and Fishman (1960) using an arc-image furnace.

Shannon and Deverall (1969) considered radiative ignition of a propellant in a neutral environment which included independent decomposition rates for liberation of fuel and oxidizer species, a heterogeneous surface reaction and a single second-order gas phase reaction. Ignition was defined by the attainment of an equality between gas-phase chemical heat generation and conductive heat loss to the solid surface.

Numerical calculations showed reasonable agreement of ignition time versus pressure with tests at low flux levels, but only qualitative similarities at high heating rates. Figure 2.13 illustrates their observed results. The greater disparity at high fluxes was attributed in part to the choosen ignition criterion. They pointed out that a reversal of the gas-phase temperature gradient, attainment of a specific temperature, a specific temperature rise, or the onset of vigorous chemical reaction did not necessarily constitute sufficient conditions to model experimental "go no-go" situations. Upon removal of the external stimulus the surface temperature was observed to decrease due to steep thermal gradients in the solid-phase existing under high flux conditions which led to a decrease in mass flux and eventually led to extinction despite the generation of an incipient flame at the time of flux cessation.

Radiative ignition of a solid fuel in an oxidizing environment with in depth radiative absorption in the solid phase was modeled by Kashiwagi (1974). Model details included surface pyrolysis of the fuel, its rate being governed by a zeroeth order Arrhenius reaction, fuel vapor and oxidizer diffusion, and a second order exothermic gas phase reaction. Attainment of ignition was specified in terms of runaway condition occuring in the gas phase.

Major conclusions based on these numerical simulations were: 1) radiative ignition times were not influenced by the thermicity of the fuel pyrolysis, 2) in-depth radiative absorption of incident radiation significantly delayed ignition times, 3) gas phase reactions must be included in radiative ignition of solid fuel and became the rate controlling factor in marginal ignition

cases and 4) ignition times and initial oxygen mole fraction increase with decreasing molecular weight of the diluent gas because of higher thermal conductivity and diffusivity of the ligher molecules.

Two observations can be made in terms of experimentally measurable effects. First, two effects are displayed in Figure 2.14, a plot of ignition time versus applied flux with a -1.9 slope value, which are operative in different incident flux regimes responsible for the change in slope at an intermediate flux level. At low absorption values and small heating rates the onset of ignition was delayed because of reduced surface heating. At high rates of heating a low absorption value led to reduced heat losses to the interior which tended to speed up ignition. Secondly, ignition times were weakly dependent on oxidizer mole fraction except at small Y_{ox} where ignitability limits increased rapidly. Finally, ignitability boundaries were identified for different sets of pyrolysis and gas phase activation energies whose values however, exceeded those commonly used in solid propellant modeling.

A similar model, except for treating a homogeneous propellant instead of a pure fuel, was considered by Kumar and Hermance (1976) with the additional feature of oxidizer generation originating from the propellant surface. Ignition was defined in terms of reaching a 50 % increase in maximum gas phase temperature; testing of other criteria led to nearly identical ignition times.

Ignition times showed a decreasing dependence on applied flux level for higher rates of heating. On a log-log plot the slope of t_{ign} vs q was approximately -1.7 for a 100 % oxygen environment. Pressure effects on ignition time were reported as being important only at sub- to atmospheric pressure levels. It was stated that, in so far as radiative ignition was considered at moderate fluxes and moderate to high pressures, the gas phase chemical diffusion time was a few orders of magnitude smaller than the solid heat-up time. Only at very low pressures the chemical-diffusion time scale became of comparable magnitude as the solid heat-up time, making the ignition time strongly dependent on gas phase chemical kinetics. Hence at low to moderate incident flux levels gas phase reactions can effectively be neglected in the ignition analysis.

Asymptotic methods were also applied to radiant ignition formulations based on exothermic runaway conditions in the gas phase. Kindelán and Williams (1975a, 1975b, 1977) considered endothermic gasification of a solid along with an exothermic gas phase reaction; in their last paper consideration was also given to in-depth absorption of radiation.

In their first paper Kindelán and Williams (1975a) placed major emphasis on differences in ignition behavior for surface pyrolysis versus distributed solid phase pyrolysis. Three different stages were identified during radiant heating of the material. After an inert heating

period a short transition stage occured in which endothermic reaction and surface regression started along with a leveling of the surface temperature. This transition stage was followed by transport-controlled gasification which tended to reach a quasi-steady state of regression. Due to the absence of a runaway condition, characteristic of an exothermic reaction, ignition times were formulated for the current endothermic gasification reaction based on the onset of gasification (τ_1) or based on the maximum surface temperature in the transition zone (τ_2). Correlation formula were developed for the τ_1 criterion. For the case of the endothermic surface reaction they obtained:

$$B = \frac{e^{[E/(1+2\sqrt{\tau_1/\pi})]}}{(1+2\alpha\sqrt{\tau_1/\pi})} \quad \text{where} \quad B = Z\rho L/q\,, \quad \alpha = cT_o/L \quad \text{and} \quad \tau = \frac{q^2 t}{k\rho c T_o^2 [1+\Gamma]^2} \qquad (2\text{-}35)$$

and for the distributed gasification reaction:

$$A = \frac{E(1/2+2\alpha\sqrt{\tau_1/\pi})\, e^{[E/(1+2\sqrt{\tau_1/\pi})]}}{(1+2\sqrt{\tau_1/\pi})^2(1+2\alpha\sqrt{\tau_1/\pi})^2} \quad \text{where} \quad A = \frac{\rho Z L k T_o}{q^2} \qquad (2\text{-}36)$$

The format of the above relations is quite similar to those presented for solid and heterogeneous ignition theories. Figures 2.15a and 2.15b display the dependence of ignition times on parameters A and E which shows remarkable agreement with thermal runaway conditions for a reactive solid undergoing exothermic decomposition.

An exothermic gas phase reaction was added to the endothermically gasifying surface by Kindelán and Williams (1975b). Features in this analysis included endothermic surface gasification, small values for Γ, the ratio of gas to solid responsivities, and the incorporation of oxidizer emanating from the solid. Without going into the complicated details, they observed that, depending upon chemical parameters, ignition could start at the onset of gasification or at some point during the transport-controlled endothermic gasification. For the first case, reported ignition times were quite similar to solid phase results because of the short chemical diffusional time scale in the gas phase. For the extended gasification case, a mixing layer developed which diffused away from the surface and ignition occured somewhere within this layer. Several plots were included that show ignition times as a function of dimensionless heat flux, parametric with different gas to gasification activation energy and frequency factor ratios.

To extend asymptotic analysis to even more realistic radiant ignition cases, Kindelán

and Williams (1977) incorporated both in-depth solid phase radiative absorption and considered ignition initiated at or slightly after onset of gasification. Other features were maintained as in their previous work. Since the development of the mixing layer and resulting ignition occured later in the transport-controlled stage, it was reported that these gas phase phenomena were not significantly affected by the solid phase absorptivity. Attention was therefore restricted to the inert and transition stages.

Graphically shown results displayed ignition time as a function of the parameter B' ($=\rho\nu L/q$) for the surface absorption case parametric with a gas phase to gasification rate parameter A" for selected pyrolysis and gas phase activation energies. These figures indicated faster ignition for the transition stage than the transport-controlled stage for different sets of activation energies. Comparison with numerical work from Kashiwagi (1974) showed poor agreement at low fluxes and better agreement at higher fluxes. Reasons for this great disparity were attributed to the stronger ignition criterion used by Kashiwagi (1974) and approximations made in the asymptotics especially in the low flux range. They noted, similarly to numerical work, that ignition times were strongly affected by solid absorption if ignition took place in the transition zone, but not so if ignition occured later. Secondly, the surface temperature and gasification rate were independent of the solid absorptivity under steady gasification rates.

More recently, radiant ignition theories have been developed which in some fashion attempt to account for the heterogeneous nature of composite propellants. The first such study by Kumar and Hermance (1972) considered ignition in a shock tube and obtained reasonable agreement with experiments. Propellant heterogenuity effects have also been applied to radiant ignition studies by Kumar (1983, 1985) and by Kumar *et al.* (1984) where in the latter case propellant samples were located in a stagnation region and subjected to rapid pressure loading conditions.

The paper by Kumar *et al.* (1984) included realistic and detailed gas phase chemical kinetics based on a realistic AP composite propellant. Excellent agreement with experiments was demonstrated where the overall ignition sequence consisted of an inert heating period, rising surface temperature and pyrolysis rates which eventually led to intense gas phase reactions provided gas phase temperature, fuel and oxidizer species concentrations were sufficiently high.

Kumar (1983) investigated the effect of surface heterogenuity for strictly gas phase ignition and gas and surface reactions for composite propellants. In the second paper Kumar (1985) noted that inclusion of surface reactions did not exhibit noticeable effects on delay times. For large oxidizer particles surface reaction did not appear to control the ignition.

With respect to radiative ignition of solid propellants, gas phase theory is capable of predicting many experimentally observed trends. Thorough investigations into the response of

pure solids subject to radiative heating were done, supplemented with asymptotic analyses. Treatment of commonly used composite propellants was undertaken most recently with careful consideration of their heterogeneous nature. Results indicated respectable agreement with experimental data provided a strong ignition criterion was selected. In general, at low and moderate flux levels the major portion of the ignition time is formed by inert heating of the solid, with chemical diffusion time in the gas phase shortened at increasing pressures. The notion of two dimensional species and energy transport effects in the gas phase for composite propelllants was clearly apparent although the solid surface itself was planar.

Significantly altered ignition behavior may be anticipated when the propellant surface is not planar but rather convex to the applied flux causing more rapid inert heating. The purpose of this thesis is to quantitatively investigate the effect of convexity of the propellant surface towards the applied heating for the simplest of physical models: the reactive solid. Based on these results further extrapolations to more complex propellant ignition models may be made based on extensive one dimensional studies.

2.6 Experimental Investigations

2.6.1 Introduction

The first objective of experimental ignition studies is to determine the time lag or ignition delay from initial application of the stimulus to attainment of a steady combustion wave as a function of pertinent parameters. Major experimental factors include applied heat flux, pressure, chemical composition of the adjacent gas phase and initial gas phase temperature. The definition of the "proper" ignition criterion forms in itself a non-obvious task.

A more basic objective consists of determining the relative contributions of condensed, surface and gas-phase reactions to the overall ignition event. It should also be noted that, in order to simulate practical rocket conditions, experimental ignition times of the order of a few milliseconds to tens of milliseconds are required. Necessary flux levels must be of the order of 100 cal/cm^2-sec, obtainable by either convective, conductive or radiative heating.

In the following sections pertinent experimental literature is reviewed with major emphasis being placed on the delineation of the functional dependencies of experimental parameters on the observed ignition time. Secondly, these results are compared to theoretical studies to pinpoint mechanisms responsible in the ignition attainment. Different experimental techniques are illuminated in terms of their manner of data acquisition and type of data obtained.

2.6.2 Shock Tube Studies

Conductive heating apparatus was developed in the late fifties by McAlevy, Cowan and Summerfield (1960) where propellant samples were mounted in the end-wall of a shock tube and exposed to the stagnant high temperature gas of the reflected shock. The major disadvantage of this method is the coupling between pressure and temperature of the shocked gas. Principal factors for investigation were the effect of total pressure and the oxidizer mole fraction in the hot gas. Ignition times were proportional to $Y_{ox}^{-1.5}$ and $p^{-1.77}$ for an AP composite propellant.

Three different double-base propellants were tested by McAlevy and Summerfield (1962) in a shock tube apparatus. Ignition times showed a strong dependence on oxygen mole fraction ($\propto Y_{ox}^{-1.7}$ to $Y_{ox}^{-3.7}$) and pressure ($\propto p^{-1.5}$ to $p^{-3.0}$) at constant gas composition. They reasoned that double-base propellants ignited via a gas phase mechanism with gaseous oxygen playing a fundamental role. Fuel molecules and oxides of nitrogen driven off the surface diffused into the hot test gas where they reacted with each other and with the test gas oxygen. It was noted that the test gas oxygen was much more reactive than the nitrogen oxides in the ignition process because of its higher temperature.

Kashiwagi *et al.* (1973) conducted an experimental program to investigate the following aspects: 1) the location of initial exothermic reaction, 2) dependence of ignition delay on partial pressure of oxidizer, 3) role of embedded oxidizer, and 4) effect of binder characteristics on ignition delay.

Testing of four polymers indicated that the ignition delay depended seperately on the oxygen mole fraction and total pressure, not simply on the partial oxygen pressure. At a fixed partial pressure of oxygen, delay times decreased with increasing pressures explained by higher surface temperatures and higher surface vaporization rates. The effect of embedded AP oxidizer was determined using a 30% PBAA, 70 % 5 μm AP propellant as shown in Figure 2.16. This effect was quite small when ambient oxidizer was present in sufficient quantities. For fixed ambient oxidizer mole fraction, the embedded AP had no effect over the entire pressure range. At fixed total pressure and low oxygen levels embedded AP played an important role in shortening ignition times caused by enhanced heating due to the higher pressure level. Figure 2.17 illustrates binder characteristics effects for two propellant systems. More rapid ignition for the PU- than the PBAA-AP propellant was explained in terms of the lower activation energy for pyrolysis of PU. They concluded that two different slope values on a log-log plot of ignition delay versus oxygen mole fraction existed, the change in slope caused by the onset of the AP effect at lowered oxygen fraction where ambient oxygen is replaced by $HClO_4$ as

controlling ignition. They based this conclusion on the two-stage character of premixed CH_4-$HClO_4$-O_2 flames as observed by Pearson (1968).

Finally, Kashiwagi *et al.* (1973) noted that no conclusive statement concerning the location of initial exothermicity could be made as both gas phase and heterogeneous theories yielded reasonable agreement with experiment. Again, differences between theoretical and experimental definition of ignition delay and incomplete knowledge of physico-chemical parameters made it impossible to determine the controlling ignition mechanism in conductive shock tube experiments.

2.6.3 Arc-Image Experiments

The arc-image system has frequently been used in ignition experiments as it enables the experimenter to select heat flux levels independent of all other environmental parameters. Typical systems employ a double elliptical mirror system with a shuttering mechanism at the secondary focus. A high intensity radiation source such as a carbon arc or high pressure xenon arc lamp located at the focus of one ellipsoid is imaged on the propellant sample positioned at the major focus of the other ellipsoid. Ignition times are determined on a "go no-go" basis where samples are exposed to successively longer pulses until first emission of visible light is observed by an photodiode or photomultiplier tube. Environmental conditions such as pressure and chemical composition of the gas phase are easily varied by enclosing the sample in a small chamber.

It should be noted that physical conditions in these experiments are drastically different from shock tube work, since in the present case the propellant is surrounded by a "cold" gas. As a result, typical ignition times are a few orders of magnitude greater than those reported for shock tube experiments.

Early work by Beyer and Fishman (1960) tested propellant samples over a pressure range from .065 to 35 atm and flux levels from 5 to 75 cal/cm^2-sec. They observed: 1) minimal effect of pressure for pressures exceeding about 4 atm., 2) existence of a lower pressure limit of .06 atm below which combustion is not self-sustaining and, 3) definite effect of gas phase composition on the ignition delay. In addition, they frequently observed a measurable time period between flux removal and visible ignition.

Rosser, Fishman and Wise (1966) reported on the ignitability of chemically simplified AP based propellants in He, Ar and N_2 atmospheres over a range of pressures and applied

heating rates. Results were all obtained using a "go no-go" criterion where no measurement was made of the elapsed time between flux removal and first appearance of a visible flame. Minimum required exposure times were established with a 5% precision.

They observed a strong effect of the inert gas composition and hence the thermal and thermodynamic properties important in solid-gas phase heat loss on the ignition time for propellant formulations using ammonium perchlorate (AP), $CuCr_2O_4$ (copper chromite or CC), carbon (C) and polyethylene (PE). In all investigations they observed the same ordering in delay times namely $\tau(Ar) < \tau(N_2) < \tau(He)$ which signified definite gas phase influences on ignition. Plots of ignition time versus heat flux exhibited slopes of -1.5 to -1.6 in 20 to 40 atm N_2 and Ar environments. Pressure proved to have a major effect on ignition times at low levels but only a minimal influence was observed at levels above $\simeq$ 5 to 10 atm.

Addition of organic fuel in the form of polyethylene in either 4%, 8% or 12 % by weight proportions to the AP/CC mixture proved to affect ignition times as displayed in Figure 2.18. The rapid rise in τ for $P_{N_2} < 15$ atm was thought to be associated with approaching the flammability limit of 4% PE, a high PE content (12%) clearly led to faster ignition. Based on supplemental experiments on AP/CC/C wafers heated by aluminum blocks they argued that ignition resulted from a runaway gas phase reaction within the pores of the sample. It was noted that the heat release associated with the formation of these gaseous reactants from the solid decomposition was unimportant based on these thermal history tests. Based on kinetic studies they found that AP decomposed by catalytic action of copper chromite into NH_4 and ClO_4 radicals. They concluded that extensive solid phase decomposition did not preceed ignition, which was dominated by gas phase reactions.

In a subsequent study on a model propellant composed of 14% PBAN, 85% AP and 1% C, Fishman (1967) reported that test results were well fit by a line of slope -2 on a log-log plot of ignition time versus heat flux up to a certain flux level. Such a relation is in accord with inert heating to a constant surface temperature according to Carslaw and Jaeger (1959). Higher fluxes showed a pressure dependence, leading to a more positive slope. Pre-ignition surface exotherms were identified by embedding thermocouples in the propellant surface. No exotherms were observed in the low heating, pressure independent regime; but in the pressure dependent regime significant exothermic reactivity was noted. He concluded that: 1) significant solid phase exothermicity occured during ignition in the pressure-dependent regime, and 2) the thermal ignition model was valid in the pressure independent regime where exothermic reactions prior to runaway were unimportant.

A relatively simple ignition theory was tested experimentally with an arc-image method

by Wise, Inami and McCulley (1967) where experimental chemical heat release data was incorporated in a solid phase ignition model which accounted for the endothermic crystal phase transition of AP as a convective transport term. Reasonable agreement was obtained for a flux range of 20 to 110 cal/cm^2-sec. Theoretical delay times were based on surface temperatures exceeding inert levels by 10 percent. Based on this agreement they noted that unless gas phase mixing and diffusion becomes rate limiting, the solid exothermic reaction will provide the trigger for ignition, especially at increasing total gas pressure.

An extensive arc-image investigation was published by Shannon (1970) while studying the ignition characteristics of AP composite propellants in a N_2 environment. Binder ingredients employed were PBAN, PU, CTPB, PIB and PEP. Ignition times were obtained under "go no-go" conditions for flux levels from 10-100 cal/cm^2-sec and over a .1 to 4.0 atm pressure range. Figure 2.19 shows the flux dependence on ignition time for an AP/PBAN propellant for different pressures. The experimental results follow the -2 slope curve, characteristic of thermal ignition behavior, only at higher pressures and low flux levels. Ignition characteristics showed no drastic changes with addition of burning rate catalysts, AP particle size and size distribution, modest increase in ignition time with a decreased oxidizer loading, and more rapid ignition by adding carbon which acts as an opacifier.

Polymer effects were reported for a 83.5% AP, .25% iron oxide and .2% carbon mix. The lower pressure limit for ignition is primarily influenced by the binder component. The hypothesis of subsurface interfacial reactions was tested by coating either oxidizer or binder with Kel-F, a well-known flame retardant for gaseous hydrocarbon flames. Since similar results were obtained irrespective of the coated component, they argued that interfacial, hypergolic type reactions were not important during radiant ignition of composite propellant.

In conclusion Shannon (1970) noted that over the investigated range of pressure and heat flux the chemistry leading to ignition involved coupling of exo/endothermic condensed-phase reactions and a significant gas phase reaction required for thermal runaway. A critical gas phase reaction rate threshold, defined as:

$$R_{zn} = (C_{oxidizer} C_{fuel})_{critical} Ze^{-E/RT} \qquad (2\text{-}37)$$

would be specified by binder and oxidizer decomposition rates, local gas temperature and local fuel and oxidizer concentrations.

Review of the arc-image ignition data and comparing it to theoretical work reveals interesting features which are further discussed in the section on CO_2 laser ignition. Most

propellants ignite predominantly with a gas phase mechanism, but their ignition behavior can be estimated to a reasonable degree by the reactive solid model concept. Its applicability depends primarily on operational conditions such as pressure and applied heat flux. In the case of above atmospheric pressure and low to moderate flux levels, the ignition time is determined mainly by the heat-up characteristics of the solid; only at low to sub-atmospheric pressures becomes the gas phase chemical diffusive time scale of similar magnitude as the inert heat-up time. Extensive work in both regimes have been reported using CO_2 laser ignition experiments.

2.6.4 Laser Ignition Experiments

In more recent years the arc-image furnace has been replaced by the CO_2 laser which provides radiative energy at 10.6 μm. Reasons for this change include the usage of a single wavelength for heating, easier operational control of the heat source and the virtual elimination of interference with visible radiation detectors compared to the arc-image apparatus.

Pure fuels were ignited by Ohlemiller and Summerfield (1971) using a CO_2 laser in N_2/O_2 mixtures of 1 to 20 atm pressure. Reasonable agreement with an ignition delay time formula, consisting of characteristic conduction, in-depth absorption and reaction/diffusion time scales proposed earlier by Ohlemiller and Summerfield (1968), were obtained provided pressure and oxygen concentration were not near the gas phase diffusion limitation. Secondly, in-depth radiative absorption had a very strong effect on ignition times.

The influence of the radiation source on the ignition behavior of several propellant formulations was investigated by DeLuca *et al.* (1976a, 1976b) using an arc-image furnace and laser stimulus. Incident fluxes ranged from 5 to 100 cal/cm^2-sec in a 5 to 21 atm N_2 environment. They observed similar ignition behavior for both double-base and composite propellants irrespective of the radiation source after the optical characteristics associated with each apparatus, such as reflection and radiative penetration, were properly taken into account.

The major difference based on the source of radiation involved fast deradiative extinction observed only for the laser apparatus for noncatalyzed double-base propellants. This phenomenon physically refers to a rapid transition to extinction of all chemical reactivity from steady combustion at and near the propellant surface as a result of rapid removal of the ignition stimulus. Explanations for this behavior were the higher opacity of these propellants at the 10.6 μm wavelength, shorter flux termination times for the laser apparatus and the more

stabilizing effect of lateral flame spread for the arc-image furnace (Ohlemiller *et al.*, 1973). Practical means for dynamic extinction are enumerated by DeLuca (1984) as rapid depressurization, fast deradiation, injection of flame inhibitors and contact with highly conductive heat sinks.

The noted differences between the arc-image and laser apparatus pertained to: 1) the nature of the nonuniformity of incident flux, 2) radiation sources emitting in different spectral regions, and 3) in general different but nonzero reflectivities and noninfinite extinction coefficients for most propellant formulations for both set-ups.

DeLuca *et al.* (1976a) established ignition maps for different propellant formulations using an IR detector, high-speed shadowgraph and color movies. The initial output of the IR detector nearly coincided with first gas phase reactivity; a fixed large signal was noted as signifying substantial gas phase flame development. Figure 2.20 shows a general ignition map for an arbitrary propellant.

The L_{1a} boundary signified the onset of gas evolution as a result of abruptly started solid phase reactions; this limit was observed to be independent of pressure. Thermal ignition theory provided the best explanation for the location and behavior of this initial boundary. The L_{1b} limit was defined by the first rise in IR signal indicative of onset of gas phase flame development. The next boundary, L_{1c}, indicated substantial gas phase flame development as recorded from the fixed, large output from the IR detector. These latter two boundaries were somewhat arbitrary as they depended on the sensitivity of the IR detector. However, these limits served to mark the rate of flame development and its dependence on ignition parameters. Only by crossing the L_{1d} boundary sustained ignition was achieved as determined by "go no-go" testing. Further radiation led for some propellants to the dynamic extinction boundary L_2 where rapid termination of the radiation induced extinguishment.

In their first paper DeLuca *et al.* (1976a) concluded that ignition delays were affected by chemical and optical factors in the propellant formulation where the latter affected the degree and manner in which the radiative energy was harnassed. The following observations were made:

1) At pressures above 21 atm the L_{1a} and L_{1d} boundaries coincided which limited the contributing factors for the ignition boundary to an interplay between surface reflection, the in-depth extinction coefficient and propellant reactivity.

2) Addition of carbon black (opacifier) changed the optical properties drastically, resulted in faster ignition and a more negative slope of the L_1 boundary. Lower pressures led to longer flame development times at high flux levels for double-base propellants; a suggested mechanism

was proposed by Price *et al.* (1964) where a weakened solid phase heat release, caused by excessive radiative degradation of the solid, produced a radiation attenuating layer of solid phase products such that longer heating was required for sustained ignition. Similar qualitative observations were made by Baer and Ryan (1968) with a simple, solid phase numerical model which included surface regression.

3) Figure 2.21 shows ignitability for double-base, AP and HMX composite propellants obtained from arc-image experiments. Although surface reflection was accounted for here, different extinction coefficients were thought to influence ignition behavior in unknown ways. Ignitability increased from HMX, AP composite, double-base (uncatalysed) and double-base (catalysed). The AP decomposition gave substantial heat release close to the surface in an AP premixed flame, followed by further heat release in a diffusion flame. This coupling of chemical heat release back to the surface exhibits a pressure dependence at lower ambient pressures (Beyer and Fishman, 1960; Shannon, 1970). Addition of oxamine (coolant) to HMX further delayed ignition because of its endothermic decomposition.

In the companion paper DeLuca *et al.* (1976b) investigated the pressure dependent, pre-ignition events in double-base propellants. It was observed that the onset of exothermicity (L_{1b}) nearly coincided with the start of gasification (L_{1a}), being somewhat longer at lower flux levels. This was followed by a relatively long, flux dependent period of radiation-assisted solid phase gasification before attainment of self-sustained ignition. Explanations specifying what condition must be reached to sustain ignition were found inadequate. Further work was needed concerning radiation attenuation and possible three-dimensional effects on the ignition process.

The separation of L_{1a} from L_{1d} increased with decreasing pressure and was observed for catalyzed DB and HMX propellants below 21 atm. AP composites showed pressure dependence only below 5 atm. Onset of the faint IR signal L_{1b} for double-base propellants was independent of pressure and environmental gas which indicated that first gasification (L_{1a}) was totally dominated by solid phase reactions. The gasification rate during the transition from L_{1a} to L_{1d} was driven by the external radiation and thermal feedback from the developing gas phase reaction. Justification for the latter was provided by enhanced gasification rates for increasing pressures. In addition, the ratio of laser assisted heating rate to the feedback rate from a steady state strand burner proved to range from 2 to 3.25 for decreasing pressures which clearly demonstrated the overall importance of the laser radiation.

Finally, the effects of the radiation source on the ignition behavior was investigated for AP composites and metallized propellants. It was stated that a decrease in ignition delay with no change in slope corresponded to a decrease in surface reflectivity; shorter ignition times with

an increase in slope meant a larger extinction coefficient (μ) as well as lowered reflectivity. Faster ignition of metallized AP propellants in the arc image furnace was attributed to the high infrared reflectivity of metals occurring with the laser apparatus.

In conclusion, it was found that, for the wide variety of propellants investigated, the dependence of ignition delay on applied radiative heat flux was related by:

$$t_{ignition} = q^n \ , \ \text{where} \quad -1.3 > n > -2.0 \tag{2-38}$$

the more positive n values corresponded to lowered pressures and increased propellant transmissivity. Minor differences were noted between arc-image and laser induced ignition.

In recent years a number of studies have investigated the ignition characteristics for composite solid propellants under sub-atmospheric conditions. This work was motivated as small solid rocket motors are increasingly used for steering and flight correction purposes at high altitudes.

Initial work by Saito *et al.* (1977) considered laminated AP-CTPB slabs, exposed to fluxes from 2 to 7 cal/cm^2-sec under sub-atmospheric pressures. A thick AP crystal was cemented on top of a slab of CTPB fuel-binder, and positioned in a He, Ar or N_2 40 or 100 Torr pressurized chamber. Ignition was initiated at or near the front of an carbonaceous layer, originating from the CTPB pyrolysis, which advanced from the fuel binder to the AP surface. This layer burnt out immediately after ignition and established a typical diffusion flame at the AP fuel binder interface. The dominant reaction directly responsible for ignition was identified as the exothermic reaction between reactive decomposition products from fuel pyrolysis and AP decomposition products. This mechanism was further supported by longer ignition times in He compared to Ar or N_2 environments as a result of a loss of buoyancy for the larger fuel degradation products and increased heat loss to the He gas.

A subsequent study by Harayama, Saito and Iwama (1983) investigated ignition of an 80 % AP, 20% CTPB propellant in a 30 to 600 Torr CO_2 environment with simultaneous measurement of surface and solid phase temperatures, surface regression and ignition delay times. Regions of non-sustained and sustained ignition were identified on a map of pressure versus heat flux. At extremely low pressures ignition did not occur because of rapid diffusion and dissipation of decomposition products in the gas phase. At sufficiently high fluxes and low pressures non-sustained ignition was observed, and explained in terms of steep thermal gradients in the solid which exceeded chemical heat production after flux cessation. At lower fluxes this conductive heat loss effect was reduced by the less steep thermal gradients such that

sustained ignition eventually resulted. Ignition times were related to incident flux levels as $t_{ign} \propto q^n$ where n= -2.1 ± .3, a correlation roughly in agreement with thermal ignition theory. Addition of aluminum particles to the AP-CTPB propellant increased its thermal conductivity which in turn led to deeper thermal layers, slower rises in surface temperature, longer ignition times and an extended self-sustaining ignition regime.

Effects of $CuCr_2O_4$ (copper chromite) and C (carbon black) addition to the 80 % AP, 20 % CTPB propellant were investigated under sub-atmospheric pressures in an Ar environment using CO_2 laser heating by Saito, Yamaya and Iwama (1985). They noted that copper chromite reduced the ignition time and improved the ignitability or the self-sustaining ignition capability of the propellant formulation. Carbon black, frequently added to reduce in-depth radiative absorption, did not exhibit catalytic activity in the ignition process during the low pressure tests. Dynamic extinction effects were only observed at pressures below 100 Torr, coincident with the moment of flux removal, irrespective of the length of laser assisted burning.

Differential thermal analysis (DTA) at various low pressures and propellant formulations indicated a recurring endotherm around 240 °C, corresponding to the crystalline phase change of AP, along with more significant exothermic reactivity and a shift to lower temperatures with the addition of copper chromite. Carbon black made the exothermic peaks less distinct. They concluded that condensed phase or heterogeneous reactions appeared to control self-sustaining ignitability with copper chromite acting as a positive catalyst, but ignition itself was rate limited by gas phase reactions.

Significant progress has been made in understanding radiative ignition of solid propellants. Radiative interaction with the solid, such as in-depth absorption, scattering and solid heat conduction form important factors as they govern the manner in which the propellant harnasses the external radiant flux. The role of pressure becomes increasingly important at low levels as the gas phase chemical diffusion time attains magnitudes comparable to the solid heat-up time. Faster observed ignition by addition of catalysts such as copper chromite and iron oxid suggest significant exothermic solid phase reactivity, although the ignition process is ultimately controlled by rapid exothermic gas phase reactions.

2.7 Concluding Remarks

Theoretical and experimental aspects of solid propellant ignition have been discussed with respect to conductive and radiative heating modes, with major emphasis on describing different mechanisms present during the ignition process. A section on convective heating by a

hot, flowing gas stream is notably absent, for example. Furthermore, common experimental methods used to obtain kinetic data on propellant ingredients have not been discussed. The intent rather has been to provide a foundation and historical perspective for the current work.

It has been observed for the radiant ignition case that a major portion of the total time for sustained ignition consists of heating the solid propellant; however, only at low pressures the gas phase chemical diffusion time becomes of comparable magnitude as the solid heat-up time. Expansion therefore of solid propellant ignition studies to multi dimensional geometries is believed to be best served by first clearly delineating geometry related effects prior to introduction of gas phase reactions, surface regression and ambient gas conditions such as its composition and pressure.

Once the effects of geometry for a reactive solid ignition model are determined and compared to established one dimensional results, possible trends predicted by more advanced models may be extrapolated at least on a qualitative basis based on existing one dimensional work. Further insight into this geometry effect is obtained by a small scale experimental program which pinpoints additional interesting features.

In subsequent chapters a reactive solid ignition model is described and solved numerically for different solid geometries. These results are cross-compared to delineate the effect of geometry. Experimental results are discussed in Chapter VI to report on actual geometric aspects during the ignition of an AP based composite propellant.

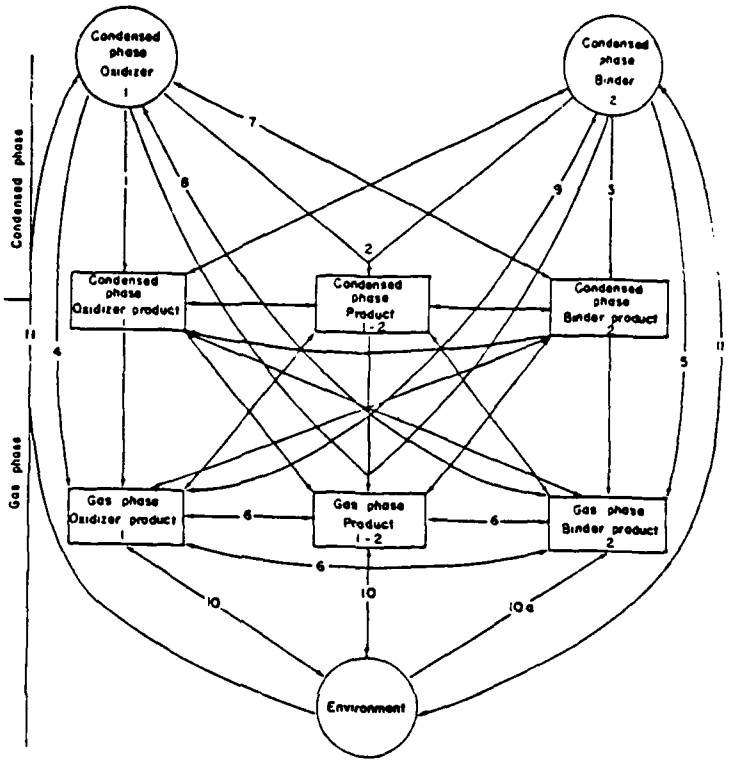

FIG. 2.1 DIAGRAM OF CHEMICAL REACTIONS DURING SOLID PROPELLANT IGNITION. Observe the various solid-to-solid, solid-to-gas and gas-to-gas chemical reactions as this classification illustrates the distinction between the solid phase, heterogeneous and gas phase ignition theories. From Price *et al.* [1966].

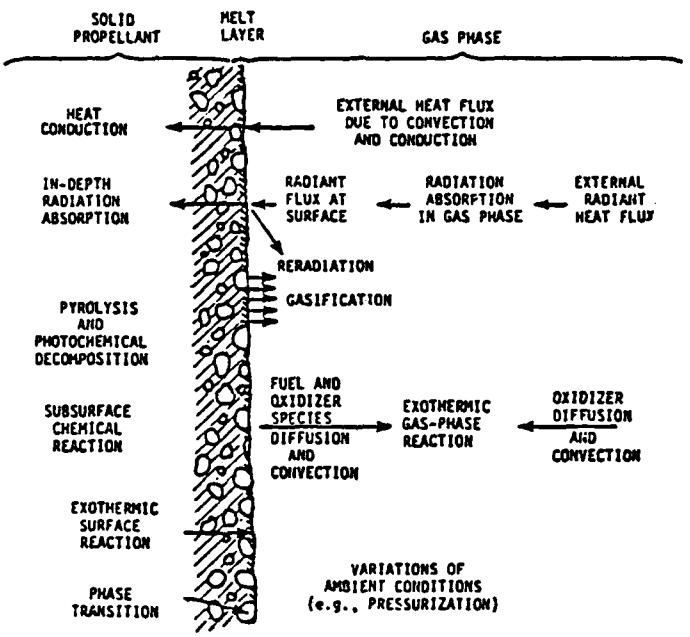

FIG 2.2 PHYSICO-CHEMICAL PROCESSES DURING PROPELLANT IGNITION. Typical physical processes occuring during radiant ignition of composite solid propellants. From Kulkarni *et al.* [1980].

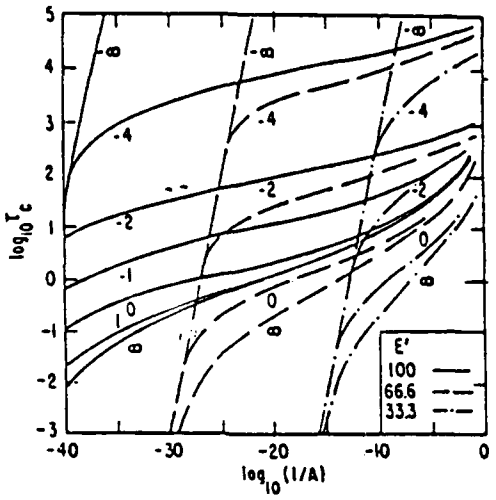

FIG. 2.3 IGNITION DELAY VS LOG(1/A) FOR 3 ACTIVATION ENERGIES AND A RANGE IN ABSORPTIVITY. The numbers that label the curves are $\log_{10}\alpha$. From Liñán and Williams [1972].

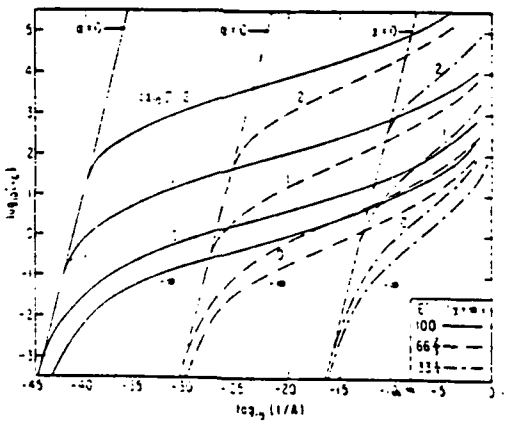

FIG. 2.4 IGNITION DELAY VS LOG(1/A) FOR VARIOUS RESPONSIVITY RATIOS AND INFINITE ABSORPTION. Curves are displayed for 3 dimensionless activation energies and for various gas-to-solid responsivity ratios Γ, for the surface absorption case ($\alpha \to \infty$). From Bush and Williams [1976].

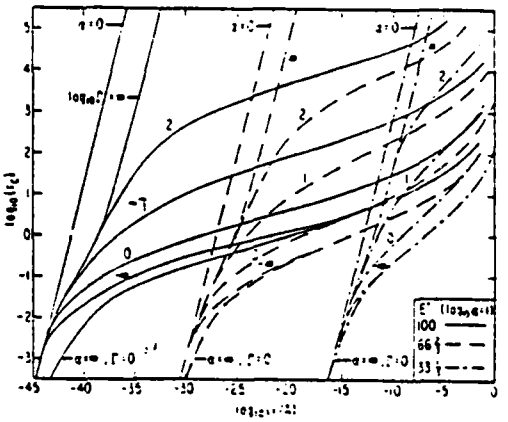

FIG 2.5 IGNITION DELAY VS LOG(1/A) FOR VARIOUS RESPONSIVITY RATIOS AND ABSORPTION= 10. Curves are displayed for 3 dimensionless activation energies and for various gas-to-solid responsivity ratios Γ, for the nondimensional absorptivity α = 10 case. From Bush and Williams [1976].

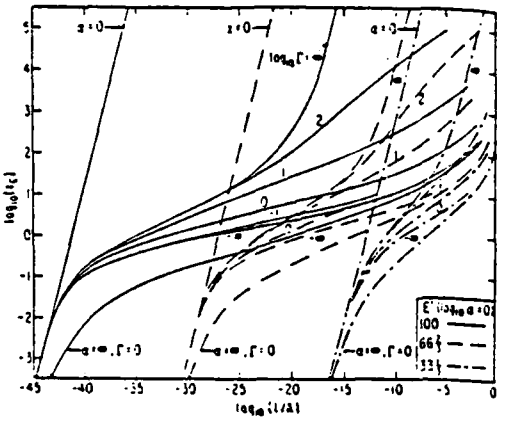

FIG. 2.6 IGNITION DELAY VS LOG(1/A) FOR VARIOUS RESPONSIVITY RATIOS AND ABSORPTION= 1. Curves are displayed for 3 dimensionless activation energies and for various gas-to-solid responsivity ratios Γ, for the nondimensional absorptivity α = 1 case. From Bush and Williams [17].

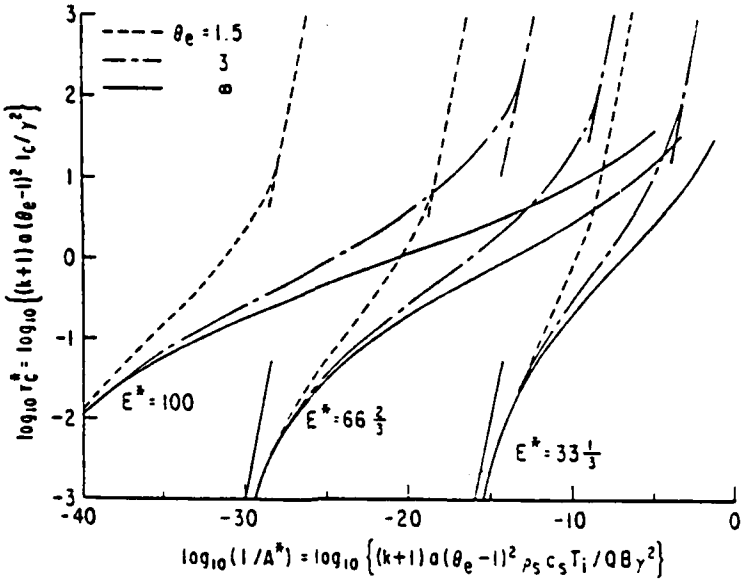

FIG. 2.7 IGNITION DELAY VS LOG(1/A) FOR CONVECTIVE HEATING. Curves displayed for 3 dimensionless activation energies, different free stream temperatures and solid phase ignition. From Niioka and Williams [1977].

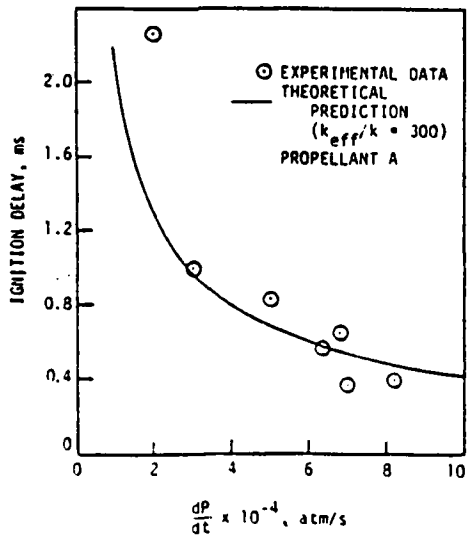

FIG. 2.8 COMPARISON OF PREDICTED AND MEASURED IGNITION TIMES. Results for solid propellant ignition under rapid pressurization. From Kumar and Kuo [1980].

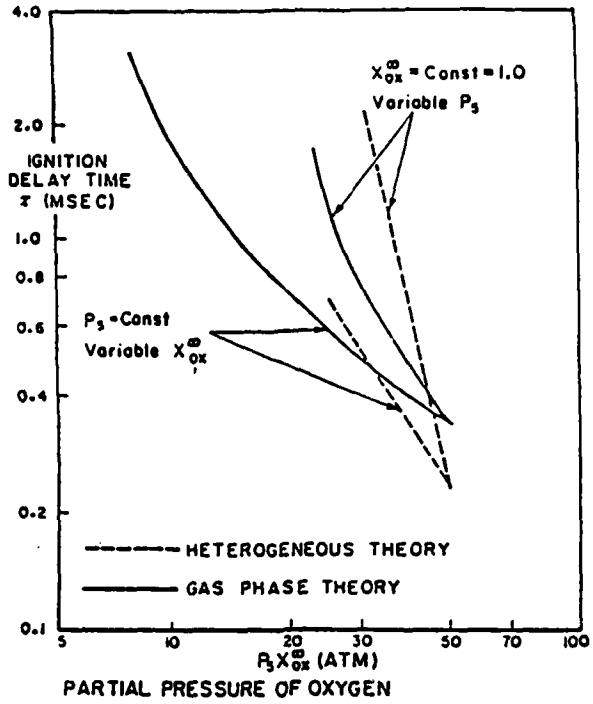

FIG. 2.9 COMPARISON OF HETEROGENEOUS AND GAS PHASE THEORY. Theoretical predictions of the effect of partial pressure of oxygen on the ignition delay in a shock tube. From Waldman *et al.* [1969], Gas phase data from Hermance *et al.* [1966].

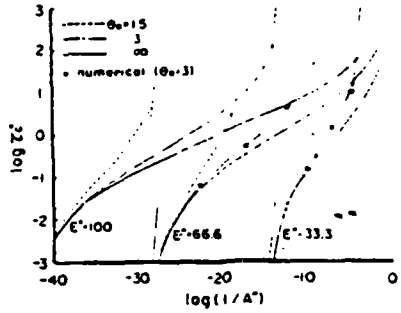

FIG. 2.10 IGNITION DELAY VS LOG(1/A) FOR CONVECTIVE HEATING. Curves displayed for 3 dimensionless activation energies, different free stream temperatures and heterogeneous ignition. From Niioka [1978].

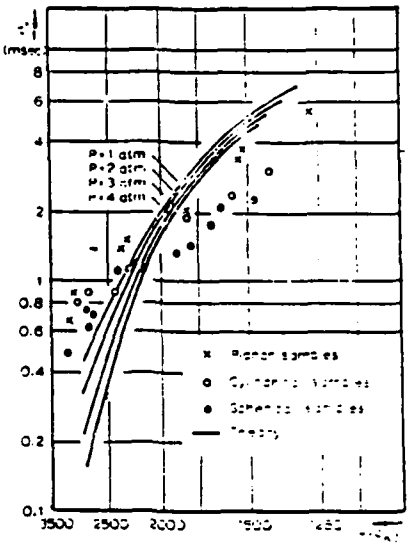

FIG. 2.11 COMPARISON OF THE THEORETICAL AND EXPERIMENTAL IGNITION DELAYS: SHOCK TUBE. Note the effect of the non planar organic fuel samples ($n\text{-}C_{18}H_{38}$), ignited in a gas driven shock tube. From Chang and Schultz-Grunow [1970].

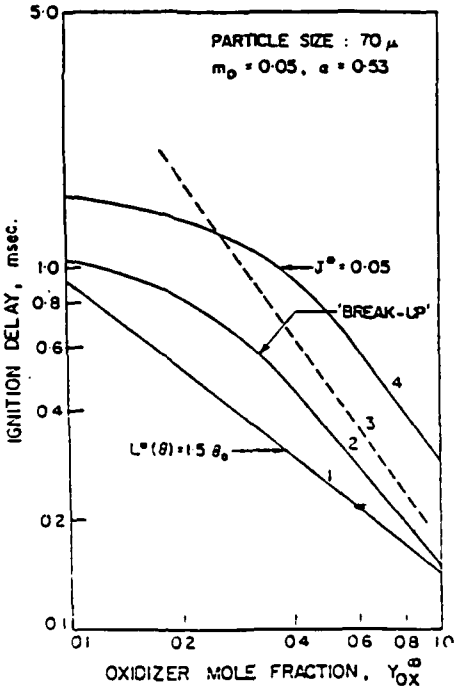

FIG. 2.12 EFFECT OF OXIDIZER MOLE FRACTION ON DELAY TIMES. Dashed curve represents experimental data; solid lines correspond to different ignition criteria based on gas phase controlled ignition. From Kumar and Hermance [1972].

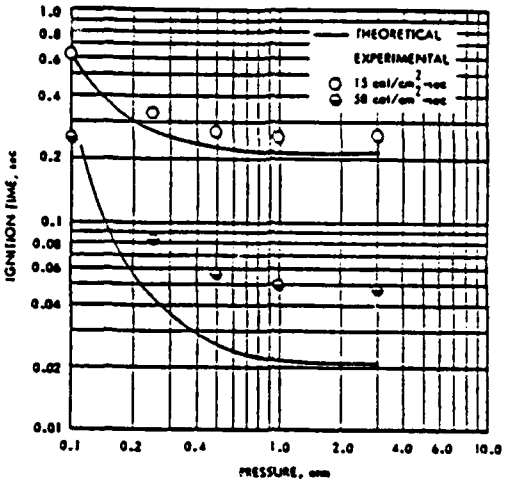

FIG. 2.13 COMPARISON OF THE THEORETICAL AND EXPERIMENTAL IGNITION DELAYS: ARC IMAGE. Radiative ignition in a neutral environment at two distinct flux levels as a function of ambient pressure. From Shannon and Deverall [1969].

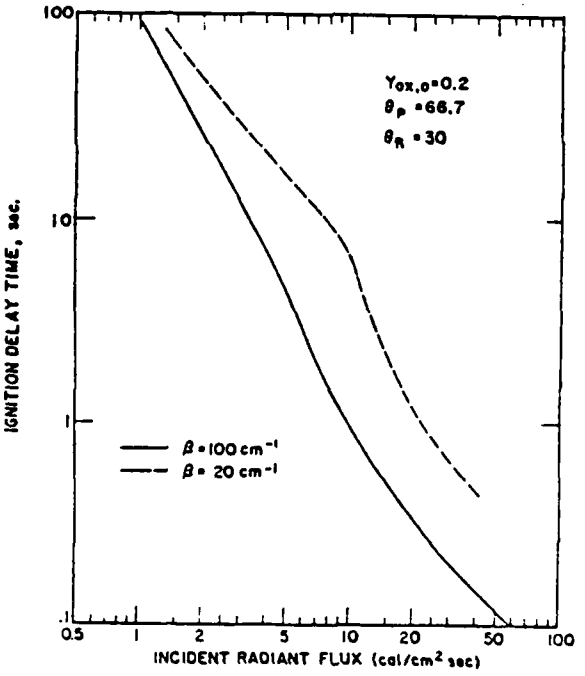

FIG. 2.14 EFFECT OF ABSORPTION COEFFICIENT ON IGNITION TIME. Solid phase pyrolysis activation energy equal to 40000 cal/mole, gas phase activation energy equal to 18000 cal/mole; note effect of the absorption coefficient both on the ignition delay value and slope value of the curve. From Kashiwagi [1974].

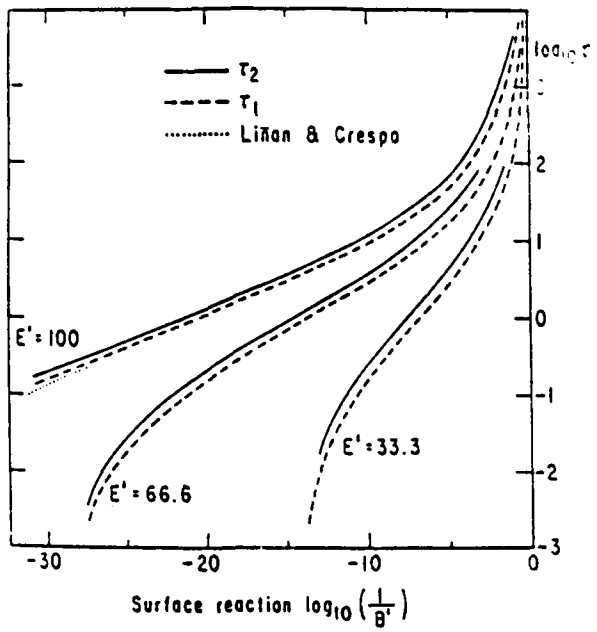

FIG. 2.15a IGNITION DELAY VS LOG(1/A) FOR DIFFERENT CRITERIA. Case of surface gasification for various activation energies. From Kindelán and Williams [1975].

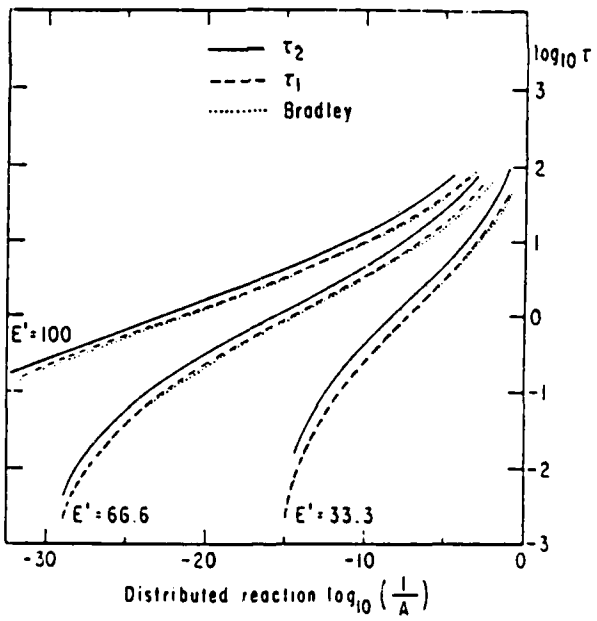

FIG. 2.15b IGNITION DELAY VS LOG(1/A) FOR DIFFERENT CRITERIA. Case of distributed gasification for various activation energies. From Kindelán and Williams [1975].

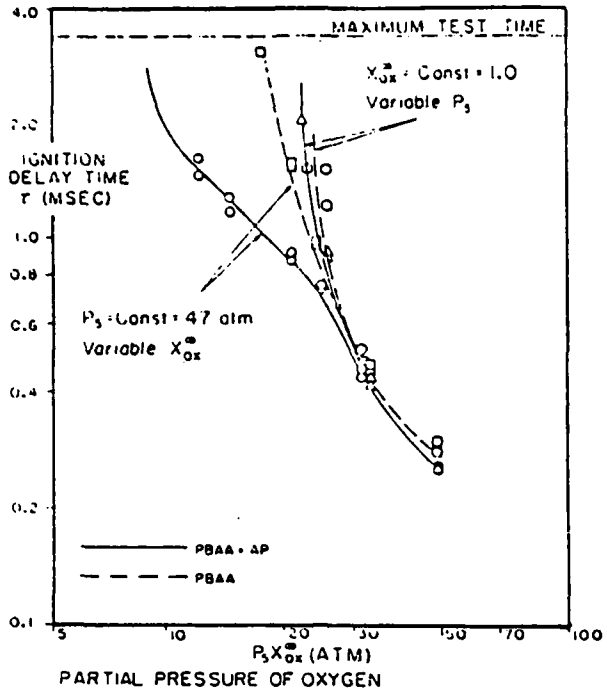

FIG. 2.16 IGNITION TIMES FOR PBAA AND PBAA+AP IN A SHOCK TUBE. Note the effect of embedded AP only at fixed total pressure, not at fixed oxidizer mole fraction. From Kashiwagi *et al.* [1973].

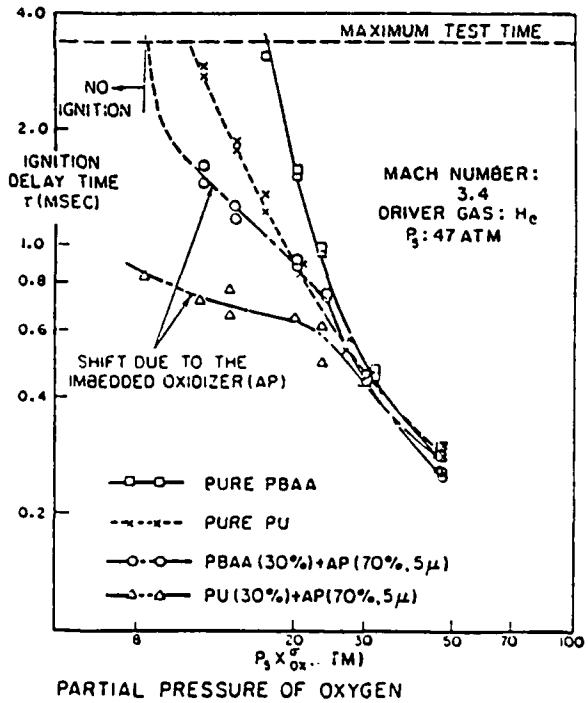

FIG. 2.17 BINDER CHARACTERISTIC EFFECTS IN A SHOCK TUBE. Note the shift in slope at lowered oxygen mole fraction due to the embedded AP. From Kashiwagi *et al.* [1973].

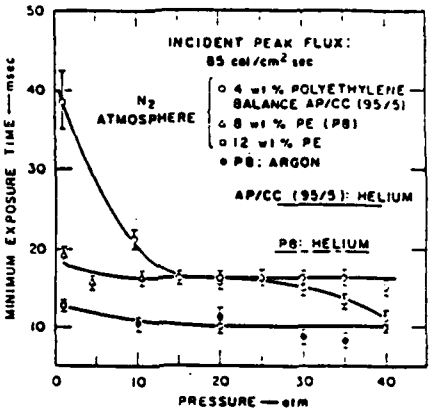

FIG. 2.18 PRESSURE EFFECT ON THE IGNITABILITY OF PROPELLANTS. Observe the effect of addition of polyethelene and nature of inert gas on ignition behavior of a NH_4ClO_4/ copper chromite/ polyethylene propellant. From Rosser *et al.* [1966].

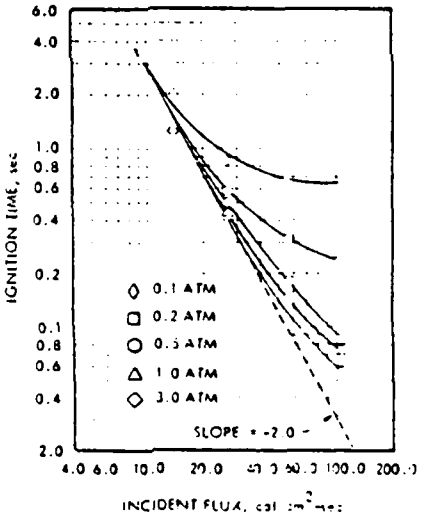

FIG. 2.19 IGNITION TIMES VS APPLIED FLUX FOR A PBAN PROPELLANT. Note increasing pressure effect as pressure decreases in a N_2 atmosphere. From Shannon [1970].

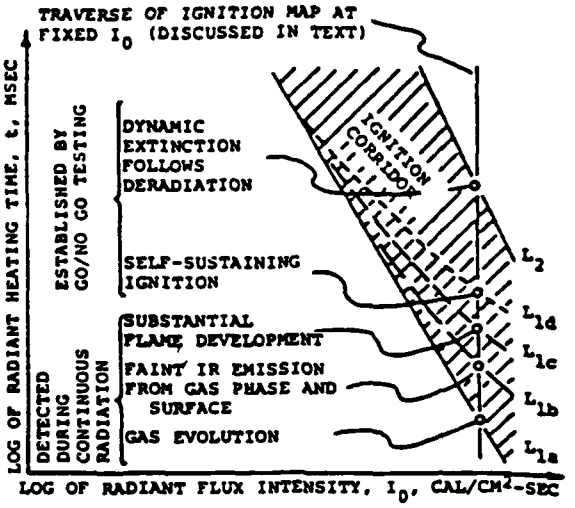

FIG. 2.20 GENERALIZED IGNITION MAP FOR RADIATIVE HEATING. The various stages during the ignition transient were detected by an IR detector, high-speed shadowgraph and color movies. From DeLuca *et al.* [1976].

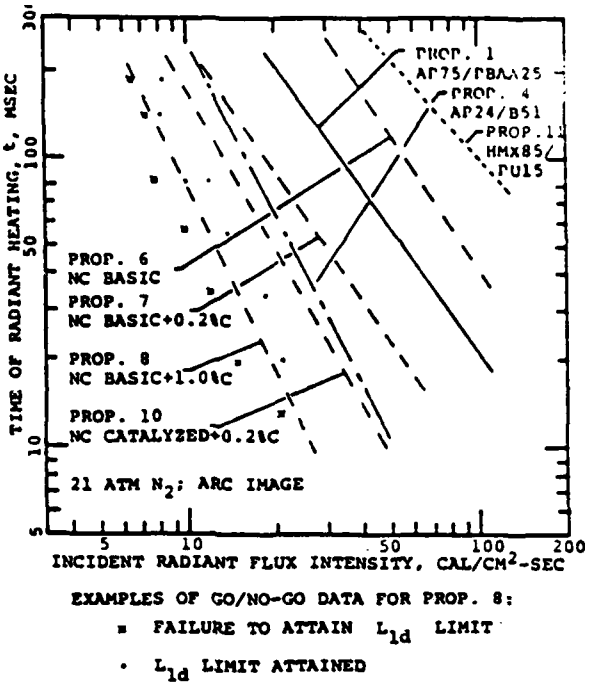

FIG. 2.21a IGNITION BOUNDARIES FOR DIFFERENT PROPELLANTS. Arc-image results for double-base, AP and HMX composite propellants based on incident flux levels. From DeLuca *et al.* [1976].

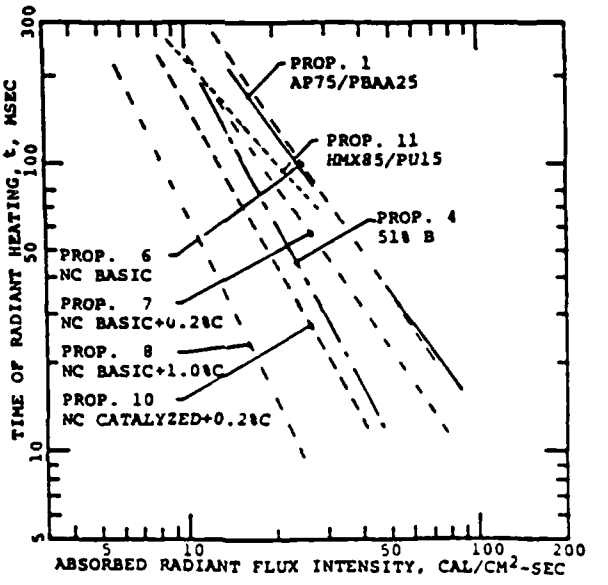

FIG. 2.21b IGNITION BOUNDARIES FOR DIFFERENT PROPELLANTS. Arc-image results for double-base, AP and HMX propellants, based on radiant flux corrected for reflection. From DeLuca *et al.* [1976].

CHAPTER III

MODEL DESCRIPTIONS

3.1 Introduction

The extension of solid propellant ignition studies to multi-dimensional geometries can be accompanied by an extensive list of qualifiers as is evident from the literature survey. Major items of this list include: i) the geometric representation of the solid and adjacent gas phase regions, ii) specification of the location(s) of strong exothermicity leading to ignition, iii) formulation of propellant reaction chemistry, and iv) appropriate initial and boundary conditions. Additional features involve the specification of thermo-physical, transport and optical properties for the different phases, the complexity of the propellant chemistry, the coupling of solid, liquid and gas phase processes, and the gas phase composition and pressure.

Clearly, a variety of models can be formulated with increasing degree of complexity by incorporating several of the above mentioned processes. The numerical results will be influenced to various degrees by the selected geometric configuration. Conversely, the effects of geometry may be obscured in unknown ways by chemical and physical processes as incorporated in the particular model formulation. For these reasons, it is imperative that the proposed model exhibits a minimum of physical and chemical complexity.

It was therefore decided to have the ignition process controlled by a solid phase reaction mechanism. This selection effectively eliminates all gas phase processes and focusses primary attention to the solid region itself. Secondly, this theory yields reasonable estimates of ignition behavior for the radiative heating case, provided conductive time scales are significantly larger than gas phase chemical diffusive time scales. Thirdly, the existence of extensive one dimensional results (Bradley, 1970), based on the same solid phase ignition theory, permits detailed comparison to delineate the effect of geometry.

As Bradley's work (1970) formed the basis for several studies which investigated the effects of different physical characteristics all based on the concept of the reactive solid, the present study attempts to establish in a similar fashion limits on geometrically related ignition behavior. In addition, previous work (Baer and Ryan, 1968; Liñán and Williams, 1971, 1972; Bush and Williams, 1975, 1976) may at least qualitatively be expanded to two dimensions based on the current comparative geometric studies.

The second question that must be answered is: what shapes should be considered to most closely resemble practical solid propellant uses? The most common use of these materials

is restricted to propulsion devices, where a cylindrical cannister is filled completely with solid propellant material except for a five or seven star shaped hollow core. Since the interior corners of such extrusions form surfaces convex to the igniter gas, a speed-up in ignition is most likely to occur at these locations.

Selected geometries include therefore a 90° corner, 45° and 22.5° sharply pointed wedges and 90°, 60° and 45° rounded tips. In all cases the solid propellant fills the noted geometry and is heated along the exposed sides at constant flux levels.

3.2 Physical Model

The model considers two dimensional heat conduction in the solid region along with a bulk, single-step, solid-to-solid exothermic Arrhenius decomposition reaction. Ignition is achieved and characterized by the occurence of a rapid thermal runaway as a result of the chemical reactivity.

The entire ignition transient from initial application of the external flux to attainment of the thermal runaway condition can be described by the following sequence of events. At time zero the solid region is heated at a constant rate which increases the surface temperature and initiates conduction of heat to the inner solid regions. Upon continued heating, local temperatures rise gradually as governed by the heat conduction process. Convergence of heat flow lines caused by geometric augmentation of the two dimensional solid domain leads locally to higher temperatures and deeper thermal wave penetration at any given time compared to the well investigated one dimensional case. These temperatures first rise gradually but later more precipitously as local chemical heat generation becomes increasingly important. Consumption of reactants locally suppresses the chemically induced temperature increases. Eventually a rapid increase in temperature takes place in the region of highest convexity, provided not all reactants have been consumed.

The "ignitedness" of the system is tested by terminating the external flux at an arbitrary time, insulating the heated boundaries and observing the subsequent thermal behavior (Hicks, 1954; Bradley, 1970). The ignition behavior is then based on the thermal characteristics during this post-heating induction period. Early or premature flux removal is accompanied by a gradual and continuous decrease in temperatures throughout the entire region. Clearly, insufficient energy is stored in the heated solid to trigger the exothermic chemical reaction necessary for ignition. Late flux removal generally leads to rapid temperature excursions, frequently without a noticeable deflection in its profile at the moment of flux cessation.

In the current work the ignition delay time is defined as the shortest external heat-up

time which produces a thermal runaway condition without total reactant consumption anywhere in the solid after the longest possible post-heating induction period. Further details are discussed in section 3.6.

3.3 Assumptions

Important assumptions in the present model formulations are:

1) constant thermal properties, independent of temperature and extent of chemical decomposition,

2) a simple, first order, exothermic solid-to-solid decomposition reaction,

3) a homogeneous, opaque reactive solid undergoing a bulk Arrhenius reaction rate,

4) reaction products remaining solid with identical thermal properties,

5) the gas-solid interface remaining stationary and no inclusion of surface regression,

6) the temperature and the extent of reaction at ignition are taken at that flux removal time which resulted in the longest post-heating induction period prior to thermal runaway, and

7) the exposed boundaries experience no heat losses and are considered insulated after flux termination.

The rationale for these assumptions rests on two pillars; first, the assumed mechanism for ignition and secondly, the desire to maintain close resemblance to the extensive one dimensional numerical results reported by Bradley (1970). Assumptions (1-4) are frequently made in the solid phase ignition theory as they constitute the definition of a reactive solid. Assumption (5) is a direct result of (4). The last two statements define the ignition temperature and fraction reacted at the moment of ignition and secondly, eliminate heat loss effects to the adjacent gas phase.

3.4 Mathematical Formulations

The three different geometries, selected for ignition analysis, are considered separately as each formulation employes a different coordinate system and presents a variety of challenges in solving its system of equations.

3.4.1 Right Angle Corner

This two dimensional geometry consists of a 90° right angle corner of a homogeneous reactive solid with surfaces parallel to the Cartesian x and y axes. Figure 3.1 shows a

schematic of the physical model. The important boundary condition consists of a constant heat flux applied normal to the sides of the corner. Along with local heat generation and reactive mass depletion, the mathematical statement of the problem, including initial and boundary conditions, is:

$$\frac{\partial\theta}{\partial\tau} = \frac{\partial^2\theta}{\partial\xi^2} + \frac{\partial^2\theta}{\partial\eta^2} + A(1-\epsilon)e^{-E/\theta} \quad (\xi > 0,\ \eta > 0) \tag{3-1}$$

$$\frac{\partial\epsilon}{\partial\tau} = \frac{A}{B}(1-\epsilon)e^{-E/\theta} \tag{3-2}$$

$$\theta(\xi,\eta,0) = \theta(\infty,\infty,\tau) = 1\ , \qquad \epsilon(\xi,\eta,0) = 0 \tag{3-3}$$

$$\frac{\partial\theta}{\partial\xi}(0,\eta,\tau) = \frac{\partial\theta}{\partial\eta}(\xi,0,\tau) = -1: \quad 0 \le \tau \le \tau_h \tag{3-4}$$

$$= 0: \qquad \tau \ge \tau_h$$

3.4.2 Sharp Wedge of Various Included Angles

This geometry consists of an infinitely long cylinder of very large outer radius with a pie slice cross section of included angle ϕ_o. Figure 3.2 displays the physical model under consideration. Constant heating is applied normal to the straight sides of the wedge; a zero rise in temperature supplies the boundary condition at the very large radius. The region of interest is located near the apex of the wedge. The reactive problem, including bulk heat production and reactant depletion, is completely defined in cylindrical coordinates by the following dimensionless equations and conditions:

$$\frac{\partial\theta}{\partial\tau} = \frac{\partial^2\theta}{\partial r^2} + \frac{1}{r}\frac{\partial\theta}{\partial r} + \frac{1}{r^2}\frac{\partial^2\theta}{\partial\phi^2} + A(1-\epsilon)e^{-E/\theta} \quad (r > 0,\ 0 < \phi < \phi_o) \tag{3-5}$$

$$\frac{\partial\epsilon}{\partial\tau} = \frac{A}{B}(1-\epsilon)e^{-E/\theta} \tag{3-6}$$

$$\theta(r,\phi,0) = \theta(\infty,\phi,\tau) = 1, \quad \epsilon(r,\phi,0) = 0 \tag{3-7}$$

$$\frac{\partial\theta}{r\partial\phi}(r,0,\tau) = -\frac{\partial\theta}{r\partial\theta}(r,\phi_o,\tau) = -1: \quad 0 \le \tau \le \tau_h \qquad (3\text{-}8)$$

$$= 0: \qquad \tau \ge \tau_h$$

The existence of a zero tangential thermal gradient along the centerline, based on symmetry considerations, reduces the solution domain and supplies an additional boundary condition as:

$$\frac{\partial\theta}{r\partial\phi}(r,\phi_o/2,\tau) = 0 \quad \text{for } \tau \ge 0, \quad r > 0 \qquad (3\text{-}9)$$

3.4.3 Rounded Tip with Variable Curvature and Angle

This configuration forms a combination of the above two formulations and the one dimensional, purely cylindrical case analyzed by Hermance (1984). In the present case, the exposed corner or wedge is modified to have a certain degree of rounding. A circular arc of radius R_o is introduced to implement this rounding effect. Other model features are maintained in the same fashion.

However, as a result of the finite radius of curvature R_o, this composite geometry has two length scales. This anomaly requires the introduction of a length parameter γ ($= qR_o/kT_i$) in addition to the regular dimensionless spatial variable ξ, η or r. Figure 3.3 shows how the physical model is implemented mathematically for this composite two dimensional geometry. Again, only one half of the domain needs to be solved because of symmetry considerations. With reference to Figure 3.3, relevant equations and initial/boundary conditions are stated as:

REGION I: Finite rounded tip sector: $\left[D_1:(r,\alpha),\ 0<r<\gamma,\ 0<\alpha<1/2(\pi-\phi_o)=\alpha_o\right]$

$$\frac{\partial\theta_1}{\partial\tau} = \frac{\partial^2\theta_1}{\partial r^2} + \frac{1}{r}\frac{\partial\theta_1}{\partial r} + \frac{1}{r^2}\frac{\partial^2\theta_1}{\partial\alpha^2} - A(1-\epsilon_1)e^{-E/\theta_1} \qquad (3\text{-}10)$$

$$\frac{\partial\epsilon_1}{\partial\tau} = \frac{A}{B}(1-\epsilon_1)e^{-E/\theta_1} \qquad (3\text{-}11)$$

$$\frac{\partial\theta_1}{r\partial\alpha}(r,0,\tau)= 0, \quad \frac{\partial\theta_1}{\partial r}(\gamma,\alpha,\tau)= 1 \tag{3-12}$$

REGION II: Finite 2-D Cartesian sector: $\left[D_2:(\xi,\eta),\ 0<\xi<\infty,\ 0<\eta<\gamma\right]$

$$\frac{\partial\theta_2}{\partial\tau} = \frac{\partial^2\theta_2}{\partial\xi^2} + \frac{\partial^2\theta_2}{\partial\eta^2} + A(1-\epsilon_2)e^{-E/\theta_2} \tag{3-13}$$

$$\frac{\partial\theta_2}{\partial\tau} = \frac{A}{B}(1-\epsilon_2)e^{-E/\theta_2} \tag{3-14}$$

$$\frac{\partial\theta_2}{\partial\eta}(\xi,0,\tau)= -1, \quad \frac{\partial\theta_2}{\partial\xi}(\infty,\eta,\tau)= 0 \tag{3-15}$$

REGION III: Finite cylindrical sector: $\left[D_3:(\hat{r},\phi),\ 0<\hat{r}<\infty,\ 0<\phi<\phi_o/2\right]$

$$\frac{\partial\theta_3}{\partial\tau} = \frac{\partial^2\theta_3}{\partial\hat{r}^2} + \frac{1}{\hat{r}}\frac{\partial\theta_3}{\partial\hat{r}} + \frac{1}{\hat{r}^2}\frac{\partial^2\theta_3}{\partial\phi^2} + A(1-\epsilon_3)e^{-E/\theta_3} \tag{3-16}$$

$$\frac{\partial\epsilon_3}{\partial\tau}= \frac{A}{B}(1-\epsilon_3)e^{-E/\theta_3} \tag{3-17}$$

$$\frac{\partial\theta_3}{\hat{r}\partial\phi}(\hat{r},\phi_o/2,\tau)= 0, \quad \frac{\partial\theta_3}{\partial\hat{r}}(\infty,\phi,\tau)= 0 \tag{3-18}$$

The three computational regions D_1, D_2 and D_3 are interconnected by equality of thermal gradients across adjoining interfaces, which are expressed as:

$$\frac{\partial\theta_1}{r\partial\alpha}(r,\alpha_o,\tau)= \frac{\partial\theta_2}{\partial\xi}(0,\eta,\tau) \tag{3-19}$$

$$\frac{\partial\theta_2}{\partial\eta}(\xi,\gamma,\tau) = \frac{\partial\theta_3}{\hat{r}\partial\phi}(\hat{r},0,\tau) \tag{3-20}$$

Initial conditions for all three regions are expressed as:

$$\epsilon_1(r,\alpha,0)= \epsilon_2(\xi,\eta,0)= \epsilon_3(\hat{r},\phi,0)= 0 \tag{3-21}$$

$$\theta_1(r,\alpha,0)= \theta_2(\xi,\eta,0)= \theta_3(\hat{r},\phi,0)= 1 \tag{3-22}$$

The numerical implementation of the system equations, formulated for the different geometries, are discussed in detail in Chapter IV and Appendix B, along with verification of the computer code and assessment of the accuracy and convergence characteristics of its results.

3.5 Variable and Parameter Definitions

The equations in section 3.4 are expressed in dimensionless form which collapses the number of variables into three dimensionless parameters A, B and E. Details of the nondimensionalization are found in Vorsteveld (1985).

The dependent temperature and time variables are now defined by:

$$\theta = \frac{T}{T_i}, \quad \tau = \frac{q^2 t}{k\rho c T_i^2} \tag{3-23}$$

and parameters A, B and E are defined as:

$$A = \frac{Q\nu k T_i}{q^2}, \quad B = \frac{Q}{\rho c T_i}, \quad E = \frac{E'}{RT_i} \tag{3-24}$$

Parameter A is the ratio of the volumetric chemical heat release rate in the solid to the external heat flux q; an identical parameter appears in many solid phase ignition studies (Bradley, 1970; Liñán and Williams, 1971, 1972; Bush and Williams, 1975, 1976). Parameter B, the heat release parameter, is the ratio of chemical heat release per unit volume to the initial sensible energy. The heat of combustion factor Q in parameters A and B signifies only that portion of the total heat of combustion of the solid propellant which is released during the solid phase exothermic chemical reaction. Parameter E is the typical dimensionless activation energy.

The current time scale (τ) appears in the exact format in the solid phase ignition studies referenced above, and in a slightly modified form in some gas phase studies (Kindelán and Williams, 1975a, 1975b, 1977). This feature facilitates direct comparison of ignition times for different models and geometric configurations.

Close examination of the different model equations shows that the solutions are of the form:

$$\tau_c = f(\phi_o,\gamma,A,B,E) \tag{3-25a}$$

$$\theta_c = g(\phi_o,\gamma,A,B,E) \tag{3-25b}$$

$$\epsilon_c = h(\phi_o,\gamma,A,B,E) \tag{3-25c}$$

A qualitative discussion of the equations reveals three different, yet mutually dependent effects. These three factors are: 1) the geometric configuration as it controls the rate of surface temperature rise based on external heating alone, 2) the values for A and E as their combination governs the approximate temperature level for strong exothermicity, and 3) the ratio (A/B) as it controls the rate of reactant consumption. Secondary effects are the magnitude of activation parameter E, as it specifies the temperature sensitivity of the chemical heat release, and the relative magnitudes of the thermal wave penetration and the rounding parameter γ. The importance of these different factors will be discussed in detail in Chapter 5.

3.6 Ignition Criteria

Theoretical definitions for the ignition delay for solid phase ignition theory can be divided into three categories. The first criterion considers the thermal behavior after removal of the external stimulus; the ignition delay is then defined as the minimum exposure time which produces the characteristic thermal runaway after some finite induction period (Hicks, 1954; Bradley, 1970). A minor variation of this criterion is based on the behavior of the surface regression rate after flux cessation (Baer and Ryan, 1968). Secondly, analyses have been performed where ignition is defined in terms of a thermal runaway condition (Baer and Ryan, 1965; Liñán, 1971, 1972; Bush and Williams, 1975, 1976). Bradley (1970) reported only minor differences in results based on these two ignition criteria. A third ignition criterion has been employed, which is based on the deviation in temperature profile due to chemical exothermicity as compared to the simple inert heating case (Wise, Inami and McCulley, 1967; Thompson and Suh, 1970; Kumar and Kuo, 1980). The different theoretical ignition criteria, used for the solid phase controlled reaction mechanism, predict similar results because of the relative simplicity of these models and the strong nonlinearity of the chemical heat release. It remains to be seen however, whether the above criteria compare favorably to those employed in experimental investigations.

In the current theoretical efforts, the ignition delay is defined in terms of the behavior of the thermal field after flux removal. More precisely, the ignition time is defined as the shortest

heating time which leads to thermal runaway conditions after the longest possible post-heating induction period without total local depletion of reactants.

Reasons for this definition are two-fold: first, in an attempt to maintain close compatibility to the extensive one dimensional investigation (Bradley, 1970), it is highly desirable to employ the same criterion. As the current models only differ in the geometric features of its solution domain, maintaining identical definitions is only logical. Secondly, the current ignition criterion refers physically to a statement of the minimum amount of incident energy needed to trigger ignition which should compare favorably to experimental "go no-go" ignition tests.

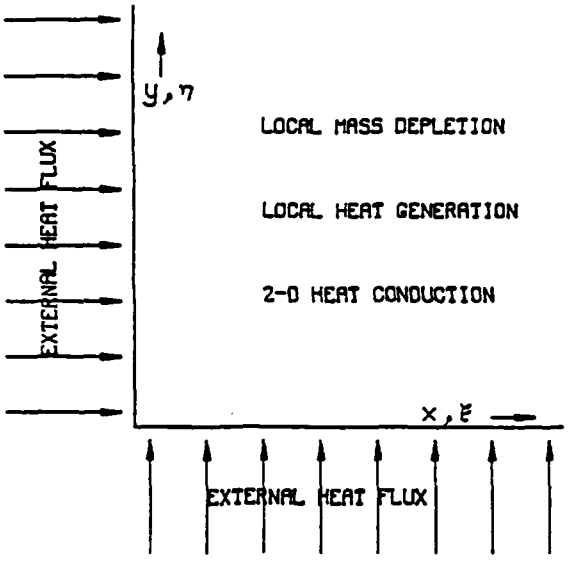

FIG. 3.1 PHYSICAL MODEL FOR THE SQUARE CORNER CASE.

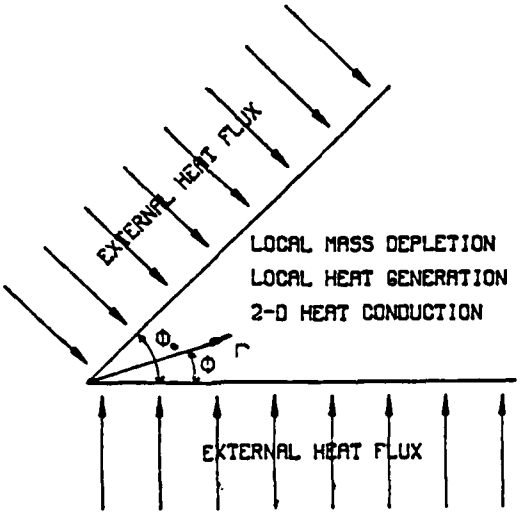

FIG. 3.2 PHYSICAL MODEL FOR THE ACUTE WEDGE ANGLE CASE.

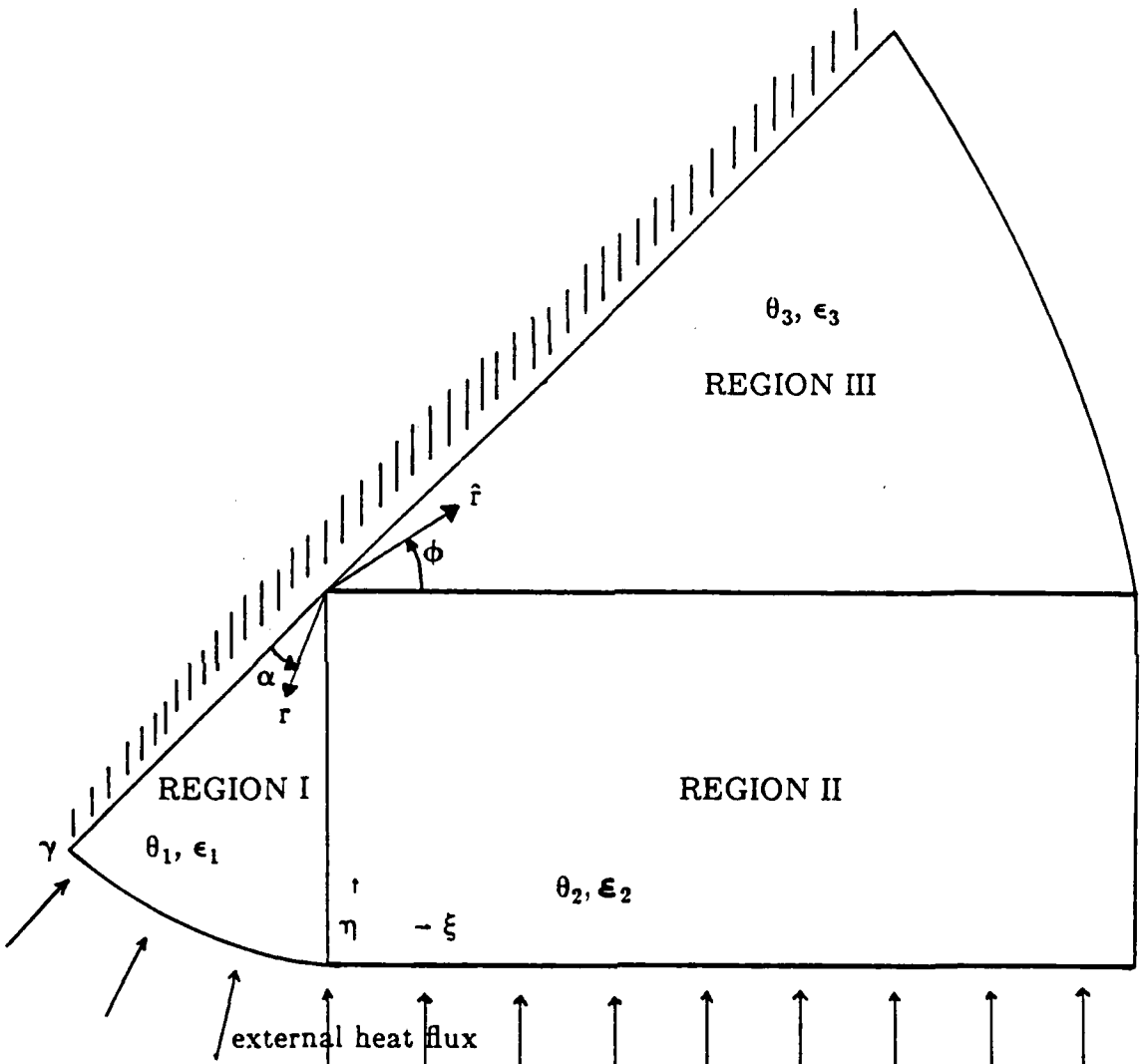

FIG. 3.3 PHYSICAL MODEL FOR THE ROUNDED TIP CASE. Coordinates, variables and computational regions are identified for all three regions. Only one half of the solution domain is required due to symmetry.

CHAPTER IV

NUMERICAL IMPLEMENTATION

4.1 Introduction

Historically the solution of proposed ignition models has proceeded in several directions. Review of the literature reveals solutions obtained via various numerical methods, asymptotic analyses, classical thermal theory and purely analytical methods such as the Laplace transform and similarity techniques. As model formulations become more complex, only asymptotic methods in terms of expansions of a very small or large parameter and numerical techniques prevail for solving these models. Since the present study considers ignition in two dimensional domains, numerical techniques are resorted to for solution.

Extensive use of finite difference methods is made in numerical ignition studies. These methods are divided into explicit and implicit schemes, based on the manner of time wise integration. A second distinction consists of single-step versus multi-step methods, where in the latter case values for the dependent variables must be known on more than one time layer (Saul'yev, 1964; Burden, Douglas Faires and Reynolds, 1981). Consider, for example, the general parabolic partial differential equation in two space dimensions:

$$\theta_\tau = \theta_{\xi\xi} + \theta_{\eta\eta} + f(\xi,\eta,\tau,\theta(\xi,\eta,\tau)) \tag{4-1}$$

A purely explicit single-step difference scheme for Eq. (4-1) is expressed as:

$$\frac{\theta_{i,j}^{k+1}-\theta_{i,j}^{k}}{\Delta\tau} = \frac{\theta_{i+1,j}^{k}+\theta_{i-1,j}^{k}-2\theta_{i,j}^{k}}{\Delta\xi^2} - \frac{\theta_{i,j-1}^{k}+\theta_{i,j-1}^{k}-2\theta_{i,j}^{k}}{\Delta\eta^2} + f(\xi_i,\eta_j,\tau_k,\theta_{i,j}^{k}) \tag{4-2}$$

where (i) and (j) refer respectively to arbitrary space points in the ξ and η directions, and (k) denotes a particular time step; $\Delta\xi$, $\Delta\eta$ and $\Delta\tau$ are increments in space and time respectively. A major advantage of the explicit formulation is that it permits node by node computation of the θ-field at the (k+1) time step, based solely on conditions existing at the k-th time step. Limitations include a severe restriction on the maximum allowable time step $\Delta\tau$, necessary to maintain stability of the numerical scheme. Accuracy and convergence is frequently assessed on a trial and error basis for nonlinear equations by varying appropriate step sizes and noting the corresponding changes in results.

A purely implicit single-step approximation for Eq. (4-1) is formulated as:

$$\frac{\theta_{i,j}^{k+1}-\theta_{i,j}^{k}}{\Delta\tau}=\frac{\theta_{i+1,j}^{k+1}+\theta_{i-1,j}^{k+1}-2\theta_{i,j}^{k+1}}{\Delta\xi^2}+\frac{\theta_{i,j+1}^{k+1}+\theta_{i,j-1}^{k+1}-2\theta_{i,j}^{k+1}}{\Delta\eta^2}+f(\xi_i,\eta_j,\tau_{k+1},\theta_{i,j}^{k+1}) \qquad (4\text{-}3)$$

This scheme produces a system of nonlinear simultaneous algebraic equations in terms of $\theta_{i,j}^{k+1}$ for i=1,.. N, j=1,.. M, which is solvable in a variety of ways. Provided the total number of nodes (NxM) is not exceedingly large, the implicit finite difference scheme is frequently used in ignition studies. Its major advantage over the explicit method is its unconditional stability which permits large time steps $\Delta\tau$ during periods of minor change in dependent variables.

Presently, the explicit method is selected because of the large number of grid points needed to discretize the various two dimensional regions. Secondly, complications that would arise in implementing the implicit scheme for a variable gridmesh and complicated domains, are easily circumvented by the explicit method.

4.2 Finite Differencing of the Model Equations

The spatial partial derivatives are presently simulated by the standard central difference approximation. By definition, the time derivative θ_τ is expressed via the forward difference scheme. The finite difference equations become more involved for a non-constant gridmesh. Employed finite difference equations along with boundary conditions are enumerated below for the three different geometries. A few comments about the computational implementation are included; details concerning code verification and assessment of its accuracy and convergent behavior of its results are found in Appendix B.

4.2.1 Right Angle Corner

The solution domain is subdivided into uniform segments $\Delta\xi$ and $\Delta\eta$ with a node located at the centroid of each segment. A finite region of integration is obtained by imposing the zero thermal gradient conditions sufficiently far away from the heated surfaces. System equations in finite difference form are:

$$\theta_{i,j}^{k+1} = \theta_{i,j}^{k} + \frac{\Delta\tau}{\Delta\xi^2}\left[\theta_{i-1,j}^{k}+\theta_{i+1,j}^{k}+\theta_{i,j-1}^{k}+\theta_{i,j+1}^{k}-4\theta_{i,j}^{k}\right] + \Delta\tau A(1-\epsilon_{i,j}^{k})\, e^{-E/\theta_{i,j}^{k}} \qquad (4\text{-}4)$$

$$\epsilon_{i,j}^{k+1} = \epsilon_{i,j}^{k} + \Delta\tau\frac{A}{B}(1-\epsilon_{i,j}^{k})\, e^{-E/\theta_{i,j}^{k}}, \quad \text{for } i=1,...N, \text{ and } j=1,...N \tag{4-5}$$

and the applied boundary conditions are:

$$\theta_{0,j}^{k} = \theta_{1,j}^{k} + \Delta\xi, \quad \text{and} \quad \theta_{i,0}^{k} = \theta_{i,1}^{k} + \Delta\eta \tag{4-6}$$

The analytical solution for the inert two dimensional conduction problem (A=0) is used to establish a starting temperature profile to lessen the overall computational time. Its solution in the present dimensionless Cartesian coordinates is given by Carslaw and Jaeger (1959) as:

$$\theta(\xi,\eta,\tau) = 1 + 2\sqrt{\tau}\left[\text{ierfc}(\frac{\xi}{\sqrt{4\tau}}) + \text{ierfc}(\frac{\eta}{\sqrt{4\tau}})\right] \tag{4-7}$$

Transition to the reactive finite difference equations is based on the relative magnitude of the A(1- ϵ)exp(-E/θ) term, being in the range of .4% to 1%, compared to the total change in internal energy for the highest temperature node. Further details concerning accuracy and convergent behavior of the computer code for this geometry have previously been reported by Vorsteveld (1985) and Vorsteveld and Hermance (1987).

4.2.2 Sharp Wedge of Various Included Angle

A cylindrical gridmesh is drawn for the solid region where the temperature θ and fraction reacted ϵ is located at the midpoint of each segment. Reasonable aspect ratio's of the grid segments are maintained by introducing two radial grid expansion factors in the low thermal gradient region. Breakdown of the central difference approximation for the radial diffusion terms in the triangular tip sector is circumvented by employing second and third order forward differences (Berezin and Zhidkov, 1965). The resulting finite difference equations are expressed as:

$$\theta_{i,j}^{k+1} = \theta_{i,j}^{k} - \frac{\Delta\tau}{(\Delta r)^2}\left[\theta_{i-1,j}^{k}(1-\frac{\Delta r}{2r_i}) + \theta_{i+1,j}^{k}(1+\frac{\Delta r}{2r_i}) - 2\theta_{i,j}^{k}\right] \tag{4-8}$$

$$- \frac{\Delta\tau}{(r_i\Delta\phi)^2}\left[\theta_{i,j-1}^{k} - \theta_{i,j+1}^{k} - 2\theta_{i,j}^{k}\right] + \Delta\tau A(1-\epsilon_{i,j}^{k})\, e^{-E/\theta_{i,j}^{k}}$$

$$\epsilon_{i,j}^{k+1} = \epsilon_{i,j}^{k} + \Delta\tau\frac{A}{B}(1-\epsilon_{i,j}^{k})\, e^{-E/\theta_{i,j}^{k}}, \quad \text{for} \quad i=1,..N, \quad \text{and} \quad j=1,..M \tag{4-9}$$

with the boundary conditions as:

$$\theta_{i,0} = \theta_{i,1} + r_i\Delta\phi, \quad \theta_{i,M+1} = \theta_{i,M} \tag{4-10}$$

Similar to the right angle corner, the analytical solution has been determined for the heating of an inert solid (A=0). This solution is accomplished via the integral transform method (Ozisik, 1980) and is shown below. Details of its development as well as investigations into its accuracy and rate of convergence are included in Appendix A.

$$\theta(r,\phi,\tau) = 1 + \frac{16}{b^2\phi_o}\sum_{\nu=0}^{\nu=\infty}\sum_{m=1}^{m=\infty}\frac{1}{\beta_m^3}\frac{J_\nu(\beta_m r)}{J'_\nu(\beta_m b)}\cos(\nu\phi) \tag{4-11}$$

$$\left[\sum_{k=0}^{k=\infty} J_{\nu+2k+1}(\beta_m b)\right]\left[1-e^{-\beta_m^2\tau}\right]$$

where J_ν's are Bessel functions of the first kind, order ν. The eigenvalues $\beta_m b$ are the positive roots for each value of ν, computed from the transcendental equation:

$$J_\nu(\beta_m b) = 0, \; m = 1,2,3,... \tag{4-12}$$

whereas the eigenvalues ν_n are determined from the roots of the expression:

$$\sin(\nu\phi_o) = 0, \quad \nu_n = n\pi/\phi_o, \quad n = 0,1,2,... \tag{4-13}$$

Use of Eq. (4-11) as an aid in overall reduction of CPU time is not feasible as an exceedingly large number of zeroes are required to compute reasonably accurate temperatures. More recently, an elegant solution has been developed for the inert problem using the similarity variable $\sigma = \tau/r^2$ and a Frobenius series in descending powers of σ (Chamberlain, 1988). Further details concerning the numerical integration scheme are located in Appendix B.

4.2.3 Rounded Tip With Variable Curvature and Angle

The numerical solution of the equations in this complex domain is accomplished by

generating three sets of finite difference code which are coupled to each other through the thermal gradient conditions expressed in Eqs. (3-19) and (3-20). Each of the three regions is briefly discussed in terms of its gridmesh characteristics, its finite difference equations and its importance during the ignition transient.

4.2.3.1 Region I

Basic features of its gridmesh include an increasing radial stepsize (Δr) upon moving inward from the heated surface to the half radius $\gamma/2$. At this point, a doubling of the angular stepsize ($\Delta\phi$) occurs along with resetting the radial stepsize to its original value to maintain approximate equality in grid segment area. Angular gridding is based on the observation that, near the surface, heat will flow predominantly in the radial direction. Hence, a relatively coarse mesh will suffice. Upon moving inward, the mesh automatically reduces in size to better approximate growing angular thermal gradients. Near the apex of region I, radial gridding is controlled manually to maintain a regular sized mesh for different γ's.

Extreme care must be exercised in deriving the finite difference equations to properly account for the variable radial gridmesh. Internodal radial spacings are denoted by increments h_i's with i=1 corresponding to surface nodes. The resulting difference equations are expressed as:

$$\theta_{i,j}^{k+1} = \theta_{i,j}^{k} + \frac{\Delta\tau}{h_{i-1}h_i}\left[\theta_{i-1,j}^{k} + \theta_{i+1,j}^{k} - 2\theta_{i,j}^{k} - \frac{h_i - h_{i-1}}{h_i + h_{i-1}}(\theta_{i+1,j}^{k} - \theta_{i-1,j}^{k})\right]$$

$$+ \frac{r_i^{-1}\Delta\tau}{h_{i-1} + h_i}\left[\theta_{i-1,j}^{k} - \theta_{i-1,j}^{k} + \frac{h_i^2 - h_{i-1}^2}{h_i h_{i-1}}\theta_{i,j}^{k} + \frac{h_{i-1} - h_i}{h_i}\theta_{i-1,j}^{k} + \frac{h_{i-1} - h_i}{h_{i-1}}\theta_{i-1,j}^{k}\right] \quad (4\text{-}14)$$

$$+ \frac{\Delta\tau}{(r_i\Delta\phi)^2}\left[\theta_{i,j+1}^{k} - \theta_{i,j-1}^{k} - 2\theta_{i,j}^{k}\right] + \Delta\tau A(1-\epsilon_{i,j}^{k})\, e^{-E/\theta_{i,j}^{k}}$$

$$\epsilon_{i,j}^{k+1} = \frac{A}{B}(1-\epsilon_{i,j}^{k})e^{-E/\theta_{i,j}^{k}} \quad \text{for } i=1,\ldots M. \text{ and } j=1,\ldots N \quad (4\text{-}15)$$

and the boundary conditions as:

$$\theta_{0,j}^{k} = \theta_{1,j}^{k} - h_1, \text{ and } \theta_{i,0}^{k} = \theta_{i,1}^{k} \quad (4\text{-}16)$$

Testing of the inert computer code for this region is accomplished by imposing adiabatic boundary conditions along the sides enclosing the $\alpha_o/2$ wedge angle to remove angular energy diffusion. Temperature profiles computed at different times are compared to exact curves, easily calculated from the inert radial temperature solution, which is expressed in current dimensionless variables with $\zeta = r/\gamma$ by Carslaw and Jaeger (1959) as:

$$\theta(\zeta,\tau) = 1 + 2\frac{\tau}{\gamma} + \gamma\zeta^2/2 - \gamma/4 - 2\gamma\sum_{n=1}^{n=\infty} e^{-\epsilon_n^2\tau/\gamma^2}\frac{J_o(\epsilon_n\zeta)}{\epsilon_n^2 J_o(\epsilon_n)} \qquad (4\text{-}17)$$

where ϵ_n are the eigenvalues of $J_1(\epsilon_n) = 0$, for $n = 1,2,...$ and J_0 and J_1 are Bessel functions of the first kind.

The curves in Figures 4.1 to 4.4 ($\gamma = 2/3$) show excellent agreement at early times for all radial stepsizes; at $\tau = .5$, slightly higher temperatures are seen for the larger stepsize Δr as a result of the forward difference approximation for the inner most mesh point. Results reported in Chapter V are all generated with a smallest possible inner stepsize to suppress this error introduced by numerical diffusion.

4.2.3.2 Region II

For ease of computations, the ξ direction is discretized into a constant stepsize under operator control. Stepsizes in the η-direction conform exactly with radial gridding in Region I for easy matching of the cylindrical and Cartesian gridmeshes. Finite difference equations with the variable stepsize in the η-direction expressed by h_i's, are formulated as:

$$\theta_{i,j}^{k+1} = \frac{\Delta\tau}{h_{i-1}h_i}\left[\theta_{i,j-1}^k + \theta_{i,j+1}^k - 2\theta_{i,j}^k - \frac{(h_i - h_{i-1})}{(h_i + h_{i-1})}[\theta_{i,j+1}^k - \theta_{i,j-1}^k]\right] \qquad (4\text{-}18)$$

$$+ \frac{\Delta\tau}{(\Delta\xi)^2}\left[\theta_{i-1,j}^k - \theta_{i-1,j}^k - 2\theta_{i,j}^k\right] + \Delta\tau A(1-\epsilon_{i,j}^k)e^{-E/\theta_{i,j}^k}$$

$$\epsilon_{i,j}^{k+1} = \epsilon_{i,j}^k - \Delta\tau\frac{A}{B}(1-\epsilon_{i,j}^k)e^{-E/\theta_{i,j}^k} \quad \text{where} \quad i = 1,...N, \quad \text{and} \quad j = 1,...M \qquad (4\text{-}19)$$

with boundary conditions as:

$$\theta_{i,0} = \theta_{i,1} - h_1, \quad \text{and} \quad \theta_{N,j} = \theta_{N-1,j} \qquad (4\text{-}20)$$

The accuracy and convergent behavior of the computer code for Region II is further discussed in Appendix B where both inert and reactive behavior is considered for the entire domain.

4.2.3.3 Region III

Upon heating of the exterior surfaces this region will experience rather small thermal gradients, especially those regions far removed from the $\phi_o/2$ apex. The $\phi_o/2$ angle is subdivided into 4 equal segments $\Delta\phi$. A constant radial stepsize is used, equal to $\Delta\xi$, for direct matching of the gridmeshes in regions II and III. Although the gridmesh leads here to segments having large angular nodal spacings far from the apex, it is felt that the induced errors are small as, first, the thermal gradients are very small, and secondly, this region is far removed from the high gradient, reactive zone and therefore only minimally influences the ignition behavior near the tip. The resulting finite difference equations are readily formulated based on previous presentations.

4.3 Determination of the Solution Domain Size

The overall size of the solution domain for a specific rounding parameter γ and wedge angle ϕ_o is determined in an approximate fashion from the zero thermal gradient condition (3-15) as ξ approaches ∞. If energy conduction is predominantly one dimensional at a distance ξ_o away from the rounded tip region, the 1-D inert solution can be used to provide an estimate for ξ_o. From this position ξ_o, a distance δ_{th} can be computed, measured inward from the heated surface, which exhibits only a minimal rise in temperature and can approximately be computed from the 1-D inert solution (Carslaw and Jaeger, 1959).

From geometric considerations shown in Figure 4.5, this distance ξ_o is readily computed from the thermal penetration depth δ_{th}, for any positive surface temperature θ_s (>1). In present dimensionless variables, the 1-D inert solution $\theta(\delta,\tau)$ and surface temperature θ_s are expressed as:

$$\theta(\delta,\tau) = 1 + 2\sqrt{\tau/\pi}\ \mathrm{ierfc}(\delta/\sqrt{4\tau}) \quad \text{and} \quad \theta_s = 1 + 2\sqrt{\tau/\pi} \tag{4-21}$$

It is found from previous work (Bradley, 1970; Vorsteveld and Hermance, 1987) that the argument of the ierfc function ranges between .1 and 5. In order to closely approximate a semi-infinite region, the contribution from the ierfc function must be kept sufficiently small. Here it

is set equal to 10^{-4} which corresponds to a value of 2.4 for its argument (Carslaw and Jaeger, 1959). This yields a direct relation between the approximate thermal penetration depth δ_{th} and the heating time τ. Upon eliminating τ, the depth of penetration δ_{th} is related to the specifiable surface temperature θ_s as:

$$\delta_{th} = 2.4\pi^{1/2}(\theta_s - 1) \tag{4-22}$$

Next, the domain size parameter ξ_o is determined from geometric considerations in terms of the estimated ignition temperature θ_s, whose value is primarily based on the selected A and E parameters.

$$\xi_o = \frac{2.4\pi^{1/2}(\theta_s - 1) - \gamma}{\sin(\phi_o/2)} \tag{4-23}$$

4.4 Computational Procedure

The entire ignition process is solved for each geometry via two independent sets of computer code. The first one generates the grid mesh, internodal spacings and computes an initial temperature distribution assuming negligible chemical heat release during the early phase of external heating. The validity of this approach has been demonstrated and used before by Bradley (1970), Liñán and Williams (1971, 1972) and Vorsteveld (1985). The second code integrates the full blown finite difference equations for each set of parameter A, B and E values.

Ignition results are calculated in an iterative fashion where several iterations are needed to narrow in on the bounds between extinction and ignition. Prior to flux removal, ignition is defined by a rapid rise in temperature, generally an order of magnitude larger than the corresponding inert temperature rise. Ignition after flux removal is assumed to have occured once $(\partial\theta/\partial\tau)_s$ becomes positive without simultaneous occurence of total reactant consumption. Extinction is assumed when either all reactants are consumed or the post heating surface temperature continues to decrease. Results reported in Chapter V have been computed using both the interrupted and continuous heating modes. Figure 4.6 shows the attainment of ignition for the square corner case using both the continuous and interrupted heating mode for a common set of parameters. Figure 4.7 displays the corresponding temperature profile curves, as well as the extinction curves, for the same parameter values but for the 45° acute wedge.

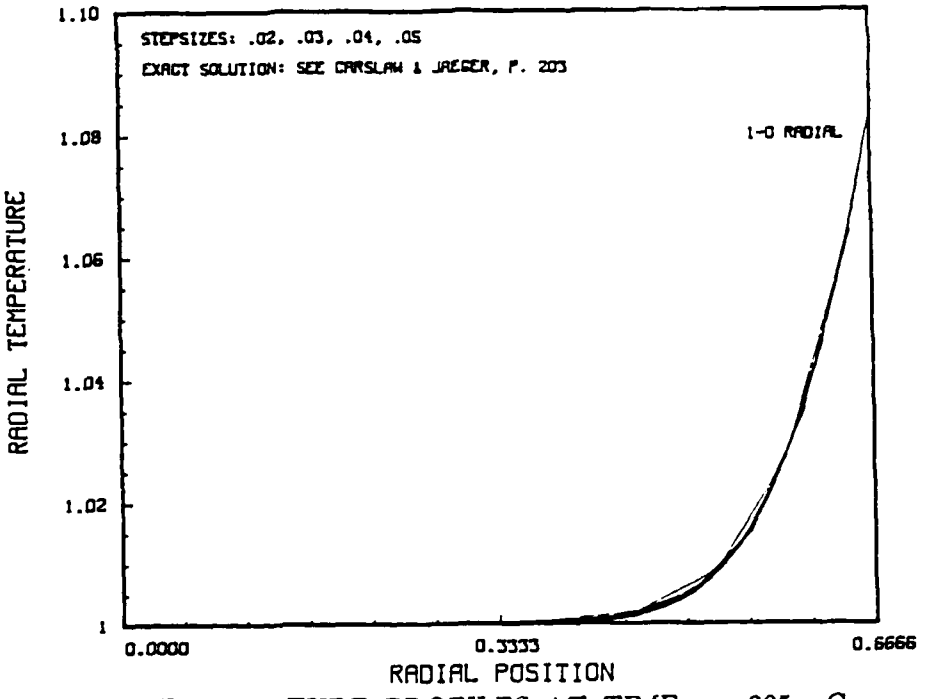

FIG. 4.1 INERT RADIAL TEMPERATURE PROFILES AT TIME = .005. Comparison between exact solution and acute angle code for Δr_o equal to .02, .03, .04 and .05.

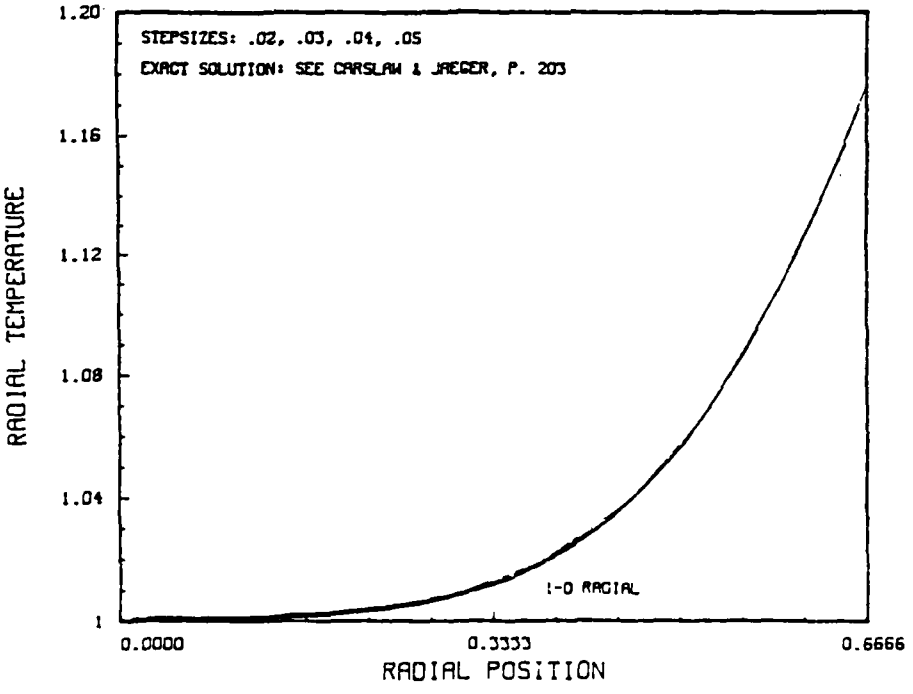

FIG. 4.2 INERT RADIAL TEMPERATURE PROFILES AT TIME = .02. Comparison between exact solution and acute angle code for Δr_o equal to .02, .03, .04 and .05.

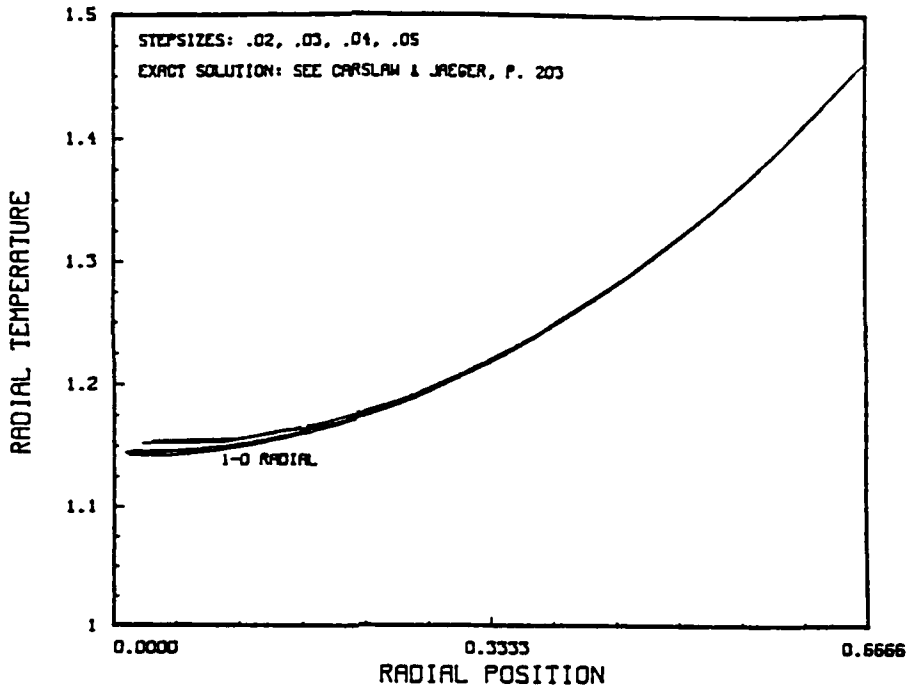

FIG. 4.3 INERT RADIAL TEMPERATURE PROFILES AT TIME = .1. Comparison between exact solution and acute angle code for Δr_o equal to .02, .03, .04 and .05.

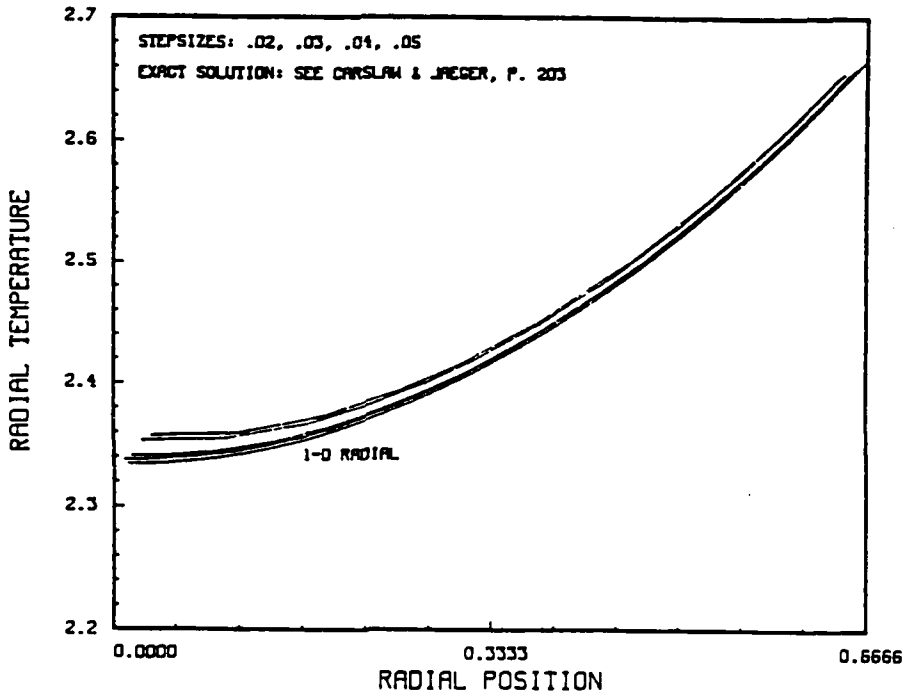

FIG. 4.4 INERT RADIAL TEMPERATURE PROFILES AT TIME = .5. Comparison between exact solution and acute angle code for Δr_o equal to .02, .03, .04 and .05.

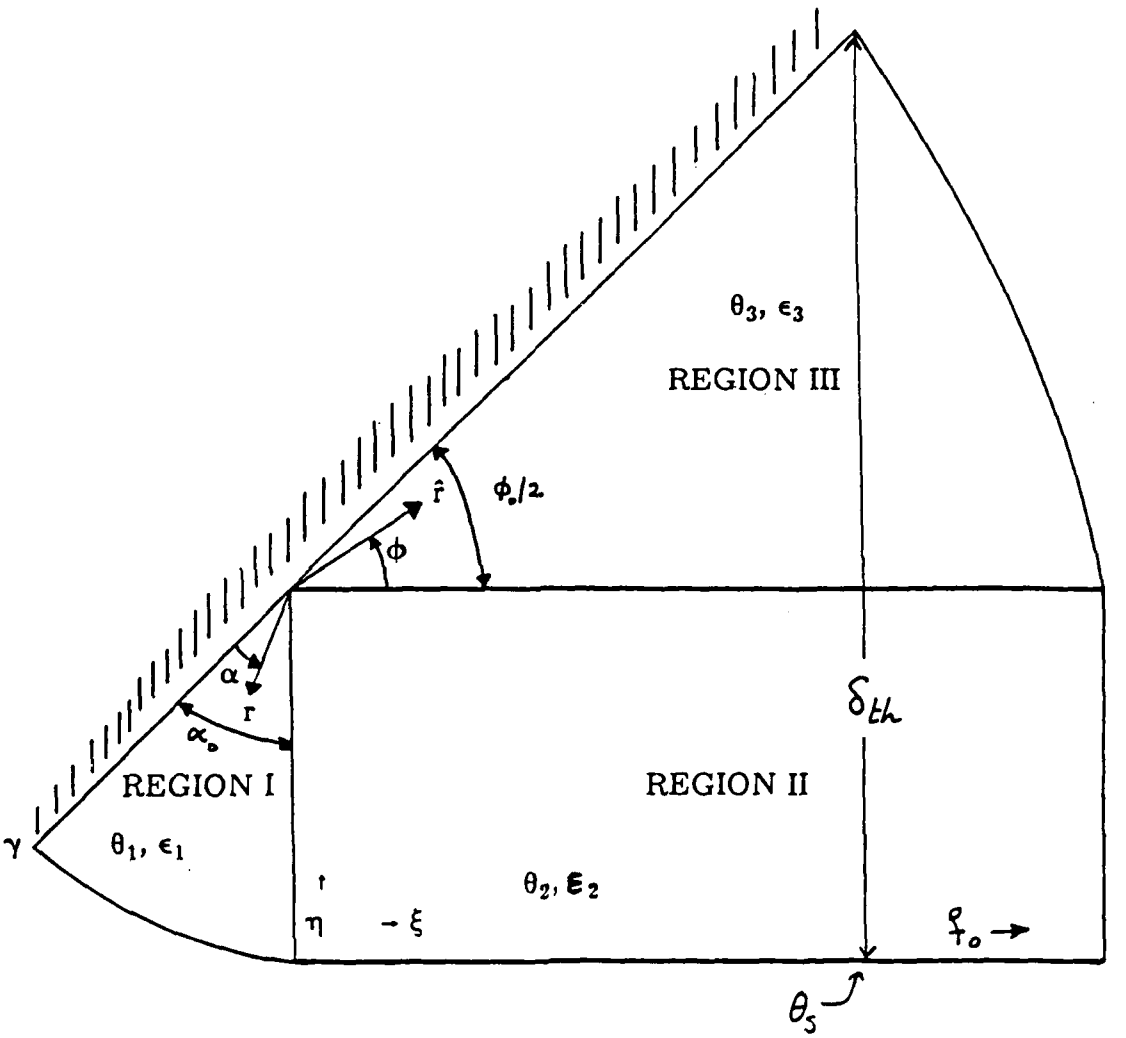

FIG. 4.5 COMPUTATION OF THE COMPOSITE DOMAIN PARAMETER. Approximate development of size parameter ξ_o for the rounded tip geometry; $\alpha_o = \pi/2 - \phi_o/2$, δ_{th} = 1-D thermal penetration depth based on surface temperature θ, as determined from the combination of A and E parameters; γ = rounding parameter.

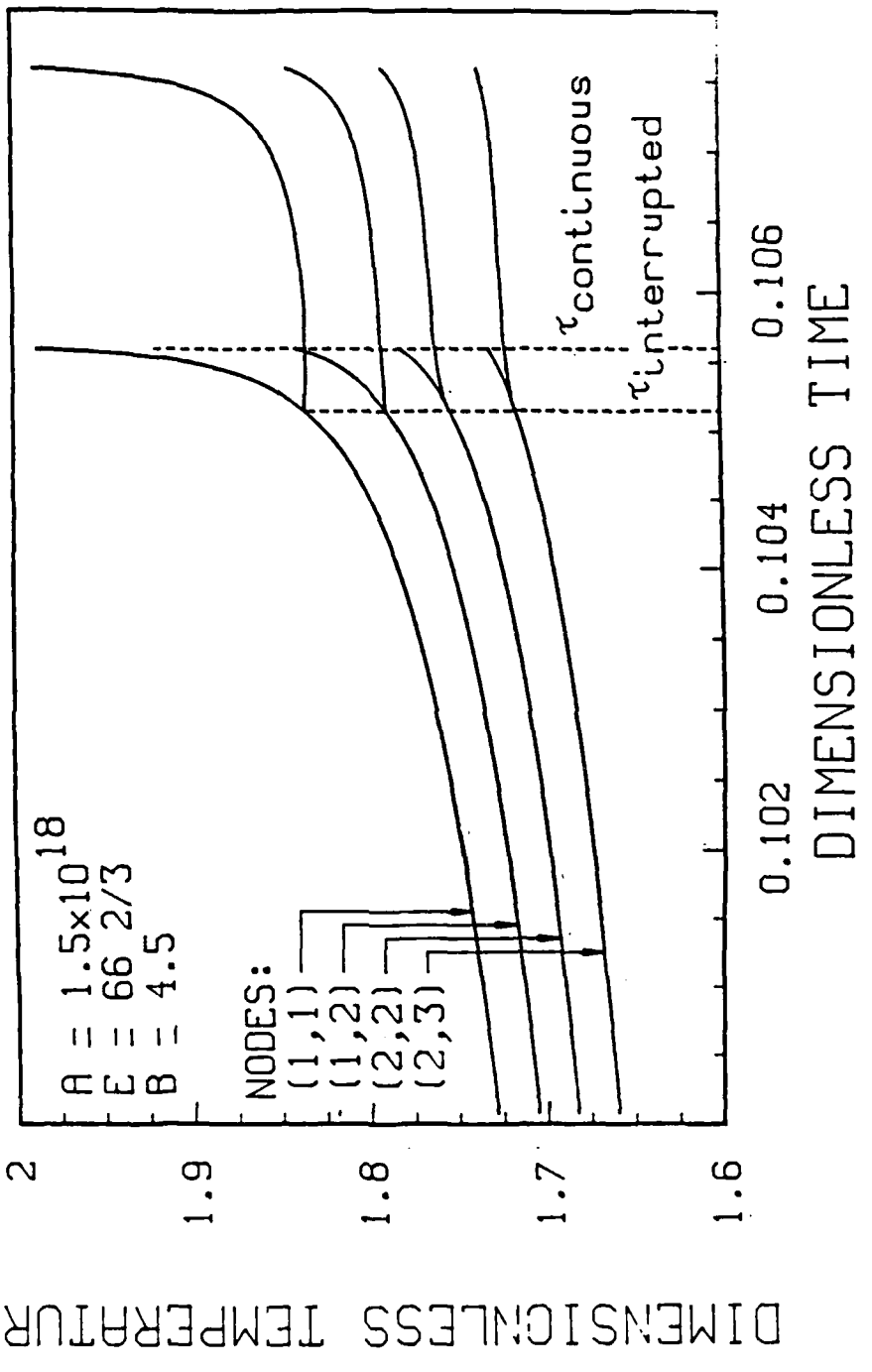

FIG. 4.6 TYPICAL TEMPERATURE PROFILES FOR SQUARE CORNER. The effect of the mode of heating (continuous vs interrupted) shown for a typical set of parameter values.

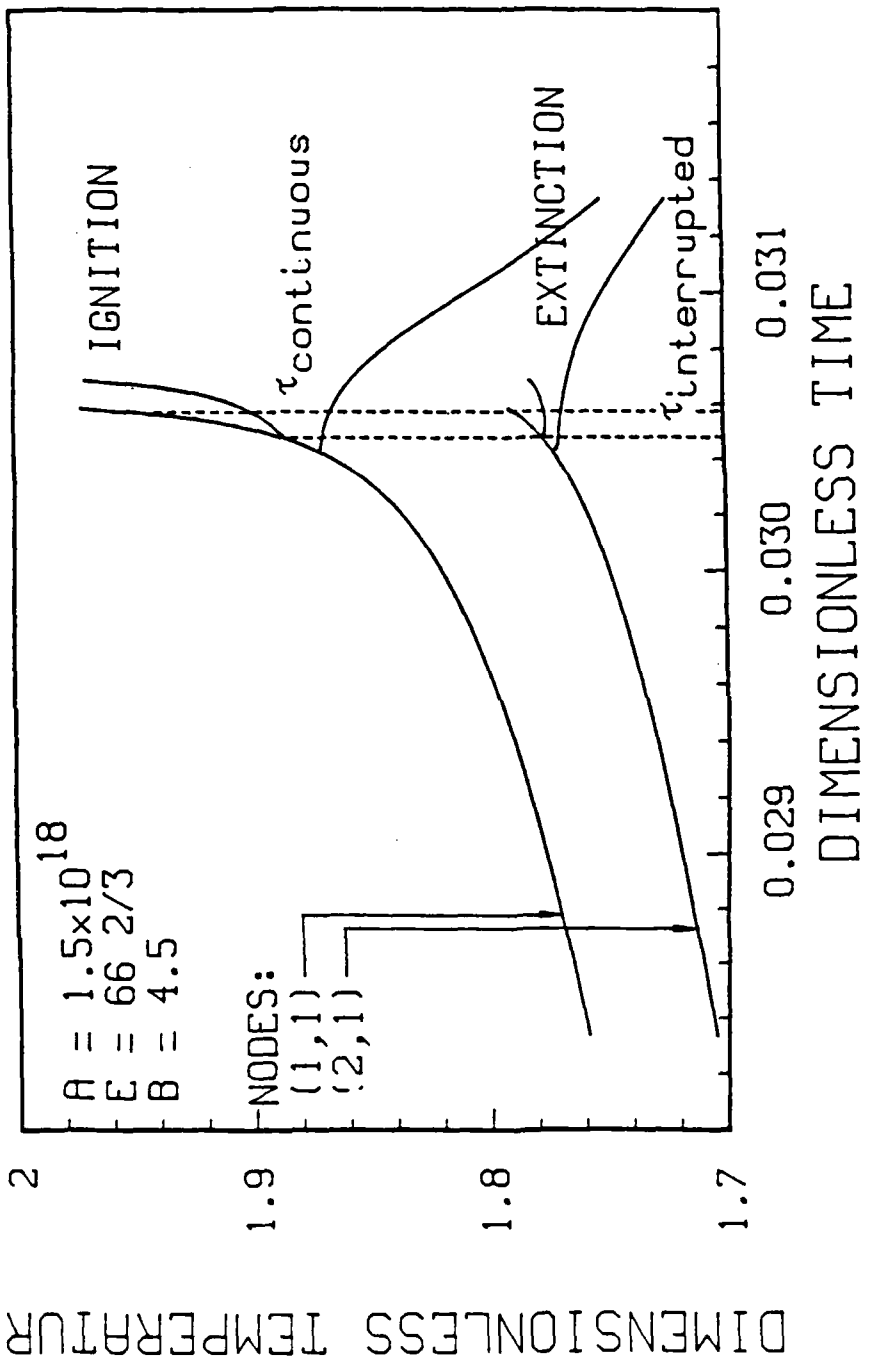

FIG. 4.7 TYPICAL TEMPERATURE PROFILES FOR THE ACUTE ANGLE. Interrupted, continuous and extinction temperature profile curves shown for the same parameter values. Note the increased nonlinearity due to the more acute geometry.

CHAPTER V

NUMERICAL RESULTS

5.1 Introduction

Theoretical aspects of the effect of geometry on the ignition behavior of reactive solids are presented and examined under three headings. First, numerical results are presented for each of the studied geometric configurations by means of graphs and correlation equations. Second, cross comparisons are performed using the present results to delineate and quantify geometric influences during the ignition process. Thirdly, current results are briefly compared to previous one dimensional work, which includes such effects as in-depth radiative absorption, thermal losses to an adjacent gas phase and surface versus distributed exothermicity. These comparisons may indicate possible avenues of model improvement for future study as well as aid in interpreting experimental data.

5.2 Present Model Results

The results reported below are all obtained using only the interrupted heating mode. In all cases the heated surfaces are mathematically considered to be insulated after flux removal (i.e. $\partial\theta_s/\partial n=0$) such that ignition is controlled by the thermal behavior of the nodes located near the high temperature surface. Several parameter sets have been solved using both continuous and interrupted heating to determine the sensitivity of the results on the selected ignition criterion. Ignition times computed for the continuous heating case exceed the interrupted heating data by less than 10 %. This difference in ignition delay for the two modes of heating is most significant for near one dimensional geometries and for those parameter values which correspond most closely to adiabatic explosion behavior.

System equations, presented in Chapter III, are solved using the following range in parameter values:

A= 10^8 to 10^{28}

E= 33 1/3, 50, 66 2/3, 83 1/3 and 100

B= 0.9 and 4.5

These values are arrived at by using the following values for the physical and chemical constants:

c= 1.547 kJ/kg-°K (.37 cal/gr-°K)

E= 83.6 to 250.8 MJ/kmole (20 to 60 kcal/mole)
k= .209 W/m-°K ($5x10^{-4}$ cal/cm-sec-°K)
q= 418 to $41.8x10^6$ W/m^2 (.01 to 10^3 cal/cm^2-sec)
Q= 669 or 3344 MJ/m^3 (160 or 800 cal/cm^3)
T_i= 300 °K
ν= $1.25x10^4$ to $6.25x10^{26}$ sec^{-1}
ρ= 1600 kg/m^3 (1.60 gr/cm^3)

Computed results consist of: τ_c, the ignition time; θ_c, the corresponding temperature at ignition; and ϵ_c, the extent of chemical reactivity at the moment of ignition. Ignition delays depend primarily on geometric factors ϕ_o and γ, and parameters A and E; the ignition temperature shows strong dependence on parameters A and E, but only a weak dependence on parameter B and geometric factors ϕ_o and γ. Fraction reacted ϵ_c depends on all factors.

5.2.1 Right Angle Corner

Major results for the sharp, 90° corner are shown in Figures 5.1 (B= 4.5) and 5.2 (B= 0.9) where the dependence of ignition time τ_c on parameter A is displayed parametric with several activation energy values. Crossdrawn on these figures are the critical fraction reacted ϵ_c and temperature θ_c as a result of the integrations. Comparison of these figures indicates two effects of parameter B on the ignition process. Smaller B values correspond physically to larger prefactors for the ratio (A/B) such that reactants are effectively consumed at a higher rate. By definition, ignition is deemed not to occur once all reactants have reacted as surface regression is not included in present model formulations. This inability to achieve ignition explains the abrupt ending of the curves for B= 0.9 in these figures. Secondly, parameter B only minimally infiuences the ignition time as the respective curves are practically identical.

Figure 5.3 shows the dependence of the temperature at ignition (θ_c) on parameter A for 5 activation energy values. Two physico-chemical aspects are apparent from these curves. Traversing vertically upward illustrates the not surprising notion of higher required temperatures for larger activation energy to attain ignition conditions. For a given set of physical and chemical properties, traversal along a particular activation curve indicates higher ignition temperatures with increasing flux levels; higher heating rates lead to steeper thermal subsurface gradients, thinner heated layers in the solid and therefore more rapid cooling after flux cessation. Thirdly, parameter B causes a small effect on the temperature at ignition only for large values for ϵ_c, where the suppression of the chemical heat release by reactant consumption

necessitates slightly higher temperatures to offset the reduced chemical heat release. Further aspects of these numerical results have been previously reported in great detail by Vorsteveld (1985) and Vorsteveld and Hermance (1987).

5.2.2 Sharp Wedge of Various Included Angle

Results have been computed for the same ranges in A, E and B with ϕ_o equal to $\pi/4$, and for the same range in A, B= 4.5 and E= 66 2/3 for ϕ_o equal to $\pi/8$. All computations are performed with the interrupted heating mode only, where ignition is based on the thermal behavior of the triangular nodes located in the extreme tip sector of the wedge shaped geometry. In general, tip temperature reductions, which exceed 5/E after flux removal, lead to extinction because of insufficient energy storage in the tip sector and rather steep thermal gradients in this region. The thermal field in the extreme tip is predominantly radial in nature because of the infinitely sharp tip representation. Ignition times computed using continuous heating exceed interrupted heating delay times by no more than 2% for these wedge angles.

Figure 5.4 displays numerical solutions of ignition time τ_c versus parameter A for the $\pi/4$ wedge angle for 5 activation energies. As before, curves of θ_c and ϵ_c are crossdrawn for a complete display of the numerical results. The dominant role of parameter B on the possible duration of the ignition process is again demonstrated for a given set of A and E parameter values as the ratio (A/B) controls the rate of consumption of reactants.

Dependence of the temperature at ignition on parameters A and E for the $\pi/4$ wedge angle is displayed in Figure 5.5. In addition to the two effects of parameter B on these curves addressed in section 5.2.1, a third aspect of increased parameter B sensitivity is portrayed by the reduced upper temperature for the large B value. In contrast to the square corner geometry where maximum temperatures θ_c's exceeded 4.5, they are limited to $\simeq$4.0 for the $\pi/4$ wedge as a result of total reactant depletion. This reduced range in temperature, for which ignition can occur, is explained by the geometric augmentation of the thermal field characteristics. The reduction of ϕ_o is accompanied physically by faster temperature rises as a result of enhanced exposure of the heated surfaces which augments the heat transfer behavior into interior regions. This geometric influence in turn leads to a highly localized site for chemical reaction which is manifested by an increased importance of the (1-ϵ) term in the energy equation. More rapid reactant consumption inhibits therefore the maximum attainable temperature. More in-depth discussions of geometric effects for these $\pi/4$ and $\pi/8$ wedge angles have recently been reported by Vorsteveld and Hermance (1988).

5.2.3 Rounded Tip With Variable Curvature and Angle

Extensive numerical solutions are obtained for a few selected geometric configurations and sets of E and B parameter values for the entire range in parameter A. Investigated combinations include: for ϕ_o equal to $\pi/2$: $\gamma = 2/3$, all E and B values, and $\gamma = .10$, E= 66 2/3, B= 4.5. For ϕ_o equal to $\pi/4$: E= 66 2/3 and both B values. In addition, a number of simulations have been performed for E= 50, ϕ_o equal to $\pi/2$ and $\pi/3$ for a range of γ values. For all cases the interrupted heating mode is used to determine the ignition characteristics in these composite domains.

The selection of these values for γ is based on practical rounding radii from experimental evidence (Baer and Ryan, 1965), practical flux levels (q) and typical solid propellant thermal conductivity values. The case of γ equal to 2/3 corresponds, for example, to a radius of curvature (R_o) of 25 μm and a flux level of 40 cal/cm^2-sec. Provided the product of qR_o remains constant, reported results are also applicable for other rounding radii (R_o) and heating levels.

General qualitative observations, based on the numerical simulations, include a lowered sensitivity of the results on the gridmesh characteristics, a longer post-heating induction period and reduced significance of reactant consumption on the ignition process. These aspects are not surprising as rounding of the solution domain leads to a diminishing influence of processes, originally exacerbated by the geometric acuteness.

Figure 5.6 displays ignition times τ_c versus log(1/A) for 5 activation energies E for the 90°, γ= 2/3 corner geometry. Crossplotted are curves of temperature (θ_c) and fraction reacted (ϵ_c) computed at the moment of ignition. For ϵ_c exceeding .60, ignition is generally unattainable as a rapid increase in temperature is inhibited by diminishing heat release rates as the fraction reacted ϵ rapidly approaches unity. Clear differences from previously presented figures include the extended nature of the curves in τ space, as well as higher values for the attainable temperature θ_c as shown by the cross plotted curves. Obviously, the introduction of rounding or smoothness to the square corner results in a lessened effect of parameter B on firstly, the possible range of ignition times and secondly, the range in temperatures as reactant consumption becomes less critical for both cases.

Further results from the rounded tip code are presented in Figure 5.7 where the variation of ignition temperature (θ_c) with parameters A and E is displayed for the rounded square corner case (γ= 2/3). The effect of reactant consumption is apparent from the slightly higher θ_c's for B= 0.9 at the upper portion of each activation energy curve. This extended range of parameter B, influencing temperatures at ignition, can be attributed to the rounding of the

corner which delocalizes and expands spatially the dominant region for ignition, in comparison to the sharp corner geometry. Secondly, higher maximum temperatures are apparent for B= 4.5 which can be explained by the delocalization of the site of high chemical reactivity as it reduces diffusive cooling effects after flux removal.

Results for other combinations of ϕ_o and γ will be presented and discussed in conjunction with the delineation of geometric and chemical effects as results for the various cases are compared. The interplay between the large scale geometric feature (ϕ_o) and small scale characteristic (γ) in terms of affecting ignition times depends primarily on the relative magnitude of the thermal wave penetration depth versus the rounding parameter γ. These aspects are further discussed when results for the different geometries are examined.

5.3 Correlation Equations

The primary result of present numerical integrations is the dependence of ignition time τ_c on system parameters A and E for different geometric configurations; values of temperature θ_c and fraction reacted ϵ_c at the moment of ignition are of secondary importance. The development of correlation expressions between results and system parameters is motivated for several reasons: 1) to enable easy reproduction of complex model results, 2) to provide alternative means of comparison to other results, and 3) to indicate physical effects or trends which are not apparent from graphs.

The development of correlation equations for the ignition time τ_c is based on the asymptotic solution derived by Liñán and Williams (1971) for the one dimensional case. The general approach consists of substituting the relation between the inert surface temperature in terms of the heating time τ_c, for each wedge shaped geometry (γ=0), into their derived correlation expression. Different wedge angles are selected by changing the value of constant C_2. An additional constant (C_1) is determined for each geometry by numerical experimentation (Hermance and Vorsteveld, 1987). Equation (5-1) the general correlation expression which relates the ignition time τ_c to system parameters A and E. Proper numerical values for matching constant C_1 and geometric constant C_2 are tabulated in Table 5.1.

$$A = C_1 E^{1/2}(\pi\tau_c)^{-1/4}[1+C_2\sqrt{(\tau_c/\pi)}]^{-1} e^{E/(1+C_2\sqrt{(\tau_c/\pi)})} \qquad (5\text{-}1)$$

TABLE 5.1		
CORRELATION FACTORS		
ϕ_o	C_1	C_2
180	.65	2
90	6	4
45	12	8
22.5	24	16

Comparison with numerical integrations shows that this correlation expression computes ignition times within 4% for all investigated wedge angles. Ignition delay times (τ_c) for other included angles (ϕ_o) are readily computed by interpolating the corresponding values for the adjustable constants C_1 and C_2.

Inspection of the figures, which show numerical solutions for the different geometries, indicates that the temperature at ignition (θ_c) is virtually constant for a specific ignition time (τ_c). Further examination indicates the existence of an approximate correlation between the temperature at ignition and ignition time, to a large degree independent of system parameters A and E, for each specific geometric configuration. For the wedge angled cases (γ=0), this relation is expressed within a $\pm$ 5 % error range by the general expression:

$$\theta_c = 1 + \alpha\sqrt{\tau_c} \tag{5-2}$$

where α is equal to 1.3, 2.57, 5.24 and 9.94, and ϕ_o is equal to π, $\pi/2$, $\pi/4$ and $\pi/8$ respectively. Increased acuteness of the angle ϕ_o is directly responsible for the faster temperature rise and accompanying reduction in ignition time. Figure 5.8 shows numerical results of ignition temperature versus ignition time for 3 acute wedge angles and different activation energies. Although the computed data exhibit a small dependence on the activation energy, it is clear from this figure that geometric aspects dominate the dependence between ignition temperature and delay times.

Eqs. (5-1) and (5-2) allow quick calculation of the ignition time τ_c and ignition temperature θ_c for a specified set of physico-chemical property values and applied flux level for different acute geometries. A knowledge of the one dimensional ignition time for a particular propellant formulation can provide an estimate of its ignitability when a specified propellant shape is

exposed to identical stimuli conditions. This conclusion, contingent upon the dominant mechanism during the actual ignition process, is based on small observed variations in ignition temperature for different geometries for a given set of A and E values. Further details are discussed in section 5.4.2.

5.4 Comparisons Between Different Geometries

In the following sections the effects of geometry are determined, within the framework of the present solid phase ignition mechanism, in terms of its effects on ignition time, ignition temperature, extent of chemical reactivity and how propellant geometry affects the dependence of dimensional ignition time on the applied heat flux. These comparisons are mainly done in a graphical manner with comments added to explain observed physical phenomena.

5.4.1 Geometry Effects on Ignition Time

Dimensionless ignition times are shown in Figure 5.9 as a function of parameter A for a variety of geometric configurations for E= 66 2/3. Not surprisingly, more acute angles ignite faster in a nearly uniform fashion. The effect of rounding the wedge angle clearly modifies the ignition behavior as parameter A decreases. At small τ_c's, which correspond to low external heating rates, and, at constant γ to large radii of curvature, the presence of rounding makes any sharp edge behave as a near planar surface, as in this region the material exhibits some adiabatic explosion characteristics. However, this aspect is not present for the sharp edges as the extreme acuteness for any applied heat flux results in more rapid ignition. Behavior on the other side of the spectrum is explained by noting that flux levels are several orders of magnitude larger, rounding radii (R_o) are reduced by the same order of magnitude and the dimensionless rounding radius (γ) forms only a small fraction of the total thermal wave penetration depth. In this region the importance of the rounding is clearly reduced and ignition times are primarily based on the overall acuteness of the protruding surface. The curves for γ equal to .1 and 2/3 clearly display the shift in governing behavior which exists between the geometric parameters ϕ_o and γ with decreasing parameter A.

Figure 5.10 displays the ratio of ignition delays for semi-infinite and semi-infinite 90° corners, both relative to 45° sectors as a function of parameters A and E. Clearly, the sharp 45° wedge ignites 3 to 4 times faster than the square corner (Vorsteveld, 1985; Vorsteveld and Hermance, 1987), 6 to 12 times faster than the planar case (Bradley, 1970).

The vertical positioning of the activation energy curves is explained by considering the inert heating process and the increasing degree of nonlinearity for larger activation energies. For inert heating to a particular temperature level, this heating ratio computes readily as 4.0 for each halving of the enclosed wedge angle. Reactive curves at high activation energy approach more closely this inert heating ratio as a result of a longer portion of the heating being characterized by the heating of a simple inert solid.

Individual E curves appear to converge as A approaches zero which implies infinite heating rates. Physically the chemical reaction time becomes very small here and increasingly independent of the activation energy E and geometric parameter ϕ_o. A nearly constant geometric effect on ignition times is observed for large A values (low heating rates). Therefore, the geometric augmentation of the ignition process remains constant for these acute configurations, even at extremely low heating rates. Ignition delay ratios reduce for the upper curves with increasing A, indicating the onset of homogeneous explosion phenomena for the planar geometry. At sufficiently small heating rates the effect of geometry diminishes, which removes the effect of solid heat conduction such that, in the limit, the respective E curves intersect the unity ratio line.

Rounding an otherwise acute angle ($\gamma = 2/3$) produces delayed onset of ignition. Figure 5.11 shows the quantitative effect of rounding a 90° corner geometry in terms of the ratio of ignition times for rounded to acute corners. Large scale geometry primarily controls ignition times for small values of A as these correspond to long heating times τ_h, deep thermal wave penetration which results in this delay ratio approaching unity. Conversely, this ratio has its maximum value for large A as thermal penetration depths are much smaller and rounding becomes rather dominant. The staggering of the activation energy curves is explained by observing that upon vertical traversal for a particular A value, corresponding ignition times τ_c increase with increasing activation energy. And, since the ignition process for large τ_c shifts from small scale to large scale geometric control, the delay ratio decreases for larger activation energy. The reduction in ignition delay ratio for small E and large A is a result of increased adiabatic chemical heat release which, in the limit, completely removes the effect of thermal diffusion (Frank-Kamenetskii, 1955).

A similar comparison is reported by Vorsteveld and Hermance (1987) and discussed above in Figure 5.10 for the ratio of ignition times for one dimensional slabs to 90° square corners. Staggering of individual activation energy curves occurs there in reverse order which is attributed to purely chemical phenomenon, as explained before, compared to the present geometric explanation. Onset of homogeneous explosion phenomena for small activation energy

and large parameter A values is reported both for square corners and the planar surface (Bradley, 1970; Vorsteveld and Hermance, 1987).

5.4.2 Geometry Effects on Ignition Temperature

As remarked in prior instances, an intricate interplay exists between the thermal field characteristics on one side, governed primarily by the geometry of the solution domain, and the chemical nature of the reactive solid on the other side, as specified by parameters A and E. Small and large scale geometry effects are further illustrated in Figure 5.12, where the dependence of θ_c on parameters A and E is shown for different geometries.

Ignition temperatures increase from rounded to sharp wedges as the latter cases exhibit faster temperature rises, steeper gradients and hence, more rapid cooling after flux cessation. Higher temperatures are required to overcome this geometrically induced thermal energy diffusion effect. Secondly, maximum attainable temperatures are significantly lowered for acute wedges as highly localized ignition consumes reactants more rapidly. Ignition is not possible anymore once all reactants at the exposed tip are consumed. Thirdly, the increased temperature sensitivity of the chemical heat release for larger activation energy is visible from the reduced variation in θ_c for the various geometries at any particular temperature level. If the ignition process is rate controlled by a solid phase, high activation energy reaction, then ignition temperatures are less sensitive to thermal field variations, caused by geometry, because of this increased nonlinearity of the chemical heat release. Finally, only a minimal effect of the wedge angle ϕ_o on the ignition temperature is observed for a given degree of rounding. Lower ignition temperatures for ϕ_o equal to $\pi/4$ compared to the $\pi/2$ case at high θ_c's or long heating times τ_h's are explained by noting that, for smaller wedge angles, the tip rounding occupies a larger cylindrical area. The thermal field contains, relatively speaking, a higher proportion of small scale rounding versus large scale acuteness at smaller wedge angles. Secondly, since the thermal wave does not penetrate as deeply for more acute angles, it further enhances the small scale smoothness contribution to the overall ignition process.

An alternate approach to illuminate geometric effects is to plot the temperature at ignition θ_c versus ignition time τ_c. Curves shown in Figure 5.13 display results for ϕ_o equal to π, $\pi/2$ and $\pi/4$ with the rounding parameter γ being equal to 0, .10 and 2/3. Increased acuteness of ϕ_o for $\gamma = 0$ is directly responsible for the faster temperature rise and corresponding reduction in ignition time since the effective heating rate is inversely proportional to the included wedge angle. In dimensional variables, Carslaw and Jaeger (1959) give the temporal inert

surface temperature T_s at a constant applied flux q_{eff} for the planar case:

$$T_s(t) = T_i + \frac{2q_{eff}}{(\pi\rho kc)^{1/2}}\sqrt{t} \qquad (5\text{-}3)$$

The corresponding inert surface temperature for different acute wedge angles ϕ_o without rounding is obtained by direct geometric augmentation of the applied heat flux via:

$$q_{eff} = \frac{\pi q}{\phi_o} \qquad (\phi_o \text{ in rads.}) \qquad (5\text{-}4)$$

The extent of rounding radius γ affecting ignition behavior depends clearly on the interplay between the duration of heating (τ_c) and magnitude of γ. For γ equal to 2/3, near planar behavior at small ignition times changes gradually with longer heating times to account for the acuteness of the solution domain. For γ equal to .10, the thermal wave penetrates even at early times significantly beyond the rounding radius γ such that ignition characteristics are more closely related to sharp tip behavior.

5.4.3 Geometry Effects on Reactant Consumption

Reactant consumption levels (ϵ_c's) influence the ignition process in two ways: first, they determine whether ignition will occur at all, and secondly, they have a small effect on the ignition temperature at high levels of reactivity. Figure 5.14 shows the typical dependence of the fraction reacted at ignition ($=\epsilon_c$) on parameter A, for E= 66 2/3 for various geometries.

A more than five-fold increase in ϵ_c is observed upon reducing parameter B by a factor of 5. Proportionally additional material is needed for the smaller B value to achieve ignition in order to overcome the reduced chemical heat release caused by the reduction of the (1-ϵ) term. Previously reported higher ignition temperatures for high levels of ϵ_c's are attributed to the same phenomenon.

Rounding acute angles is clearly accompanied by a reduction in critical fraction reacted. Interestingly, lower ϵ_c levels are computed for more acute ϕ_o angles as proportionally more rounded surface area is exposed to the applied heat flux which effectively delocalizes the ignition process. This in turn extends the possible range of ignition within the context of the current model formulation. Inclusion of convective transport will certainly affect present results, especially at elevated fraction reacted levels, which should not be ignored as stipulated by Hermance (1984). It must be noted that comparison to the sharp angled cases is somewhat

skewed by the gridmesh system employed. For instance, the extreme tip node for the square corner case experiences applied heating from two sides whereas the corresponding node for the sharp $\pi/4$ and $\pi/8$ cases is heated only from one side.

5.4.4 Dimensional Ignition Time Dependence on Heat Flux

To compare present results to experimental data, plots of $\log(A\tau_c)$ versus $\log(1/A^{1/2})$ are directly proportional to the typical logarithmic experimental plots of ignition time (t_{ign}) versus heat flux (q). Figure 5.15 shows theoretical curves for activation energy E equal to 66 2/3 for the different geometries under consideration. First, for strictly acute angles (γ=0), the speed-up in ignition delay for more acute angles is nearly uniform over the applied flux range. This means that, at any flux level, geometric augmentation of the 1-D ignition results can be anticipated. This ignition delay speed-up can theoretically exceed one dimensional predictions by more than one order of magnitude.

With respect to the rounded corner cases, it must first be noted that the dimensional radius of curvature R_o changes inversely proportional to the applied heat flux. Large values for A correspond to low heating rates and large radii of curvature; small values for A on the other hand indicate high flux levels and small radii of curvature, for a constant held value for γ.

At low heating rates (large A), the magnitude of γ is much more important than the overall wedge angle ϕ_o in affecting ignition times. It was observed in the numerical computations that at these A values the thermal penetration depth at the moment of ignition is of comparable magnitude to the rounding parameter γ equal to 2/3. Conversely, at small A or high rates of heating, the large scale geometric character of the domain (ϕ_o) influences ignition times significantly more than the rounding parameter γ. This is demonstated by faster ignition for the $\phi_o = \pi/4$, $\gamma = 2/3$ case compared to the sharp $\pi/2$ case. In these computations, the thermal wave consistently penetrated the solution domain by more than one order of magnitude beyond the rounding radius γ at the moment of ignition. The overall effect of rounding is clearly to moderate the extreme speed up in ignition observed for the highly acute wedge angles.

Slope values, computed from Figure 5.15 and similar curves for other activation energies, are compiled in Table 5.2. It should be noted that these values are based on a constant γ but changing R_o dimension. These slope values exhibit only minor variation with respect to the geometric features ϕ_o and γ; the more negative values for a given activation energy

correspond to the rounded tip cases. This data clearly shows that slope values are primarily influenced by the activation energy of the solid phase reaction and only minimally by the geometric features of the solid region.

TABLE 5.2

Theoretical Slopes of Ignition Time versus Flux Curves

Activation Energy	minimum	maximum
33 1/3	-1.50	-1.57
50	-1.67	-1.72
66 2/3	-1.75	-1.79
83 1/3	-1.80	-1.83
100	-1.84	-1.86

These slope values are frequently employed to identify mechanistic steps during the ignition process of practical propellant formulations. In an experiment, all edges are probably rounded to some degree, and the data in Table 5.2 indicates that the presence of a slope $>$ -2.0 is not necessarily indicative of ignition mechanisms other than solid phase reaction. Conversely, similar slope values may occur in cases where a major portion of the ignition transient is characterized by solid phase heating, although ignition itself is definitely controlled by a rapid gas phase heat release. These aspects are further addressed in Chapter VI during the discussion of experimental observations.

Present numerical results can be briefly compared to other solid phase theoretical work, where additional effects are incorporated. Figure 5.16 shows a map of ignition time τ_c versus log(1/A) for the 66 2/3 activation energy. One dimensional curves are computed using correlation equations presented in the literature survey. Clearly, inclusion of a conductive heat loss effect or in-depth radiative absorption modifies and retards the theoretical onset of ignition significantly. In effect, based on these curves, it appears just as important for improved theoretical ignition predictions, to have semi-quantitative knowledge of the extent of surface heat loss and in-depth radiative absorption versus knowing the geometric details of the propellant surface. No quantitative statements can be made at this point concerning the effects of these factors on ignition behavior of reactive solids in multi dimensional geometries.

Qualitatively, the extent of these effects can be approximately assessed based on a knowledge of their respective significance and effects in planar cases. Experimental work in Chapter VI will report on the practical extent of geometric effects during the ignition process.

Numerical solutions to a solid phase ignition model, concerned with geometric aspects on the ignition process, predict significant speed up in ignition times when a surface is convex to the applied stimulus. For infinitely sharp wedges, ignition proceeds approximately three times faster with each halving of the enclosed angle. Introduction of rounding cuts back drastically on the rapidity of ignition; however, the effect of non planar surfaces produces, within the present model formulation, a non-negligible factor which must be further investigated as it could be employed as a means of more reliable igniter transfer in marginal ignition cases or as a viable approach of achieving faster ignition in presently functioning igniter systems.

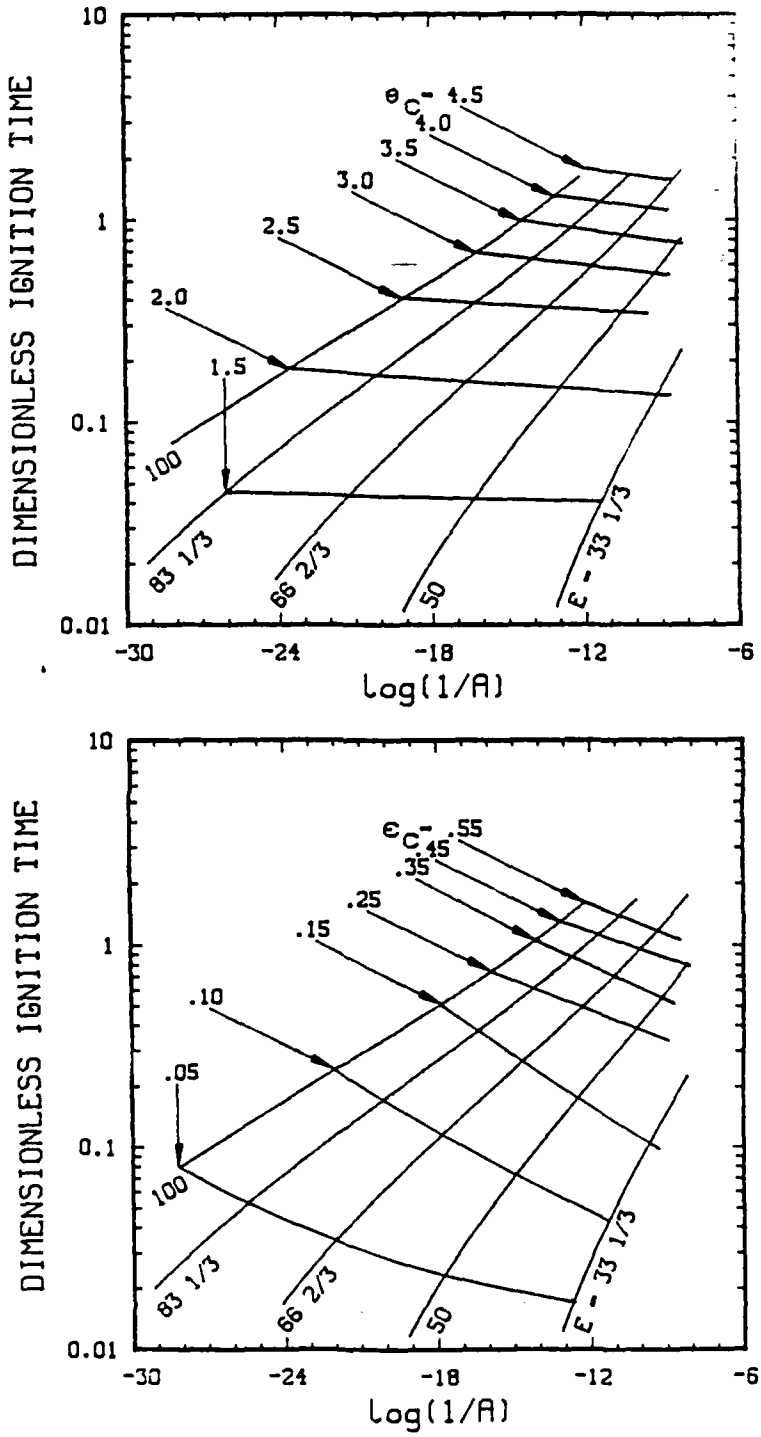

FIG. 5.1 SQUARE CORNER RESULTS: IGNITION DELAY TIMES. Ignition delay τ_c vs log(1/A) for 5 activation energies, B= 4.5; θ_c and ϵ_c curves included.

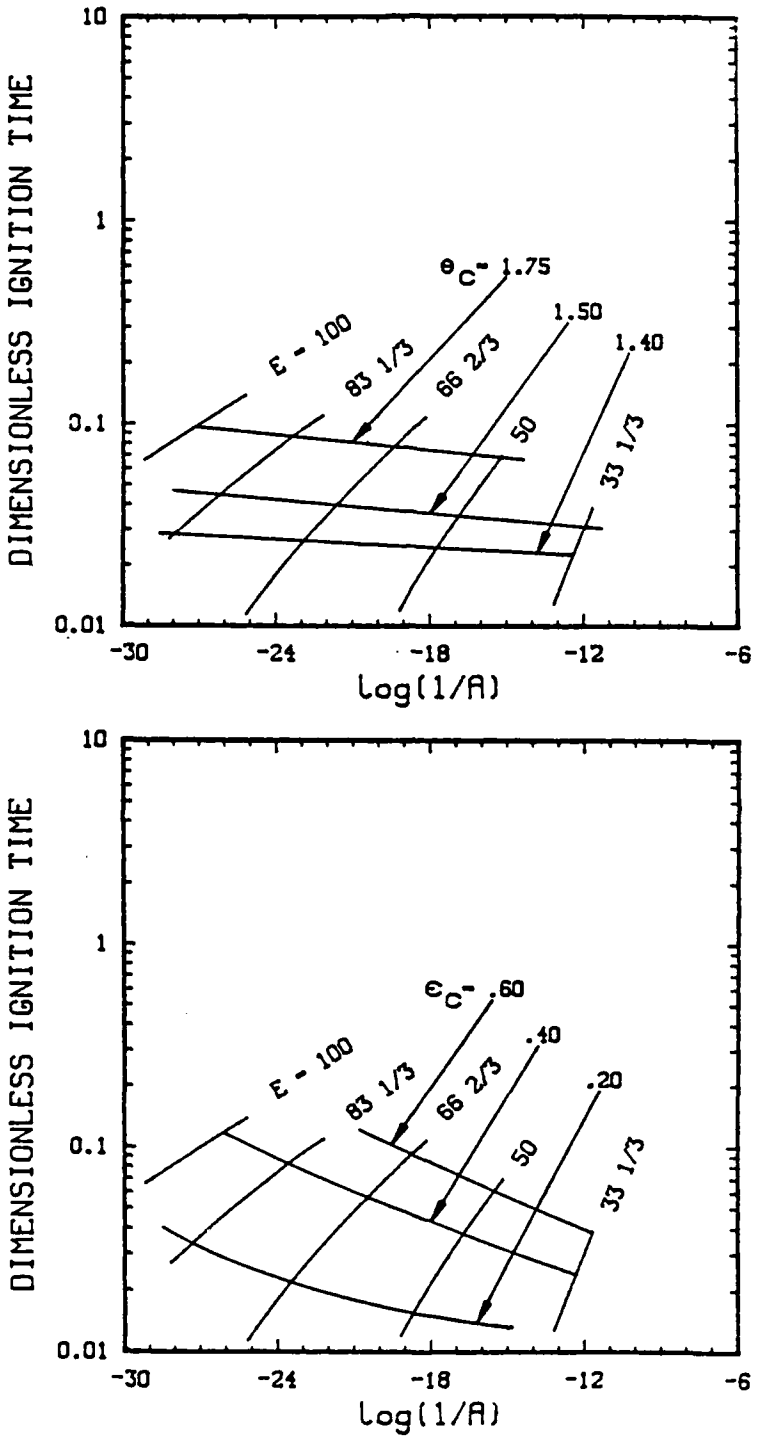

FIG. 5.2 SQUARE CORNER RESULTS: IGNITION DELAY TIMES. Ignition delay τ_c vs log(1/A) for 5 activation energies, B= .9; θ_c and ϵ_c curves included.

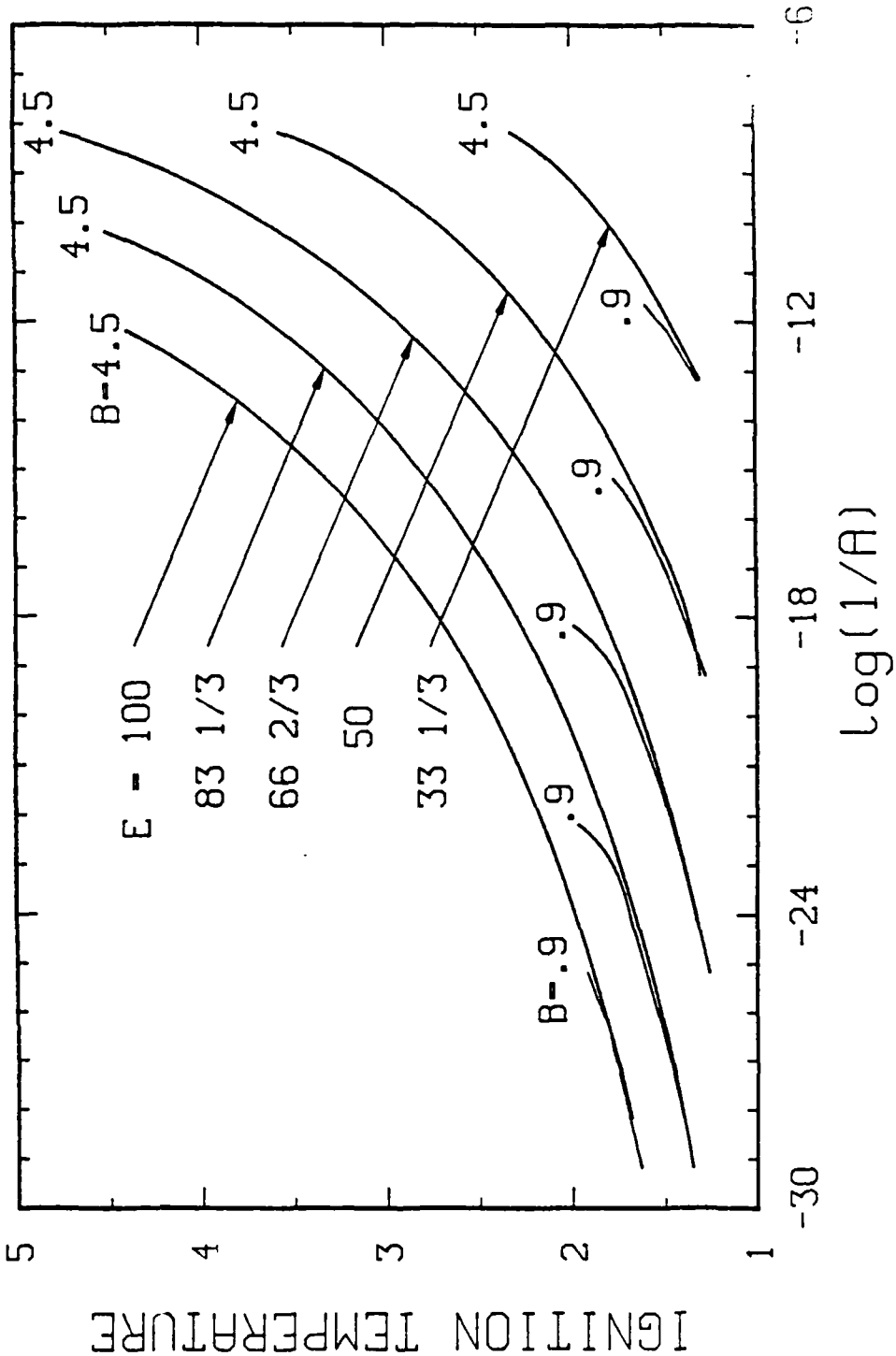

FIG. 5.3 SQUARE CORNER RESULTS: IGNITION TEMPERATURES. Ignition temperature θ_c vs log(1/A) for constant activation energy E, B equal to 4.5 and .9.

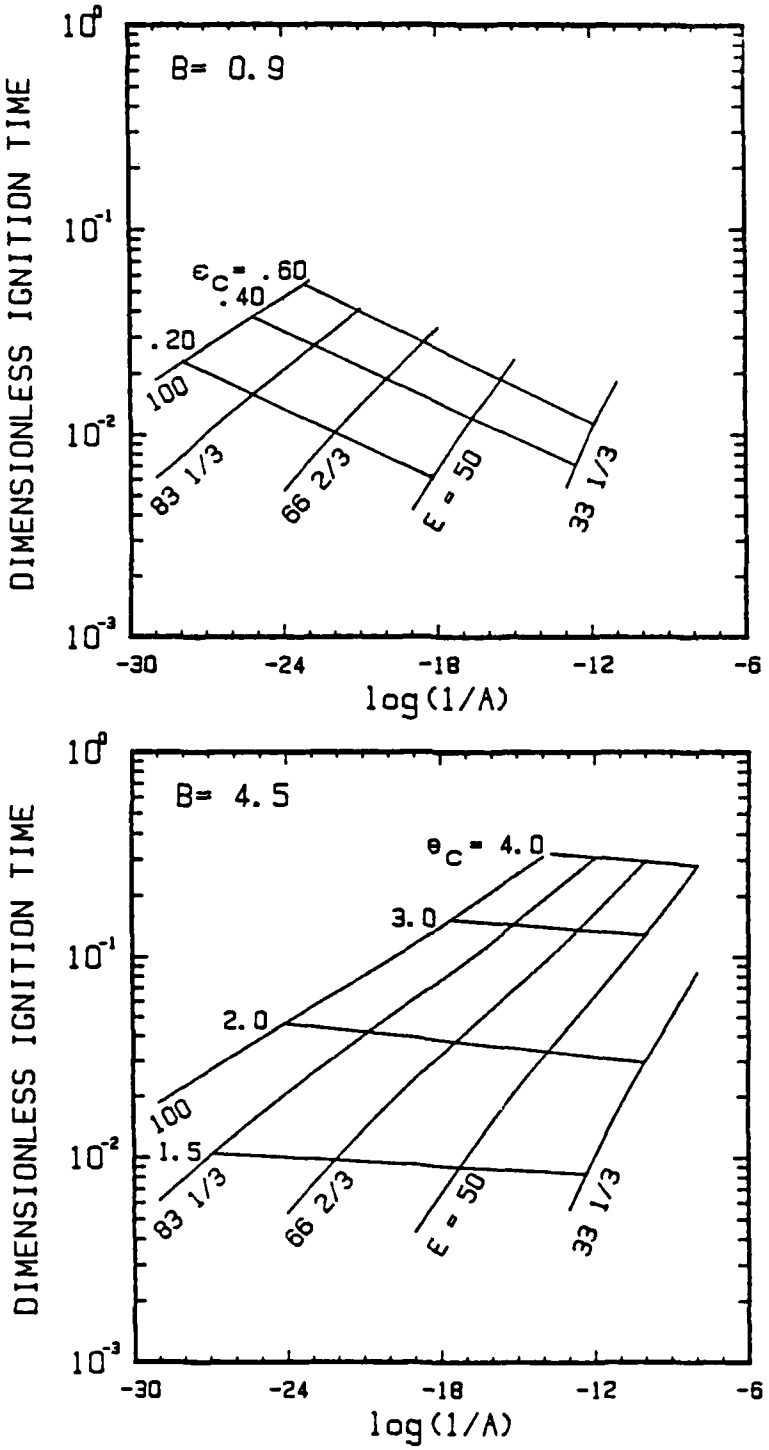

FIG. 5.4 ACUTE (45°) WEDGE RESULTS: IGNITION DELAY TIMES. Ignition delay τ_c vs log(1/A) for 5 activation energies, B= 4.5 and .9, θ_c and ϵ_c curves included.

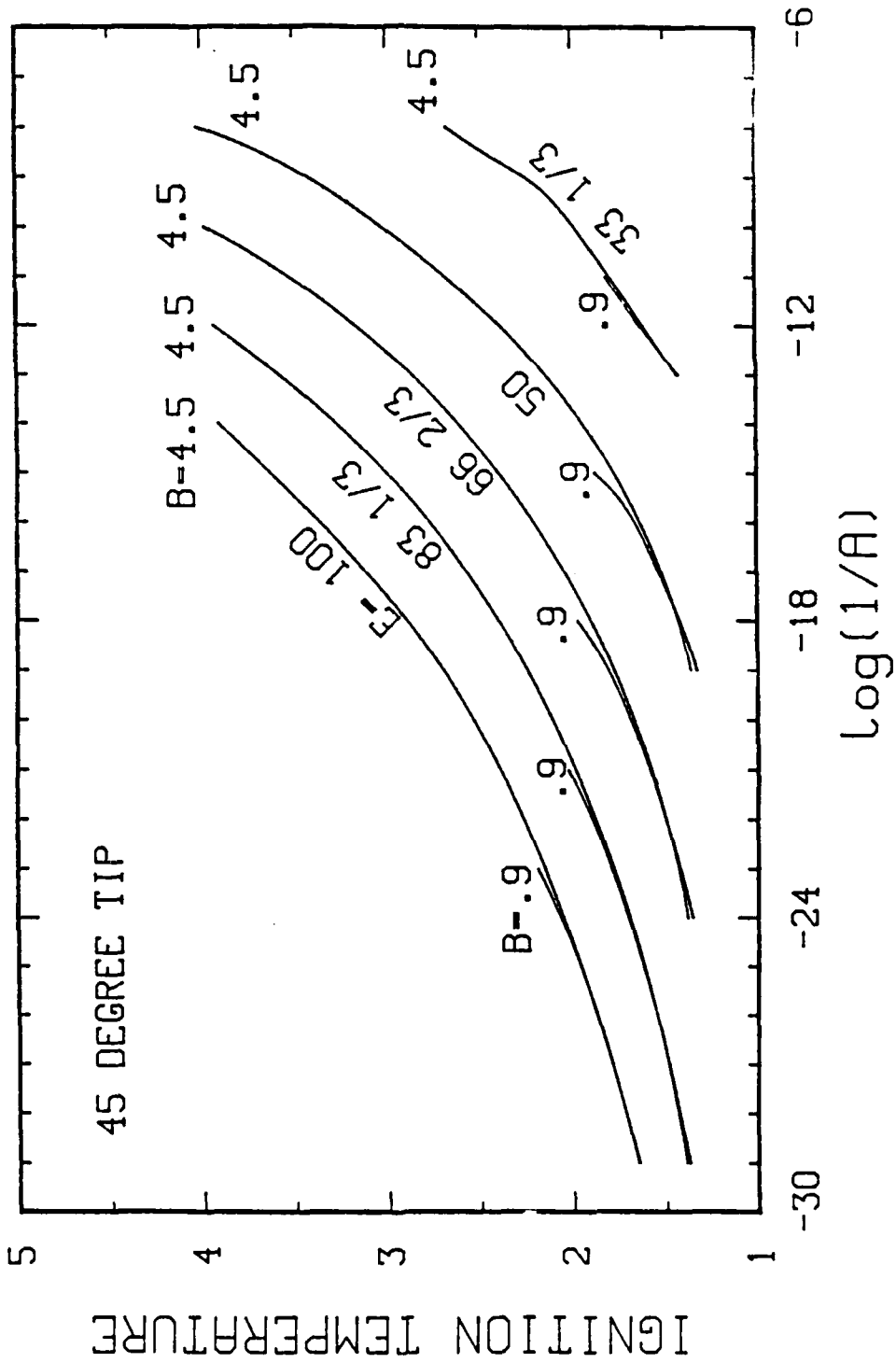

FIG. 5.5 ACUTE (45°) WEDGE RESULTS: IGNITION TEMPERATURES. Ignition temperature θ_c vs log(1/A) for 5 activation energies, B equal to 4.5 and .9.

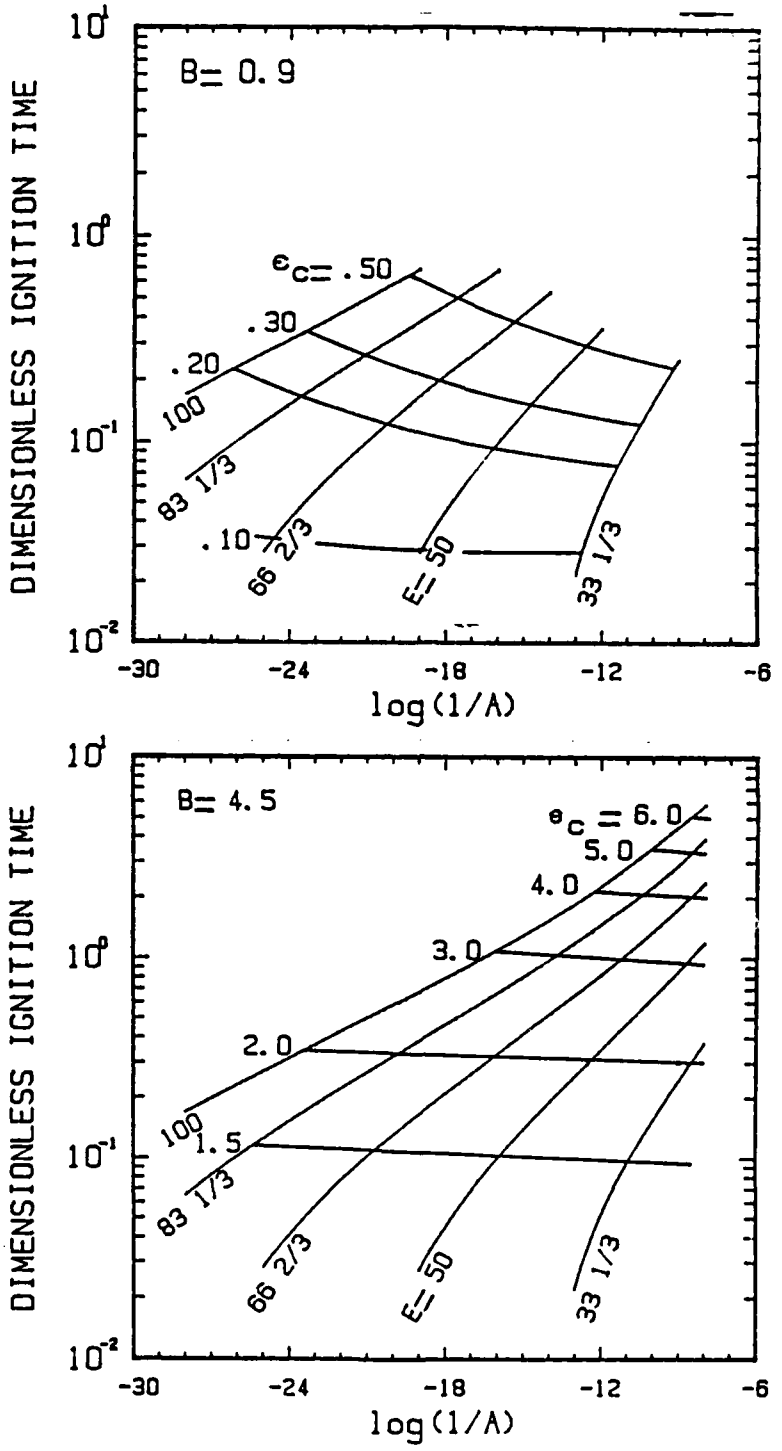

FIG. 5.6 ROUNDED TIP RESULTS: IGNITION DELAY TIMES. Ignition delay τ_c vs $\log(1/A)$ for the $\phi_o = \pi/2$, $\gamma = 2/3$ geometry with parameter B equal to .9 and 4.5; θ_c and ϵ_c curves included.

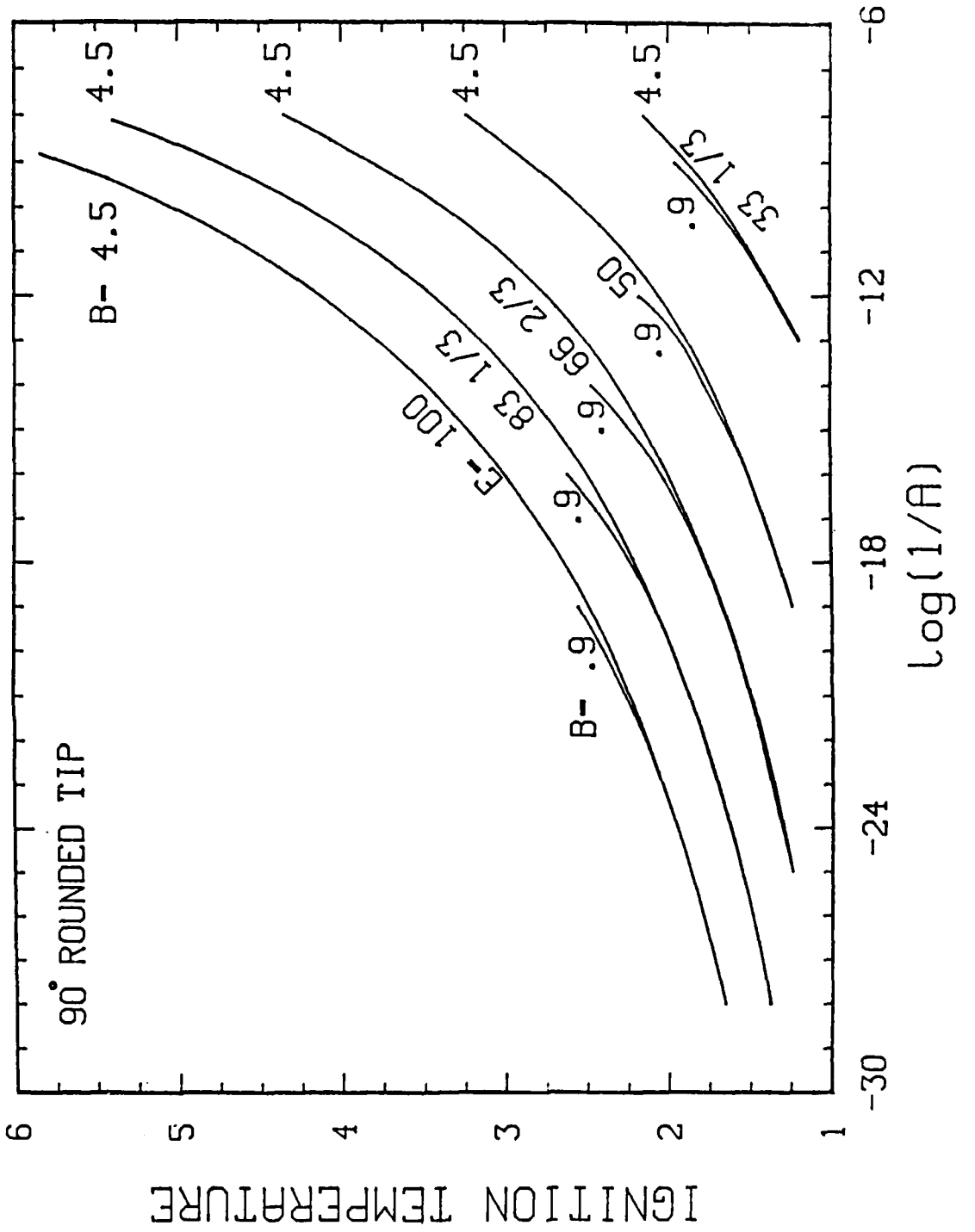

FIG. 5.7 ROUNDED TIP RESULTS: IGNITION TEMPERATURES. Ignition temperature θ_c vs log(1/A) for 5 activation energies, B equal to 4.5 and .9, and the $\phi_o = \pi/2$, $\gamma = 2/3$ geometry.

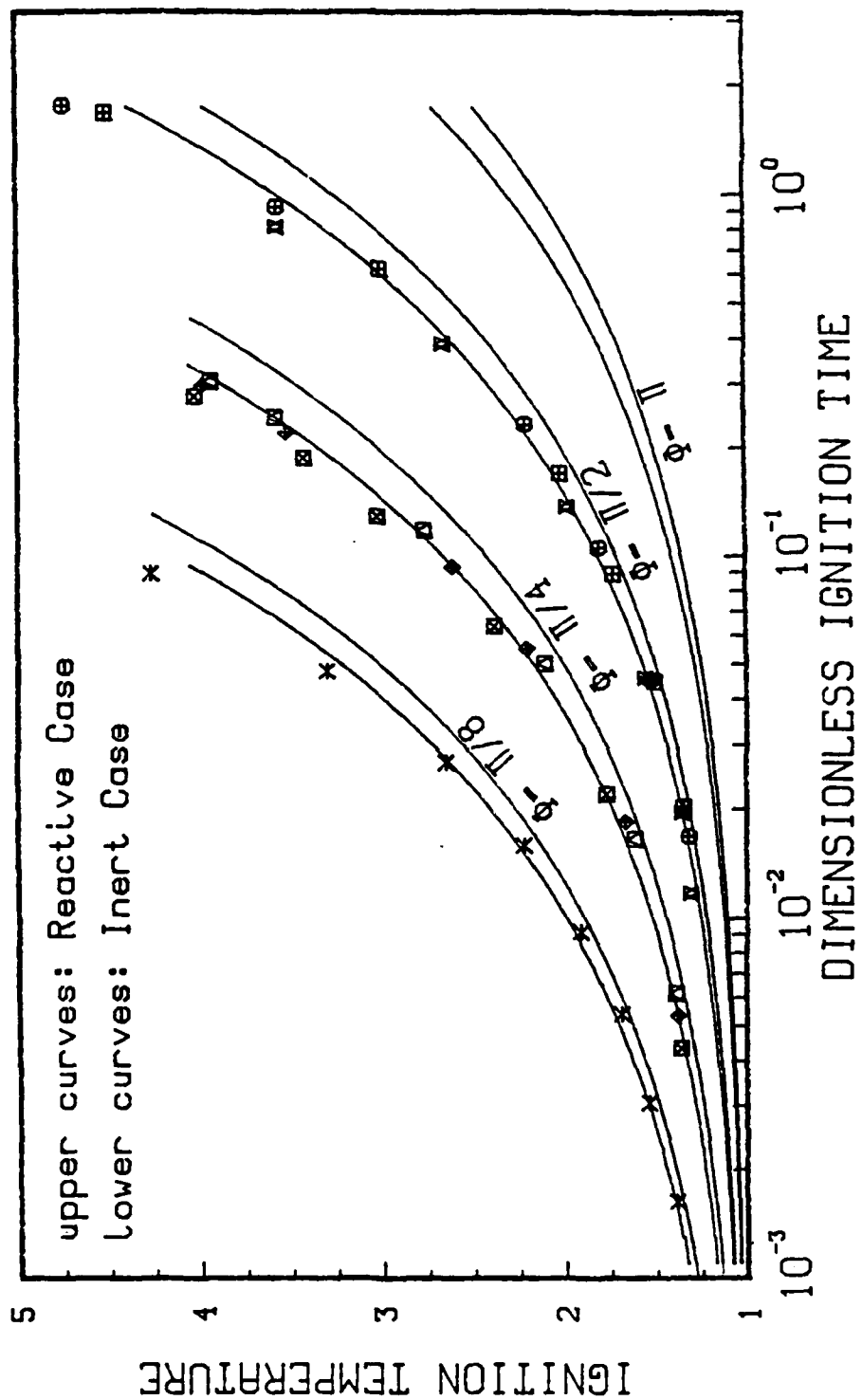

FIG. 5.8 IGNITION TEMPERATURES VERSUS IGNITION DELAY TIMES. Inert and reactive correlations shown for ϕ_o equal to π, $\pi/2$, $\pi/4$ and $\pi/8$ ($\gamma = 0$); Typical numerical data points included.

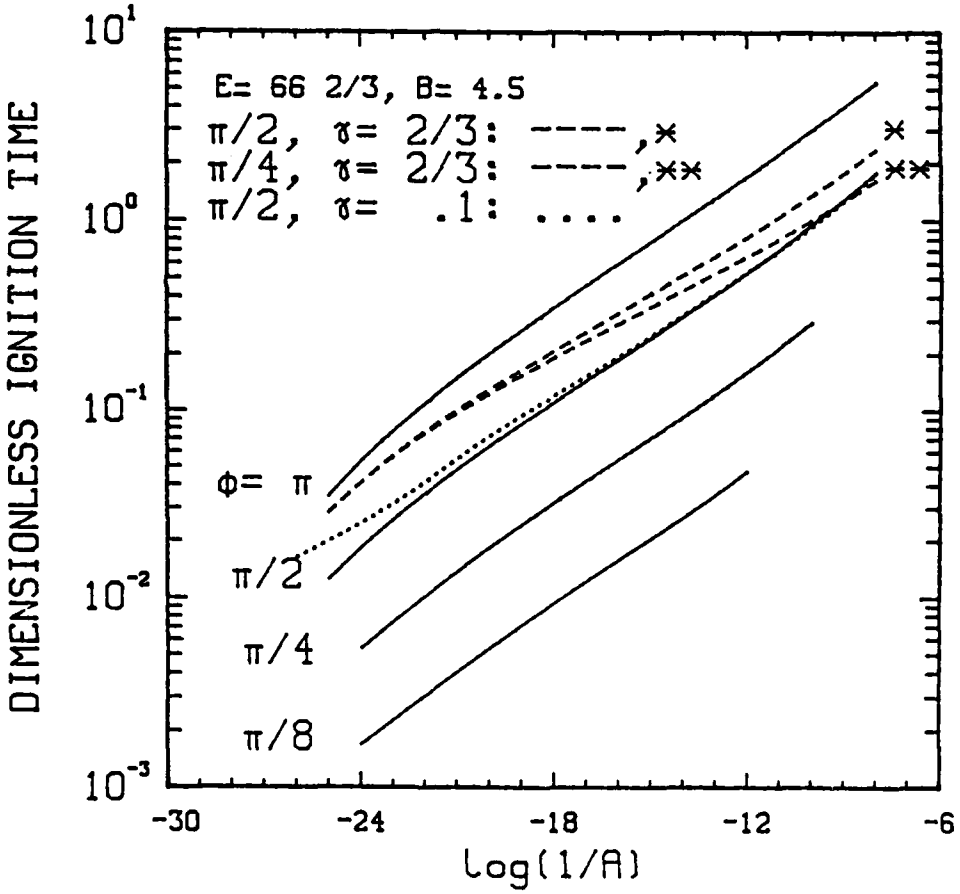

FIG. 5.9 EFFECT OF GEOMETRY ON IGNITION DELAY TIME. Ignition delay τ_c vs log(1/A) for activation energy E= 66 2/3 and 7 geometric cases. Note the shift in behavior for the rounded tip curves with decreasing A. Also observe the effect of the rounding parameter γ as parameter A decreases.

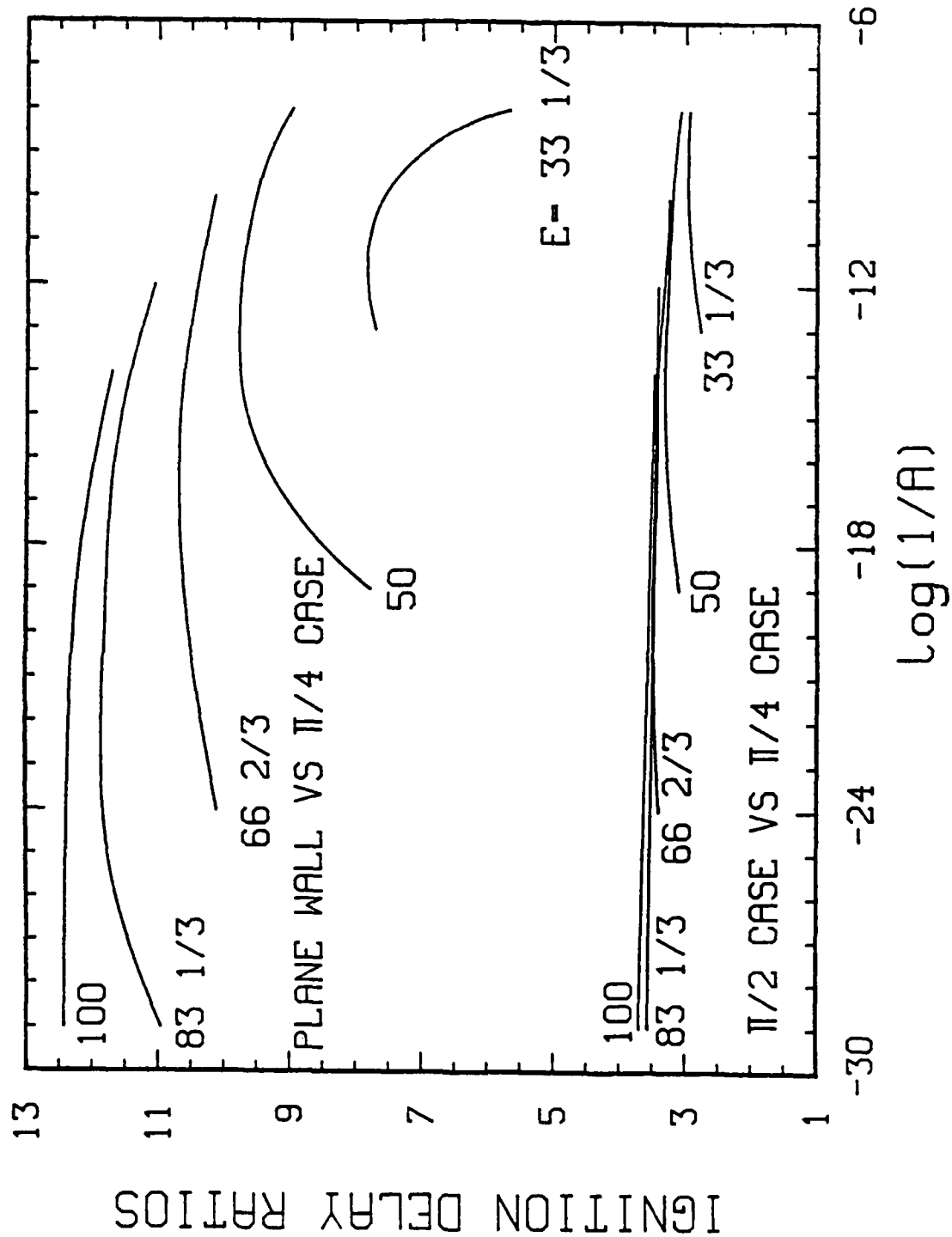

FIG. 5.10 QUANTITATIVE IGNITION DELAY COMPARISON FOR WEDGES. Ratio of ignition delays for planar and 90° wedges compared to 45° wedges as a function of log(1/A) and 5 activation energies.

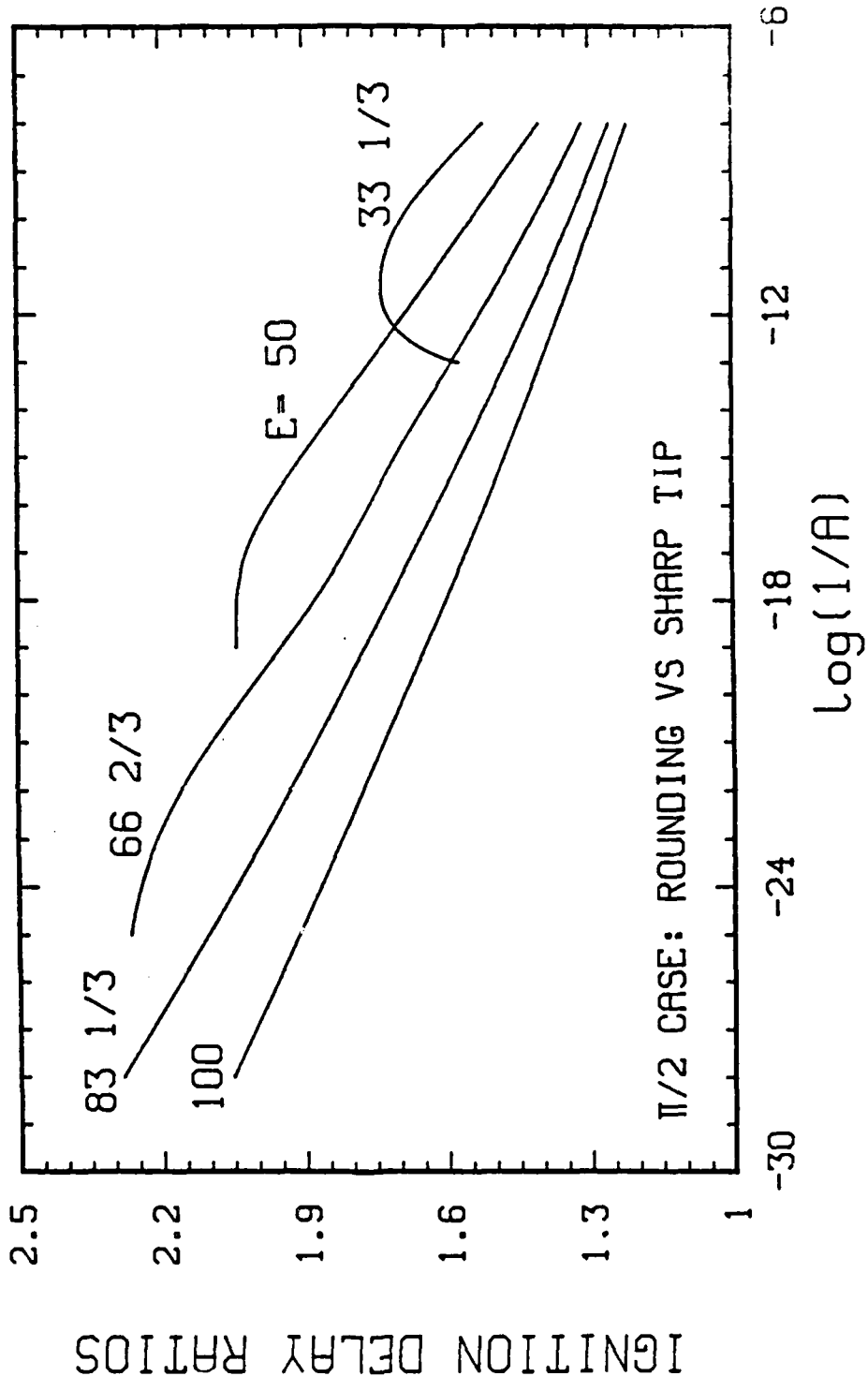

FIG. 5.11 QUANTITATIVE IGNITION DELAY COMPARISON FOR TIPS. Ratio of ignition delays for rounded to acute 90° corners vs log(1/A) and 5 activation energies.

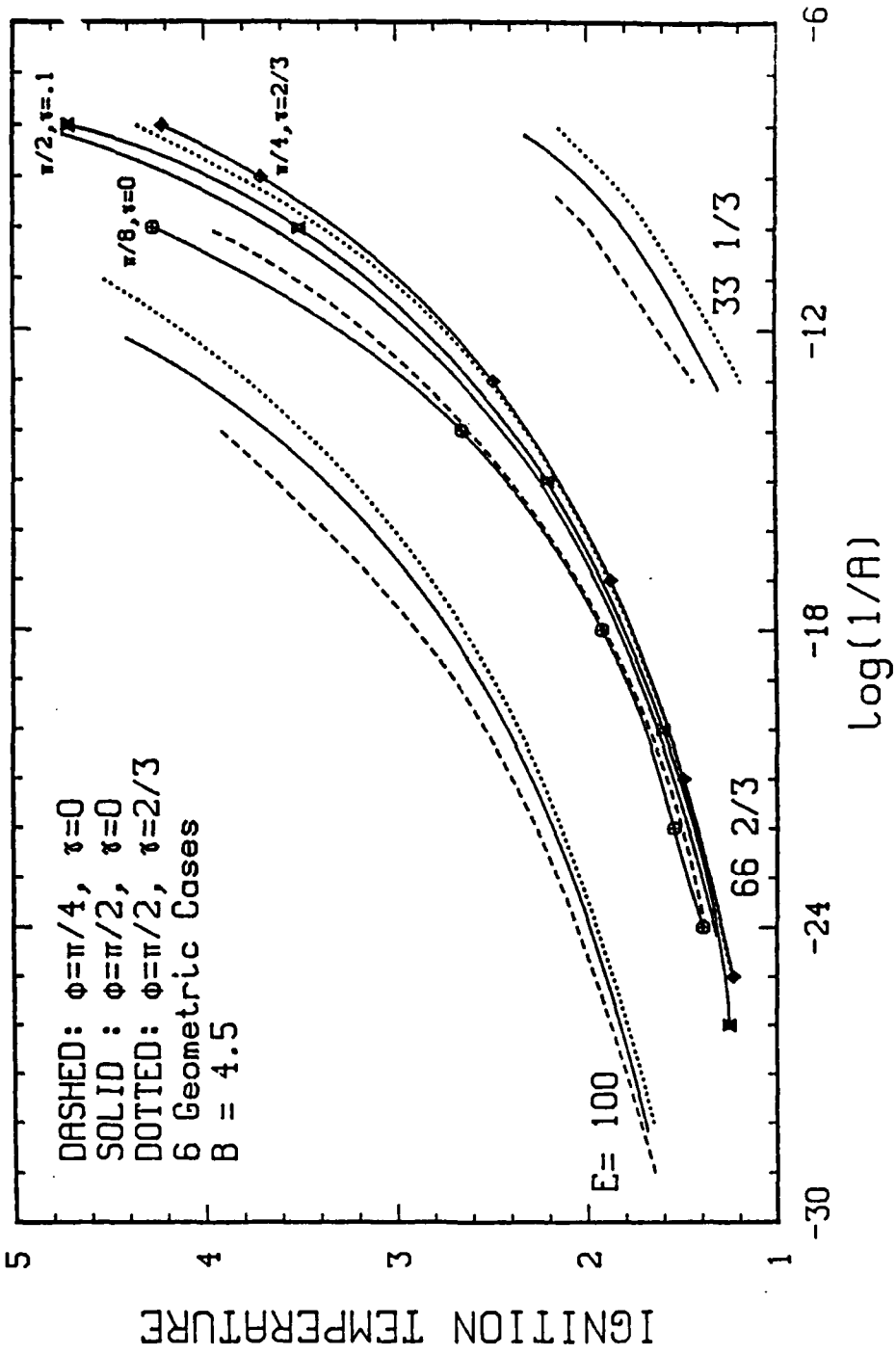

FIG. 5.12 EFFECT OF GEOMETRY ON IGNITION TEMPERATURE. Ignition temperature θ_c vs log(1/A) for 6 geometric cases and 3 activation energies. Note both the effect of the degree of acuteness (ϕ_o) and rounding (γ).

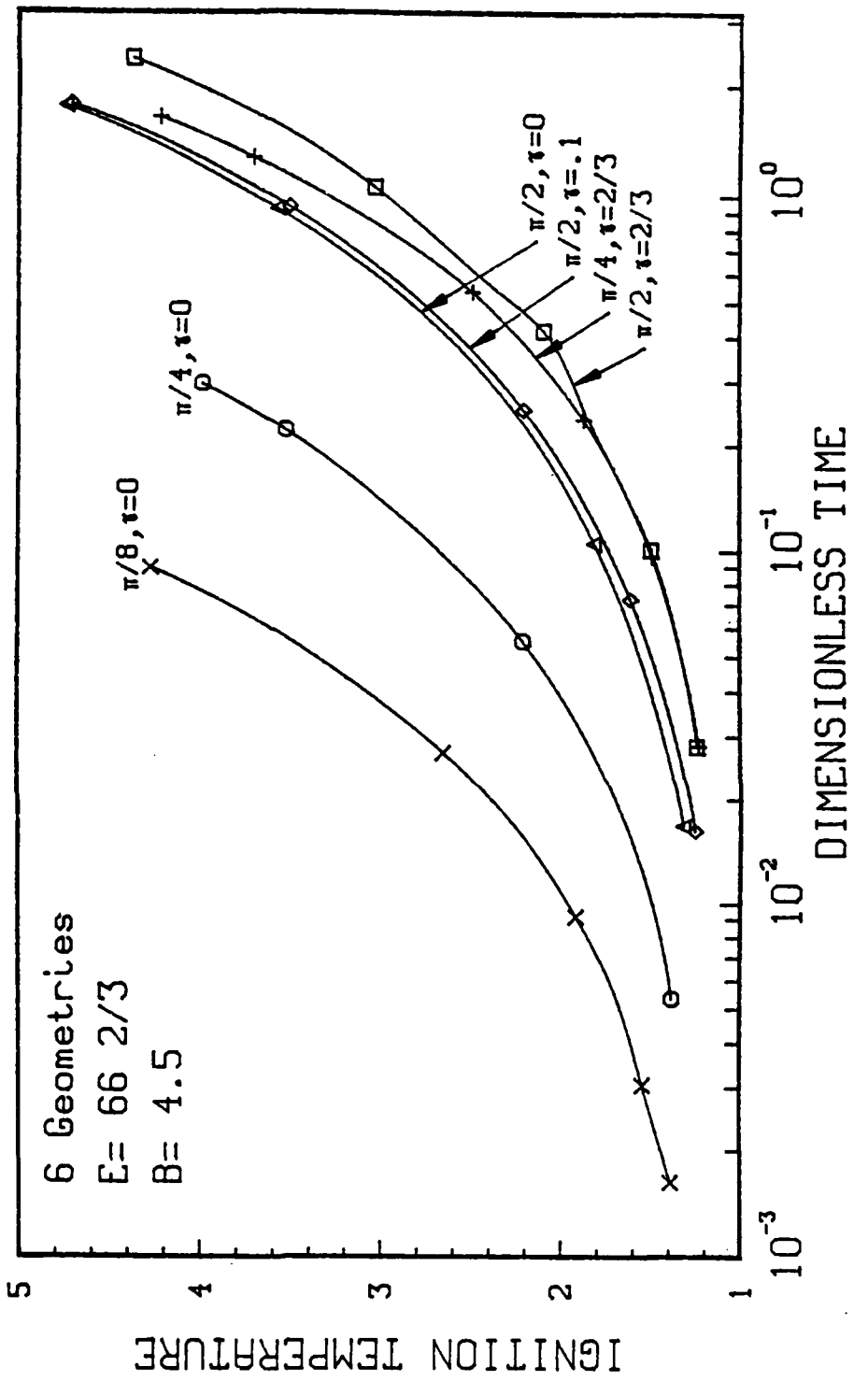

FIG. 5.13 GEOMETRY EFFECT ON IGNITION TEMPERATURE VERSUS TIME. Curves indicate shift in controlling behavior from small scale geometric feature ($=\gamma$) at short times, to large geometric feature ($=\phi_o$) at long times.

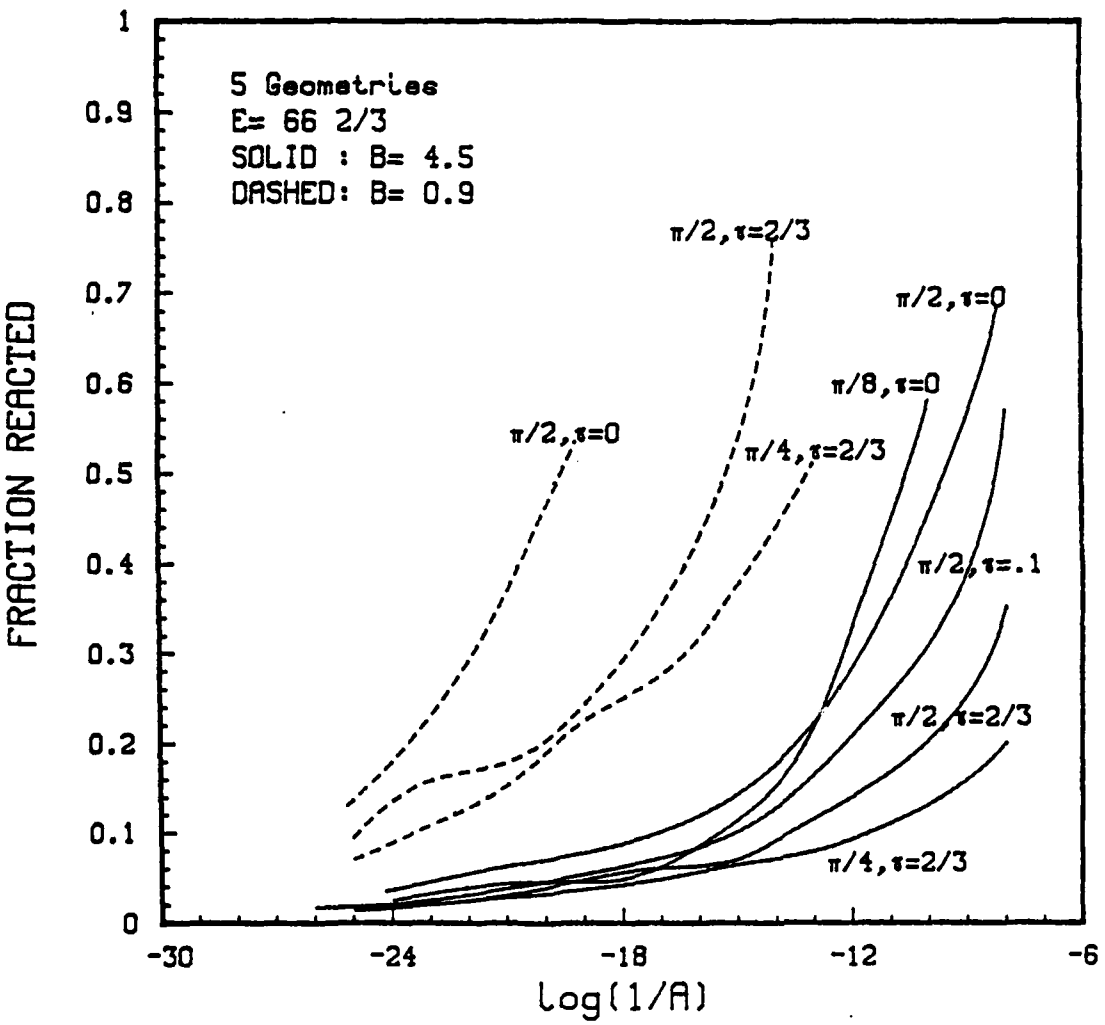

FIG. 5.14 GEOMETRY EFFECTS ON CRITICAL FRACTION REACTED. ϵ_c vs log(1/A) for the E= 66 2/3 activation energy; note the moderating effect on the rate of reactant consumption, apparent for large γ, as rounding delocalizes the ignition site.

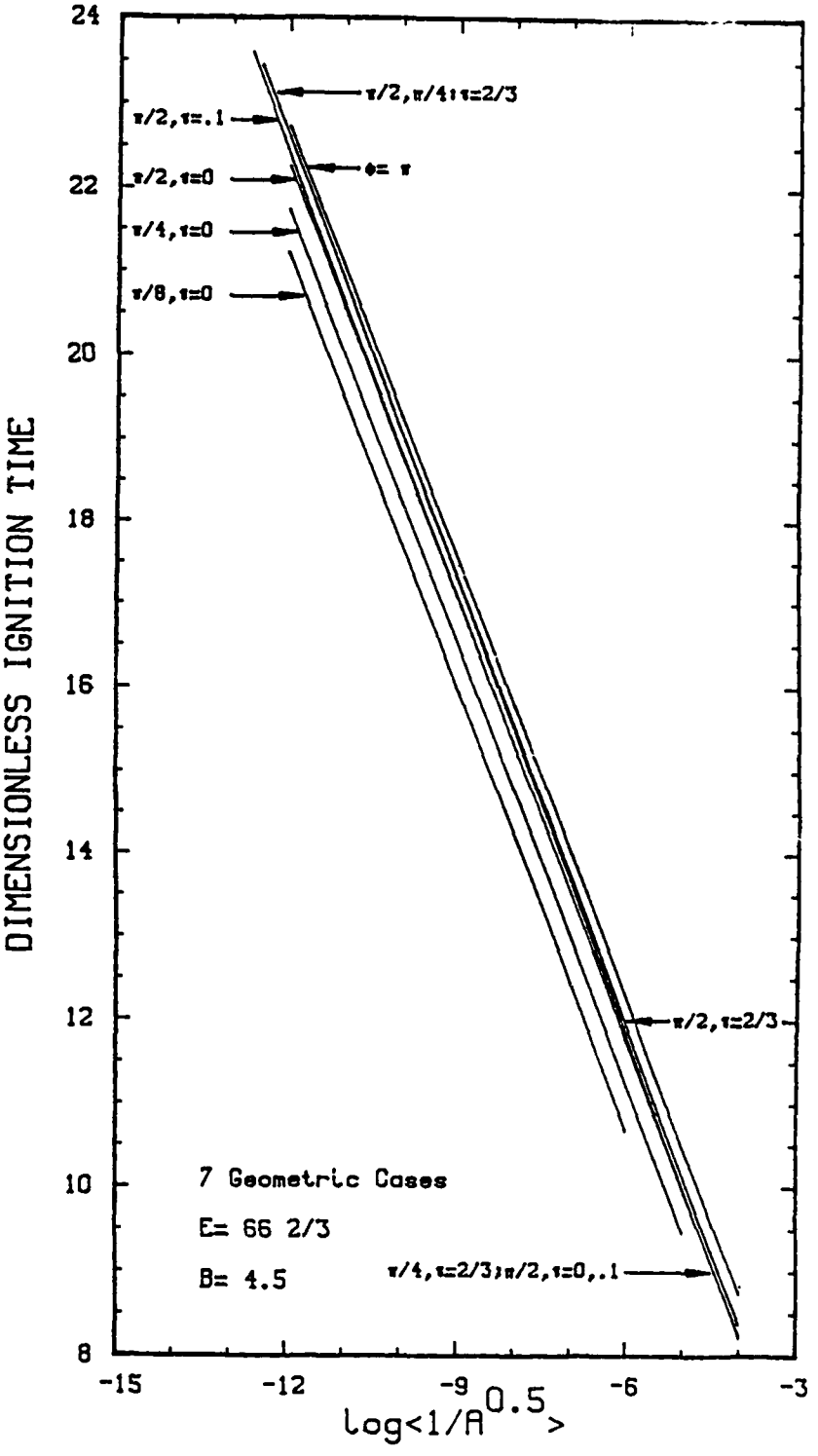

FIG. 5.15 DIMENSIONLESS IGNITION TIME VS APPLIED HEAT FLUX. $\text{Log}(A\tau_c) = \log((Q\nu/\rho c T_i)t_c) \propto \log(t_c)$ versus $\log(1/A^{1/2}) = \log(q/\sqrt{Q\nu k T_i}) \propto \log(q)$ for the E= 66 2/3 activation energy and 7 different geometric cases. Observe shift in behavior for the rounded tip cases.

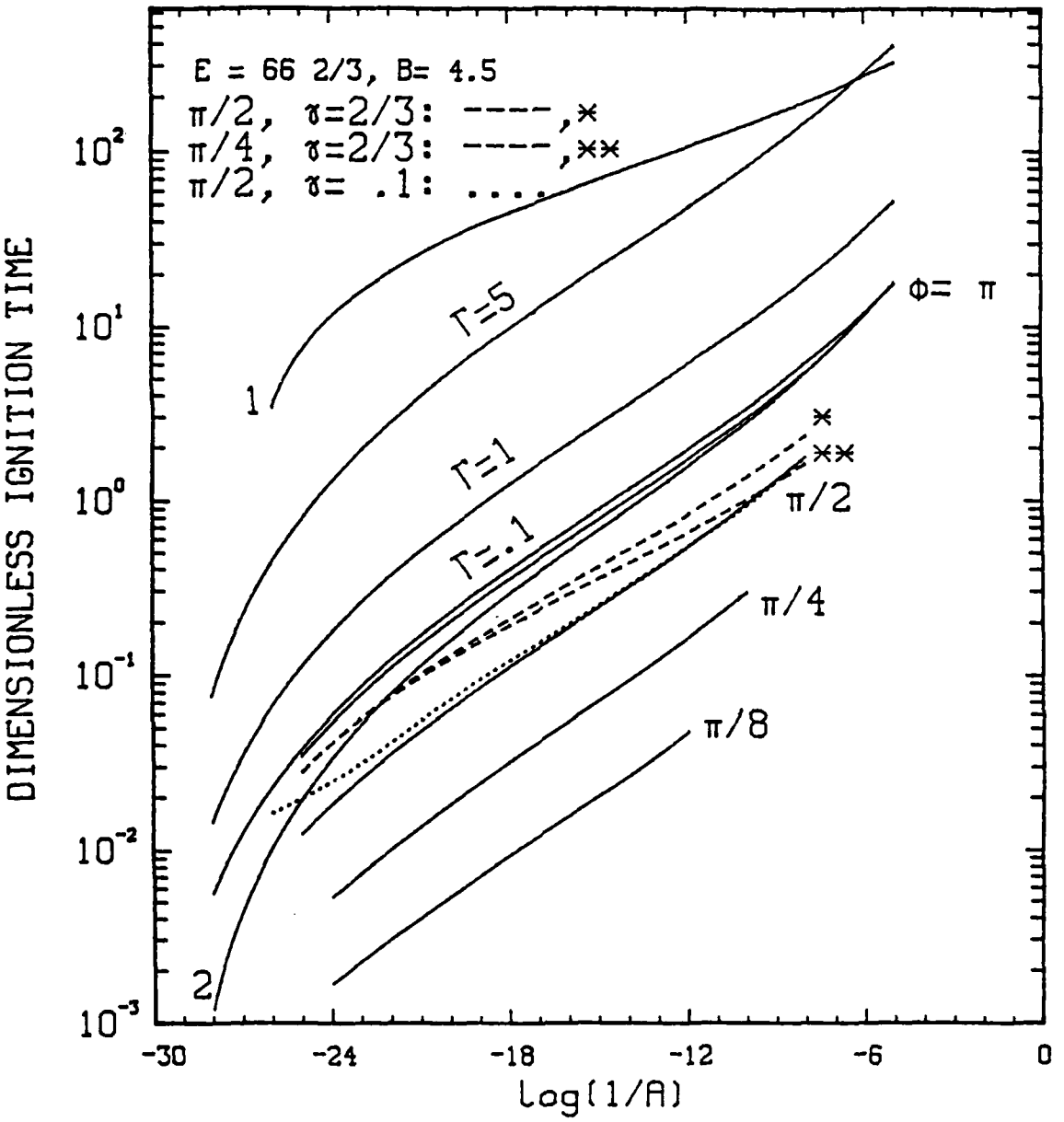

FIG. 5.16 COMPARISON TO OTHER PHYSICAL FACTORS. Ignition delay τ_c vs log(1/A) for the E= 66 2/3 activation energy, present geometries and published solid phase work. Curve 1: from Liñán and Williams (1972) including in-depth radiative absorption, $\alpha = \mu k T_i/q = 10^{-2}$; Curve 2: from Bush and Williams (1975), first order term for surface absorption, no surface cooling case; Γ curves: from Bush and Williams (1976), surface absorption and conductive heat loss to gas phase through an adjustable Γ parameter.

CHAPTER VI

EXPERIMENTAL WORK

6.1 Introduction

A small scale experimental program was undertaken in order to determine the validity of the geometrically related numerical predictions. Solid propellant samples having different geometric configurations, were heated by a CO_2 laser and the dependence of ignition time on applied heat flux was determined experimentally.

Usage of CO_2 laser systems has emerged in the past two decades as a reliable source of radiative energy as it provides a clean and reproducable means of heating an exposed surface. Radiative ignition behavior of two polymeric fuels in N_2/O_2 environments from 1 to 10 atm's pressures was investigated by Ohlemiller and Summerfield (1971). The ignition delay was taken to be equal to the first light detection as measured by a photomultiplier tube. Dynamic extinction effects on the ignition and steady burning behavior of double base propellants were determined experimentally in a subsequent study with a CO_2 laser system (Ohlemiller *et al.*, 1973). A detailed comparison of sources effects (arc-image versus laser) on ignition behavior of both double-base and composite propellants, at pressures from 5 to 21 atm's, was reported by DeLuca *et al.* (1976a, 1976b). Similar characteristics for both types of propellants were observed, provided optical factors associated with each ignition source, were accounted for properly. Results obtained by arc image techniques can therefore be compared to laser ignition results contingent upon properly accounting for surface reflection and in-depth absorption of incident radiation. Laser systems have also been employed in a series of subatmospheric tests on AP composite propellants in Ar, He and N_2 environments (Saito *et al.*, 1977; Harayama, Saito and Iwama, 1983; Saito, Yamaya and Iwama, 1985).

Measurement of the ignition delay, frequently defined as the time span between start of heating and onset of light emission, is either determined by a photomultiplier tube with its output displayed on an oscilloscope, a heat sensitive infra-red detector or a photo-transistor. Alternative ignition detection includes the use of small fine-wire thermo couples attached to or embedded under the propellant surface for temperature monitoring (Suh *et al.*, 1970; Rogers and Suh, 1970; Harayama, Saito and Iwama, 1983). Based on thermo-couple time traces Fishman (1967) reported two different ignition mechanisms for a 85% AP, 14% PBAN propellant depending on the applied flux levels. The onset of the surface exothermicity was clearly

detectable from these temperature traces.

Sample exposure times are frequently controlled by a double set of iris leaf type, fast acting shutters with generally the first one opening rapidly and the second one closing rapidly, each having an action time of a few milliseconds (Ohlemiller and Summerfield, 1971; Ohlemiller *et al.*, 1973; DeLuca *et al.*, 1976a).

Experimental ignition delay criteria can be divided into two basic categories. Most often. ignition boundaries are established based on 50% of the samples igniting under interrupted flux conditions on a plot of ignition time versus applied heat flux (Beyer and Fishman, 1960; Rosser, Fishman and Wise, 1966; Shannon, 1970). The second approach involves either continuous or interrupted irradiation of the propellant surface but measurement of first light emission (Ohlemiller and Summerfield, 1971; DeLuca *et al.*, 1976a, 1976b; Saito *et al.*, 1977). These results depend to some extent on the sensitivity of the detection system as mere sensing of an incipient flame does not necessarily correspond to attainment of a state of successfull ignition. Employment of a so-called "strong" ignition criterion in experimental testing of solid propellants is imperative as ignition can not be termed successful unless subsequent deflagration of the sample occurs.

Several chemical aspects play important roles during the ignition of AP-based propellants. Their importance and relevance in explaining observed phenomena vary depending on physical conditions during experimental testing. The first and foremost influencing factor is formed by the chemical ingredients of the propellant itself, mainly the AP oxidizer, binder material and performance enhancing additives such as burning rate catalysts, stabilizers and opacifiers. Since solids loading (% AP by weight) generally range from 70% to 90%, ignition is frequently controlled by the AP decomposition rate. Shannon (1970) reported that binder characteristics become important only at subatmospheric pressures. Further proof of oxidizer control during the ignition process is demonstrated by Shannon (1970) where use of advanced oxidizer systems led to faster ignition and lower minimum pressure limits for identical binder systems. Precise specification of the dominant chemical reaction is not clear at this point because the activation energy E of thermal decomposition of AP nearly coincides with other possible exothermic processes such as fuel oxidation by $HClO_4$ or ClO (Kishore and Gayathri, 1984).

A substantial amount of work has been done on the chemical decomposition of AP in order to determine the underlying chemical mechanisms involved in steady AP deflagration. Following a heating period during which the AP undergoes a crystalline phase transition, it is generally recognized that 70% of the AP undergoes an exothermic degradation into gaseous products with the remaining 30% subliming into NH_3 and $HClO_4$ which subsequently react in a

premixed flame close to the surface (Lengelle, Brulard and Moutet, 1970; Kumar *et al.*, 1984). Pellett (1972) identified H_2O, HCl, Cl_2, O_2, N_2O, NO_2 and N_2 products resulting from the exothermic condensed phase decomposition of AP as well as the formation of gaseous NH_3 and $HClO_4$ from the endothermic dissociative evaporation of AP, based on time resolved mass spectrometry. Detailed kinetic reaction schemes were proposed by Jacobs and Pearson (1969) and Guirao and Williams (1971) for the chemical decomposition and burning of pure AP.

Binder decomposition is usually of thermal origin where the particular mechanisms depend on the polymer itself and crosslinking and curing agents. Mechanisms of binder degradation are scission of C-C bonds, which includes both random and weak link scission, as well as reverse polymerization by end and random initiation and unzipping of the long C-C polymer backbone (Rabinovich, 1965). Energetically, the binder decomposition is usually endothermic and results in the production of small gaseous hydrocarbon monomers. These fuel species engage in a diffusion type reaction with the products of the exothermic AP decomposition and products of the premixed NH_3 and $HClO_4$ reaction.

Cohen, Fleming and Derr (1974) reported, while investigating the role of binders on the combustion process, that the kinetics of pyrolysis were independent of environmental pressure, presence of AP and catalysts in the sample. In general, the propellant surface was covered with a molten, boiling surface with the binder decomposition products contributing to the gas phase processes. Substantial evidence of polymer melting and flowing was demonstrated by Shannon (1970) based on photomicrographs of propellant surfaces heated for a period just short of that required for ignition. Dramatic pressure effects were noted for steady propellant deflagration in terms of the nature of the surface morphology. Boggs, Derr and Beckstead (1970) reported AP crystals protruding from the surface at high pressure but recession of these crystals with liquid binder flowing over the AP at low pressure. The role of binders in composite propellant ignition is generally limited to their influence on the low pressure ignitability limit and the effects of its decomposition products on gas phase reaction processes.

A third chemical factor is the effect of additives to the basic propellant formulation and observing their effects. Commonly tested ingredients are burning rate enhancers $CuCr_2O_4$ (copper chromite) and Fe_2O_3 (iron oxid), optical opacifier C (carbon black) as well as a host of other materials. Shannon (1970) reported faster ignition by addition of iron oxid and copper chromite for some propellant formulation. Catalytic influences were attributed to accelerated AP decomposition and enhanced gas phase reactivity. Dominant modes of operation in catalytic action were identified by Pearson (1971) for the AP propellant system as accelerating the $HClO_4$ decomposition into reactive intermediates, promoting heterogeneous chemical reaction

between solid fuel and perchlorate acid on the fuel surface and accelerating the gas phase reaction between gaseous fuel species and $HClO_4$. Consistently faster ignition was reported by Ramaprabhu and Bhaskaran (1983a, 1983b) for addition of CuO or Fe_2O_3 to an AP-PVC propellant in shock tube experiments. Catalytic effects of these metal oxides were thought to lower the initial decomposition temperature and thereby accelerate the decomposition process. Saito, Yamaya and Iwama (1985) noted in subatmospheric pressure, CO_2 laser experiments, faster ignition and enhanced ignitability after copper chromite addition to an AP-CTPB propellant system. It was reasoned that the copper chromite acted as a positive catalyst in both the condensed phase and heterogeneous reactions. This conclusion is in general accord with early work where catalytic action of metal oxides accelerated $HClO_4$ decomposition, which then reacted with fuel pyrolysis products (Pearson and Sutton, 1967).

Addition of carbon black (C) generally reduces optical transparancy along with faster ignition. DeLuca *et al.* (1976a, 1976b) concluded that detailed propellant formulation comparisons can only be made after optical factors are eliminated by carbon addition. Longer ignition times reported by Saito, Yamaya and Iwama (1985) for carbon addition can be attributed to smaller exothermicity as shown by DTA curves compared to the baseline AP-CTPB propellant. Kishore and Gayathri (1984) in their review noted that the effectiveness of catalysts in the ignition process can be related to its effectiveness in promoting thermal AP decomposition. With these preliminaries in mind, present experimental results must be commented on within the context of the above remarks.

6.2 Experimentation

6.2.1 Experimental Apparatus

Figure 6.1a shows the apparatus for the ignition experiment using an Adkin MIRL-50 CO_2 laser (100W max cw mode) to provide the radiant energy. Incorporation of the LP-1 Laser Pulser module enables single pulse operation of the laser cavity with precise control of exposure duration and total energy output. The laser beam is directed through a mirror system for intensity profile smoothing. A convex lens focusses the slightly divergent beam unto the propellant sample, thereby irradiating a circular area of approximately .10 cm^2. At two locations along its path. portions of the CO_2 beam are deflected by beam splitters for monitoring purposes. Exposure duration is accurately determined from a highly attenuated deflected beam by a Cd-Hg-Te detector operating in a differentiated mode. Total beam energy is measured by a

Scientech Model 365 Laser Power-Energy Meter operating in the single pulse energy mode. The radiation enters an airtight, N_2 purged chamber through a transmissive ZnSe window. Quartz windows allow visual access to the propellant sample for monitoring purposes. A HeNe laser, positioned collinear with the CO_2 laser beam, is employed for accurate placement of each propellant sample prior to the test run. A schematic of the experimental set-up is shown in Figure 6.1b, along with a sketch illustrating the interaction of the laser radiation with the propellant surface. The incident laser radiation is unidirectional for all geometries.

Light emissions from the propellant surface are detected by a Hamamatsu, model R955, side-on type photomultiplier tube (PMT) and displayed on a storage-scope. The laser pulse width, measured by the Cd-Hg-Te detector, is simultaneously recorded on the scope where its triggering is synchronized with the execution of the experiment by an output signal from the manual activation of the LP-1 laser pulser. In addition, each test run was taped using a 30 frames/sec video recorder system. A second HeNe laser provided supplementary light for these recordings in the otherwise dark test surroundings.

Propellant specimens were carefully prepared using a microtome and X-acto knife to produce samples with either a plane surface, a 90^o or a 60^o wedge angle. Figure 6.2 shows representative test samples, produced from 5 mm x 5 mm propellant sticks and mounted on reusable holders. Careful measurement of the rounding of the edge indicated a 20-30 μm radius of curvature. Prior to insertion in the chamber, the sample surface was cleaned by blowing off with dry, contaminant free air.

6.2.2 Procedure

Each test run started with placement of the sample holder in the chamber, proper positioning of the propellant sample with respect to the incoming CO_2 radiation using the collinear HeNe laser and translation stages located inside the chamber, and activation of the N_2 purge. The CO_2 beam was temporarily blocked by a firebrick to check reliable operation of the laser cavity. Proper operating settings concerning pulse duration and output level were set on the LP-1; oscillator and amplifier gas pressures and currents were selected on a trial basis to obtain the desired power output level. Proper laser operation was assured by repeated testing and measurement of output energy levels.

After removal of the beamstop, the purging rate was decreased to minimize flow conditions in the chamber, scope and video recording system were activated, and functioning of the LP-1 control panel triggered the scope and tested the ignitability of the sample. Approximate

"go" and "no-go" ignition limits have been established by varying the exposure time, as controlled by the LP-1, for a given laser output power for each geometric sample configuration. Samples were ignited over an incident flux range of 40 - 400 W/cm^2 in an atmospheric pressure N_2 environment.

6.3 Experimental Results

Recorded data consists of laser gas pressure and current settings, an energy measurement of the total laser pulse, a video recording of each run and scope traces from the Cd-Hg-Te detector and photomultiplier tube (PMT). Three time values for each PMT trace were recorded which correspond respectively to the initial deflection, midpoint and steady high level of the trace. A permanent record of each successful run is obtained by photographing the oscilloscope screen.

It was attempted to have the termination of the laser exposure coincide as closely as possible with the initial rise in the PMT output, indicative of ignition. This procedure resembles most closely the established "go" "no-go" criterion, frequently used in experimental studies except, presently, for simultaneous monitoring of light emissions. For cases when ignition does not occur, the corresponding "no-go" time is taken as the total radiative exposure time. Approximately 30 to 40 runs for each geometry were performed to establish the ignition boundary as a function of the applied heating rate.

The test propellant was an AP-HTPB composite propellant, type X63ASROC (85% AP, 11% HTPB, $\approx$ 2.5% Al and $\approx$ .4% Fe_2O_3). The propellant was supplied by Naval Weapons Center, China Lake, CA. Reasons for its selection were its low smoke character, excellent safety record and low aluminum content in the formulation.

Figures 6.3 through 6.5 show "go" and "no-go" results on a plot of ignition time versus applied heat flux for the 3 different geometries with ignition times based on the initial deflection of the PMT trace. Least squares curve fits of the form $t_{ign} \propto aq^b$ are included for the successful runs. Values for constants a and b based on the first and second ignition criterion are tabulated in Table 6.1 with t_{ign} in seconds, heat flux q in W/cm^2, readily enabling numerical reproduction of these curves.

Figures 6.6 through 6.8 display similar results with the exception that here ignition times are based on the midpoint of the PMT trace. Measured slope values of these curves and those shown in Fig.'s 6.3 through 6.5 are included within parentheses in Table 6.1 and are employed in further considerations.

TABLE 6.1			
Values of Curve Fit Constants a and b			
geometry	criterion	constant a	constant b
π	first	921.313	-1.5626 (-1.56)
π	second	614.956	-1.4670 (-1.47)
$\pi/2$	first	159.394	-1.3147 (-1.31)
$\pi/2$	second	114.152	-1.2040 (-1.20)
$\pi/3$	first	102.363	-1.3077 (-1.31)
$\pi/3$	second	39.729	-1.0284 (-1.03)

The speed up in ignition delay, computed for each ignition criterion, is displayed in Figure 6.9 for the acute wedges, relative to the planar case. These speed up factors are computed based on the least squares curve fits. Figure 6.9 shows that, based on the first rise in PMT trace, square corners ignite 1.3 to 2.3 times faster than planar samples for flux levels decreasing from 400 to 40 W/cm^2-sec; 60° edges ignite 2.0 to 3.6 times faster over the same flux range. These ratios decrease respectively to 1.2 to 2.0 for the square corner and to 1.2 to 3.1 for the 60° edges if the second criterion is used. This reduction in ignition speed up is simply attributed to longer flame development times for edges, after initial ignition, to reach similar flame intensities as the planar samples. A more important observation is the reduction in speed up with increasing heating rates as this might indicate a shift in ignition mechanism, induced or enhanced by the sample geometry. These aspects will be addressed in the Discussion section 6.4.

A set of typical scope traces is displayed in Figure 6.10 where the applied heating rate is approximately equal to 250 W/cm^2 for each geometric configuration. Examination of these traces accentuates the effect of acuteness of the edge in terms of longer flame development times for these cases. Primary reason for the slower signal rise is simply the much smaller area initially ignited for the acute angles. Similar trends are displayed in Figure 6.11 for lower flux levels. Video recordings support this observation as ignition is always seen to commence along the protruding propellant edge and more frames are required for acute samples to reach similar flame intensities.

Further PMT trace observations show the frequent existence of a temporary, short-lived rise in PMT signal prior to the typical steady signal rise indicative of successful ignition. (See Fig.'s 6.10 and 6.11) Frequency of occurence of this phenomenon is about 40%, 20% and 13% for the 60°, 90° and planar samples respectively. This behavior can be attributed to either high intensity spots in the CO_2 laser beam causing highly localized ignition, or more likely, liberation of volatile matter on the surface giving rise to "hot spots", which are definitely

exacerbated by the protruding propellant edge.

For marginally heated test runs where the onset of detectable light emission nearly coincides with laser radiation termination, Figures 6.12 and 6.13 show PMT traces which exhibit a rather long, low level signal prior to attaining full scale levels. This behavior is most apparent and most frequent for the 60° and 90° samples. This phenomenon pertains to a post-heating "cooking" period where, for a substantial time interval, a balance exists between processes related to gaseous species and chemical heat production on one hand, and reactant consumption and heat loss effects on the other. These longer development times for edges clearly indicate a shift in importance of contributing ignition mechanisms as a result of the sample geometry.

Three interesting observations are made based on the frame-by-frame inspection of the video recordings. First, recordings of "no-go" runs sometimes show short liberation of gases from the surface as well as a slight movement of the sample caused by thermal stresses development below the propellant surface during laser radiation. Secondly, under high flux conditions and sharp edges, short-lived, small flamelets are observed emanating from different locations on the irradiated surface, presumably at AP crystal sites. Their brief existence can be explained by rapid chemical reaction of gasified species, but their limited quantity and heat release is insufficient to trigger ignition. Interestingly enough, these observations are made for both "go" and "no-go" test runs. Thirdly, the temporal flame development for the 60° and 90° samples can roughly be partitioned into three overlapping phases despite limitations imposed by the framing rate of the video system. Initially a single flame is observed standing erect on the edge, which gradually grows in strength and spreads down along the sides. At this point a three-clover structure can briefly be identified with the central portion originating from the downward burning of the edge and two side lobes as a result of ignition and burning of both edges. Upon continued surface regression the three structures coalesce and disappear to produce a bright, steady flame.

6.4 Discussion of Experimental Results

Prior to an in-depth discussion of the experimental results, the validity and accuracy of the data must be assessed. Experimental variables are the laser exposure time ($t_{exposure}$) measured by the Cd-Hg-Te detector, laser pulse energy content (E_{laser}) determined from the calorimeter, fraction of the laser beam deflected for monitoring purposes (ω) and nominal beam area (A_o). The average incident heat flux based on unidirectional propellant surface irradiation is

expressed as:

$$q = \frac{1}{A_o}\frac{1-\omega}{\omega}\frac{E_{laser}}{t_{exposure}}\sin(\phi_d/2) \qquad (6\text{-}1)$$

Careful calibrations have determined the value of the deflection factor (ω) of the beam splitter to equal .05337 $\pm$ .6%. The accuracy of the calorimeter is verified by the manufacturer to be within $\pm$ 3%. Laser exposure times are determined well within 1% because of the pulsed laser capability. The nominal beam area (A_o) is computed from paper burns and optical considerations. Its calculated and measured value is taken as .0944 cm^2 $\pm$4%. Sample angles are reproduced within $\pm$ 3°. As a result of these considerations, the presented results have an uncertainty in the applied heat flux of 6%; its largest contributors are the nominal beam area A_o and measured energy level.

Although the exact determination of the "proper" ignition delay time depends to a large extent on the employed definition itself, in the current circumstances the low detection sensitivity assures subsequent combustion. This detection sensitivity is needed to prevent saturation of and damage to the photomultiplier tube during steady burning of the propellant sample. Therefore, equipment limitations are partly responsible for the current selection of a "harsh" or "strong" ignition criterion.

Comparison of current one dimensional results to reported work in the literature shows good agreement in terms of slope values for curves of ignition time versus applied flux levels. Table 6.2 contains a list of experimentally determined slope values based on radiative ignition of small cubes of solid propellant. All works except for those of Baer and Ryan (1965), Saito *et al.* (1977) and Harayama, Saito and Iwama (1983) employed heating rates ranging from 10 to 100 cal/cm^2-sec.

The less negative slope for the more advanced ignition definition as shown in Table 6.1 can be attributed to similar time intervals between the two criteria, independent of the applied flux level. Based on the reasonable agreement with previous work, current one dimensional results are explained in terms of the typical AP premixed flame and AP/hydro carbon diffusion flame as controlling the ignition behavior. Video recordings further support this conclusion as luminosity occurs in the gas phase, a small distance away from the solid surface.

TABLE 6.2

Experimental Slope Values in the Literature: Ignition Time versus Heat Flux

Propellant	Environment	slope(arc-image)	slope(laser)	Reference
80% AP+PBAA, PU, PS	N_2, 1 atm	-1.82^		Baer and Ryan
95% AP, 5% CC	N_2, 25-40 atm	-1.45*		Rosser, Fishman, Wise
95% AP, 2.5% CC, 2.5% C	N_2, 25-40 atm	-1.6*		Rosser
87.4% AP, 4.6% CC, 8% PE	N_2, 25-40 atm	-1.5*		Rosser
95% AP, 5% CC	N_2, 20 psig	-1.45*		Wise, Inami, McCulley
84% AP, 16% PBAN	N_2, 1 atm	-1.70*		Shannon
epoxy	O_2, 1 atm		-1.45**	Ohlemiller and Summerfield
75% AP, 25% PBAA	N_2, 21 atm	-1.3*	-1.4*	DeLuca *et al*
75% AP, 24% PBAA, 1% C	N_2, 21 atm	-1.6*	-1.5*	DeLuca *et al*
80% AP, 20% PBAA	N_2, 21 atm	-1.3*		DeLuca *et al.*
24% AP, 51% B	N_2, 21 atm	-2.0*	-2.0*	DeLuca *et al.*
laminated AP+CTPB	N_2, Ar, 40 Torr		-2.90	Saito *et al*
laminated AP+CTPB	N_2, Ar, 100 Torr		-3.60*	Saito
80% AP, 20% CTPB, 0-1% Al	CO_2, 30-600 Torr		-2.1±.3	Harayama

^ first light detection criterion, radiation furnace apparatus.

* "go no-go" ignition criterion based on 50% of samples ignited.

** first light detection ignition criterion.

Detailed comparison to published work is difficult because the exact propellant formulation is classified and therefore unknown. The presence of carbon black is not known. Studies most suitable for comparison are those at a similar pressure range, i.e. those by Baer and Ryan (1965), Wise, Inami and McCulley (1967), Shannon (1970) and Northam, Pellett and Cofer III (1972). Without addition of catalysts or metals, slope values range between -1.70 and -1.98 when carbon is included in the formulation. Inclusion of catalysts such as copper chromite or iron oxid results in a less negative slope as was demonstrated by Shannon (1970) for an AP/PBAN system and by Wise, Inami and McCulley (1967). Since the present formulation includes both Al and Fe_2O_3, the -1.56 slope corresponds well with previous work.

Based on the current one dimensional results and their agreement with published work, geometry effects are extrapolated from the 60° and 90° experimental data to understand and develop possible mechanisms responsible for their observed ignition behavior. Faster ignition for the edges is first of all attributed to the convergence of the heat flow lines in the solid which is accompanied by faster solid phase temperature rises. However, if this solid phase conductive mechanism is the single factor, then more rapid ignition for acute geometries should exhibit no dependence on the applied heat flux. But, the speed up depends rather strongly on the applied heating rate as is shown in Figure 6.9. This geometrically induced, solid conductive factor is most significant at low flux levels as square corners ignite presently up to 2.5 times faster than planar samples. Baer and Ryan (1965) reported square corners igniting 3.0 to 3.5 times faster for flux levels from 30 W/cm^2-sec down to 5 W/cm^2-sec in a hot radiation furnace. Hence, solid phase heat conduction provides only part of the explanation for more rapid ignition,

especially at higher rates of heating.

The less negative slopes reported in Table 6.1 for the two dimensional samples indicate a departure from the above described, one dimensional ignition mechanism for the present AP propellant formulation. Greater sensitivity of the results on the ignition criterion is clearly illustrated as well in Table 6.1, by noting corresponding slope values. Further qualitative insight in these experimental results is obtained by considering the total ignition delay time as the sum of a set of characteristic time scales.

$$\tau_{ign} = \tau_{solid\ cond} + \tau_{chem\ diffusion} + \tau_{convection} + \tau_{thermal\ losses} \qquad (6\text{-}2)$$

The first term ($\tau_{solid\ cond}$) considers the solid inert heating time to an approximate temperature level for a specific geometric configuration with inclusion of in-depth radiative absorption. The term $\tau_{chem\ diffusion}$ deals with the mixing time scale in the gas phase for interdiffusion of oxidizer and fuel decomposition products for the exothermic ignition reaction; it depends in a complicated manner on the overall geometry, AP particle size and chemical ingredient aspects. The third time ($\tau_{convection}$) pertains to the time scale needed for sufficient build-up of gas phase reactants due to surface regression. Inclusion of this term seems imperative because of the two dimensional nature of the propellant surface. The last term ($\tau_{thermal\ losses}$) considers gas phase cooling effects as a result of the concave nature of the exposed propellant edge to the surrounding "cold" gas phase.

This concept of different time scales is a result of experimental phenomena observed from the PMT traces and video recordings. Long, low level flame development times can be explained by large convective and gas phase diffusive times where a near quasi-steady condition exists between surface gasification and species production versus gas phase species, chemical reaction and thermal diffusion. This phenomenon is clearly depicted on scope traces where laser termination nearly coincides with onset of low level light emissions (See Fig.'s 6.12 and 6.13). Although this behavior is observed for the planar case as well, the length of this quasi-steady, low level of chemical reactivity is definitely lenghtened by the acute sample shapes. Species are projected away from the surface in a divergent "spray" fashion which exacerbates diffusive mixing and promotes heat transfer to the adjacent "cold" inert gas phase. In addition, the initial gasifying propellant area is very small and increases only gradually, compared to an entire gasifying surface in the one dimensional case.

As the initial area undergoing gasification and/or solid phase reactions is limited to the edge, intermittent flamelet development, as observed on the video recordings, can be explained

by rapid localized gasification and gas phase reactions, followed by cooling in the "cold" and inert gas phase. This behavior is most frequently observed for the 60° samples under high flux conditions.

Geometry effects diminish at higher rates of heating. This can be attributed to two factors. First, the cut corner is not infinitely sharp but careful measurement indicates a 25-30 μm rounding radius. This value compares well to the 20 μm radius of curvature reported by Baer and Ryan (1965) for a square corner. Thermal wave penetration at the moment of ignition is of comparable magnitude as this rounding radius under high flux conditions. Secondly, the extreme tip can undergo rapid heating and subsequent burn off without leading to continued deflagration. The newly created surface underneath presents a more one dimensional like geometry such that the overall ignition time does not deviate much from the 1-D result. Temporary spikes on some PMT traces could have originated from the fast burn-off of the protruding propellant edge.

Based on the current experimental investigation, restricted to an one atmospheric N_2 environment, it is clear that propellant geometry can be a significant factor in the ignition process. A dramatic speed up in ignition time is attained over planar surfaces, but its magnitude diminishes rapidly at increasing flux levels. For marginally performing igniter systems, roughening or serrating the propellant surface will most likely ease the ignitability of the propellant and thus improve the reliability of the igniter system. A potentially added benefit consists of the more gradual nature of the build-up to steady burning for sharp edges which could contribute to a more uniform attainment of a totally ignited propellant surface in the interior of a solid rocket motor.

6.5 Comparison between Experimental and Theoretical Results

In this section a comparison is performed between numerical model predictions and experimental data. Model results are presented for 60° and 90° wedge angles having either an infinitely sharp or a 25 μm radius of curvature edge. Trends are identified on a plot of ignition time versus practical heat flux levels.

Sharp edge results are easily generated from the correlation expressions. The rounded tip computer code is slightly modified to handle small dimensionless rounding radii γ as a result of the constant physical radius of curvature. Selection of chemical and physical parameters, listed in Table 6.3, is based on: (1) the X63ASROC data sheet (CPIA M-2 Manual) supplied with the test propellant, (2) published physical properties for AP by Rosser, Inami and Wise (1966) and, (3) careful review of the literature.

TABLE 6.3

Physical Properties and Input Parameters

property	symbol	value	Reference
thermal capacity	c	1338 J/kg-K	Rosser, Inami and Wise (1966)
activation energy	E	30 kcal/mole	Summerfield and Kuo (1984)
thermal conductivity	k	.46 W/m-°K	Rosser, Inami and Wise
heat of combustion	Q	$2x10^9$ J/m^3	X63ASROC data sheet
pre-exponential factor	ν	10^8 sec^{-1}	
solid density	ρ	1727 kg/m^3	X63ASROC data sheet

The numerical value for Q used in the simulations represents 50% of the total heat of combustion of the test propellant. It should be noted that the model predictions are highly sensitive to the selection of numerical values for the activation energy E and pre factor ν. The activation energy value is based on frequently reported values in the literature; pre-factor ν is selected to obtain ignition times comparable to those found in the experiment.

Figures 6.14 (a-c) show numerically computed results along with experimental data on a graph of ignition time versus applied flux. Results are displayed for both sharp and rounded edges. Table 6.4 contains slope values for all displayed curves. The dotted lines represent results for an alternative chemical parameter set (E=100, ν=2.5x10^{18}) based on the correlation equations developed for the acute cases.

TABLE 6.4

Theoretical and Experimental Slope Values

geometry	experiment	E=50, R_0=0	E=50, R_0=25 μm	E=100
π	-1.56	-1.68		-1.84
$\pi/2$	-1.31	-1.66	-1.47	-1.84
$\pi/3$	-1.31	-1.65	-1.37	-1.84

First of all, the deviation in ignition time itself does not constitute a significant mechanistic problem in that selection of other values for E and ν can easily produce better numerical agreement between theory and experiment. Smaller activation energies result in less negative slopes of t_{ign} versus heat flux as shown in Table 5.2; changes in ν shift the curve vertically. The effect of rounding becomes most visible at high heating rates as, for a fixed R_o, the parameter γ increases which reduces the overall acuteness of the wedge angle. This leads to a significant slope adjustment towards better correspondence with the experimental curves. It seems imperative to include some degree of rounding for future modeling of geometric effects, based on the improved slope agreement. Selection of a smaller activation energy would likewise result in a less negative slope for the theoretical predictions. Use of small activation energies is

reported by Kumar and Hermance (1976) and Kumar (1983, 1985) in radiative gas phase ignition theories with reasonable success.

Major theoretical shortcomings consist of minor differences in slope, as tabulated in Table 6.4, but most importantly, computed ignition temperatures which exceed experimentally quoted values by 100 to 300 °K. Kumar *et al.* (1984) reported surface temperatures of $\approx$ 450 °K for an AP-PBAA propellant under rapid pressure loading conditions. Rosser, Fishman and Wise (1966) reported surface temperatures at ignition from 500 to 650 °K for a 95% AP, 2.5% CC and 2.5% C formulation. Wise, Inami and McCulley (1967) computed surface ignition temperatures from 700 to 850 °K; experimental values ranged from 800 to 975 °K for a 75% AP, 20% CTPB propellant, ignited in hot wire tests. Presently computed ignition temperatures range from 900 to 1200 °K which are clearly much higher than accepted experimental values.

Based on the comparisons above, it is clear that the present model formulations do not contain sufficient provisions to describe all of the experimental observations. This fact is not surprising because of the assumed simple reactive solid ignition model. Points for improvement within the framework of the solid phase theory include incorporation of a surface heat loss to the gas phase, as it will slow down the surface temperature rise, and inclusion of convective transport, which will also limit surface temperatures and thus the surface exothermicity, by simple depletion or disappearance of material. Both of these factors will lenghten the time of onset of significant chemical heat release and are expected to produce better agreement between theory and experiment.

Kumar and Hermance (1976) have shown that, for planar but inhomogeneous propellants, reasonable estimates of its ignition characteristics can be made based on simple solid phase theory, provided pressures do not extend to sub-atmospheric levels. Therefore, for multi dimensional domains or non planar samples, the present theoretical approach provides a partial explanation of the experimental observations. Most importantly, the inclusion of rounding or roughness moderation is imperative for future geometric considerations in the study of solid propellant ignition.

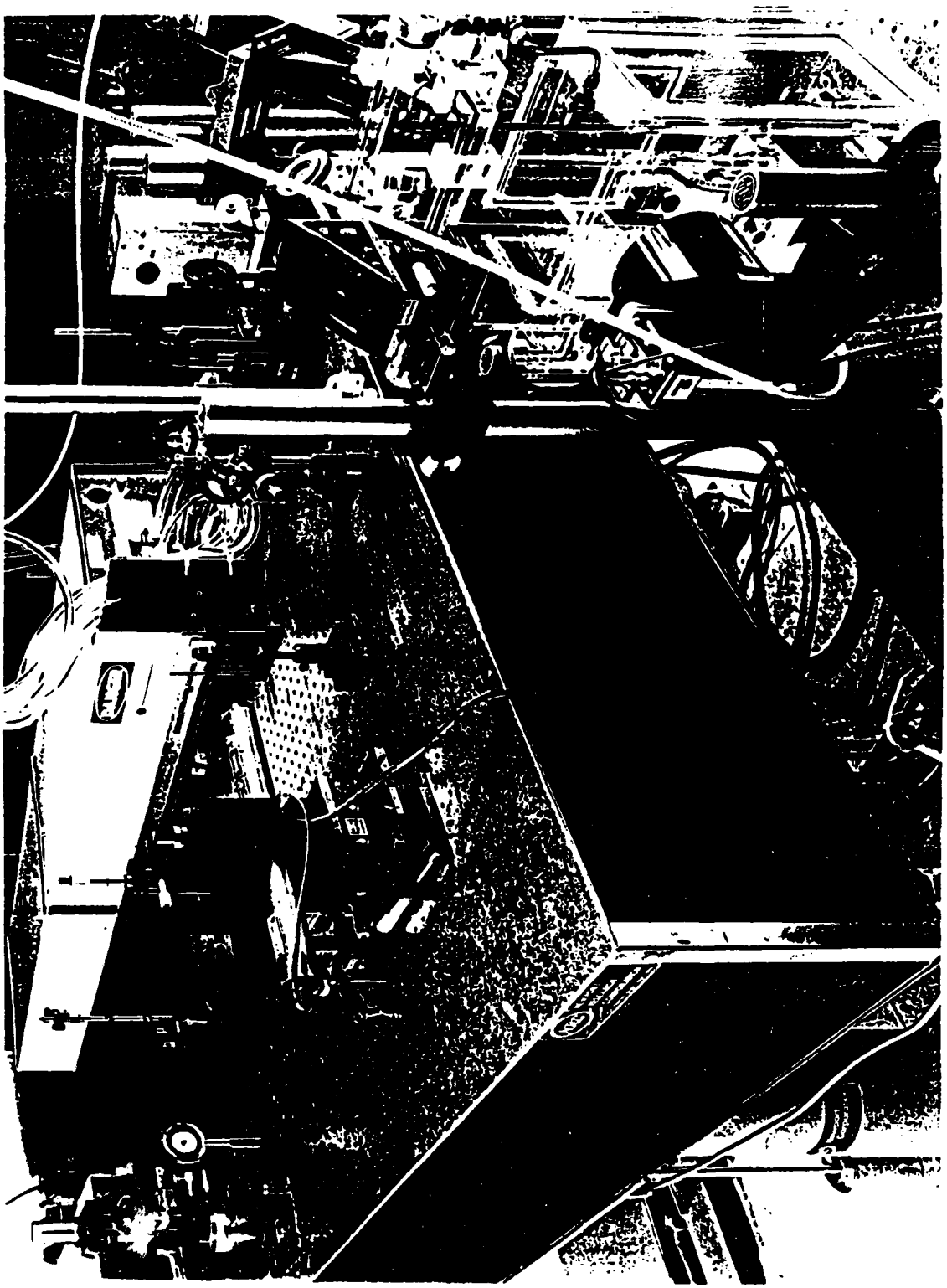

FIG 6.1a LASER IGNITION AND DETECTION APPARATUS.

EXPERIMENTAL SET-UP:

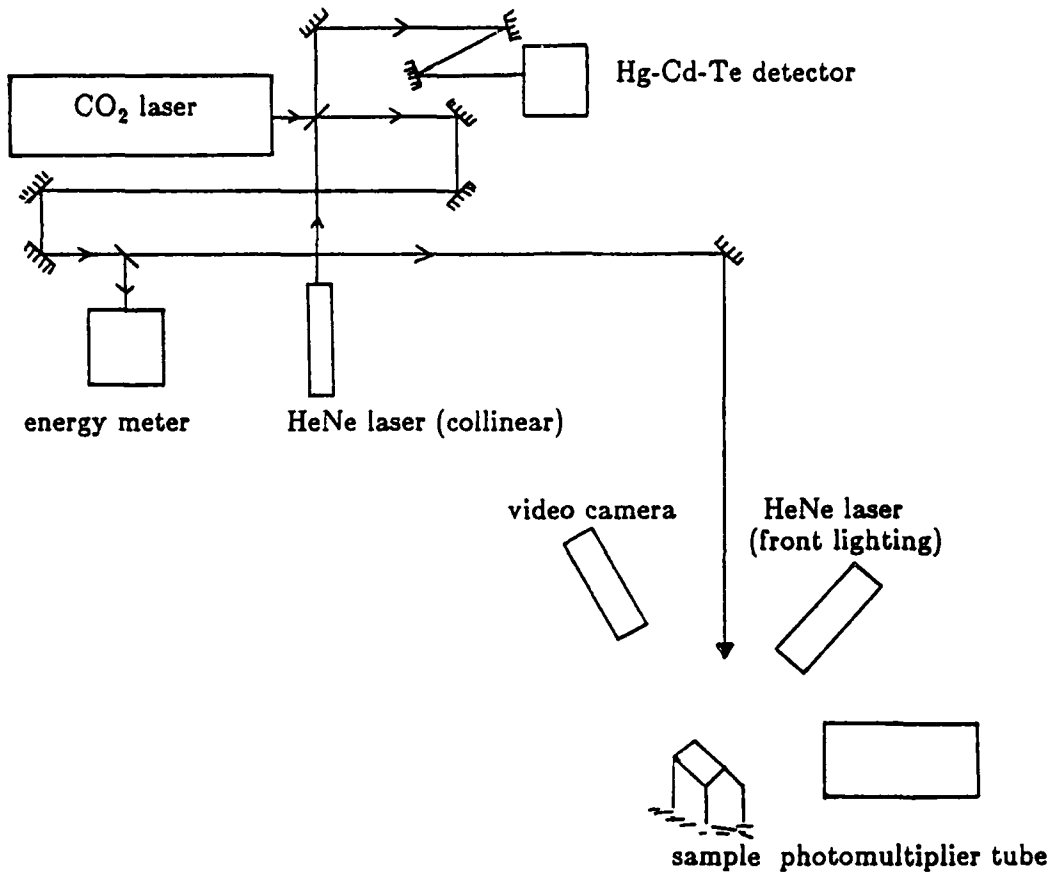

SAMPLE ORIENTATION W.R.T. LASER LIGHT:

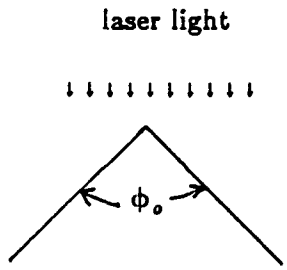

FIG. 6.1b SCHEMATIC OF EXPERIMENTAL SYSTEM, INCLUDING ORIENTATION OF SAMPLES WITH RESPECT TO INCIDENT LASER LIGHT.

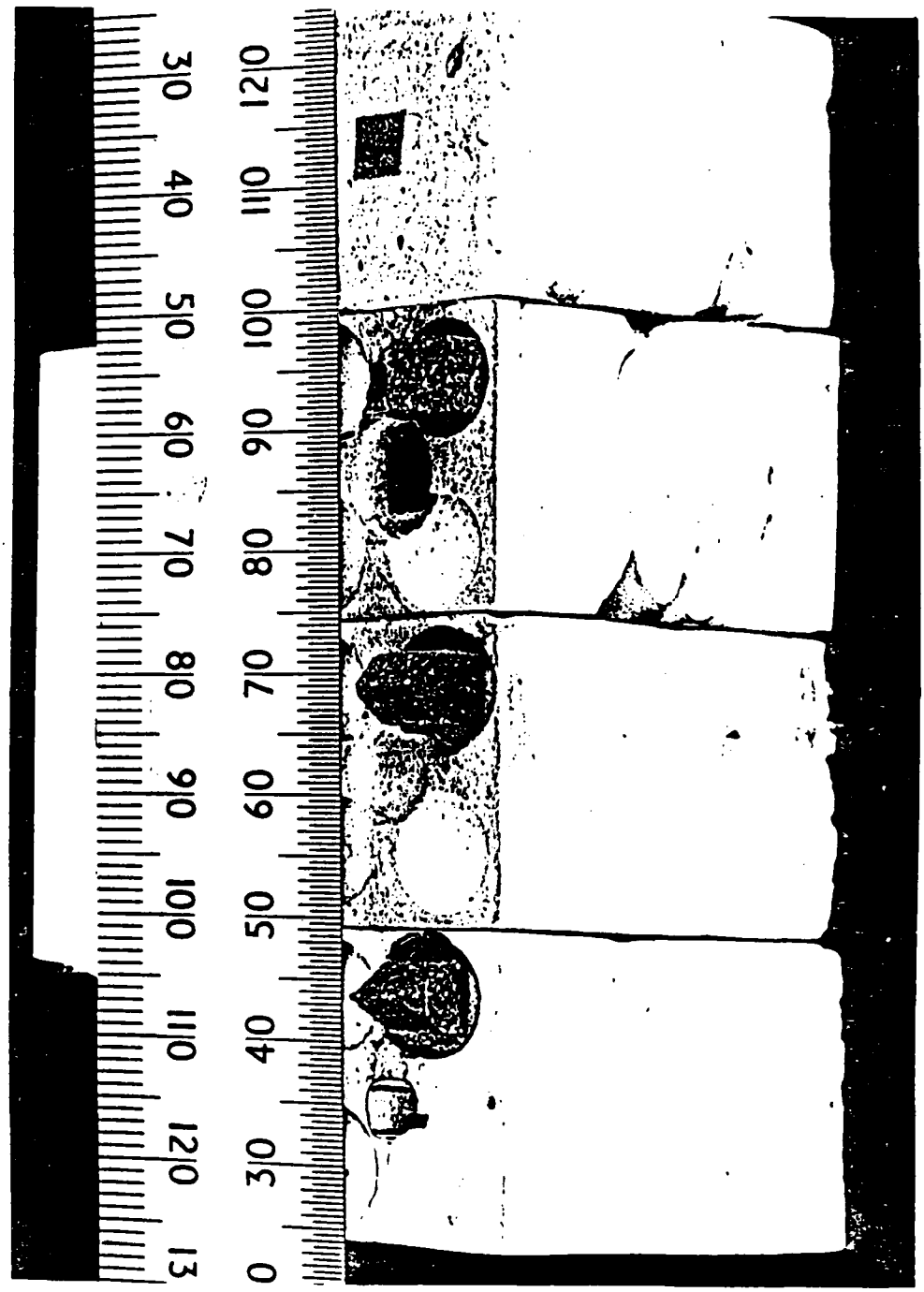

FIG. 6.2 INVESTIGATED AP-HTPB PROPELLANT SAMPLE GEOMETRIES. Ruler graduations in mm. Small 180°, 90° and 60° composite propellant samples mounted on gray-white holding compound.

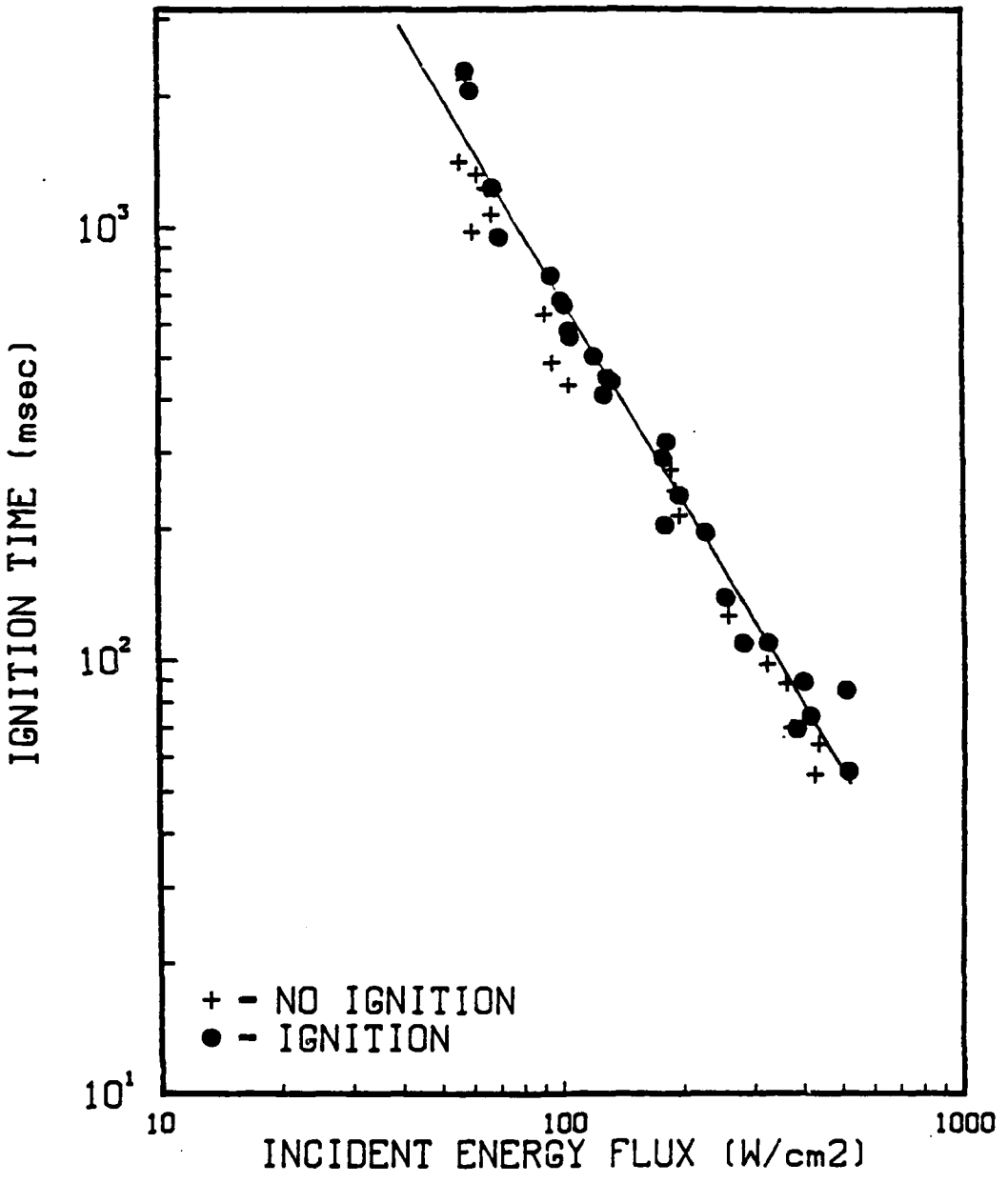

FIG. 6.3. EXPERIMENTAL IGNITION TIME VERSUS INCIDENT FLUX: 180° CASE. First rise in PMT output as ignition criterion.

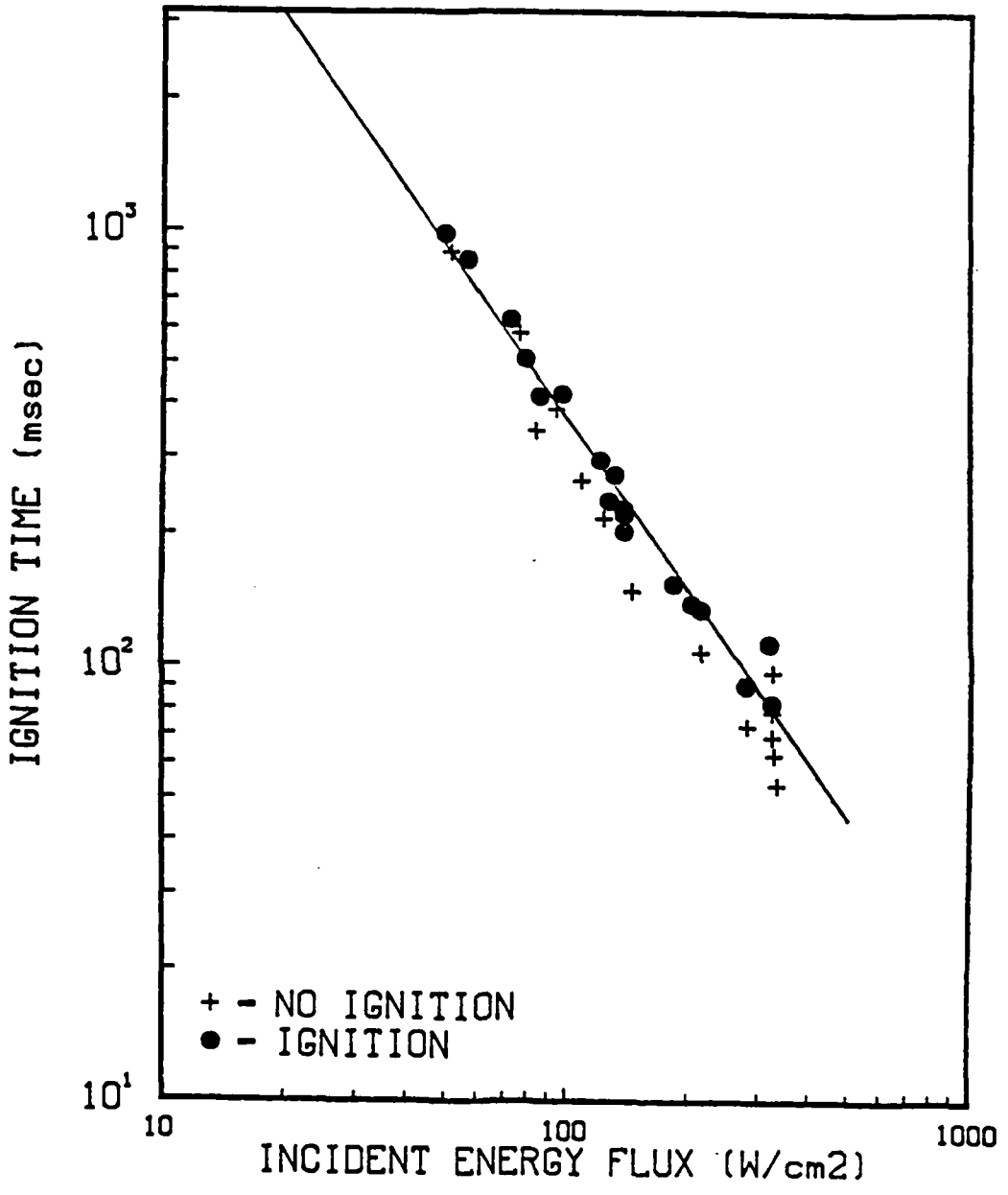

FIG. 6.4. EXPERIMENTAL IGNITION TIME VERSUS INCIDENT FLUX: 90° CASE. First rise in PMT output as ignition criterion.

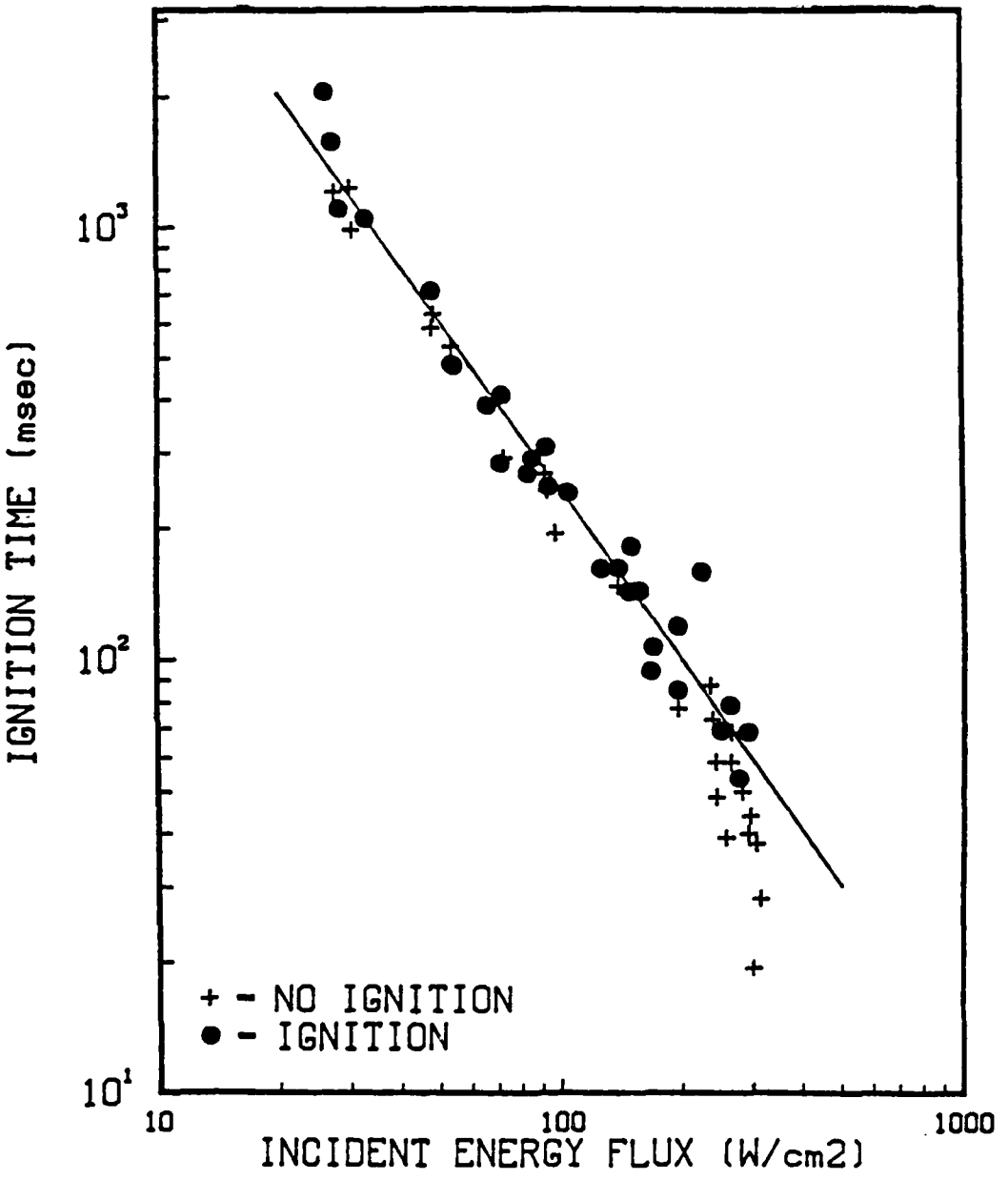

FIG. 6.5. EXPERIMENTAL IGNITION TIME VERSUS INCIDENT FLUX: 60° CASE. First rise in PMT output as ignition criterion.

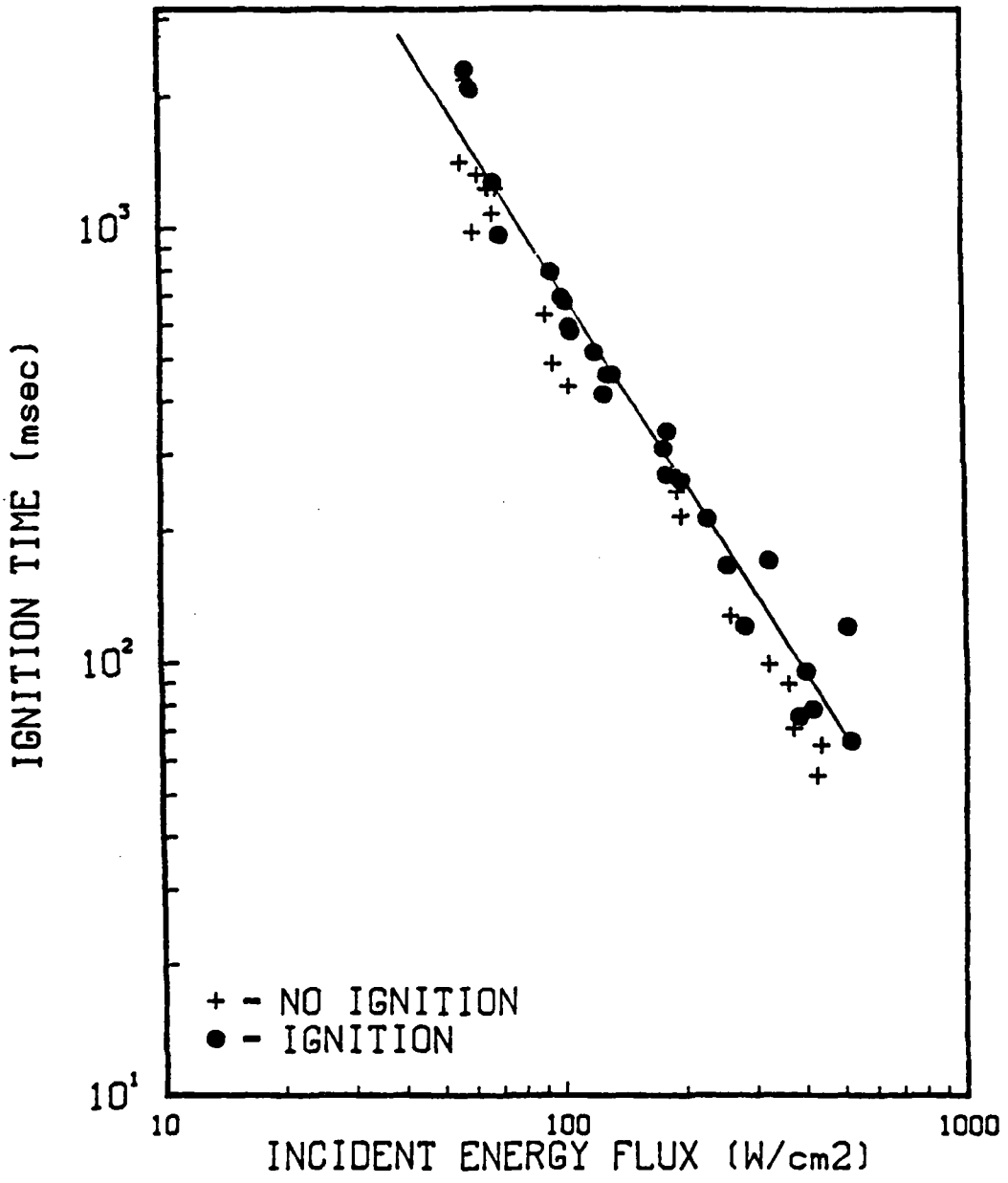

FIG. 6.6. EXPERIMENTAL IGNITION TIME VERSUS INCIDENT FLUX: 180° CASE. Midpoint level of PMT signal is used as the ignition criterion.

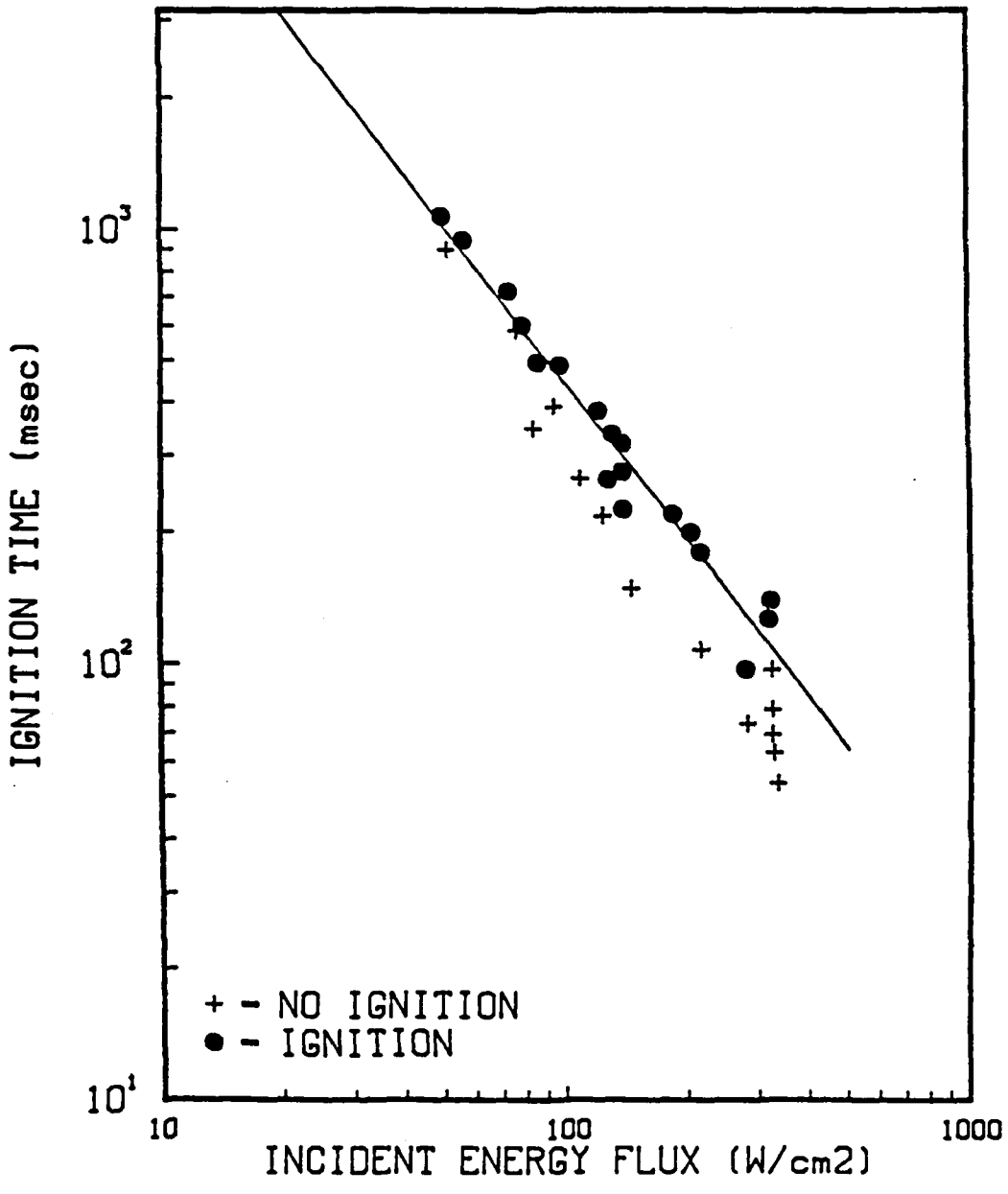

FIG. 6.7. EXPERIMENTAL IGNITION TIME VERSUS INCIDENT FLUX: 90° CASE. Midpoint level of PMT signal is used as the ignition criterion.

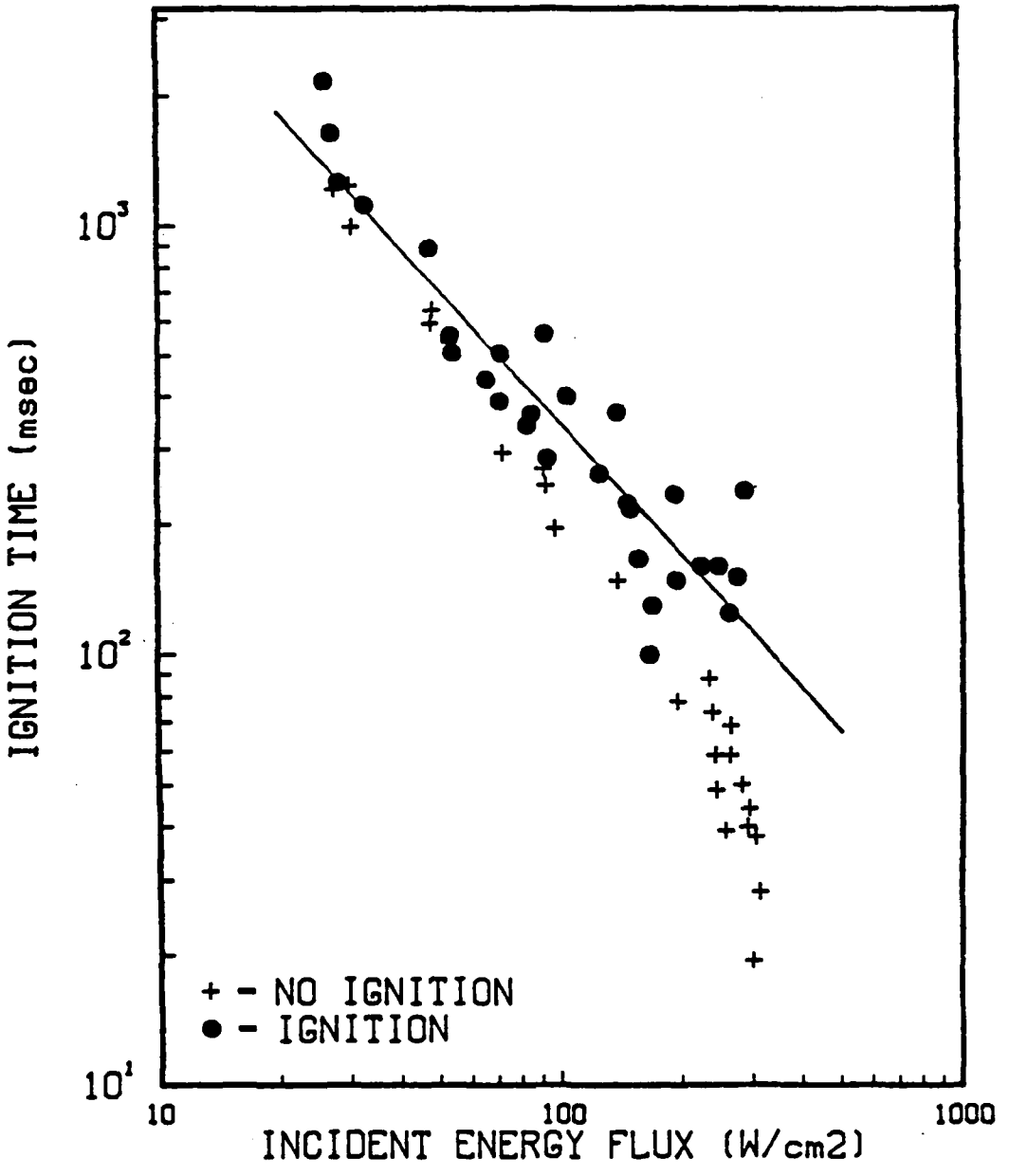

FIG. 6.8. EXPERIMENTAL IGNITION TIME VERSUS INCIDENT FLUX: 60° CASE. Midpoint level of PMT signal is used as the ignition criterion.

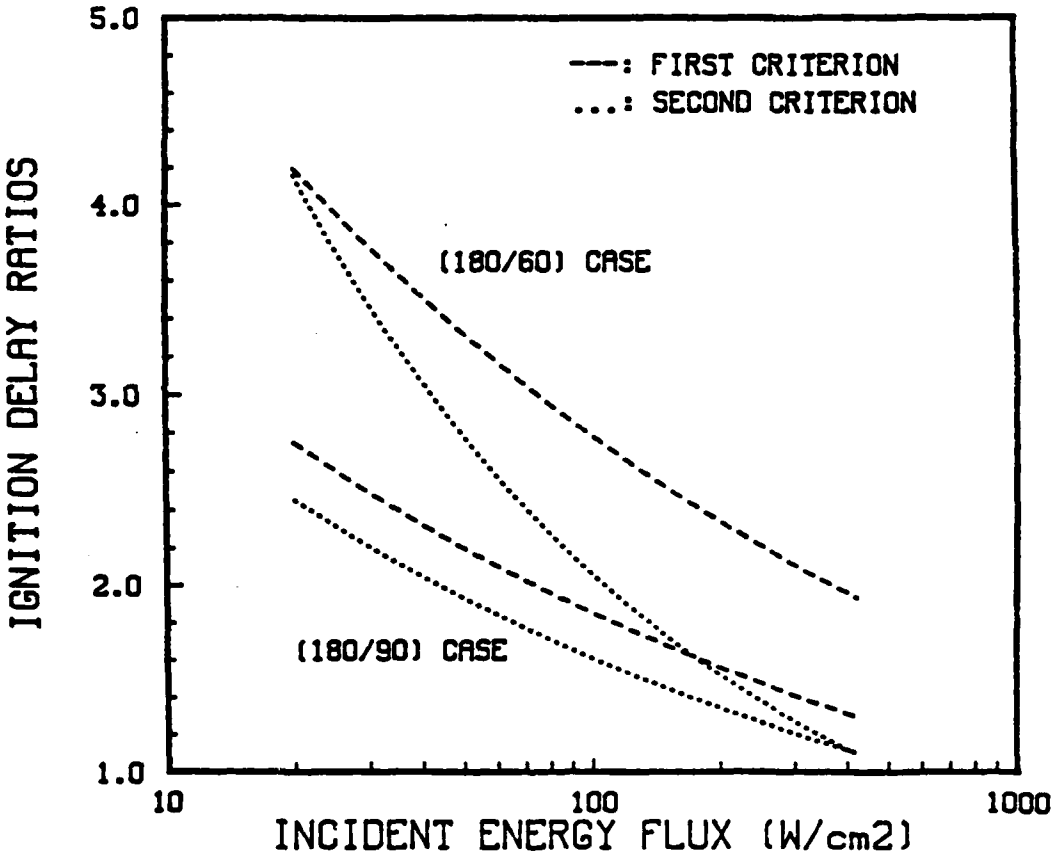

FIG. 6.9 IGNITION DELAY RATIOS OF ACUTE EDGES TO A PLANE SURFACE VERSUS INCIDENT FLUX. Curves shown are computed for both ignition criteria; note the strong dependence of 60° samples on the ignition criterion.

180° sample

$q = 240\ W/cm^2$
$t_{ign} = 139.5$ msec
$t_{laser} = 147$ msec
$t_{rise} = 48.5$ msec

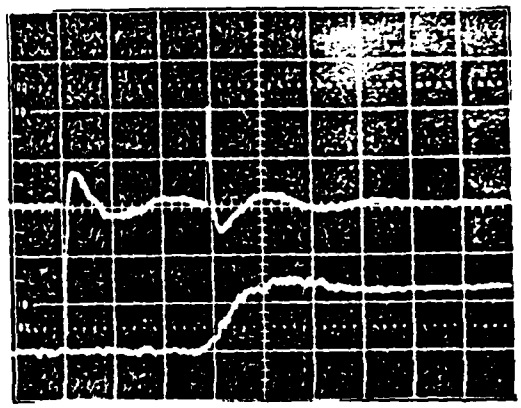

90° sample

$q = 261\ W/cm^2$
$t_{ign} = 91$ msec
$t_{laser} = 98.4$ msec
$t_{rise} = 64.2$ msec

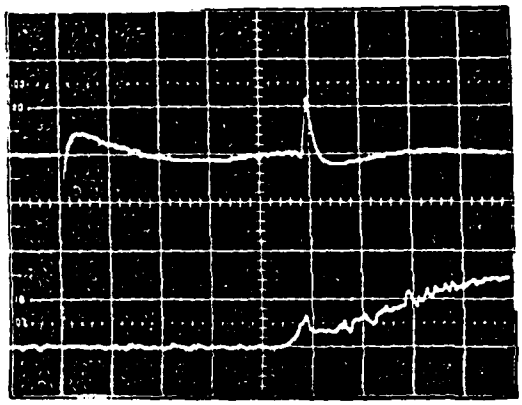

60° sample

$q = 247\ W/cm^2$
$t_{ign} = 79.4$ msec
$t_{laser} = 88.6$ msec
$t_{rise} = 71$ msec

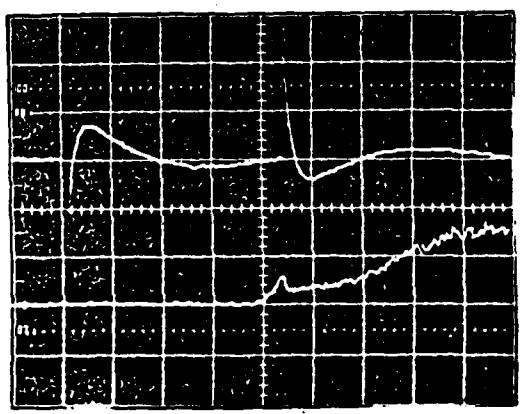

FIG. 6.10. PMT TRACES AT HIGH INCIDENT HEAT FLUXES. Note similar magnitude in signal development time for the different geometries. [upper trace: Cd-Hg-Te detector; lower trace: PMT]

180° sample

$q = 89\ W/cm^2$
$t_{ign} = 776$ msec
$t_{laser} = 844$ msec
$t_{rise} = 50$ msec

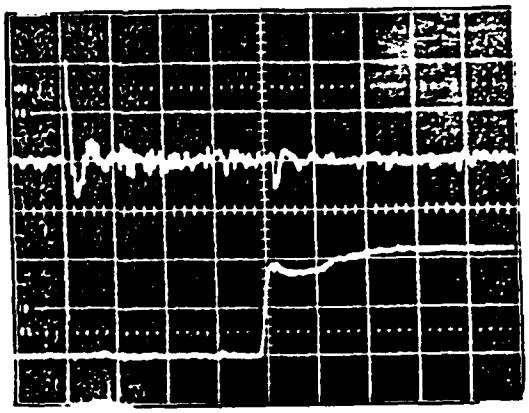

90° sample

$q = 92\ W/cm^2$
$t_{ign} = 424$ msec
$t_{laser} = 491$ msec
$t_{rise} = 209$ msec

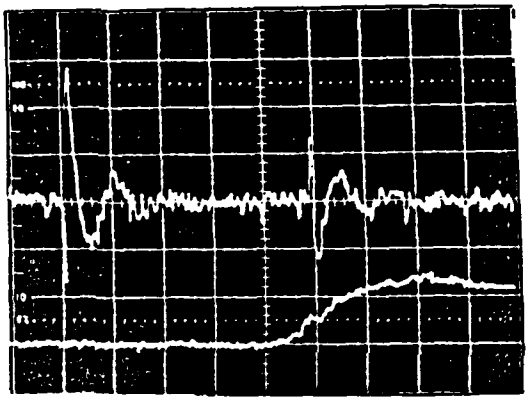

60° sample

$q = 79\ W/cm^2$
$t_{ign} = 270$ msec
$t_{laser} = 349$ msec
$t_{rise} = 358$ msec

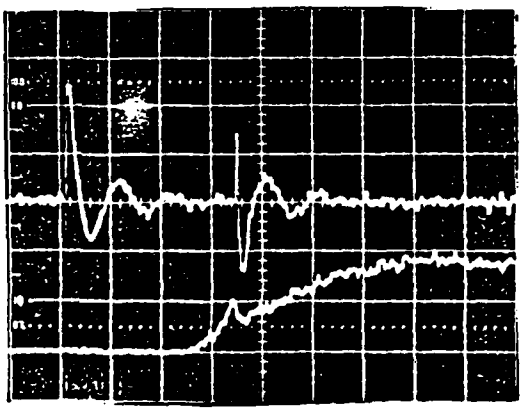

FIG. 6.11. PMT TRACES AT LOW INCIDENT HEAT FLUXES. Note large differences in signal development time for different geometries. [upper trace: Cd-Hg-Te detector; lower trace: PMT]

180° sample

$q = 477\ W/cm^2$
$t_{ign} = 86$ msec
$t_{laser} = 70.6$ msec
scale= .02 sec/div

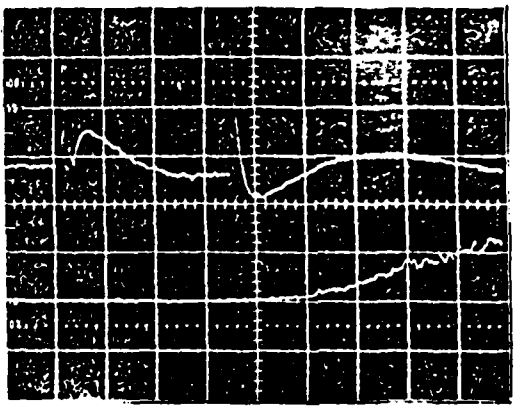

90° sample

$q = 303\ W/cm^2$
$t_{ign} = 83$ msec
$t_{laser} = 83.6$ msec
scale= .02 sec/div

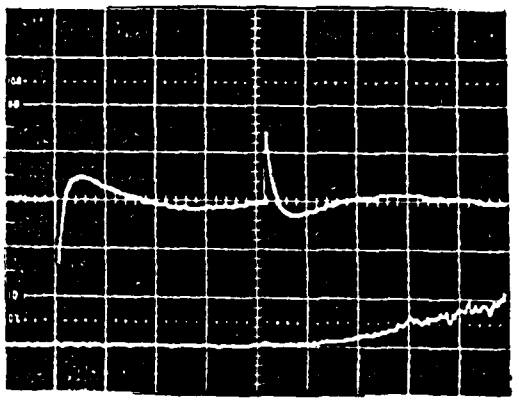

60° sample

$q = 273\ W/cm^2$
$t_{ign} = 69$ msec
$t_{laser} = 48.1$ msec
scale= .05 sec/div

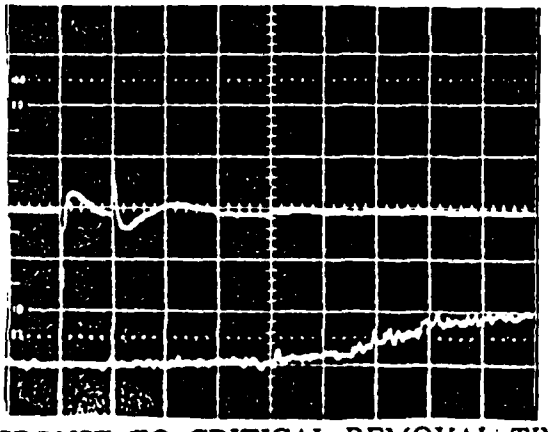

FIG. 6.12. PROPELLANT RESPONSE TO CRITICAL REMOVAL TIME OF RADIATION, HIGH FLUX LEVELS. Scales are indicated to facilitate comparison for different propellant samples. Note more gradual flame development for sharp samples. [upper trace: Cd-Hg-Te detector; lower trace: PMT]

180° sample

q= 100 W/cm^2
t_{ign} = 437 msec
t_{laser} = 441 msec
scale= .10 sec/div

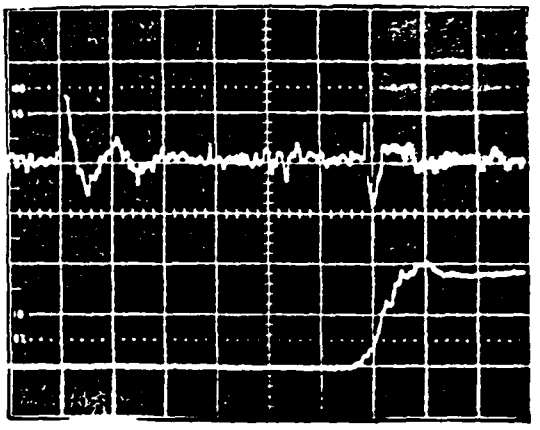

90° sample

q= 100 W/cm^2
t_{ign} = 575 msec
t_{laser} = 588 msec
scale= .10 sec/div

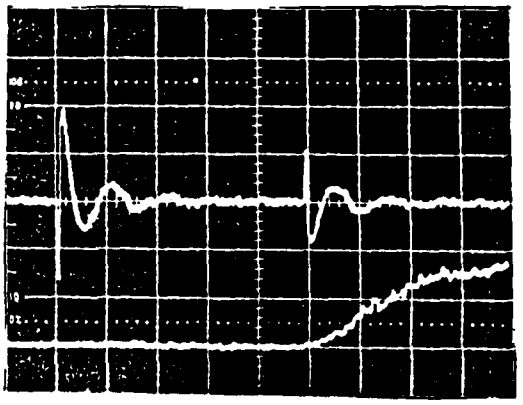

60° sample

q= 87 W/cm^2
t_{ign} = 312 msec
t_{laser} = 272.5 msec
scale= .10 sec/div

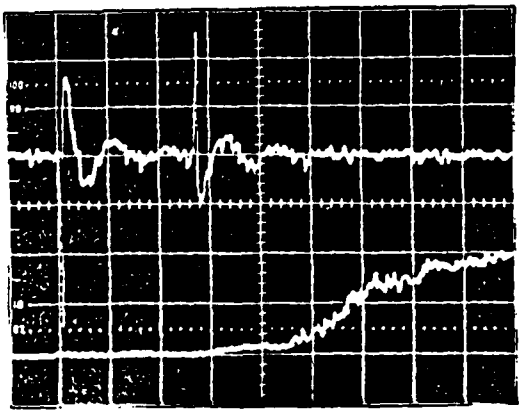

FIG. 6.13 PROPELLANT RESPONSE TO CRITICAL REMOVAL TIME OF RADIATION, LOW FLUX LEVELS. Observe "cooking" behavior for the 60° case. [upper trace: Cd-Hg-Te detector; lower trace: PMT]

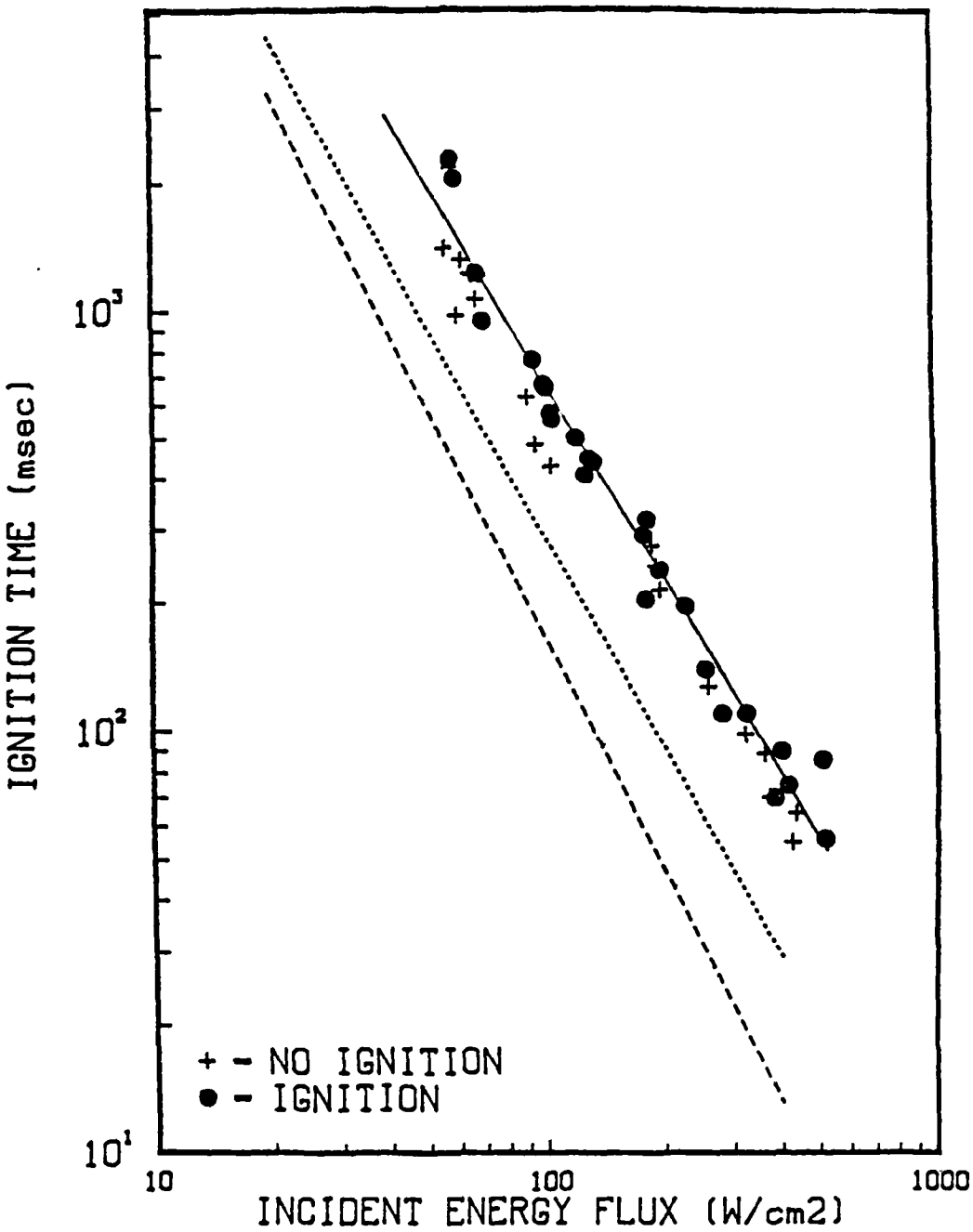

FIG. 6.14(a) COMPARISON OF THEORY AND EXPERIMENT FOR PLANAR CASE: IGNITION TIME VERSUS INCIDENT FLUX. Initial rise in PMT output defined as ignition criterion. [Dotted line: E= 50, $\nu = 10^8$ sec^{-1}; dashed line: E= 100, $\nu = 2.5 \times 10^{18}$ sec^{-1}]

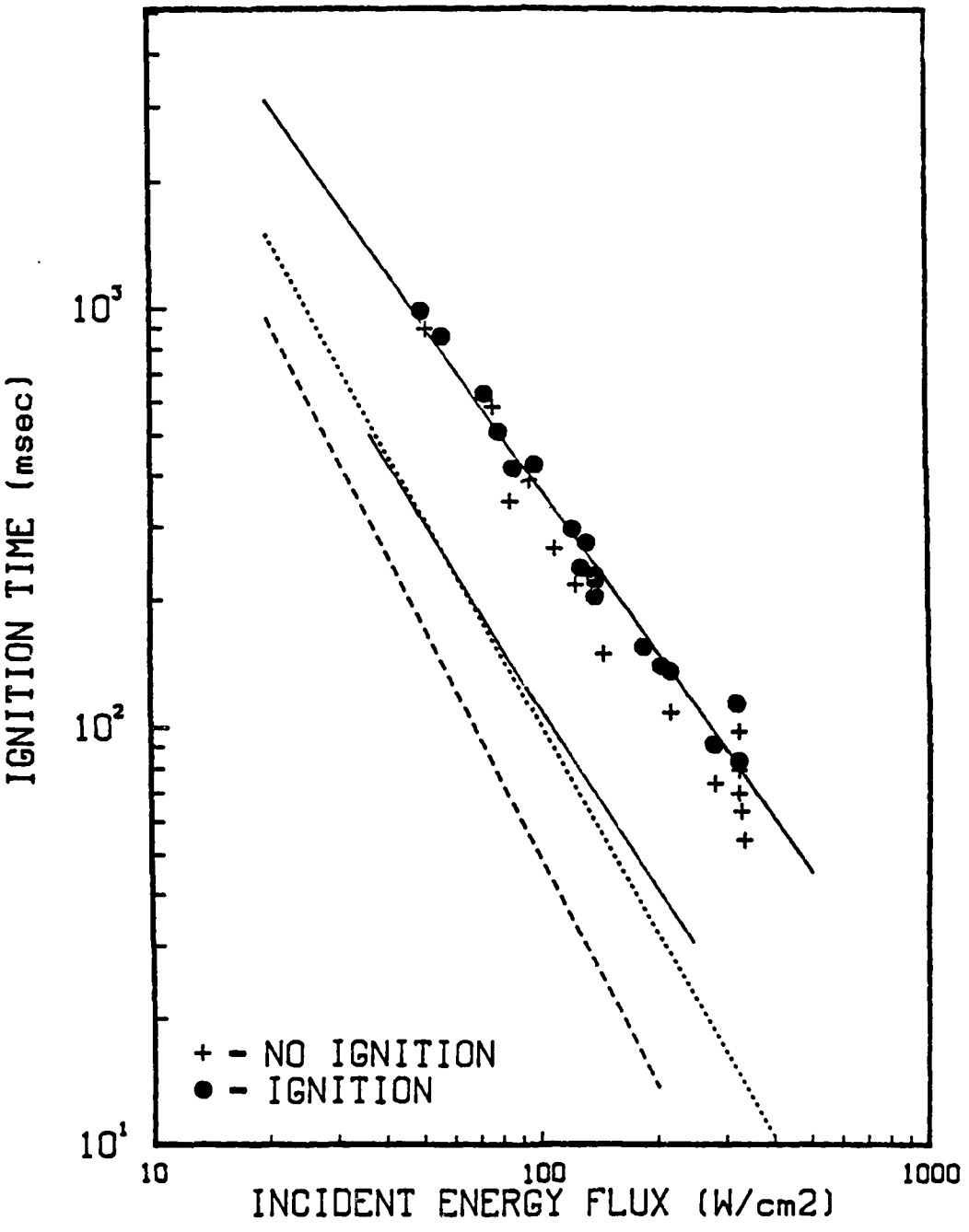

FIG. 6.14(b) COMPARISON OF THEORY AND EXPERIMENT FOR 90° CASE: IGNITION TIME VERSUS INCIDENT FLUX. Initial rise in PMT output defined as ignition criterion. [Dotted line: E= 50, $\nu = 10^8$ sec^{-1}, no rounding; solid line: E= 50, $\nu = 10^8$ sec^{-1}, 25 μm rounding; dashed line: E= 100, $\nu = 2.5 \times 10^{18}$ sec^{-1}, no rounding]

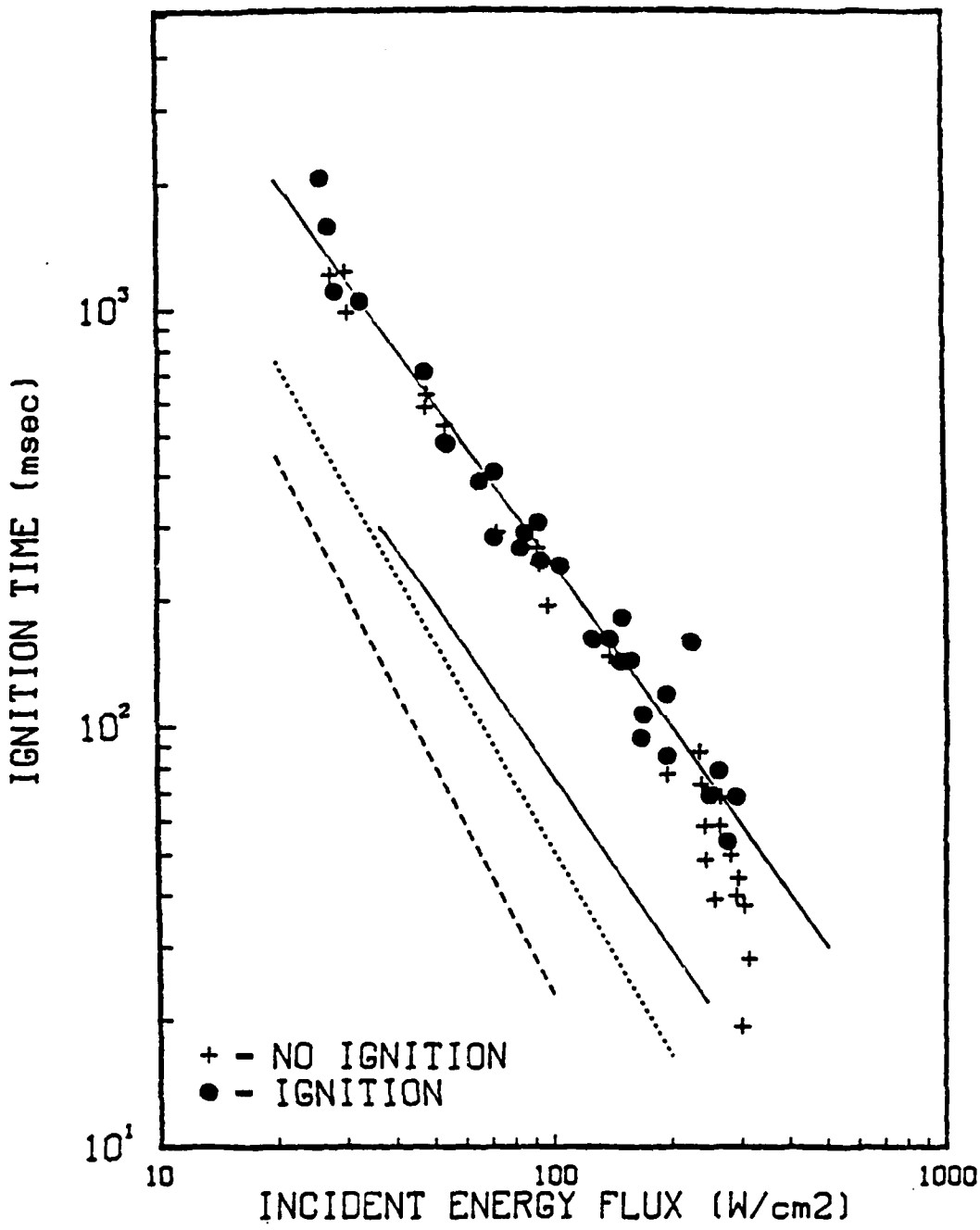

FIG. 6.14(c) COMPARISON OF THEORY AND EXPERIMENT FOR 60° CASE: IGNITION TIME VERSUS INCIDENT FLUX. Initial rise in PMT output defined as ignition criterion. [Dotted line: E= 50, $\nu = 10^8$ sec^{-1}, no rounding; solid line: E= 50, $\nu = 10^8$ sec^{-1}, 25 μm rounding; dashed line: E= 100, $\nu = 2.5 \times 10^{18}$ sec^{-1}, no rounding]

CHAPTER VII

CONCLUDING REMARKS

7.1 Summary

This work is one of the first extensive studies concerned with solid propellant ignition in multi-dimensional geometries. Specific recommendations with respect to future theoretical research include the need for surface rounding in complex propellant shapes, inclusion of surface regression, and incorporation of gas phase processes, provided simulated conditions warrant these considerations. Practical suggestions from an engineering standpoint as a result of having edges and corners on solid propellant surfaces are improved ignitability for marginal igniter systems, and more rapid ignition under low to medium heating conditions and low pressures. This latter aspect could have potential application in restart and/or steering rockets used in space flight.

Multi-dimensional effects on the ignition characteristics of a solid propellant have been investigated using several geometric configurations. To meet this objective, both theoretical and experimental programs of study were initiated. Mathematical models have been formulated, solved numerically, and compared to established one dimensional results. A small experimental program has been conducted where ignition characteristics of geometrically different propellant samples have been determined in terms of the dependence of ignition delay on applied heating rate. These results indicate several interesting features which could potentially contribute to more reliable and faster ignition of ordnance by making the exposed surface convex with respect to the applied igniter flux. In solid rocket motor configurations, roughening or serrating the interior propellant surface could result in faster ignition and more reliable and faster flame spreading behavior.

The basic rationale for the present physical model is to accentuate the effect of geometry by totally ignoring gas phase processes and therefore have the ignition process controlled by a simple, solid phase reaction mechanism. Secondly, the existence of extensive one dimensional results from otherwise identical models has permitted detailed comparisons to delineate geometric effects. As several physico-chemical aspects have been investigated in the past using the one dimensional, solid phase ignition theory, the current work establishes a baseline of results, based on the same theory, for ignition in multi-dimensional geometries.

The mathematical models are solved numerically using the explicit finite difference method. Use of this method is dictated by the large number of computational nodes as a result

of the two dimensional nature of the solution domain, which makes the use of implicit methods prohibitively expensive computationwise. In addition, the implementation of gridstep variations and incorporation of non-similar grid meshes is readily accomplished with the explicit method. Stability is maintained by selecting sufficiently small integration timesteps. Convergence of the numerical results has been assessed by determining their dependence on the spatial stepsize. The trade-off between accuracy and computational time restricts the accuracy of the present results to a few percentage points.

Major results of the computations deal with the changes in ignition delay time (τ_c), the corresponding ignition temperature (θ_c) and fraction reacted (ϵ_c) for identical system parameters, as a result of geometrically different solution domains.

Not surprisingly, the major effect of geometry exhibits itself most distinctly in terms of shorter delay times for geometries having a high degree of convexity towards the applied heat flux. It is shown in chapter V that this geometrically induced ignition time enhancement can exceed one order of magnitude, compared to the planar case. Inclusion of small scale rounding has a significant slowing effect on the overall speed up in ignition. This moderating effect depends primarily on the relative magnitudes of the thermal wave penetration depth at the moment of ignition and rounding radius.

The temperature at ignition (θ_c) is influenced primarily by system parameters A and E and to a lesser extent by geometric factors ϕ_o and γ. Parameters A and E together specify the chemical reactivity of the solid, whereas ϕ_o and γ govern the thermal diffusion aspects during the transient heating process. Maximum temperatures, achieved at the moment of flux removal, are influenced by geometric factors as they control the thermal diffusion process. The observed maximum dip in temperature after flux cessation and prior to final thermal runaway is much less pronounced when a high degree of small scale acuteness is present. Maximum attainable temperatures at ignition become increasingly limited for more acute geometries as local chemical decomposition proceeds more rapidly, which ultimately inhibits thermal runaway due to total reactant consumption.

Geometry influences the amount of reacted material (ϵ_c) in a similar manner as it influences the ignition temperature (θ_c), in that a more acute domain experiences more localized external heating and, as a result, more localized chemical heat production. Fractions reacted increase significantly for more acute geometries such that attainment of ignition becomes rapidly restricted within the context of the current solid phase model as a result of rapid total reactant consumption.

Experimental results reported in chapter VI indicate a noticeable but less significant

effect of geometry in terms of achieving faster ignition. In addition, a much stronger dependence on the applied heating rate is observed for the ignition speed up ratio. Collected data shows other aspects, contrary to predicted model behavior, such as more gradual flame development after initial light detection for sharp samples and short lived, temporary light emissions prior to successful ignition. All these observations indicate mechanisms operational during the experiment which are not predicted by the physical model. This fact is not surprising at all, as no theoretical provisions are incorporated in the model to describe these phenomena.

From the experimental data it is clear, however, that faster ignition is possible, provided the applied flux levels are limited, and that the ignition process is possibly controlled by similar mechanisms as in the one dimensional case, except that these mechanisms have different relative importance during the ignition process. The improved agreement between theory and experiment, by including a physically realistic radius of curvature, definitely indicates the importance of small scale smoothness when investigating geometric effects on solid propellant ignition.

7.2 Conclusions

[1] The speed up in ignition delay time for acute geometries ($\gamma = 0$), in comparison to the planar case, ranges from 2.5 to 3.4 for ϕ_o equal to $\pi/2$, from 6.5 to 12 for $\pi/4$ edges, and from 28 to 36 for $\pi/8$ wedge angles. This more rapid ignition depends slightly on the activation energy of the chemical reaction; the higher the activation energy, the more rapid the onset of ignition.

[2] The introduction of curvature to the exposed sector of angle ϕ_o reduces significantly the abovestated speed up in ignition delay; its extent depends on the relative magnitude of the radius of curvature γ and the thermal wave penetration depth. For a given γ, large scale parameter ϕ_o becomes more important in the overall ignition process for those (A,E) sets which require high temperature levels for ignition.

[3] Ignition delays for the various acute geometries ($\gamma=0$) can be correlated to system parameters A and E by a single empirical equation with two adjustable constants in a form which also accounts for the one dimensional case.

[4] Reactant consumption becomes increasingly important for smaller wedge angles ϕ_o ($\gamma=0$), as it not only affects the ability to achieve ignition but also influences the ignition temperature. For cases where $\gamma>0$, the physical region of strong exothermicity is spatially more distributed and results are less sensitive to ϵ_c.

[5] Temperatures at ignition are influenced primarily by small scale geometric features (γ) and not by the overall wedge angle ϕ_o, for a given set of physiochemical parameters.

[6] Experimental results show faster ignition as a result of geometric convexity of the propellant surface with respect to the applied heat flux. Reported results suggest additional mechanisms responsible during ignition of HTPB-AP propellant samples based on video recordings, PMT traces, and the dependence of ignition time versus applied heat flux.

[7] Solid phase thermal diffusion constitutes a significant portion of the entire delay time, based on the improved agreement between theory and experiment by prescribing a realistic radius of curvature. Additional mechanisms at work are surface gasification, gas phase thermal and species diffusion, and chemical reactivity in the gas phase, as is evident from video recordings and PMT traces.

7.3 Suggestions for Future Work

Future modeling efforts for determining geometric effects should include an adjacent gas phase along with solid surface regression, undergoing either an endothermic or exothermic gasification, as well as species and thermal diffusion and chemical reaction in the gas phase. The starting solid geometry must have a realistic radius of curvature which could be based on some mean AP crystal size. A judicious choice between solid, surface and gas phase exothermic heat release must be made based on the ingredients of the modeled propellant. Major emphasis should be placed on obtaining ignition time dependence on applied flux levels similar to experimental results.

More experimental testing of AP based propellants having a carefully characterized two dimensional geometry is required, especially at low and high pressures and in different gaseous environments. The generation of an experimental three dimensional map for a few common propellants, showing the geometric effect on ignition delays versus applied heating rates and pressure, would be most beneficial for the design of igniter systems. This would enable quick, approximate assessment of surface convexity effects under specified stimuli conditions.

Although somewhat beyond the scope of this current work, it appears worthwhile to deliberately introduce a measure of roughness unto the propellant surface interior to a rocket motor. Its effects can then be observed in terms of the onset of ignition, flame spreading characteristics and the chamber filling, pressurization stage. Interesting observations may possibly be made with respect to flame spread behavior and combustion instability suppression.

BIBLIOGRAPHY

Abramovitz, M., and Stegun, I.A., *Handbook of Mathematical Functions.* Dover Publications, Inc., New York, 1970.

Altman, D., and Grant, A.F., "Thermal Theory of Solid Propellant Ignition by Hot Wires," *4th Symposium (International) on Combustion,* Williams and Wilkins Co., Baltimore, Md., 1953, p. 158.

Andersen, W.H., "Theory of Surface Ignition with Application to Cellulose, Explosives and Propellants," *Combustion Science and Technology,* Vol. 2, 1970, pp. 213-221.

Andersen, W.H., "Analysis of Ignition Behavior of M2 Propellant," *Combustion Science and Technology,* Vol. 5, 1972a, pp. 43-46.

Andersen, W.H., "Model of Transient Ignition of Self-Sustained Burning," *Combustion Science and Technology,* Vol. 5, 1972b, pp. 75-81.

Baer, A.D., and Ryan, N.W., "Ignition of Composite Propellants by Low Radiant Fluxes," *AIAA Journal,* Vol. 3, 1965, pp. 884-889.

Baer, A.D., and Ryan, N.W., "An Approximate but Complete Model for the Ignition Response of Solid Propellants," *AIAA Journal,* Vol. 6, No. 5, May 1968, pp. 872-877.

Beresin, I.S., and Zhidkov, N.P., tr., *Computing Methods.* Pergamon Press Ltd., 1965.

Beyer, R.B., and Fishman, N., "Solid Propellant Ignition Studies with High Radiant Energy as a Thermal Source," *ARS Progress in Astronautics and Rocketry: Solid Propellant Research, Vol. 1,* edited by M. Summerfield, Academic Press, New York, 1960, pp. 673-692.

Boggs, T.L., Derr, R.L., and Beckstead, M.W., "The Surface Structure of AP Composite Propellants," *AIAA Journal,* Vol. 8, Feb. 1970, pp. 370-372.

Bradley, H.H. Jr., "Theory of Ignition of a Reactive Solid by Constant Energy Flux," *Combustion Science and Technology,* Vol. 2, 1970, pp. 11-20.

Bradley, H.H., Jr., and Williams, F.A., "Theory of Radiant and Hypergolic Ignition of Solid Propellant," *Combustion Science and Technology,* Vol. 2, 1970, pp. 41-52.

Burden, R.L., Douglas Faires, J., and Reynolds, A.C., *Numerical Analysis,* 2nd Ed., Prindle, Weber & Schmidt, Boston, Mass. 1981.

Bush, W.B., and Williams, F.A., "Radiant Ignition of a Surface-Cooled Reactive Solid," *Acta Astronautica,* Vol. 2, 1975, pp. 445-462.

Bush, W.B., and Williams, F.A., "Influence of Strong Conductive Cooling on Radiant Ignition of a Reactive Solid," *Combustion and Flame,* Vol. 27, No. 3, Dec. 1976, pp. 321-329.

Carslaw, H.S., and Jaeger, J.C., *Conduction of Heat in Solids.* 2nd Ed. Oxford: Clarendon Press, 1959.

Chamberlain, E.W., Personal Comm., 1988.

Chang, C.M., and Schultz-Grunow, F., "Theoretical and Experimental Study of the Gas-Phase Ignition

of an Evaporating Fuel in a Stagnant Hot Oxidizing Gas," *AIAA Journal*, Vol. 8, No. 1, Jan. 1970, pp. 107-114.

Cohen, N.S., Fleming, R.W., and Derr, R.L., "Role of Binders in Solid Propellant Combustion," *AIAA Journal*, Vol. 12, No. 2, Feb. 1974, pp. 212-218.

CPIA M-2 Manual, X63ASROC, unit 1186, p. 1186.

DeLuca, L., "Extinction Theories and Experiments," Chapter 12, *Fundamentals of Solid-Propellant Combustion, Progress in Astronautics and Aeronautics, Vol. 90*, edited by M. Summerfield and K.K. Kuo, American Institute of Aeronautics and Astronautics, 1984.

DeLuca, L., Caveny, L.H., Ohlemiller, T.J., and Summerfield, M., "Radiative Ignition of Double-Base Propellants: I Some Formulation Effects" *AIAA Journal*, Vol. 14, No. 7, July 1976a, pp. 90-946.

DeLuca, L., Ohlemiller, T.J., Caveny, L.H., and Summerfield, M., "Radiative Ignition of Double Base Propellants: II Pre-ignition and Source Effects," *AIAA Journal*, Vol. 14, No. 8, August 1976b, pp. 1111-1117.

Fishman, N., "Surface Exotherm during Ignition of Ammonium Perchlorate Propellants," *AIAA Journal*, Vol. 5, No. 8, 1967, pp. 1500-1501.

Frank-Kamenetskii, D.A., tr., *Diffusion and Heat Exchange in Chemical Kinetics*. Princeton Univ. Press, 1955.

Frazier, J.H., and Hicks, B.L., "Thermal Theory of Ignition of Solid Propellants," *Journal of Physical and Colloid Chemistry*, Vol. 54, 1950, pp. 872-876.

Guirao, C. and Williams, F.A., "A Model for Ammonium Perchlorate Deflagration between 20 and 100 atm," *AIAA Journal*, Vol. 9, No. 7, July 1971, pp. 1345-1356.

Harayama, M., Saito, T., and Iwama, A., "Ignition of Composite Solid Propellant at Subatmospheric Pressures," *Combustion and Flame*, Vol. 52, 1983, pp. 81-89.

Hermance, C.E., "Geometrical Augmentation of the Ignition of Pyrotechnic Formulations," *Proceedings of the Ninth Pyrotechnic Seminar*, IIT Research Institute, Colorado Springs, August 1984, pp. 289-302.

Hermance, C.E., "Solid Propellant Ignition Theories and Experiments," Chapter 5, *Fundamentals of Solid Propellant Combustion, Progress in Astronautics and Aeronautics, Vol. 90*, edited by M. Summerfield and K.K. Kuo, American Institute of Aeronautics and Astronautics, 1984.

Hermance, C.E., and Kumar, R.K., "Gas Phase Ignition Theory for Homogeneous Propellants Under Shock Tube Conditions," *AIAA Journal*, Vol. 8, No. 9, Sept. 1970, pp. 1551-1558.

Hermance, C.E., Shinnar, R., and Summerfield, M., "Ignition of an Evaporating Gas Containing an Oxidizer," *AIAA Journal*, Vol. 3, No. 9, 1965, pp. 1584-1592.

Hermance, C.E., Shinnar, R., and Summerfield, M., "Ignition of an Evaporating Fuel in a Hot Oxidizing Gas, Including the Effect of Heat Feedback," *Astronautica Acta*, Vol. 12, No. 2, March 1966, pp. 95-112.

Hermance, C.E., and Vorsteveld, L.G., "How Much Do Edges Affect the Ignition of a Homogeneous Reactive Solid: Summary to Date," paper presented at the 1987 JANNAF Fall Meeting, Monterey, CA, Oct. 3-6, 1987.

Hicks, B.L., "Theory of Ignition Considered as a Thermal Reaction," *Journal of Chemical Physics,* Vol. 22, 1954, pp. 414-429.

Hildebrand, F.B., *Introduction to Numerical Analysis.* McGraw-Hill. New York. 1956.

Inami, S.H., McCulley, L., and Wise, H., "Ignition Response of Solid Propellants to Radiation and Conduction," *Combustion and Flame,* Vol. 13, 1969, pp. 531-536.

Jacobs, P.W.M., and Pearson, G.S., "Mechanism of the Decomposition of Ammonium Perchlorate," *Combustion and Flame,* Vol. 13, No. 4, 1969, pp. 419-430.

Kashiwagi, T., "A Radiative Ignition Model of a Solid Fuel," *Combustion Science and Technology,* Vol. 8, 1974, pp. 225-236.

Kashiwagi, T., Waldman, C.H., Rothman, R.B., and Summerfield, M., "Ignition of Polymers in a Hot Oxidizing Gas," *Combustion Science and Technology,* Vol. 8, 1973, pp. 121-131.

Kindelán, M., and Williams, F.A., "Theory for Endothermic Gasification of a Solid by a Constant Energy Flux," *Combustion Science and Technology,* Vol. 10, 1975a, pp. 445-462.

Kindelán, M., and Williams, F.A., "Radiant Ignition of a Combustible Solid with Gas Phase Exothermicity," *Acta Astronautica,* Vol. 2, 1975b, pp. 955-979.

Kindelán, M., and Williams, F.A., "Gas Phase Ignition of a Solid with In-Depth Absorption of Radiation," *Combustion Science and Technology,* Vol. 16, 1977, pp. 47-58.

Kishore, K., and Gayathri, V., Chapter 5, "Chemistry of Ignition and Combustion of Ammonium Perchlorate-Based Propellants," *Fundamentals of Solid Propellant Combustion, Progress in Astronautics and Aeronautics, Vol. 90,* edited by M. Summerfield and K.K. Kuo, American Institute of Aeronautics and Astronautics, 1984.

Kubota, N., "Survey of Rocket Propellants and Their Combustion Characteristics," Chapter 1, *Fundamentals of Solid-Propellant Combustion, Progress in Astronautics and Aeronautics, Vol. 90,* edited by M. Summerfield and K.K. Kuo, American Institute of Aeronautics and Astronautics, 1984.

Kulkarni, A.K., Kumar, M., and Kuo, K.K. "Review of Solid Propellant Ignition Studies," AIAA Paper 80-120, June 1980; also *AIAA Journal,* Vol. 20, No. 2, Feb. 1982, p. 243.

Kumar, R.K., "Gas Phase Ignition of a Composite Solid Propellant Subjected to Radiant Heating," *Combustion Science and Technology,* Vol. 30, 1983, pp. 273-288.

Kumar, R.K., "Importance of Surface Reactions During Radiative Ignition of Composite Solid Propellants," *Combustion and Flame,* Vol. 59, 1985, pp. 63-68.

Kumar, R.K., and Hermance, C.E., "Ignition of Homogeneous Solid Propellants Under Shock Tube Conditions: Further Theoretical Development," *AIAA Journal,* Vol. 9, No. 8, Aug. 1971, pp. 1615-1620.

Kumar, R.K., and Hermance, C.E., "Gas Phase Ignition Theory of a Heterogeneous Solid Propellant Exposed to a Hot Oxidizing Gas," *Combustion Science and Technology,* Vol. 4, 1972, pp. 191-196.

Kumar, R.K., and Hermance, C.E., "Role of Gas Phase Reactions During Radiant Ignition of Solid Propellants," *Combustion Science and Technology,* Vol. 14, 1976, pp. 169-175.

Kumar, M., and Kuo, K.K., "Ignition of Solid Propellant Crack Tip under Rapid Pressurization," *AIAA Journal,* Vol. 18, No. 7, July 1980, pp. 825-833.

Kumar, M., Wills, J.E., Kulkarni, A.K., and Kuo, K.K., "A Comprehensive Model for AP-Based Composite Propellant Ignition," *AIAA Journal,* Vol. 22, No. 4, April 1984, pp. 526-534.

Kuo, K.K., "Present Challenges in Solid-Propellant Combustion Research," Proceedings of Fall Technical Meeting of Eastern Section: The Combustion Institute, Nov. 2-5, 1987.

Lengelle, G., Brulard, J., and Moutet, H., "Combustion Mechanisms of Composite Solid Propellants," *16th Symposium (International) on Combustion,* Pittsburg, PA, 1976, pp. 1257-1269.

Liñán, A., and Crespo, A., "An Asymptotic Analysis of Radiant and Hypergolic Heterogeneous Ignition of Solid Propellants," *Combustion Science and Technology,* Vol. 6, 1972, pp. 223-232.

Liñán, A., and Williams, F.A., "Theory of Ignition of a Reactive Solid by Constant Energy Flux," *Combustion Science and Technology,* Vol. 3, 1971, pp. 91-98.

Liñán, A., and Williams, F.A., "Radiant Ignition of a Reactive Solid with In-Depth Absorption," *Combustion Science and Technology,* Vol. 18, Feb. 1972, pp. 85-97.

McAlevy, R.F. III, Cowan, P.L., and Summerfield, M., "The Mechanism of Ignition of Composite Solid Propellants by Hot Gases," *ARS Progress in Astronautics and Rocketry: Solid Propellant Research,* Vol. 1, edited by M. Summerfield, Academic Press, New York, 1960, pp. 623-652.

McAlevy, R.F. III, and Summerfield, M., "Ignition of Double Base Solid Rocket Propellants," *ARS Journal,* Vol. 32, No. 2, 1962, pp. 270-273.

Niioka, T., "Heterogeneous Ignition of a Solid Fuel in a Hot Stagnation-Point Flow," *Combustion Science and Technology,* Vol. 18, 1978, pp. 207-215.

Niioka, T., and Williams, F.A., "Ignition of a Reactive Solid in a Hot Stagnation-Point Flow," *Combustion and Flame,* Vol. 29, No. 1, 1977, pp. 43-54.

Northam, G.B., Pellett, G.L. and Cofer III, W.R., "Effects of Low-Temperature Ammonium Perchlorate Decomposition on the Ballistic Properties of a CTPB Propellant," *AIAA Journal,* Vol. 10, No. 8, pp. 1068-1072, 1972.

Ohlemiller, T.J., Caveny, L.H., DeLuca, L., and Summerfield, M., "Dynamic Effects on Ignitability Limits of Solid Propellants Subjected to Radiative Heating," *14th Symposium (International) on Combustion,* Combustion Institute, Pittsburg, PA, 1973, pp. 1297-1307.

Ohlemiller, T.J., and Summerfield, M., "A Critical Analysis of Arc Image Ignition of Solid Propellants," *AIAA Journal,* Vol. 6, No. 5, May 1968, pp. 878-886.

Ohlemiller, T.J., and Summerfield, M., "Radiative Ignition of Polymeric Materials in O_2/N_2 Mixtures," *13th Symposium (International) on Combustion,* Combustion Institute, Pittsburg, PA, 1971, pp. 1087-1094.

Ozisik, M.N., *Heat Conduction.* John Wiley and Sons, New York, 1980.

Pearson, G.S., "Perchloric acid Flames VIII- methane-rich flame with oxygen," *Combustion and Flame,* Vol. 12, 1968, pp. 54-62.

Pearson, G.S., "The Role of Catalysts in the Ignition and Combustion of Solid Propellants," *Combustion Science and Technology,* Vol. 3, 1971, pp. 155-163.

Pearson, G.S. and Sutton, D., "Composite Propellant Ignition: Ignition of Ammonia and Other Fuels by Perchloric Acid Vapor," *AIAA Journal,* Vol. 5, No. 2, 1967, pp. 344-346.

Pellett, G.L., "Ammonium Perchlorate Gasification and Combustion at High Heating Rates and Low Pressures," *14th Symposium (International) on Combustion,* Pittsburg, PA, 1972, pp. 1317-1330.

Price, E.W., Bradley Jr. H.H., Dehority, G.L., and Ibiricu, M.M., "Theory of Ignition of Solid Propellants," *AIAA Journal,* Vol. 4, No. 7, July 1966, pp 89-124.

Price, E.W., Bradley, H.H., Jr., and Fleming, R., "Ignition of Solid Propellants," Western States Section, Paper WSS/CI 63-6, April 29-30, 1963.

Price, E.W., Bradley, H.H., Jr., Hightower, J.D., and Fleming, R.O., Jr., "Ignition of Solid Propellants," AIAA Paper 65-120, 1964.

Rabinovitch, B., "Regression Rates and the Kinetics of Polymer Degradation," *10th Symposium (International) on Combustion,* The Combustion Institute, 1965, pp. 1395-1404.

Ramaprabhu, R. and Bhaskaran, K.A., "Thermal Behavior of Solid Propellants Using a Shock Tube," Proc. of the 16th Southeastern Seminar on Thermal Sciences, Vol. 2, 1983a, pp. 863-869.

Ramaprabhu, R. and Bhaskaran, K.A., "Role of Catalyst on the Ignition Mechanism of Composite Solid Propellant," Proc. of the 16th Southeastern Seminar on Thermal Sciences, Vol. 2, 1983b, pp. 871-879.

Rogers, C.R., and Suh, N.P., "Ignition and Surface Temperatures of Double Base Propellants at Low Pressures: II. Comparison of Optical and Thermocouple Techniques," *AIAA Journal,* Vol. 8, No. 8, August 1970, pp. 1501-1506.

Rosser, W.A., Fishman, N., and Wise, H., "Ignition of Simulated Propellants Based on Ammonium Perchlorate," *AIAA Journal,* Vol. 4, No. 9, Sept. 1966, pp. 1615-1622.

Rosser, W.A., Inami, S.H., and Wise, H., "Thermal Diffusivity of Ammonium Perchlorate," *AIAA Journal,* Vol. 4, No. 4, April 1966, pp. 663-666.

Saito, T., Maruyama, T., Higashi, K., and Iwama, A., "Ignition of Laminated Composite Propellants Composed of Ammonium Perchlorate Single Crystal and Fuel-Binder by Means of a CO_2 Laser," *Combustion Science and Technology,* Vol. 15, 1977, pp. 161-168.

Saito, T., Yamaya, T., and Iwama, A., "Effects of Additives on the Ignition of AP-Based Propellants at Subatmospheric Pressures," *Propellants, Explosives, Pyrotechnics,* Vol. 10, 1985, pp. 129-138.

Saul'yev, V.K., *Integration of Equations of Parabolic Type by the Method of Nets.* The Macmillan Company, New York, 1964.

Shannon, L.J., "Composite Solid-Propellant Ignition by Radiant Energy," *AIAA Journal,* Vol. 8, No. 2, Feb. 1970, pp. 346-353.

Shannon, L.J., and Deverall, L.I., "A Model of Solid Propellant Ignition in a Neutral Environment," *AIAA Journal,* Vol. 7, No. 3, 1969. pp. 497-502.

Suh, N.P., Tsai, C.L., Thompson, C.L. Jr., and Moore, J.S., "Ignition and Surface Temperatures of Double Base Propellants at Low Pressure: I. Thermocouple Measurements," *AIAA Journal,* Vol. 8, No. 7, July 1970, pp. 1314-1321.

Summerfield, M., and Kuo, K.K., *Fundamentals of Solid-Propellant Combustion, Progress in Astronautics and Aeronautics, Vol. 90,* American Institute of Aeronautics and Astronautics, 1984.

Thompson, C.L. Jr., and Suh, N.P., "The Interaction of Thermal Radiation and M2 Double-Base Propellant," *Combustion Science and Technology,* Vol. 2, 1970, pp. 59-66.

Vorsteveld, L.G., "Two Dimensional Ignition Theory of a Reactive Solid by Constant Energy Flux," *Master's Thesis,* Univ. of Vermont, Burlington, VT, Oct. 1985.

Vorsteveld, L.G. and Hermance, C.E., "Effect of Geometry on Ignition of a Reactive Solid: Square Corner," *AIAA Journal,* Vol. 25, No. 4, April 1987, pp. 592-597.

Vorsteveld, L.G., and Hermance, C.E., "Effect of Geometry on Ignition of a Reactive Solid: Acute Angles," to be published in Journal of Propulsion and Power, July-Aug. 1988.

Waldman, C.H., "Theory of Heterogeneous Ignition," *Combustion Science and Technology,* Vol. 2, 1970, pp. 81-93.

Waldman, C.H., and Summerfield, M., "Theory of Propellant Ignition by Heterogeneous Reaction," *AIAA Journal,* Vol. 7, July 1969, pp. 1359-1361.

Williams, F.A., "Theory of Propellant Ignition by Heterogeneous Reaction," *AIAA Journal,* Vol. 4, Aug. 1966, pp. 1354-1357.

Wise, H., Inami, S.H., and McCulley, L., "Role of Condensed-Phase Reactions in Ignition and Deflagration of Ammonium Perchlorate Propellants," *Combustion and Flame.* Vol. 11, 1967, pp. 483-488.

APPENDIX A: INERT HEATING OF A SECTOR

A.1 Problem Solution

Consider the problem of a wedge of enclosed angle ϕ_o and large radius b, initially at an uniform temperature $u(r,\phi,0)= \theta(r,\phi,0)-1= 0$, and subject to constant heating along the rays at $\phi= 0$ and $\phi= \phi_o$ for time $t>0$. This transient diffusion problem is mathematically expressed for an isotropic, constant thermal properties, inert solid in dimensionless variables as:

$$\frac{\partial^2 u}{\partial r^2}+\frac{1}{r}\frac{\partial u}{\partial r}+\frac{1}{r^2}\frac{\partial^2 u}{\partial \phi^2}=\frac{\partial u}{\partial t} \qquad (0<\phi<\phi_o,\ 0<r<b) \tag{A-1}$$

subject to the uniform initial condition:

$$u(r,\phi,0)= 0 \tag{A-2}$$

and mixed boundary conditions:

$$\frac{\partial u}{r\partial \phi}(r,0,t)= -1,\quad \frac{\partial u}{r\partial \phi}(r,\phi_o,t)= 1 \quad u(b,\phi,t)= 0 \tag{A-3}$$

For strictly homogeneous boundary conditions Eq. (A-1) is easily solved by the classical method of separation of variables (Carslaw and Jaeger, 1959). Separation equations and their particular solutions for the above system are expressed as:

$$\frac{d\Gamma}{dt}+\beta^2\Gamma = 0:\ \Gamma(t)=e^{-\beta^2 t} \tag{A-4a}$$

$$\frac{d^2\Phi}{d\phi^2}+\nu^2\Phi = 0:\ \Phi(\phi)= \cos(\nu\phi) \text{ or } \sin(\nu\phi) \tag{A-4b}$$

$$\frac{d^2R}{dr^2}+\frac{1}{r}\frac{dR}{dr}+(\beta^2-\frac{\nu^2}{r^2})R = 0:\ R(r)= J_\nu(\beta_m r) \text{ or } Y_\nu(\beta_m r) \tag{A-4c}$$

where J_ν and Y_ν are Bessel functions of order ν of the first and second kind respectively. The variables have been separated in the form:

$$u(r,\phi,t)= R(r)\ \Phi(\phi)\ \Gamma(t) \tag{A-5}$$

To solve the above system with inhomogeneous conditions, spatial variables are removed sequentially by integral transforms. First, define the following integral transform and its inversion formula to remove the ϕ-variable dependence from Eq. (A-1):

$$\tilde{u}(r,\nu,t)= \int_0^{\phi_o} K(\nu,\phi)u(r,\phi,t)d\phi \tag{A-6}$$

$$u(r,\phi,t)= \sum_{\nu=0}^{\nu=\infty} K(\nu,\phi)\tilde{u}(r,\nu,t) \tag{A-7}$$

The kernel $K(\nu,\phi)$ is tabulated for different boundary conditions in Ozisik (1980); for the present inhomogeneous boundary conditions in the ϕ direction, $K(\nu,\phi)$ becomes:

$$K(\nu,\phi)= \sqrt{2/\phi_o}\cos(\nu_n\phi) \tag{A-8}$$

and eigenvalues ν_n's are found from:

$$\sin(\nu_n\phi_o)= 0, \quad \nu_n = n\pi/\phi_o, \quad n = 0, 1, 2,... \tag{A-9}$$

Next take the integral transform of Eq. (A-1) by applying the integral transform (A-6), using the eigenfunction separation in Eq. (A-4b) and the ϕ-variable boundary conditions from Eq. (A-3) to obtain:

$$\frac{\partial^2\tilde{u}}{\partial r^2} + \frac{1}{r}\frac{\partial\tilde{u}}{\partial r} - \nu^2\tilde{u} + \frac{1}{r}\left[K(\nu,\phi)_{\phi_o} + K(\nu,\phi)_0\right] = \frac{\partial\tilde{u}}{\partial t} \tag{A-10}$$

Introduce next the radial integral transform and its inversion formula to remove the r-variable from Eq. (A-10):

$$\hat{u}(\beta_m,\nu,t)= \int_0^b rK_\nu(\beta_m,r)\tilde{u}(r,\nu,t)dr \tag{A-11}$$

$$\tilde{u}(r,\nu,t)= \sum_{m=1}^{m=\infty} K_\nu(\beta_m,r)\hat{u}(\beta_m,\nu,t) \tag{A-12}$$

Again, the kernel $K_\nu(\beta_m,r)$ is tabulated for a variety of boundary conditions in Ozisik (1980). For the present homogeneous boundary condition of the first kind, expressed by Eq. (A-3), this kernel is given as:

$$K_\nu(\beta_m,r)= \frac{\sqrt{2}}{b}\frac{J_\nu(\beta_m r)}{J'_\nu(\beta_m b)} \tag{A-13}$$

and eigenvalues are determined from:

$$J_\nu(\beta_m b)= 0, \quad m = 1, 2, 3,... \tag{A-14}$$

Next take the integral transform of Eq. (A-10) by applying integral transfrom (A-11), using Eq. (A-4c) and the homogeneous radial boundary condition from Eq. (A-3) to yield:

$$-\beta_m^2\hat{u} + \int_0^b \left[K(\nu,\phi)_{0,\phi_o}\right]K_\nu(\beta_m,r)dr = \frac{d\hat{u}}{dt} \tag{A-15}$$

In order to evaluate the integral in Eq. (A-15), the terms within the brackets must be determined explicitly as a function of ν. Evaluation of $K(\nu,\phi)$ at ϕ equal to 0 and ϕ_o produces:

$$K(\nu,\phi)= 2\sqrt{2/\phi_o} \quad \text{for even } n, \quad K(\nu,\phi)= 0 \text{ for odd } n \tag{A-16}$$

The integral in Eq. (A-15) is then expressed as:

$$A(\beta_m,\nu)= \frac{4}{b\sqrt{\phi_o}} J'^{-1}_{\nu}(\beta_m b)\int_0^b J_\nu(\beta_m r)dr \tag{A-17}$$

Abramovitz and Stegun (1970) give the answer for the integral in Eq. (A-17) in terms of an infinite series as:

$$A(\beta_m,\nu)= \frac{8}{\beta_m b\sqrt{\phi_o}} J'^{-1}_{\nu}(\beta_m b)\sum_{k=0}^{k=\infty} J_{\nu+2k+1}(\beta_m b) \tag{A-18}$$

The resulting ordinary differential equation (A-15) and its initial condition Eq. (A-2) in the time variable of the temperature transform are then rearranged as:

$$\frac{d\hat{u}}{dt} + \beta_m^2\hat{u} = A(\beta_m,\nu) \qquad \hat{u}(\beta_m,\nu,0)= 0 \tag{A-19}$$

The solution to Eq. (A-19) is directly written down in terms of the transformed temperature variable $\hat{u}$ as:

$$\hat{u}(\beta_m,\nu,t)= \frac{A(\beta_m,\nu)}{\beta_m^2}\left[1-e^{-\beta_m^2 t}\right] \tag{A-20}$$

By straightforward backsubstitution of Eq. (A-18) into Eq. (A-20), application of inversion formula Eq. (A-12) along with the kernel $K_\nu(\beta_m,r)$ expressed by Eq. (A-13), and finally application of inversion formula Eq. (A-7) with kernel $K(\nu,\phi)$ from Eq. (A-8), produces the complete solution in the original temperature variable θ (= u+1) as:

$$\theta(r,\phi,t)= 1 + \frac{8}{b^2\phi_o}\sum_{\nu=0}^{\nu=\infty}\sum_{m=1}^{m=\infty}\frac{1}{\beta_m^3}\frac{J_\nu(\beta_m r)}{J'^2_\nu(\beta_m b)}\cos(\nu\phi) \tag{A-21}$$

$$\left[1-e^{-\beta_m^2 t}\right]\sum_{k=0}^{k=\infty} J_{\nu+2k+1}(\beta_m b)$$

By slightly expanding this double series solution, Eq. (A-21) can be written as:

$$\theta(r,\phi,t) = 1 - \frac{8}{b^2\phi_o}\sum_{m=1}^{m=\infty}\frac{1}{\beta_m^3}\frac{J_0(\beta_m r)}{J'^2_0(\beta_m b)}[1-e^{-\beta_m^2 t}]\sum_{k=0}^{k=\infty}J_{\nu+2k-1}(\beta_m b) \qquad \text{(A-22)}$$

$$+\frac{16}{b^2\phi_o}\sum_{\nu_n=n\pi/\phi_o}^{\nu=\infty}\sum_{m=1}^{m=\infty}\frac{1}{\beta_m^3}\frac{J_\nu(\beta_m r)}{J'^2_\nu(\beta_m b)}[1-e^{-\beta_m^2 t}]\cos(\nu\phi)\sum_{k=0}^{k=\infty}J_{\nu+2k+1}(\beta_m b)$$

A.2 Numerical Implementation of the Series Solution

The numerical evaluation of the series was broken down into four general segments for a selected wedge angle ϕ_o to verify its accuracy and convergence characteristics.

1) Determination of eigenvalues β_m from $J_\nu(\beta_m b) = 0$ for desired values of order ν.

2) Evaluation of the infinite series $\sum_{k=0}^{k=\infty}J_{\nu+2k+1}(\beta_m b)$ for each order ν.

3) Numerical development of common summation terms $C_{\nu,m}$ expressed as:

$$C_{\nu,m} = \frac{1}{\beta_m^3}\sum_{k=0}^{k=\infty}J_{\nu+2k+1}(\beta_m b) \qquad \text{(A-23)}$$

4) Computation of individual terms for a given set of values for (r,ϕ,t) and summing these terms over the selected orders (ν's) and zeroes (m's).

Computational details of steps 1-4:

1) Each root of $J_\nu(\beta_m b) = 0$ was initially approximated using McMahon's Expansion for Large Zeros (Abramovitz and Stegun, 1970). The exact value was then converged upon within a tolerance of 10^{-14} using the Secant Method (Burden, Douglas Faires and Reynolds, 1981). The IMSL library package available on the *VAX 8600* was used for Bessel function computation. Roots for each order ν were then stored in data files.

2) Computation of the infinite series $\sum_{k=0}^{k=\infty}J_{\nu+2k+1}(\beta_m b)$ was accomplished by returning to the original integral and manipulating it into a more palatable form via the following integral relations.

$$\int_o^\infty J_\nu(x)dx = 1 \qquad \text{(A-24)}$$

$$\int_0^z J_{2n}(x)dx = \int_0^z J_0(x)dx - 2\sum_{k=0}^{k=n-1}J_{2k+1}(z) \qquad \text{(A-25)}$$

$$\int_z^\infty \left[J_0(x)+iY_0(x)\right]dx = x^{-1/2}e^{i(z-\pi/4)}\left[\sum_{k=0}^{k=7}(-1)^k a_k(x/8)^{-2k-1} - i\sum_{k=0}^{k=7}(-1)^k b_k(x/8)^{-2k}\right] \qquad \text{(A-26)}$$

After some manipulation, the original integral can then be expressed for integer values of the order index ν (= 2n) as:

$$\int_0^b J_\nu(x)dx = 1 - \int_b^\infty J_0(x)dx - 2\sum_{k=0}^{k=n-1} J_{2k+1}(b) \qquad \text{(A-27)}$$

The first integral on the right hand side is evaluated using the real part of Eq. (A-26). For cases were b< 8, Simpson's Rule was employed as the approximation in Eq. (A-26) is limited to large x.

3) For efficient evaluation of the series solution, the $C_{\nu,m}$ terms were computed once for each order ν and several hundred β_m's. Results were stored in data files. Use was made of the recurrence relation:

$$J_{\nu-1}(x) - J_{\nu+1}(x) = 2J'_\nu(x) \qquad \text{(A-28)}$$

4) Finally, the double series was developed for a given set of r, ϕ and t for a specific number (N) of each order ν and number of zeroes (M) per order ν. Previously computed β_m's and $C_{\nu,m}$'s were inputted directly from the created data files.

A.3 Accuracy and Convergence of Series Solution

The accuracy and speed of convergence of Eq. (A-22) was investigated to determine the overall feasibility and usefulness of the inert solution as an aid in reducing overall computational times for the reactive case.

This investigation was undertaken in two directions:

(i) Compare the results of Eq. (A-22) for $\phi_o = \pi/2$ to the exact closed form solution expressed in Cartesian coordinates to the identical heat conduction problem.

(ii) Compare the Double Series solution to results of a numerical finite difference scheme for $\phi_o = \pi/6$.

The solution to the one-dimensional heat equation for a semi-infinite region with Neumann conditions at x= 0 is given in Carslaw and Jaeger (1959). Application of the principle of superposition permits development of the solution for a semi-infinite corner ($\phi_o = \pi/2$) geometry subject to Neumann conditions along x= 0 and y= 0 by algebraic addition of the individual one-dimensional solutions. The result in Cartesian coordinates for $\phi_o = \pi/2$ is expressed as:

$$\theta(x,y,t) = 1 - 2\sqrt{t/\pi}\left[e^{-x^2/4t} + e^{-y^2/4t}\right] - x\ \mathrm{erfc}(x/2\sqrt{t}) - y\ \mathrm{erfc}(y/2\sqrt{t}) \qquad \text{(A-29)}$$

The finite difference scheme was integrated only for an angle of $\pi/12$ due to symmetry; the pie slice section was subdivided into 50 nodes in radial direction, 5 nodes in tangential direction. Nodes were placed $\Delta\phi/2$ away from the physical boundary analogous to a previous investigation (Vorsteveld, 1985).

A.4 Results

For the special case of $\phi_o = \pi/2$, radial temperature profiles for 2 selected angles of $\phi_1 = \pi/80$ and $\phi_2 = \pi/5$ were computed and plotted along with the result of equation (A-29) for an arbitrary time of .02 sec. Different computational cases are tabulated below.

Table A.1 Square Corner Comparison
Computational Cases

Case	Orders(ν's)	# of Zeroes(m's)	Terms in Series
I	1-9	100	900
II	1-9	200	1800
III	1-9	300	2700
IV	1-4	800	
	5-9	300	4700

Figures A.1 and A.2 show radial temperature profiles for ϕ_1; Figures A.3 and A.4 for ϕ_2. Associated CPU times on a VAX 8600 system for the 4 cases range from 4.1 sec for case I up to 49.4 sec for case IV per evaluated node. A few remarks concerning these figures are appropriate at this point.

1. Oscillatory behavior around the exact temperature curve in Fig.'s A.1 and A.3 for case I is clearly visible. The small number of terms involved is the culprit in that positive and negative contributions of the $J_\nu(\beta_m b)$ term are not spatially balanced.

2. The mismatch displayed in Figure A.2 at large radii is caused by the relatively few orders involved and better agreement is anticipated by incorporating higher orders in the summation. Higher orders are strictly necessary for very small angular arguments to yield negative $\cos(\nu\phi)$ terms which will result in a slight drop in temperature.

3. Better agreement is reached by employing more terms in the series evaluation as is anticipated and illustrated in these figures. Secondly, series temperatures appear to converge faster in regions of low thermal gradients as can be concluded by comparing Fig.'s A.2 and A.4. All this leads to the conclusion that the temperatures of most interest, namely those near the tip and boundary, are computed with more difficulty than those within the interior.

For the second investigation where $\phi_o = \pi/6$, temperatures at selected nodes are compared at an arbitrary time. Eq. (A-22) is evaluated for two cases: case I with 1200 zeros for $\nu = 0$, 300 zeros for $\nu = 12$, 24 and 36; case II with only 300 zeros for $\nu = 0$, 12, 24 and 36. Table A.2 indicates the % error between numerical and series results. Data in Table A.2 indicate errors ranging from -.4 to .3% for case I. Discrepancies increase only to a few percent in the extreme tip region for case II; results in the remaining region are virtually unaffected by the reduced number of terms carried in the summation. Hence a large number of zeros must be carried along in the summation to achieve reasonable accuracy in the extreme tip region.

Table A.2 30° Acute Wedge Comparison				
Error Percentages between Numerical and Series Solution				
r	ϕ	Temperature	Case I	Case II
(-)	(rad)	(-)	(% error)	(% error)
.005	$\pi/120$	1.2907	+.02	-1.90
.005	$\pi/24$	1.2904	+.05	-1.90
.015	$\pi/120$	1.2568	-.11	-.28
.015	$\pi/24$	1.2557	-.025	-.19
.075	$\pi/120$	1.1236	-.40	-.45
.075	$\pi/24$	1.1181	+.08	+.04
.24	$\pi/120$	1.0488	-.19	-.19
.24	$\pi/24$	1.0313	+.15	+.15
.83	$\pi/120$	1.0328	+.17	+.17
.83	$\pi/24$	1.0031	-.25	-.25

A.5 Conclusions

1. The integral transform technique yields the solution to the equations (A-1), (A-2) and (A-3) in the form of a double infinite series. Main advantage of this solution is that Eqs. (A-22), (A-9) and (A-14) can compute temperature values for any enclosed angle ϕ_o. Secondly, these equations provide a means of checking numerical schemes.

2. Detailed comparison to an exact solution for $\phi_o = \pi/2$ indicates good convergence of the series solution provided a sufficiently large number of terms are evaluated. The use of equation (A-22) as an aid in overall reduction of CPU time is rendered obsolete due to the needed CPU time for reasonable accuracy.

3. The double series can, however, be used to quickly check individual nodal temperatures calculated by a numerical scheme. Especially in the exposed tip region close agreement to the exact answer can be reached provided a sufficiently large number of terms are evaluated. Practical usefulness of the series solution is restricted therefore to verify local temperatures as an aid in the determination of a maximum allowable stepsize to maintain certain error bounds.

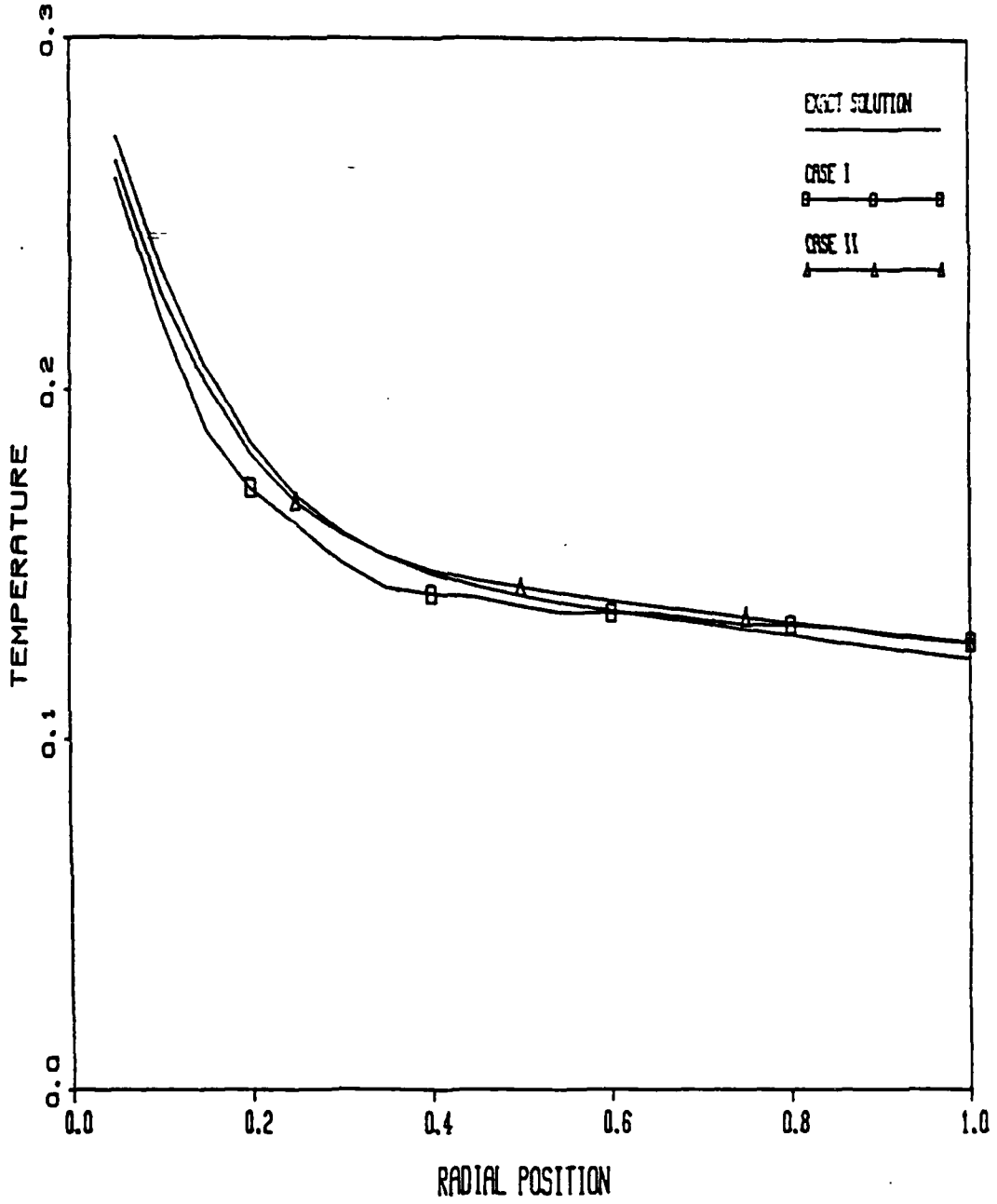

FIG. A.1 SURFACE TEMPERATURE PROFILES FOR EXACT AND SERIES SOLUTION: CASE I AND II. Case I: 100 zeroes for first 9 orders, Case II: 200 zeroes for first 9 orders.

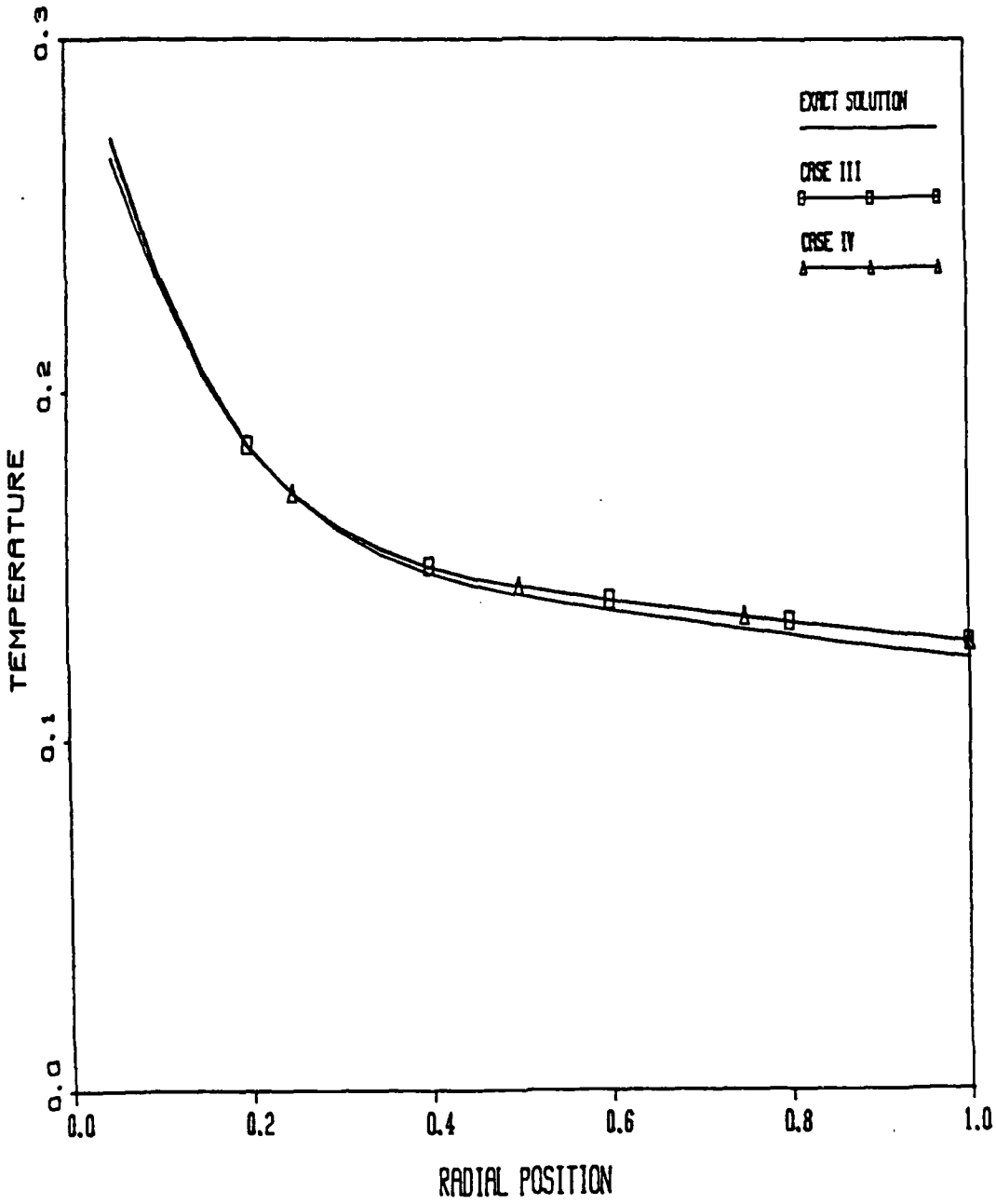

FIG. A.2 SURFACE TEMPERATURE PROFILES FOR EXACT AND SERIES SOLUTION: CASE III AND IV. Case III: 300 zeroes for first 9 orders, Case IV: 800 zeroes for first 4 orders, 300 zeroes for next 5 orders.

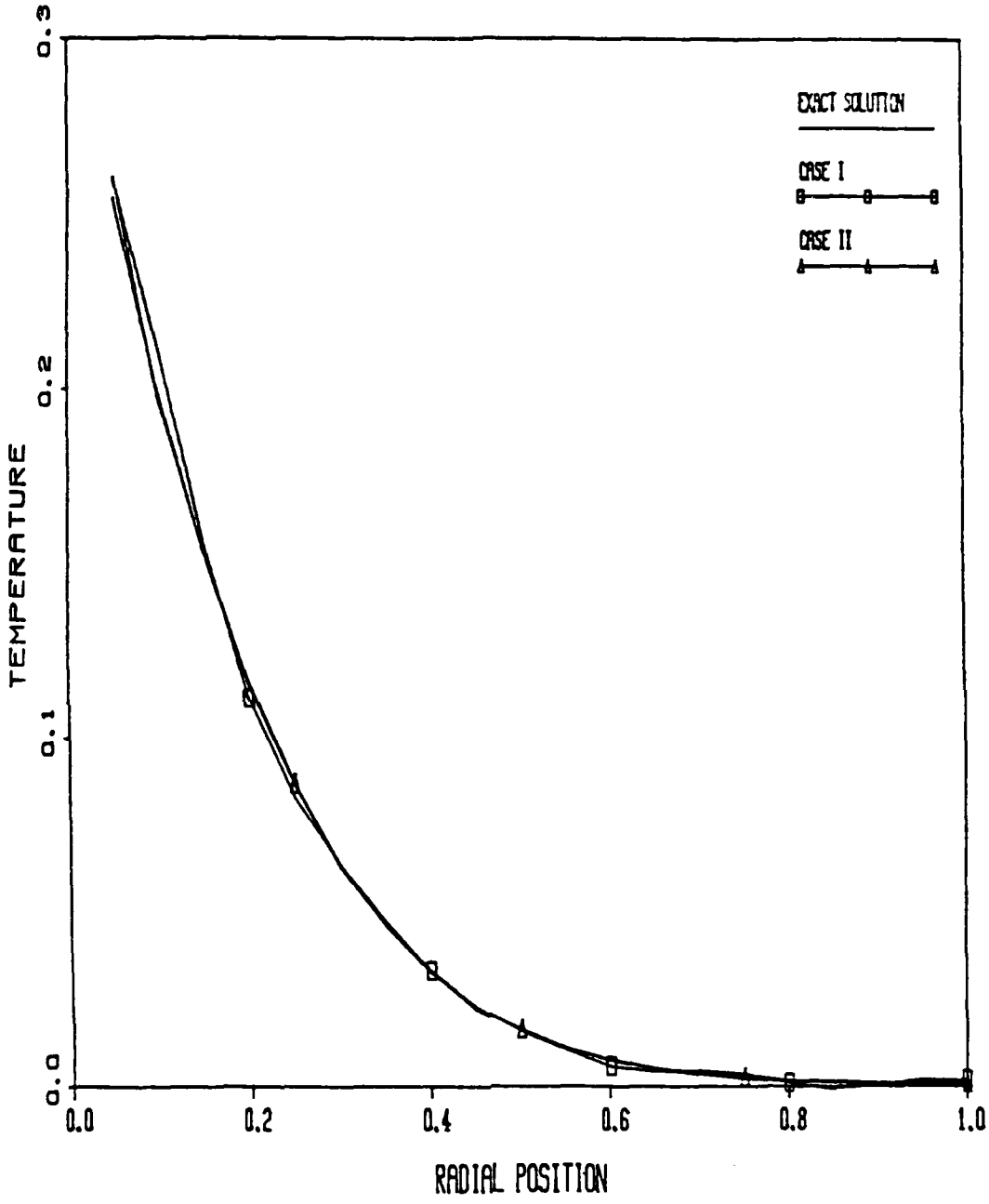

FIG. A.3 INTERIOR TEMPERATURE PROFILES FOR EXACT AND SERIES SOLUTION: CASE I AND II. Case I: 100 zeroes for first 9 orders, Case II: 200 zeroes for first 9 orders.

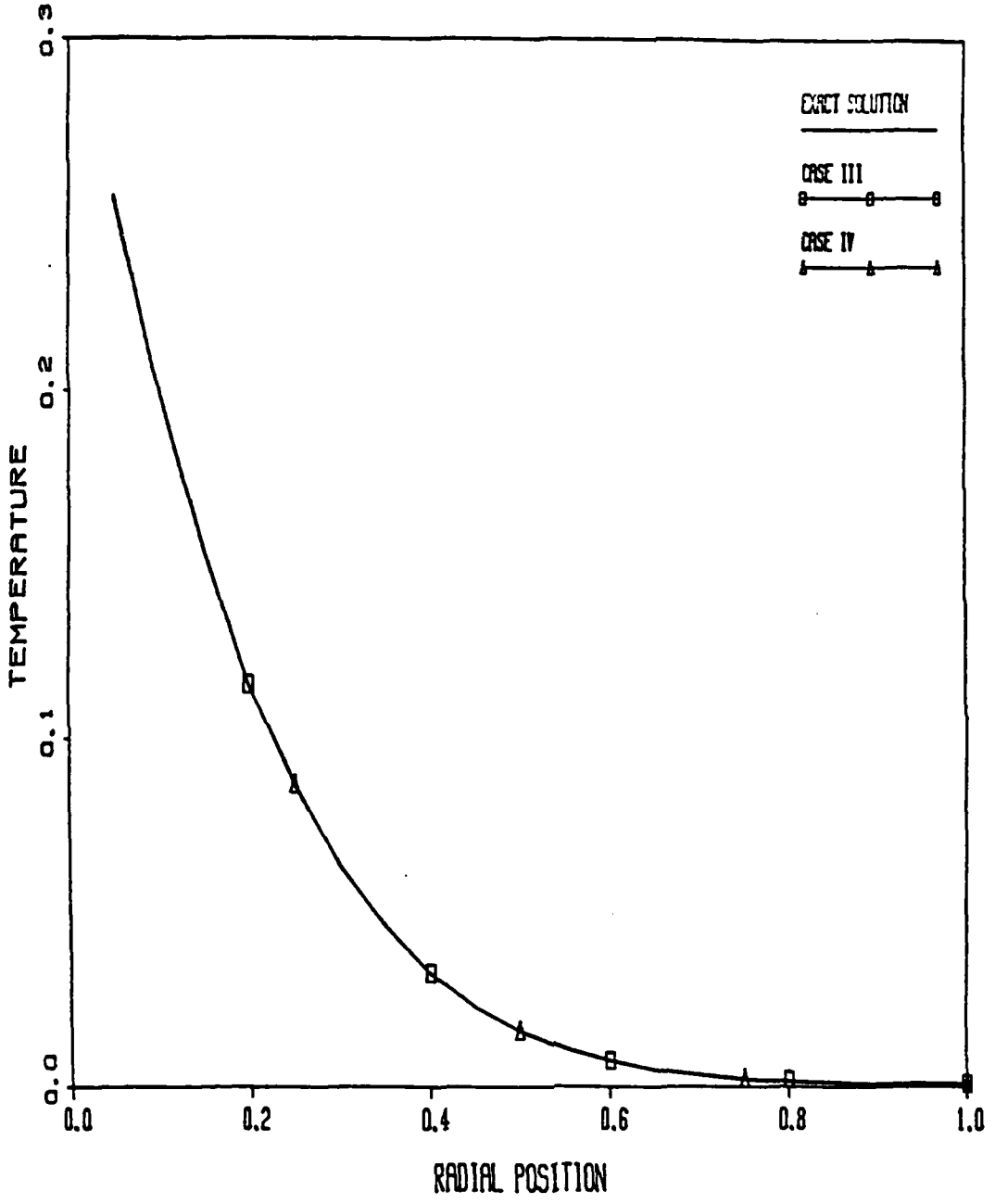

FIG. A.4 INTERIOR TEMPERATURE PROFILES FOR EXACT AND SERIES SOLUTION: CASE III AND IV. Case III: 300 zeroes for first 9 orders, Case IV: 800 zeroes for first 4 orders, 300 zeroes for next 5 orders.

APPENDIX B: COMPUTER CODE VERIFICATION

B.1 Square Corner Code

Accuracy and convergent behavior of this computer code has been thoroughly tested for the square corner geometry, and has been reported in great detail by Vorsteveld (1985). Major observations from this work and used in the present simulations are: (1) dimensionless stepsizes ranging from .02 to .05; (2) the justified neglect of both reactant consumption and chemical heat production during the initial heating phase (up to half of total heating time); and (3) monotonically convergent ignition data. Spatial stepsizes were selected based on a less than 3% reduction in ignition time for halving the current stepsize.

B.2 Acute Angle Code

Accuracy and convergence behavior of this computer code have been investigated and assessed in two steps. For parameter A equal to zero (inert heating) and ϕ_o equal to $\pi/2$, numerical solutions have been compared to the exact closed form solution, expressed by Eq. (4-7), as a first step in assessing its accuracy. Numerical simulations have been performed for different Δr's and for second and third order forward differences approximating radial diffusion in the extreme tip sector. These first and second order forward difference approximations, based on an uniform stepsize h, are presented by Berezin and Zhidkov (1965) as:

$$\dot{y}_0 = \frac{1}{6h}\left[-11y_0 - 18y_1 - 9y_2 + 2y_3\right] + O(h^3) \qquad \text{(B-1)}$$

$$\ddot{y}_0 = \frac{1}{24h^2}\left[70y_0 - 208y_1 + 228y_2 - 112y_3 + 22y_4\right] + O(h^3) \qquad \text{(B-2)}$$

Temporal deviations in temperature from the exact value, as computed from Eq. (4-7), have been monitored at certain physical locations in the numerical gridmesh. These deviations, expressed as an error percentage, are displayed in Figures B.1 through B.4 for these physical locations, illustrating the accuracy of the numerical scheme. Based on these figures several observations are enumerated here which will be instrumental in assessing the convergence behavior of the reactive code.

1) The largest errors occur in the extreme tip of the exposed corner. It is therefore of eminent importance that temperatures are resolved sufficiently in this region.

2) Numerically computed tip region temperatures exhibit larger negative errors at early times, and more positive errors at later times, with increasing stepsize Δr.

3) Third order differencing of radial diffusion yields reduced error peaks at early times but increasingly underestimates temperatures at longer times. Second order forward differences are therefore preferred.

Although the above analysis is performed for ϕ_o equal to $\pi/2$ and M= 10, applicability of the above error behavior of the acute angle code can be inferred to hold qualitatively for smaller wedge angles because of equality in equations, conditions and stepsizes. Since the material heats up faster for smaller wedge angles, the temporal and stepsize related error

variations, produced by the code, become more important in explaining convergence related aspects of the numerical simulations. These remarks establish bounds of accuracy of the acute angle code.

The second step consists of assessing the convergence characteristics of the acute angle code which is done by computing ignition times for two values of the fundamental stepsize Δr for wedge angle ϕ_o equal to $\pi/4$. The percent deviation in ignition time due to a halving of the gridstep Δr as defined by Eq. (B-3), is shown in Figure B.5 on a map of ignition time τ_c versus log(1/A) for 5 activation energies. Shaded regions indicate regimes exhibiting similar heat transfer characteristics and convergence behavior. In Eq. (B-3) $\tau_c(a)$ represents the computed value of τ_c at Δr= a.

$$\% \text{ dev} = 100 \frac{\tau_c(.04) - \tau_c(.02)}{\tau_c(.02)} \qquad \text{(B-3)}$$

Whereas in the square corner case the above term always remained positive and less than 3 percent, deviations range from -10% to +5% for the acute angle code. Brief explanations for each of the shaded regions, displayed in Figure B.5, are given to justify this seemingly erratic convergence pattern in the ignition time data.

I) Smaller τ_c's in region I for Δr equal to .04 are explained in terms of larger positive errors for this stepsize at early times, as is clear from Fig.'s B.1 through B.4.

II) In this region the chemical heat release becomes significant only later in time such that the abovementioned gridstep related mechanism is not present anymore or has reduced significantly. A finer grid resolves slightly higher tip temperatures and hence faster ignition.

III) Ignition in this regime is delayed by higher levels of ϵ_c for small Δr which require therefore additional heat input and result in larger ignition times to attain thermal runaway.

IV) Numerical results in region IV are not strongly affected by variations in Δr because of a diminished discretization effect since both meshes better approximate the thermal gradients at longer heating times.

A special investigation has been undertaken for the most erroneous data point (A=10^{13}, E=33 1/3) with Δr = .01, .02, .04 and second and third order forward approximations for radial diffusion in the tip sector. Results are displayed in Table B.1.

Table B.1 Convergence Test

Results for E= 33 1/3, log(A)= 13, B= .9

order	Δr	τ_c	θ_c	ϵ_c	% error*
2	.04	.00500	1.342	.114	-10.4
3	.04	.00513	1.344	.116	-8.1
2	.02	.00558	1.430	.293	0.0
3	.02	.00562	1.423	.300	+0.7
2	.01	.00577	1.450	.423	+3.4

* % error computed relative to second order forward approximation, Δr= .02.

Differences displayed in Table B.1 lend further support to abovementioned explanatory statements concerning the convergent behavior of the acute angle computer code. For the

above set of A and E parameter values these discrepancies are exacerbated as chemical heat release becomes substantial even at very small temperature rises. The numerical errors of the code are most apparent in this region as is evident from Figures B.1 to B.4.

Results reported in Chapter V for the acute angle geometry with $\phi_2 = \pi/4$ and $\pi/8$ must therefore be considered in light of the limitations inherent to the code. the extreme sharpness of the exposed tip and the accompanying discretization effects.

B.3 Rounded Tip Code

Prior to discussing the accuracy and convergence characteristics of the rounded tip code, two minor items are briefly addressed here. The first problem concerns the implementation of diffusion terms across gridmesh interfaces. Here the internodal distance between nodes directly adjacent to the interface is taken as the sum of the half of the relevant stepsizes. With respect to the interfaces between Regions I and II and between Regions II and III respectively, the following expressions for these internodal distances are derived:

$$D_{I-II} = (r_i)_I \Delta\alpha/2 + \Delta\xi/2, \text{ and } D_{II-III} = (r_i)_{II} \Delta\phi/2 + r_{1I} \tag{B-4}$$

As will be shown shortly, the rounded tip code maintains overall stability and yields reasonably convergent results as various stepsizes are reduced. Despite the approximate nature of the interface grid mesh implementation, sufficiently accurate results are generated by the code.

Secondly, the approximation of the radial diffusion terms for the central nodes located at the apex of Regions I and III is achieved using order $\Delta\xi$ forward difference expressions as:

$$\dot{y}_0 = \frac{1}{2\Delta\xi}(-3y_0 + 4y_1 - y_2) + O(\Delta\xi) \tag{B-5}$$

$$\ddot{y}_0 = \frac{1}{\Delta\xi^2}(2y_0 - 5y_1 + 4y_2 - y_3) - O(\Delta\xi) \tag{B-6}$$

Due to possible numerical diffusion, it is imperative that stepsizes near the apex of each region are as small as computationally feasible.

The rounded tip code, generated to solve the ignition problem in composite geometries, is verified in two steps. First, the accuracy of the code is verified by comparing its results for A=0 to simple 1-D temperature profiles and observing qualitative differences as a result of the composite geometry. and secondly, the convergent character of the reactive code is established by noting the effect of gridsize reductions on reactive results.

Testing of the inert code (A=0) proceeds in several ways to investigate the following aspects:

1) Stepsize dependence on temperature profiles: ideally, no differences in profiles should occur as it will indicate sufficient spatial resolution of gradients.

2) Effect of angular diffusion in region I at early and long times. From intuition one recognizes that at early times thermal penetration is less than tip radius γ, such that heat flow is

governed primarily by radial diffusion. At longer times the distance γ constitutes only a minor portion of the total thermal wave; hence angular diffusion must be more apparent in region I at this point.

3) Nature of heat flow far away from the rounded tip region. Strictly speaking, the validity of the imposed "no-flow" boundary condition at ξ_o is verified by comparing temperature profiles in Region II.

Figures B.6 and B.7 show radial temperature profiles in Region I at τ equal to .1 and .5 for $\alpha = 0$ and $\alpha_o/2$ along with the 1-D radial profile. These curves show qualitative agreement with the 1-D curves as well as a rather small gridstep effect. Further, angular energy diffusion is apparent in Figure B.7 but not in Figure B.6.

Both radial and Cartesian profiles are shown in Figures B.8 through B.10 for τ equal to .02, .1 and .5 respectively. Displayed profiles are taken from $\alpha = \alpha_o/2$ in Region I, and from Region II at $\xi \simeq .09$ and at $\xi \simeq .9\xi_o$. These figures clearly show that the heat transfer characteristics change from predominantly one dimensional at short times to two dimensional at long times.

Finally, Figures B.11 and B.12 show profiles in Region II at $\xi \simeq .09$, $.5\xi_o$ and $.9\xi_o$ for τ equal to .1 and .5. The existence of a thermal gradient at small ξ but not at large ξ is quite obvious which lends further credibility to the imposition of the zero gradient condition at large ξ.

In summary, highest accuracy of the inert code is achieved at early times, irrespective of the employed stepsize Δr_o. Stepsizes ranging from .02 to .04 yield sufficient accuracy at larger times. The reasonable agreement in the radial temperature profiles at all times τ for different stepsizes Δr_o is especially promising as the ignition process is controlled by the thermal field in this region.

Convergence of the reactive rounded tip code is investigated by running the code for selected gridmesh sizes for identical system parameters A and E. Tables B.2 through B.5 list the ignition time τ_c for 4 data sets, computed with different gridmesh characteristics.

Table B.2 Convergence Test

Results for E= 66 2/3, log(A)= 21, B= 4.5

Δr	$\Delta \xi$	τ_c	% error
.05	.06	.1020	1.30
.04	.05	.1010	.30
.03	.04	.1009	.20
.02	.03	.1007	0.0

Table B.3 Convergence Test

Results for E= 50, log(A)= 13, B= 0.9

Δr	$\Delta \xi$	τ_c	% error
.04	.06	.26380	.26
.03	.045	.26224	0.0

Table B.4 Convergence Test			
Results for E= 100, log(A)= 23, B= 4.5			
Δr	$\Delta \xi$	τ_c	% error
.05	.06	.37384	1.73
.04	.05	.37336	1.60
.03	.04	.36747	0.0

Table B.5 Convergence Test			
Results for E= 83 1/3, log(A)= 9, B= 4.5			
Δr	$\Delta \xi$	τ_c	% error
.05	.07	2.995	2.20
.03	.05	2.931	0.0

In all these simulations only a very small temperature rise is observed in the low temperature region of the solution domain. From the above tables it is clear that: 1) the code produces monotonically convergent results as stepsizes $\Delta \xi$ and Δr are reduced. and 2) the percent error in ignition times is significantly smaller than for the acute wedge geometries, with its magnitude being comparable to those for the 90° square corner. Based on the tabulated results, the following guidelines have been established for computing results over ranges in A and E parameter values. Results reported in Chapter V are obtained according to the recommendations in Table B.6.

Table B.6		
Practical Gridmesh Values		
τ_c	Δr	$\Delta \xi$
.02-0.5	.02-.03	.03-.04
.50-5.0	.04-.05	.06-.07

As a final check on the rounded tip code, Figures B.13 and B.14 show both inert and reactive temperature profiles inward from 4 different surface locations close to the point of ignition. Chemical heat release is visible throughout a significant portion of the solution domain, but most apparent near the surface in the rounded tip region.

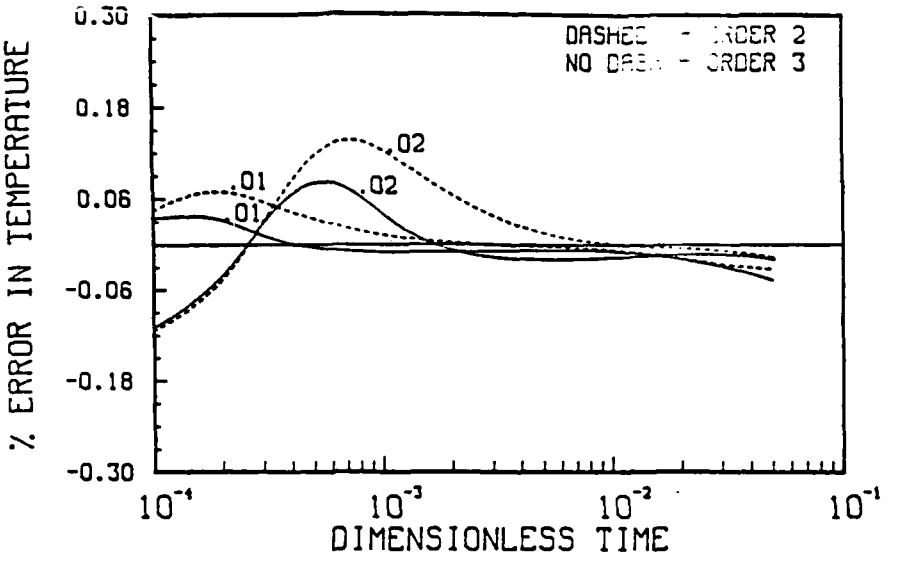

FIG. B.1 ERROR PROFILES FOR TIP NODE (1,1) COMPUTED BY 90° ACUTE ANGLE CODE. Comparison between exact inert solution and numerical code using 2nd and 3rd order forward tip approximations and Δr_o equal to .01 and .02.

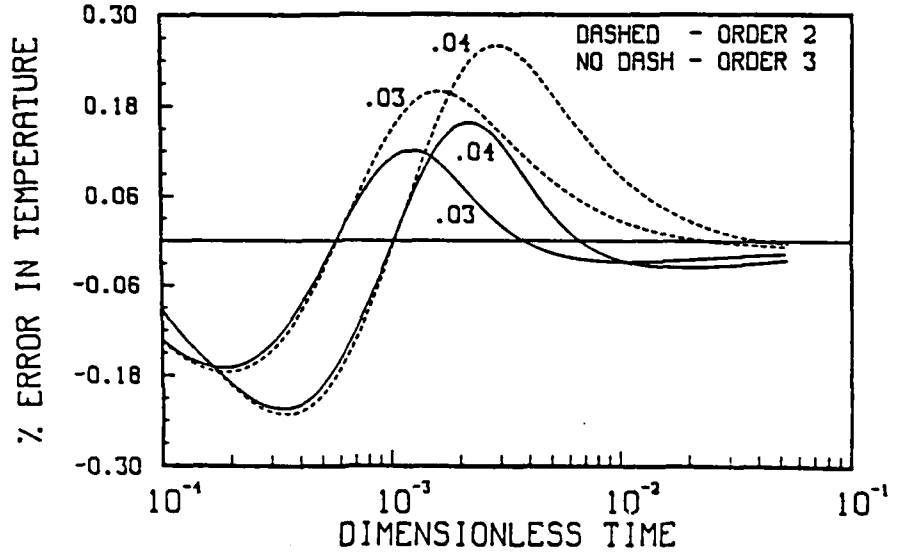

FIG. B.2 ERROR PROFILES FOR TIP NODE (1,1) COMPUTED BY 90° ACUTE ANGLE CODE. Comparison between exact inert solution and numerical code using 2nd and 3rd order forward tip approximations and Δr_o equal to .03 and .04.

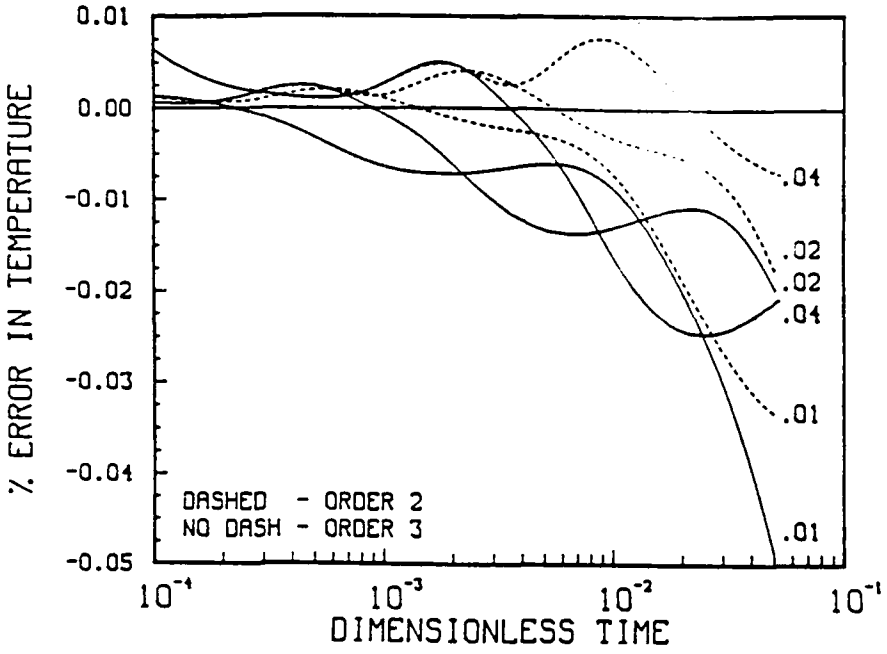

FIG. B.3 ERROR PROFILES FOR SURFACE NODE (4,1) COMPUTED BY 90° ACUTE ANGLE CODE. Comparison between exact inert solution and numerical code using 2nd and 3rd order forward tip approximations and Δr_o equal to .01, .02 and .04.

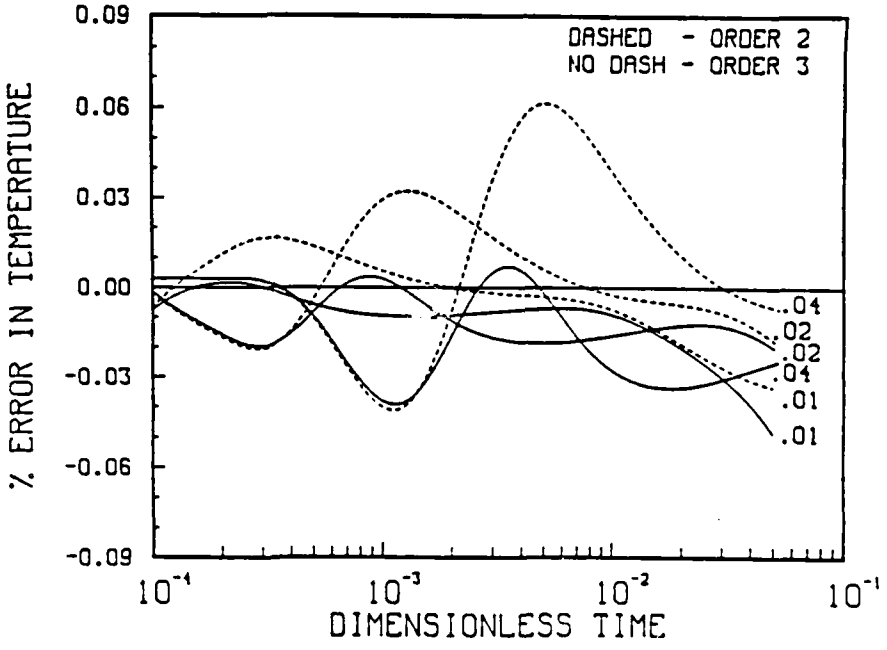

FIG. B.4 ERROR PROFILES FOR INTERIOR NODE (2,3) COMPUTED BY 90° ACUTE ANGLE CODE. Comparison between exact inert solution and numerical code using 2nd and 3rd order forward tip approximations and Δr_o equal to .01, .02 and .04.

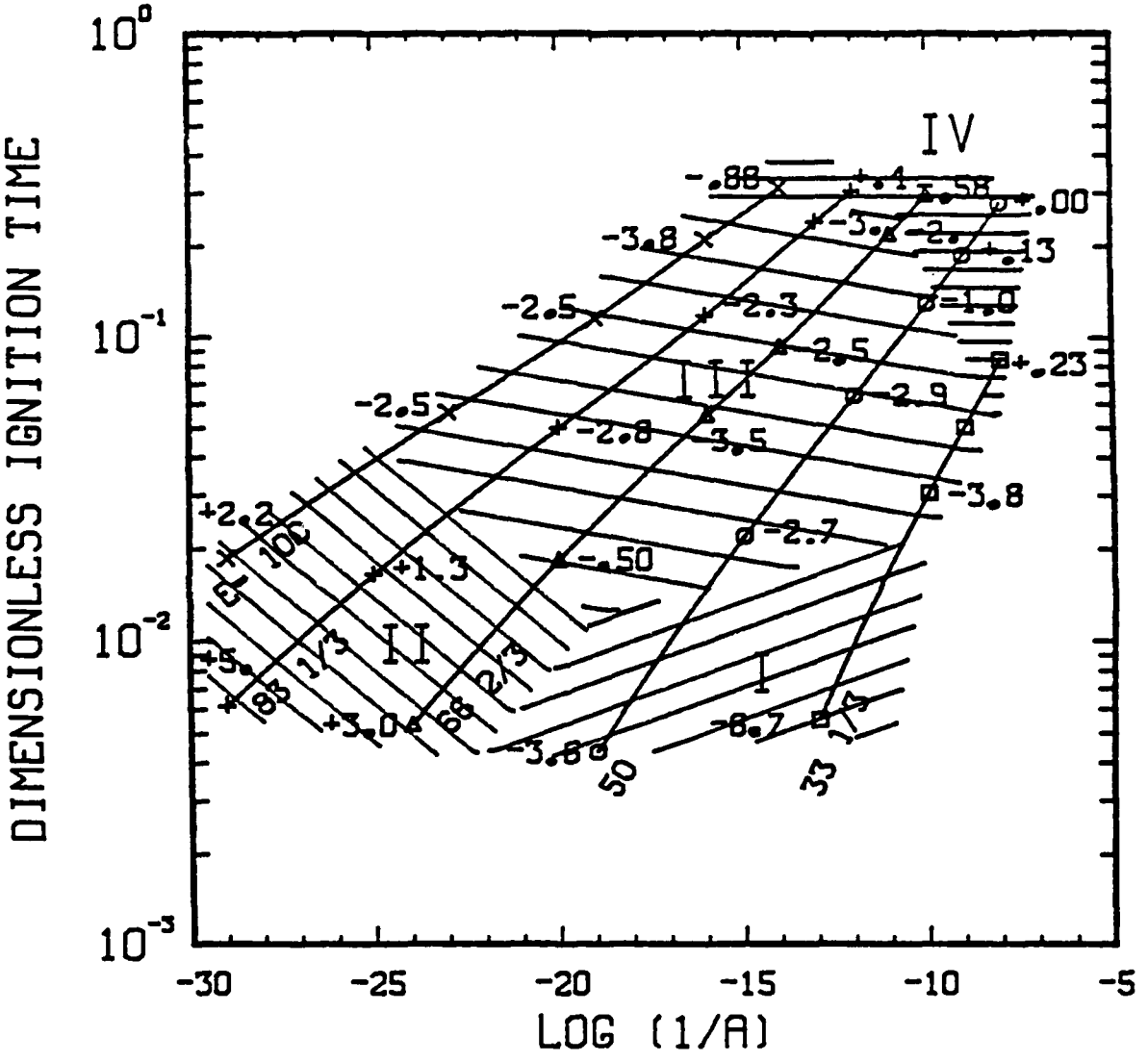

FIG. B.5 MAP SHOWING CONVERGENT BEHAVIOR OF IGNITION TIMES FOR 45° ACUTE WEDGE. Percent deviation in ignition time τ_c displayed for Δr_o equal to .02 and .04. Shaded areas exhibit similar convergence characteristics.

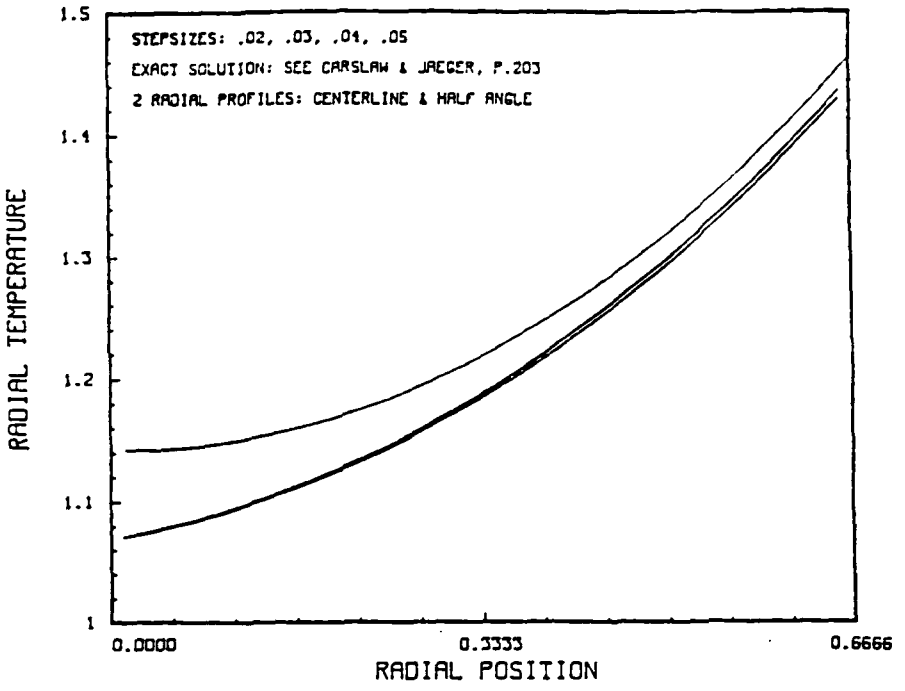

FIG. B.6 INERT RADIAL TEMPERATURE PROFILES FOR $\gamma = 2/3$, $\tau = .1$ FOR ROUNDED TIP CODE. Upper curve represents the 1-D profile, middle curve shows profile along $\alpha = 0°$ ray, lower curve along $\alpha = \alpha_o/2$ ray.

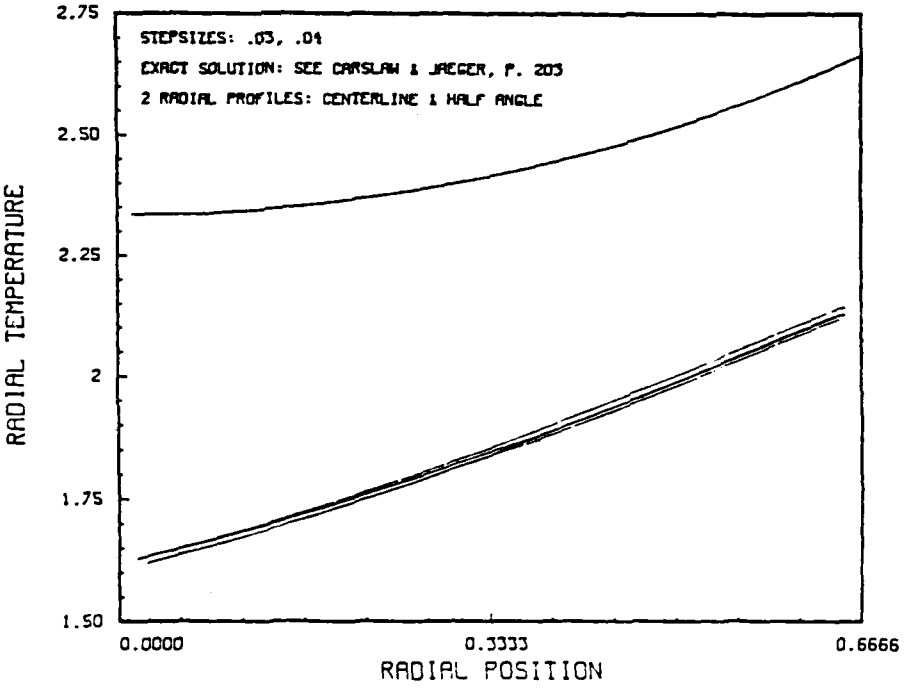

FIG. B.7 INERT RADIAL TEMPERATURE PROFILES FOR $\gamma = 2/3$, $\tau = .5$ FOR ROUNDED TIP CODE. Upper curve represents the 1-D profile, middle curve shows profile along $\alpha = 0°$ ray, lower curve along $\alpha = \alpha_o/2$ ray.

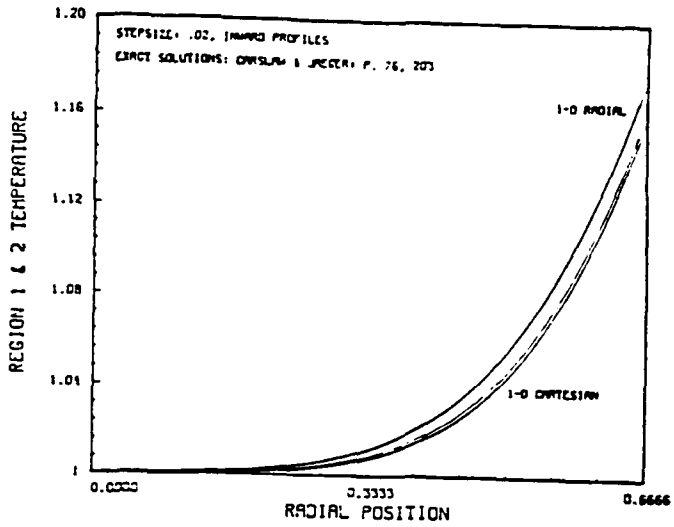

FIG. B.8 REGION I AND II TEMPERATURE PROFILES AT $\tau = .02$, $\gamma = 2/3$. Upper curve at $\alpha = \alpha_o/2$, middle curve at $\xi \simeq .09$, lower curve at $\xi \simeq .9\xi_o$. (1-D radial and Cartesian profiles included).

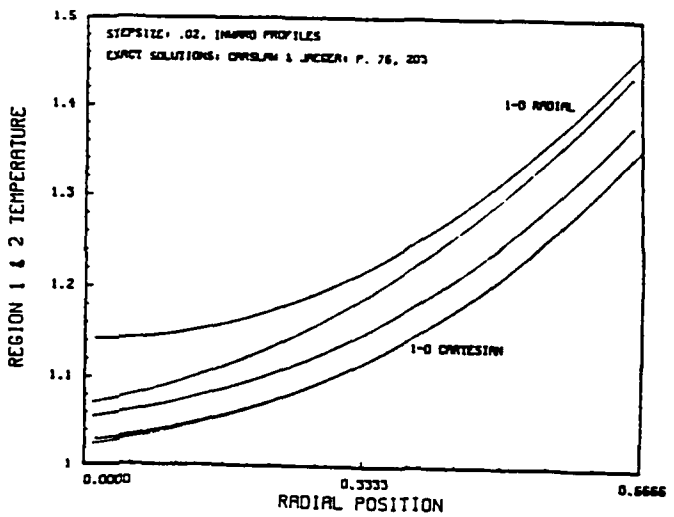

FIG. B.9 REGION I AND II TEMPERATURE PROFILES AT $\tau = .10$, $\gamma = 2/3$. Upper curve at $\alpha = \alpha_o/2$, middle curve at $\xi \simeq .09$, lower curve at $\xi \simeq .9\xi_o$. (1-D radial and Cartesian profiles included).

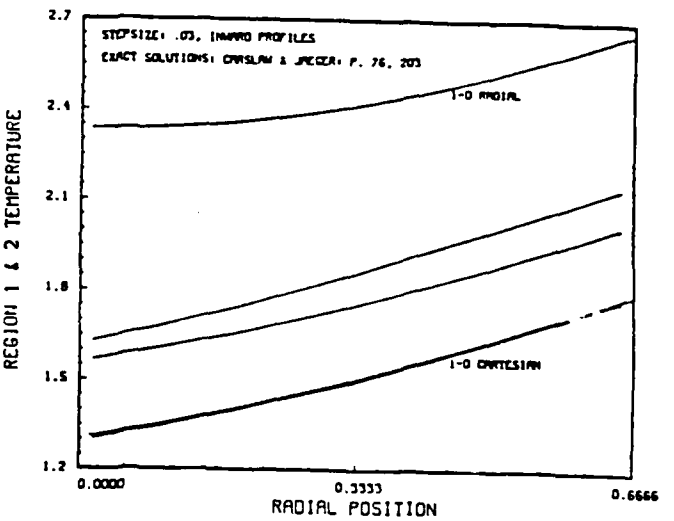

FIG. B.10 REGION I AND II TEMPERATURE PROFILES AT $\tau = .50$, $\gamma = 2/3$. Upper curve at $\alpha = \alpha_o/2$, middle curve at $\xi \simeq .09$, lower curve at $\xi \simeq .9\xi_o$. (1-D radial and Cartesian profiles included).

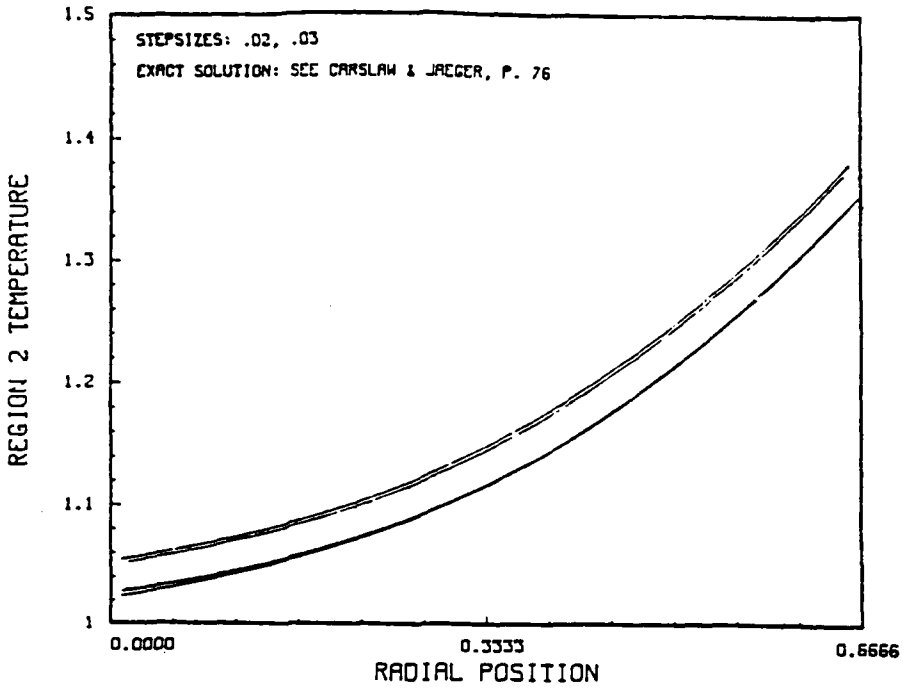

FIG. B.11 INERT TEMPERATURE PROFILES IN REGION II AT $\tau = .1$, $\gamma = 2/3$. Upper curve at $\xi = .09$, middle curve at $\xi = .5\xi_o$, lower curve at $\xi = .9\xi_o$. (1-D Cartesian curve included).

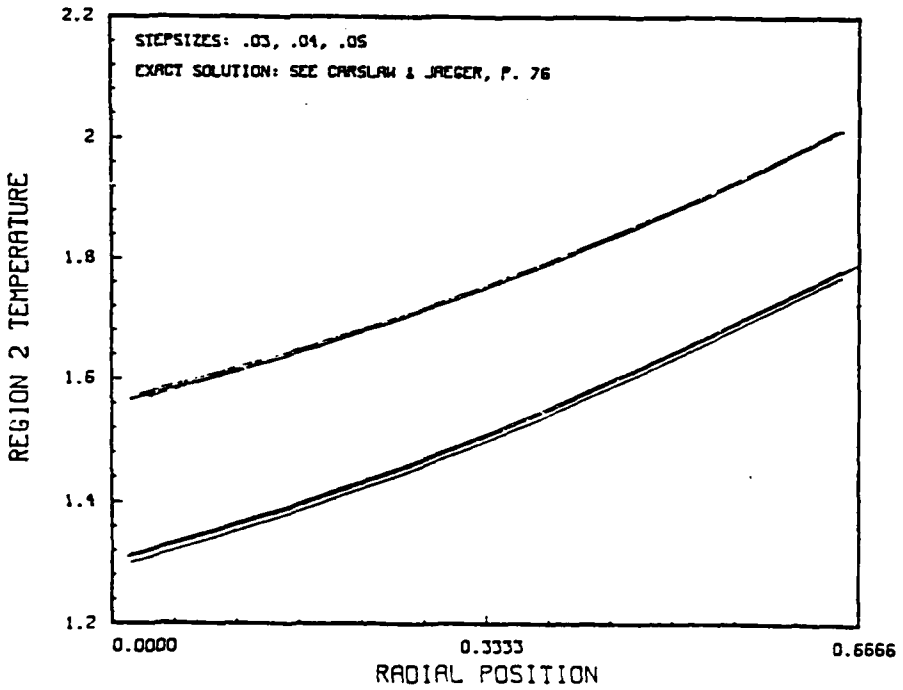

FIG. B.12 INERT TEMPERATURE PROFILES IN REGION II AT $\tau = .5$, $\gamma = 2/3$. Upper curve at $\xi = .09$, middle curve at $\xi = .5\xi_o$, lower curve at $\xi = .9\xi_o$. (1-D Cartesian curve included).

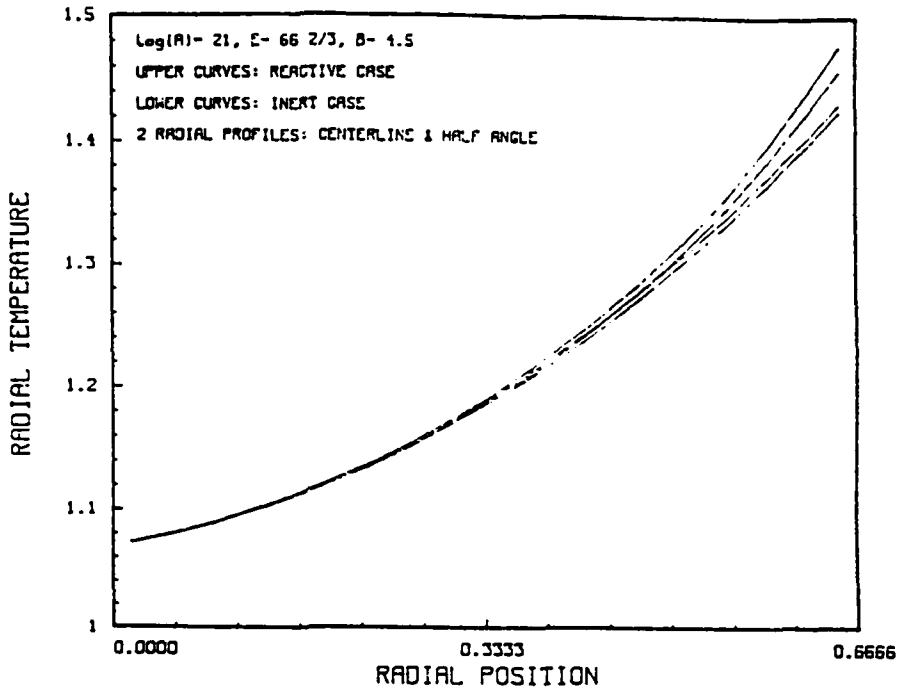

FIG. B.13 RADIAL PROFILES FOR REACTIVE AND INERT CASES: SHORTLY BEFORE IGNITION. Radial curves taken along $\alpha = 0°$ and $\alpha_o/2$. ($\gamma = 2/3$)

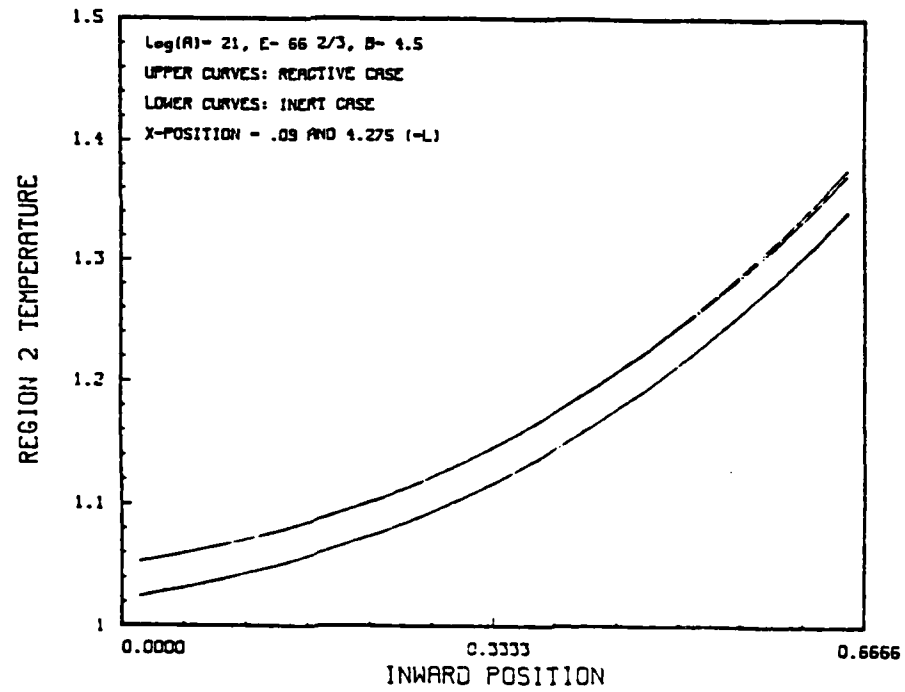

FIG. B.14 REGION II PROFILES FOR REACTIVE AND INERT CASES: SHORTLY BEFORE IGNITION. Profiles inward from $\xi = .09$ and $.5\xi_o$. ($\gamma = 2/3$)